

USING RESISTIVITY PSEUDOSECTIONS TO MONITOR MOISTURE MIGRATION THROUGH THE VADOSE ZONE

Research performed
in partial fulfillment
of the requirements for the degree of
MASTER OF SCIENCE
in HYDROLOGY

by
Paul Michalak



TABLE OF CONTENTS

	<u>Page</u>
ABSTRACT	iv
I. PURPOSE OF WORK	1
II. INTRODUCTION	3
A. Geology	3
B. Hydrogeology	4
C. Background Information	5
III. PREVIOUS WORK	6
IV. THEORY	8
A. Electrical Resistivity in the Vadose Zone	8
B. Factors Affecting Interpretation of Resistivity Data	12
V. METHODS	17
A. Instrumentation	17
B. Surveying Techniques	17
1. Wenner Electrode Configuration	17
2. Dipole-Dipole Electrode Configuration	18
3. Vertical Electrical Sounding	19
4. Horizontal Profiling	19
5. Pseudosection	20
C. Interpretational Techniques	20
1. Wenner VES Data	20
2. Dipole-Dipole Pseudosection	22

VI. PRESENTATION OF RESULTS	25
A. Vertical Electrical Soundings	25
1. Wenner VESs	25
2. Dipole-Dipole VESs	26
B. Horizontal Profiles	26
C. Dipole-Dipole Pseudosections	26
VII. DISCUSSION	31
A. VES Interpretation	31
B. Horizontal Profile Interpretation	33
C. Dipole-Dipole Pseudosections	34
1. Pseudosection Modeling	34
2. Moisture Content vs Resistivity	34
a) Upper zone	35
b) Middle zone	37
c) Lower zone	37
3. Qualitative Analysis	39
VIII. CONCLUSIONS	41
IX. RECOMMENDATIONS	43
X. REFERENCES	50
XI. FIGURES	53-89
XII. TABLES	90-103
APPENDIX A. Summary tables of pseudosection resistivity measurements and their standard deviations	104-123
APPENDIX B. Computer program for the forward calculation and automatic inversion of Wenner sounding curves from Zohdy and Bisdorf (1975).	124-140
Resistivity modeling program to invert dipole-dipole pseudosections from Dey and Morrison (1976).	141-168

APPENDIX C. A Resistivity Study of the La Union Lower
Landfill.
by Paul Michalak and Kim Edlund

169-220



ABSTRACT

A study of moisture migration was conducted at a site located near the New Mexico Institute of Mining and Technology. As part of this project, numerous boreholes and tensiometers were placed within the research area to monitor the movement of water through the system as well as to define the lithology of the earth below the site. For this paper, resistivity pseudosections, using a dipole-dipole configuration, were measured and analyzed to study the migration of moisture in the vadose zone. The analysis of the pseudosections included both numerical modeling using an integrated finite difference code, as well as qualitative grouping of resistivity measurements into intervals. Additionally, Wenner vertical electrical soundings and horizontal profiles were conducted to supplement the pseudosection data. The Wenner vertical electrical soundings were analyzed using an inversion code based on the Dar Zarrouk parameters. As a result of the lateral inhomogeneities found within the research area and likely resistivity changes within the pore water, no quantitative analysis of the relationship between moisture content and resistivity measurements was possible. Recommendations to alleviate some of the difficulties experienced in this research are included.



I. PURPOSE OF WORK

This research study was undertaken in order to apply earth resistivity techniques, with an emphasis on dipole-dipole pseudo-sections, in the monitoring of water infiltration in the vadose zone. This research is an attempt to supplement a classical vadose zone infiltration study technique, termed an instantaneous profile, which was developed by Watson (1966) and extended by Hillel et al. (1972). An instantaneous profile utilizes the following general equation which describes the flow of water in a vertical soil profile.

$$\frac{\partial \theta}{\partial t} = \frac{\partial}{\partial z} \left(K(\theta) \frac{\partial H}{\partial z} \right)$$

where θ is the volumetric moisture content, t is time, z the vertical depth, K the hydraulic conductivity, and H the hydraulic head. Thus, two important physical parameters, matrix suction head and soil moisture, must be measured with respect to depth and time. These measurements can be made using both a tensiometer and a neutron moisture probe. This requires the introduction of neutron meter access tubes as well as of the tensiometers themselves throughout the soil profile. Essentially, this means drilling holes to specified depths which disturbs the soil profile and is expensive. Moreover, measurements of this type only yield point values whereas moisture distribution throughout a volume of ground is desired.

Procedurally, once the instruments are in place, water is either ponded on the surface or a constant flux is achieved just below the surface. At this point, readings over a specified time interval can be made of both soil matrix suction and soil moisture. From these data, an infiltration rate through the soil profile can be derived.

Resistivity measurements, although labor intensive, require no drilling. Thus, as stated earlier, the goal of this study was to use earth resistivity techniques in observing moisture movement in the vadose zone. This was accomplished by taking resistivity readings before and after the introduction of water into the soil profile. Although no actual infiltration rates are reported in this paper, the techniques presented and suggested could help in the mapping of moisture migration, especially if combined with direct measurement of soil moisture at suitably spaced points, as outlined.

II. INTRODUCTION

A. Geology

Socorro, New Mexico is located in Socorro County, approximately 75 miles south of Albuquerque, on Interstate 25. The infiltration study site is located at T3S, R1W; within the city limits of Socorro, on the western border of the New Mexico Institute of Mining and Technology (NMIMT) golf course. Figure 1 is a sketch of the study area.

Geologically, the top 30 feet of sediment, the interval of interest in this paper, corresponds to part of the Sierra Ladrones Formation of the Santa Fe Group. The Sierra Ladrones Formation, deposited during early Pliocene to middle Pleistocene consists of alluvial fan, piedmont slope, alluvial flat, flood plain, and axial stream deposits (Machette, 1978). Specifically, two facies of the Sierra Ladrones Formation are encountered here. The upper facies, corresponding approximately to the top 12 feet of material at the study site, is defined as the Piedmont slope facies of the Sierra Ladrones Formation (Chamberlin, 1980). It consists of silty sands and pebbles derived from Socorro Peak, which lies just west of the study site. The next 18 feet, defined as the fluvial sand facies, is predominantly composed of clean, tan-colored, fluvial sands derived from the ancient Rio Grande.

On a local scale, the stratigraphy of the study area was investigated by Parsons (1988) through the installation of a series of boreholes located throughout the study area. Parsons (1988) defined a grid system for the study area through which the location of each borehole could be defined. For consistency, the same grid locations are

referred to in this work. Figure 1 identifies the location of five boreholes, 15-15, 11-15, 19-15, 15-19, and 15-11, that are of particular interest to this study. Figure 2, adapted from Parsons (1988), identifies the lithologic symbols utilized in Figures 3 to 9. Figure 3, a borehole geologic log located at 15-15, presents the general depositional sequence of the Sierra Ladrones Formation encountered at the site. Generally, the stratigraphy at the site alternates between fine sand and silt to coarse sand, pebbles, and cobbles. Figures 4 to 7 are the borehole geologic logs located at 11-15, 19-15, 15-19, and 15-11, respectively. These shallow borings illustrate the stratigraphy in the upper 6 feet of the study area. Boreholes 11-15 and 19-15 indicate a coarser upper zone (coarse sand and pebbles) while boreholes 15-19 and 15-11 represent a finer textured material (sand and silt). Figures 8 and 9, adapted from Parsons (1988), are geologic cross sections of the study area oriented along the a'-a (south to north) and f-f' (west to east) center lines (Figure 1). Both cross sections illustrate the site's subsurface heterogeneity.

B. Hydrogeology

Hydrogeologically, there are two regional aquifers present in Socorro Basin (Anderholm, 1983). The phreatic aquifer, located 70 to 75 feet from the surface, was the only aquifer penetrated by the resistivity soundings conducted in this study. This unconfined aquifer, with a saturated thickness not exceeding 300 feet, is in the Sierra Ladrones Formation. The gradient is in a southeasterly direction.

C. Background Information

As stated above, the interval of interest is the top 30 feet of sediment. Specifically, resistivity surveys were conducted both before and after the introduction of a continuous flow of water into the research area. The actual infiltration area was approximately 30.5 feet squared. Prior to the pre-infiltration resistivity measurements, this 30.5 feet x 30.5 feet area was dug out to a depth of about 3 feet. After the pre-infiltration resistivity measurements, PVC drip lines were placed on the bottom of the dug out area. These drip lines, covered for protection with halves of larger diameter PVC pipe, were used to introduce water into the system. Placed over the drip lines, in ascending order, was a plastic liner, 6 to 12 inches of hay, backfill, another plastic liner, and finally a thin layer of soil. In this study, the two plastic liners proved troublesome because of their non-conducting properties. Compaction during this construction stage resulted in a level surface. The infiltration rate introduced into the soil profile was 1×10^{-5} cm/s or 100 times less than the estimated saturated hydraulic conductivity of the soil. For details on site setup see Matson (1989) and Parsons (1988).

Pre-infiltration resistivity measurements were conducted between August 11, 1986 and October 31, 1986. The actual introduction of water into the system did not occur until January 29, 1987. The post infiltration resistivity measurements were started after approximately three months of continuous water infiltration into the system. These measurements were collected between May 6, 1987 and June 8, 1987.

III. PREVIOUS WORK

Historically, direct current earth resistivity methods have been used extensively in conjunction with groundwater studies. In almost all cases, the application of resistivity techniques in hydrology has been either in detecting a water table or detecting and monitoring leachate from disposal/landfill sites. The first published study on monitoring moisture migration in the vadose zone was issued by Kean et al. (1987). A brief review of this paper seems in order.

Kean et al. (1987) used a reverse Schlumberger array, in conjunction with a central circuit board and data logger, to continuously monitor apparent resistivity both before and after a rainfall, at four sites exhibiting geoelectrical horizontal layering and lateral homogeneity. The resistivity data were modeled using a Ghosh-Koefoed inversion computer algorithm (Koefoed, 1970). This model assumes horizontal layering. The layer thicknesses were found by hand-augering. From their resistivity inversions and augering, the authors deduced a three-layered earth at three of the four study sites. It should be noted that these simple models were possible, in part, because the water tables at all four reported study sites were between depths of only 4.5 and 42 feet. The shorter the distance between the surface and the water table, the less likely it is that a complex multi-layered model will be necessary. In addition to the resistivity measurements, gravimetric moisture measurements and tensiometer measurements were used at some of the sites to define relevant soil parameters further. Kean et al. (1987) concluded that, "(1) moisture is retained for long periods

of time in clay/silt-rich soils, (2) moisture migration is slow below a moist soil zone and is not readily detected by surface resistivity measurements, and (3) near-surface moisture changes can be defined by surface resistivity."

The first of these conclusions appears rather obvious. The second conclusion is difficult to substantiate with the data presented in the present research since the time intervals between dry and wet resistivity measurements were significantly different in both works. Kean's assertion that moisture migration is not readily detected by surface resistivity measurements may be true using his more conservative modeling approach; however, the more flexible resistivity modeling techniques used in this paper are better suited to interpret unsaturated zone resistivity measurements. As a result it does appear, based on our results, that the modeling techniques presented in this paper can differentiate moisture migration in successive sets of vadose zone resistivity measurements. Although, for reasons that will be discussed later, no quantitative evaluation of moisture resistivity changes was possible from this work, it is believed that with the proper equipment and a geologically and/or geoelectrically simpler site, a quantitative appraisal of moisture movement in the vadose zone using resistivity techniques may be possible. Finally, the results presented in this paper qualitatively concur with Kean's third conclusion, that near-surface moisture changes can be defined by surface resistivity.

IV. THEORY

A. Electrical Resistivity in the Vadose Zone

When monitoring the infiltration of water through the vadose zone using resistivity methods it is important to consider the effects of partial saturation of the soil profile on resistivity measurements. Almost exclusively, the research relating groundwater hydrology with electrical geophysical methods has involved the relationship between saturated soil or rock and electrical resistivity measurements. In this study, the unsaturated conditions characteristic of the vadose zone result in a more complicated relationship between electrical resistivity and a partially saturated soil profile. Therefore, it is important to develop the conceptual differences between resistivity measurements taken in a saturated profile, an unsaturated profile, and an unsaturated profile experiencing infiltration.

When considering resistivity in a saturated soil system a good starting point is the formation factor, originally defined by Archie (1942) as

$$F = \rho_o / \rho_w$$

where ρ_o is the bulk resistivity of the soil system and ρ_w is the pore water resistivity. The term formation factor can be further defined as apparent formation factor, where the effect of surface conductance and other intergranular pore water contributions are considered, and the intrinsic formation factor, where the rock matrix is assumed to be perfectly nonconducting (Urish, 1981). In brine filled sediments, the

apparent formation factor approaches the intrinsic formation factor (Barker and Worthington, 1973) because the surface conductance effects are much smaller than the pore water conductivity. An empirical form of the formation factor was also given in Archie (1942) as

$$F = a\phi^{-m}$$

where ϕ is the porosity of the soil system and a and m are constants representing the intrinsic properties of the grain matrix. This relationship works well in brine filled sediments but does not apply to fresh-water systems since the formation factor, in systems with high pore water resistivities, varies with pore water resistivity and grain size as well as with porosity.

A model of the electrical transport process in sediments completely saturated with fresh water (low salt content) must account for several factors. In terms of conductance, the grain matrix, pore water, and solid-liquid interface (surface conductance) contribute to the process. Usually, the conductivity of the grain matrix can be ignored; however, pore water and surface conductivity are integral components of the electrical transport process. For a localized model of electrical transport, pore water and surface conductance can be considered constant. Additionally, the tortuosity of the current flow path, porosity of the matrix material, and the internal pore area (defined as the total interstitial surface area of the pore per unit pore volume) must be considered in a model of electrical flow in fresh-water sediments (Urish, 1981).

In the unsaturated zone, the intergranular spaces of the soil matrix are not completely filled with water. For a partially saturated profile, the intergranular spaces are made up of differing proportions of a nonconductive gaseous phase (air) and a liquid phase (water). In dry soils with very small moisture contents, water exists in an adsorbed state immediately adjacent to the soil particle surface. This water, known as "hygroscopic water" exists as extremely thin films surrounding soil particles. Electrical current when applied to a soil containing only hygroscopic water is conducted along this thin surficial film. This aspect of unsaturated electrical transport is equivalent to surface conductance in the saturated model. Because of the absence of a conductive pore water to enhance current flow, the tortuosity of the current path is great. As a result, the resistance to current flow is generally greater in this system than in a saturated system.

When moisture content in a soil increases slightly (i.e., less than 20% of the intergranular space is filled with water) pore water will remain almost entirely in capillary wedges at the contact points of the particles (Figure 10). This results in the formation of separate and discontinuous pockets of pore water. Electrical current paths in this system also have a much more tortuous route than in a saturated medium.

Infiltration in a partially saturated profile further complicates electrical resistivity models in the vadose zone. As stated earlier, in a saturated profile electrical current moves in a tortuous path through the intergranular spaces. The actual path traveled by the current is probably complex; however, the path itself should remain fairly constant between measurements taken at the same location (assuming effective

porosity and pore water resistivity do not change). During infiltration in an unsaturated system, this may not be the case. As water passes through a dry profile, capillary wedge interconnection is in a transient state. This is primarily true directly behind the wetting front of an infiltration moisture profile. It is in this wetting zone that moisture levels are in the range where pore water exists mainly in capillary wedges (Hillel, 1980a). As a result, electrical resistivity measurements taken at the same location over time may experience random effects during infiltration since the medium through which the electrical current travels is changing. Thus, in an unsaturated system experiencing infiltration, the electrical flow lines generated from a given electrode spacing may not be constant over time.

When a soil profile is experiencing infiltration under unsaturated conditions, the interaction between the ionic constituents of the pore water and matrix must be considered. During its passage through the vadose zone, the wetting front tends to dissolve additional solids (Hillel, 1980b). This additional load consists primarily of electrolytic salts. As the infiltrated water moves further through the profile, it carries this load in its convective stream, leaving some of the salts behind to the extent that they are adsorbed or precipitated whenever their concentrations exceed their solubility. Consequently, soil water chemistry during infiltration is probably not constant throughout the profile. Moreover, since soil water is dissolving and/or precipitating salts, the soil portion of the system is also not constant. The result of being unable to assume constant soil water or

soil matrix during an infiltration event complicates the comparison of resistivity measurements taken before and after the infiltration event.

As can be seen, a model of electrical transport in an unsaturated medium is more complex than one for a saturated medium. Not only must the grain matrix conductance, pore water conductance, surface conductance, tortuosity, effective porosity, and internal pore area be accounted for, but the moisture content must be considered. Additionally, the chemical composition of the pore water is not necessarily constant. All these factors must be considered when interpreting the results of an electrical resistivity survey in the vadose zone.

B. Factors Affecting Interpretation of Resistivity Data

Before electrical resistivity data can be analyzed, it is necessary to consider factors that may complicate the interpretation. Two factors that affect the interpretation of any set of resistivity data are the thicknesses and the resistivities of the geoelectric layers being surveyed. It should be recognized that the geoelectric section of a profile may not be the same as the geologic section for a given survey area. Geoelectric sections are synonymous with geologic sections only when the boundaries between geologic layers coincide with the boundaries between layers characterized by different resistivities (Zohdy et al, 1974). Theoretical type curves derived for the purpose of interpreting vertical electrical soundings (VES) are an expression of the relationship between layer thicknesses and resistivities in a geoelectric section. However, a measured VES can correspond to several subsurface distributions of thickness and resistivity. Thus, the

inversion of the data is not unique. Interpretations of VES data must utilize any geological information available about the study area to help eliminate models that do not fit into the known geologic picture.

Another factor that complicates VES interpretation is lateral inhomogeneities. The formation of a cusp, a pointed segment on a VES curve, indicates the presence of a lateral inhomogeneity. Wenner VES curves affected by lateral heterogeneities are particularly complicated when the potential electrodes cross over or near an inhomogeneity (Zohdy et al, 1974). Cusps and other deviations from smooth theoretical curves such as those published by Mooney and Wetzel (1956) or Elliot (1974), make interpretation of these geoelectric sections difficult. The characteristic smoothness in theoretical curves results from the assumption of horizontal layering in geoelectric sections. Consequently, fitting or inverting complicated non-smooth field curves does not result in a meaningful interpretation since the boundary conditions used in deriving the analytical solutions were not met.

Dipole-dipole resistivity measurements are particularly sensitive to lateral inhomogeneities. In a classical study of dipole methods, Al'pin et al (1966) found that dipole-dipole VES curves taken in the same area showed widely different results. They attributed these discrepancies to "lateral changes in the total conductance of the rocks above the basement." Thus, it was concluded that the dipole methods showed a high degree of resolution in detecting such inhomogeneities. Keller (1966) also discusses the extreme effects of lateral resistivity changes on dipole-dipole measurements when the dipole source is over a resistive zone. He recommends that the most conductive overburden be

found and utilized as the sounding area. Frohlich (1968) found that dipole methods are more affected by lateral resistivity changes than the Schlumberger technique and concluded that interpretations based on a horizontal layer case can provide uncertain results.

From the discussion above, it is concluded that VES curves derived from dipole-dipole measurements can show a greater ambiguity than either Wenner or Schlumberger arrays when lateral variations in resistivity are present. This problem results from the laterally homogeneous layer assumption in VES curve interpretations. This assumption is believed to be unnecessary when modeling pseudosections. The purpose of pseudosections is to model inhomogeneities that, because of their irregularity, can not be simulated by other models. A logical question that follows is: can all lateral inhomogeneities be accounted for in two-dimensional dipole-dipole pseudosections?

To answer this question the modeling process itself must be addressed. The operation of defining a model using either a finite-difference or finite element approach can be quite laborious. Given a pseudosection of field data, the modeler tries to match his model-generated pseudosection by adjusting or "tweaking" the electrical conductivity matrix input. The capacitance matrix that produces the "best fitting" match to the field pseudosection is considered the earth model. In Dey and Morrison (1979a), the integrated finite-difference approach to pseudosection interpretation views the resultant model as "two-dimensional structures defined as geologic bodies of arbitrary cross section with infinite extent along the strike." Thus, along the cross section, all inhomogeneities, within the modeling grid, are

accounted for and modeled; however, inhomogeneities along the strike, i.e., in a direction normal to the modeled section, can not be handled with presently available methods.

One solution to this problem would be the application of a three-dimensional pseudosection model (Dey and Morrison, 1979b). The capacitance grid used in the numerical solution of a three-dimensional pseudosection model would contain conductivity information perpendicular to the orientation of the pseudosection. Dey and Morrison (1979b) in their three-dimensional pseudosection model applied mathematical techniques very similar to the ones presented in their earlier two-dimensional study (Dey and Morrison, 1979a). One difference between Dey and Morrison's two- and three-dimensional models, however, involves the use of a Fourier transform in their two-dimensional model. This transformation resulted in a two-dimensional capacitance matrix, as input, and a two-dimensional solution (see Chapter V, page 22). Their three-dimensional model, on the other hand, does not require a transformation. It utilizes a three-dimensional capacitance matrix as input which, in turn, results in a three-dimensional solution.

The real difficulty in applying Dey and Morrison's three-dimensional model involves the size of the solution grid. In realistic simulations of geologic models in three-dimensions for dipole-dipole pseudosections, the discretization grid generally results in 10,000 to 15,000 nodes at which total potentials are evaluated for multiple injection points (Dey and Morrison, 1979b). Such discretizations result in matrices that are rather unwieldy to handle even on very fast main frames. Reducing the size of the grid in the third dimension, to

decrease the size of the solution grid, defeats the purpose of using a three-dimensional model. This is in contrast to a two-dimensional model where much smaller grids (100 to 1000 nodes) are usually applied.

Although two-dimensional pseudosection modeling can account for lateral inhomogeneities along the section's axis, a cross section showing large heterogeneities is almost impossible to match using a hit or miss "best fit" approach. As an example, the Dey and Morrison (1979a) model, which was utilized in this report (Appendix B) has a 58 x 16 conductance matrix or 928 electrical conductivity values as input. When these conductivity values show great variation, the possibility of matching a model to field data can become a hopeless exercise. In addition, it should be remembered that the inverse modeling method described above does not produce a unique solution. Consequently, even if a reasonable fit is found, the modeler must subjectively decide the accuracy of his solution. Uncertainty increases in proportion to the complexity of the modeled earth.

V. METHODS

A. Instrumentation

A Soiltest R-60 Earth Resistivity Meter (power unit and D.C. millivoltmeter) was used to conduct the resistivity soundings. In this system the power unit is connected to two steel stakes (current electrodes), from which the battery generated current enters the earth. The D.C. millivoltmeter is connected to two porous pots filled with saturated copper sulfate solution (potential electrodes) between which voltage is measured.

B. Surveying Techniques

Two types of electrode configurations, the Wenner and the dipole-dipole array, were used to conduct the resistivity surveys presented in this work. In this study, the Wenner surveys included horizontal profiles as well as vertical electrical soundings (VES). In the case of the dipole-dipole configuration, an additional form of presentation, termed a pseudosection, was also employed.

1. Wenner Electrode Configuration

As illustrated in Figure 11, four electrodes are placed along the ground surface (in the order shown) so that an equal distance (defined as a) exists between any two adjacent electrodes. The equation for the apparent resistivity measured with the Wenner array is

$$\rho_a = 2\pi a \frac{\Delta V}{I}$$

where a is the electrode spacing, ΔV is the potential difference, and I is the current.

The depth of investigation for the Wenner array, as determined by Roy and Apparao (1971) is 11% of the total Wenner electrode spread (or $0.33a$). Depth of investigation is defined as that depth at which a thin horizontal layer of ground contributes the maximum amount to the total measured signal at the ground surface. It should be noted that the depth of investigation is not the depth at which the entire measured signal originates. Obviously, other portions of the earth have contributed to the signal; however, the largest contribution comes from the depth of investigation. As a result, depth of investigation aids in determining horizontal profiling spacings when the general depth of the object or layer is known.

2. Dipole-Dipole Electrode Configuration

The dipole-dipole configuration is commonly used in resistivity surveys. Al'pin et al (1966) developed much of the necessary theory for this configuration. In this work a polar or axial dipole-dipole array was employed. Figure 12 illustrates the position of the current and potential electrodes for the polar dipole-dipole array. The equation for the apparent resistivity measured with the dipole-dipole array is

$$\rho_a = \pi n (n+1)(n+2)a \frac{\Delta V}{I}$$

where a is the distance between electrodes in either dipole, n is an integer multiple of the distance, ΔV is the potential difference, and I

is the current (Figure 12). The dipole-dipole array has one of the greatest depths of investigation among all electrode configurations used in surface resistivity methods. Roy and Apparao (1971) found the depth of investigation for a dipole-dipole array in a homogeneous earth to be about 20% of the dipole separation. Roy and Apparao (1971) define dipole separation as the distance between the midpoints of the two dipoles (see Figure 12). This was in contrast to 11% for a Wenner array (discussed above) and 12.5% for the Schlumberger configuration, where these percentages refer to distance between the current electrodes. Essentially, this means that in order to get similar information in resistivity soundings, the Wenner and Schlumberger arrays would have to be almost twice as long as the dipole-dipole array. The dipole-dipole configuration, however, requires more electrical power than the Wenner and Schlumberger arrays. Keller (1966) estimates that this increase may be an order of magnitude.

3. Vertical Electrical Sounding

In a vertical electrical sounding, the center of the electrode configuration is fixed. Measurements are made at various electrode spacings. We assume that wider electrode spacings produce greater current penetration resulting in more information about deeper structures. In this report, both Wenner and dipole-dipole vertical electrical soundings were utilized.

4. Horizontal Profiling

In horizontal profiling, the electrode separation is maintained at a constant value and the entire array is moved along a traverse. Readings are taken at uniform intervals along this traverse.

A lateral inhomogeneity or anomaly will cause a rise or fall in observed readings. In this study Wenner horizontal resistivity profiles with spacings of 30 and 50 feet were conducted.

5. Pseudosection

A pseudosection is a sort of electrical resistivity cross-section. Although any electrical resistivity configuration can be used, it is most frequently seen in conjunction with the dipole-dipole array. In a pseudosection, the apparent resistivity values for each station are plotted on a vertical section, the points of which are the intersections of 45 degree lines, drawn from the surface, beginning at the respective midpoints of the current and potential dipoles (Telford et al. 1976). The technique is illustrated in Figure 12. From this definition, it is easy to see that each vertical line of data in a pseudosection represents an expansion of the array about a fixed center and constitutes a VES curve. In addition, if we take each horizontal line of data in the pseudosection, we find that it comprises a horizontal profile.

C. Interpretational Techniques

1. Wenner VES Data

The Wenner VES models presented in this paper were developed using a computer program written by Zohdy and Bisdorf (1975). Within this program, modified Dar Zarrouk (MDZ) functions are utilized in an iterative fashion to calculate the proper model parameters. Appendix B contains a copy of this computer code.

The automatic inversion of vertical electrical soundings using modified Dar Zarrouk functions is an interesting procedure. Zohdy (1975)

gives a detailed derivation of the procedure. This derivation has several typographical errors and care should be taken when comparing its equations to the computer code of Zohdy and Bisdorf (1975). Briefly, the points on the digitized VES field curve are considered to be points on an MDZ curve. The MDZ curve is then solved for layer thicknesses and resistivities. The total kernel function (TKF) curve for this set of thicknesses and resistivities is calculated using Sunde's recursion formula (Sunde, 1949), and the VES curve is calculated by convolution using Ghosh's coefficients (Ghosh, 1971). After comparing this generated VES curve with the field curve, adjustments are initiated and a new modified Dar Zarrouk curve is calculated. The process continues as described above until a fit, within a prescribed tolerance, is obtained between the generated and field VES curves.

The Zohdy inversion method for VES curves has some distinct advantages. Unlike most direct interpretation methods, this technique does not require initial assumptions on the number of layers or about the layer resistivities or thicknesses. Instead, the VES curve is digitized (at the rate of six points per logarithmic cycle), and the number of layers is automatically fixed as equal to the number of points on the digitized curve. In addition, the technique automatically smoothes its output, so that most models do not contain an inordinate number of layers. Frequently, the model is reduced even further by visual inspection. The automatic smoothing process is especially useful when inverting a distorted field curve, since the output of the computer code will result in two solutions: one based on the inversion of the

distorted field curve and the other on the inversion of the automatically smoothed VES curve.

There are also some disadvantages to this method; the most important of these involves the use of the Ghosh filter coefficients (Ghosh, 1971). Zohdy (1975) reports that for VES curves with steeply descending branches, the Ghosh filter coefficients will result in inaccurate apparent resistivity values and therefore mean a poor fit. Specifically, Zohdy (1975) reported that this becomes a problem when the ratio of the minimum apparent resistivity to the maximum apparent resistivity is less than 0.025. While testing the Zohdy and Bisdorf (1975) code for use in this work, it was discovered that this technique could not properly invert several of the theoretical curves derived by Mooney and Wetzel (1956). Not all of these theoretical curves fell exactly into Zohdy's troublesome category, although all did have descending branches. In terms of applying the Zohdy method, if the visual inspection reveals a poor fit between the field and generated VES curves, or if a known marker bed or depth (such as a clay/sandstone boundary or a water table) does not correspond with the inverted model's interpretation, the technique should not be considered accurate. Experience has shown that application of the Zohdy computer codes as an interpretation tool should be decided on a case by case basis.

2. Dipole-Dipole Pseudosections

For the dipole-dipole electrode configuration, the computational method employed in this work is a finite-difference technique which solves a three-dimensional potential distribution about a point source of current located in or on the surface of a half-space

containing an arbitrary two-dimensional distribution of conductivity. The theory is well described by Dey and Morrison (1979a) and the computer code used was published by the same authors three years earlier (Dey and Morrison, 1976). Appendix B contains a copy of the pseudosection modeling code used in this report.

Essentially, the finite-difference equations are derived for Poisson's equation (Dey and Morrison, 1979a, Equation 1) by using an area discretization of the subsurface. This results in a block-centered finite-difference grid. The governing equation (Poisson's) is in three dimensions, but through a Fourier transform, Dey and Morrison (1979a) are left with a two dimensional space and a Fourier constant. The potential values at all points in the grid are simultaneously obtained for multiple point sources of current injection. In this report, the multiple point sources of current are the current electrodes used in a dipole-dipole resistivity survey. The solution to this problem is obtained using a direct explicit matrix inversion. Since the capacitance matrix (matrix of input conductivity values) is symmetric and positive definite, the most practical matrix inversion solution technique is the Cholesky decomposition method. Finally, this solution technique achieves a three-dimensional distribution as an answer by discretizing the Fourier constant into five distinct intervals, inverting the entire capacitance matrix in each interval using the Cholesky decomposition technique, and then combining each of the five discretized solution sets. Although the potential solution is in three dimensions, it should be kept in mind that the conductivity matrix, the most important aspect in this work, is a two-dimensional structure. By

a two-dimensional structure, it is meant that the geologic body producing the conductivity matrix is an arbitrary cross-section with infinite extent in the perpendicular direction.

There are two distinct advantages to this modeling method. In a computational sense, this technique uses very little computer time. The eloquence of the mathematical derivation along with the utilization of the Cholesky decomposition method combine to make this computer modeling method extremely efficient. It should be kept in mind that this technique does invert five 58×16 matrices, so that even on a main-frame computer the computation is not instantaneous. The other advantage is the ability to model arbitrary cross-sections of conductivity. Many electrical techniques, including the Zohdy method previously discussed, must assume horizontal layer stratification. The Dey and Morrison method has no such limitation.

Two disadvantages exist for this method. Even though the input conductivity matrix is only about half the size of the actual inverted matrix (58×16), one of the real problems with this technique is deriving 928 conductivity values for a heterogeneous pseudosection. Another problem with pseudosection modeling is the technique's inability to handle heterogeneities perpendicular to the cross section.

VI. PRESENTATION OF RESULTS

A. Vertical Electrical Soundings

1. Wenner VESs

Two Wenner vertical electrical soundings were conducted at the study site. Figures 13 and 14 are the Wenner resistivity data and Zohdy VES inversions of these data, centered at locations 15-15 and 15-11, respectively (Figure 1). The Wenner VES data centered at 15-15 was conducted before any water infiltration had taken place, whereas the VES data centered at 15-11 was conducted after three months of soil moisture infiltration. A post-infiltration Wenner VES centered at 15-15 was not possible because of the two plastic liners placed above the infiltration lines during the construction stage of the project (see Section 2, Background Information). Most VESs require a considerable amount of electrode movement; moreover, the Wenner configuration requires moving all four electrodes after each reading. For the smaller Wenner electrode spacings (less than 10 feet), reproducing the exact locations of the pre-infiltration measurements would have required extensive excavation of the infiltration area, to insure penetration of the plastic liners. Consequently, the post-infiltration Wenner VES was moved approximately 15 feet south and was centered at 15-11.

Tables 1 and 2 are the computer output from the Zohdy VES inversions of the Wenner resistivity data centered at 15-15 and 15-11, respectively. The inverted geoelectric sections can be found under the columns titled reduced depth (or reduced thickness) and reduced resistivity. Figures 15 and 16 are the graphical representation of the

inverted geoelectrical sections presented in Tables 1 and 2, respectively.

2. Dipole-Dipole VESs

Figures 17 to 21 are the dipole-dipole VESs centered at 15-17.3, 15-19, 15-20.6, 15-22.3, and 15-24, respectively (Figure 1). These data correspond to 5 vertical lines of data taken from the a-a' pre-infiltration pseudosection (Figure 1). The dipole-dipole VESs include additional data collected using wider electrode spacings than are presented in the a-a' pseudosection. These additional data points were not included in the a-a' pseudosection because they were only measured during the pre-infiltration collection phase. Consequently, no corresponding post-infiltration dipole-dipole VESs are presented.

B. Horizontal Profiles

Two Wenner horizontal resistivity profiles were conducted from south to north along the a'-a survey line. Figures 22 and 23 are the Wenner horizontal resistivity profiles with electrode spacings of 30 and 50 feet, respectively. The station numbers refer to the locations of the resistivity measurements. For both profiles, resistivity measurements were taken at 10 foot intervals. The locations of the station numbers corresponding to those presented in Figures 22 and 23 are identified in Figure 24. Both profiles were generated after approximately 3 months of infiltration.

C. Dipole-Dipole Pseudosections

Pre- and post-infiltration pseudosections were conducted along 5 lines situated on or around the infiltration area (Figure 1). All

pseudosections presented in this work were constructed using a dipole-dipole electrode configuration with a dipole spacing of 10 feet. Figure 25 is the legend of resistivity intervals represented in the graphical illustrations of these pseudosections (Figures 26 to 35). Figures 26 and 27 are the pre- and post-infiltration pseudosections conducted along the a-a', north-south center line. Figures 28 and 29, 30 and 31, 32 and 33, and 34 and 35 are the pre- and post-infiltration pseudosections conducted along the b-b' (west boundary), c-c' (east boundary), d-d' (north boundary), and e-e' (south boundary) lines, respectively. The pre- and post-infiltration dipole-dipole resistivity measurements and their standard deviations are presented in Appendix A.

Table 3 is the computer output of the numerical inversion of the pre-infiltration a-a' pseudosection using a computer code developed by Dey and Morrison (1976). The first page in Table 3 is the capacitance matrix for the resistivity model. Each number in the matrix corresponds to a resistivity value, which is defined at the bottom of the page under the heading "resistivity key". The second page is the resulting pseudosection inversion.

The a-a' (north-south center line) pseudosection required only four electrode positions directly within the plastic lined infiltration area. Thus, it was possible to conduct this pseudosection along the a-a' line for both the pre- and post-infiltration resistivity measurements. This was achieved by digging four holes through the top three feet (containing the 2 plastic liners) of the infiltration area at the approximate pre-infiltration electrode locations. All of the other dipole-dipole post- infiltration resistivity measurements were also

conducted over the same survey lines as the pre-infiltration measurements.

Tables 4 through 8 present a comparison between pseudosection resistivity measurements and soil moisture readings collected at the same locations. The dipole-dipole measurements used to construct the pseudosections were centered directly over boreholes which contained neutron access tubes. As a result, the center vertical column of data within each pseudosection corresponds to points within the earth in which the moisture content was measured (Parsons, 1988). As illustrated in Figure 1, borehole location 15-15 corresponds to the center of the a-a' pseudosection. In addition, borehole locations 11-15, 19-15, 15-19, and 15-11 (Figures 3 to 7) correspond to the center vertical columns in pseudosections b-b', c-c', d-d', and e-e', respectively. Only borehole 15-15 was installed and sampled deep enough in the infiltration area to supply a complete vertical lithologic profile of the infiltration area. Consequently, this is the only location where a complete pre- and post-infiltration resistivity and soil moisture profile can be compared to lithology.

Tables 4 through 8 represent the center vertical columns of resistivity measurements as well as percent moisture content by volume of rock and percent saturation at particular depths. The resistivity measurements and their standard deviations are presented in alternating rows of two and three measurements. Given the geometric configuration of dipole-dipole pseudosections used in this study, a resistivity measurement directly in line with the centrally located neutron access tubes was not available for every depth (see Figure 12). For example,

in the a-a' pseudosection, a resistivity measurement directly in line with borehole 15-15 was only available at the n equals 2, 4, 6, 8, 10, and 12 electrode spacings. As can be seen in Table 4, these depths are represented by three resistivity values, the center value corresponding approximately to the neutron tube location and the two values adjacent to the center column being supplied to better illustrate resistivity values at these depths. The n equals 1, 3, 5, 7, 9, and 11 electrode spacings are only represented by two values. These depths did not have a resistivity reading directly in line with the borehole. Consequently, these two values represent resistivity readings directly adjacent to borehole 15-15.

The depths corresponding to each horizontal row of resistivity in Tables 4 through 8 were calculated using the analytical formula for resistivity depth of investigation derived by Roy and Apparao (1971). For example, with a dipole-dipole separation (as defined by Roy and Apparao, see Figure 12) of 20 feet (the $n = 1$ line of data in each pseudosection) the depth of investigation, using the Roy and Apparao (1971) technique is approximately 20% of the dipole separation or 4 feet. Thus, the percent moisture content by volume of rock at the 4 foot depth is compared with the n equals 1, or 20 foot, dipole-dipole electrode separation directly over the neutron measuring point.

Percent moisture in Tables 4 through 8 is presented in two forms: percent moisture content by volume of rock and percent saturation. To calculate this latter value, an average porosity of 43.4% (standard deviation 6.23%, 68 samples tested) was used for the sediments from ground surface to 12 feet below the surface (Piedmont Slope facies) and

a porosity of 36% (standard deviation 4.53%, 21 samples tested) was used for the sediments from 12 feet below surface to about 27 feet below ground surface (Fluvial Sand facies). These average porosities, taken from Parsons (1988), are useful when considering the effect of saturation.

VII. DISCUSSION

A. VES Interpretation

Two Wenner vertical electrical soundings (Figures 13 and 14), and five dipole-dipole vertical electrical soundings (Figures 17 to 21) were conducted at the study site. Inspection of these curves reveals two distinct characteristics: the undulatory shape of all the VES field curves and the sharp maxima/minima (singularities) evident in the dipole-dipole curves. The undulating nature of the VES curves indicates heterogeneity beneath the study site. The sharp maximum or minimum points can be indicative of a buried resistive or conductive layer of limited lateral extent (Zohdy et al., 1974). As can be seen in Figures 15 and 16, the Zohdy inversions of the field data clearly indicate a multilayered geoelectric section. It should be noted; however, that the inverted curves poorly fit the field data.

A comparison of the Zohdy inversion of the pre-infiltration Wenner resistivity data centered at 15-15 with the 15-15 borehole geologic log (Figures 3 and 15) shows only a poor correlation. Most significantly, the Zohdy inversion lumped a 13 foot section (the 8 to 21 foot depth interval from ground surface) containing an alternating sequence of cobbles and sand with pebbles into a single geoelectric unit. If this sounding had been conducted solely to find the location of the water table, a resolution of this magnitude would be acceptable. However, for a study involved in monitoring the migration of an infiltration profile, lumping a sequence of layers into one unit is not satisfactory.

The post-infiltration Wenner VES centered at 15-11 (Figure 14) shows a different kind of complexity in curve shape than does the Wenner sounding centered at 15-15 (Figure 13). This difference may be the result of the infiltration profile not being horizontally continuous in a geoelectric sense, which violates the assumption of lateral homogeneity necessary in VES inversions. As before, the poor inverted fit coupled with the complexity of the inverted curve does not lend itself to a useful interpretation of moisture migration in the vadose zone. On the whole, resistivity is lower in this post-infiltration profile (Figure 16).

Since the dipole-dipole configuration is oriented differently from the Wenner array, similar looking VES field curves would not be expected. All of the dipole-dipole field curves (Figures 17 to 21), generated from the a-a' pre-infiltration pseudosection show the same general characteristic complexity as do the Wenner field data. However, the dipole-dipole curves do have a common feature: all 5 dipole-dipole curves exhibit a number of sharp maxima and minima (singularities) over a much smaller range of electrode spacings than the Wenner field curves. This difference probably stems from two factors: a greater depth of investigation (Roy and Apparao, 1971) and a greater sensitivity to lateral inhomogeneities (Keller, 1966) that characterize the dipole-dipole array. The south-north oriented geologic cross section presented in Figure 8 illustrates the lateral inhomogeneities found in the infiltration area. Specifically, within the 20 to 25 foot depth interval a silt-clay layer is interrupted directly under the infiltration area by an interval of fine to coarse sand. This

particular sequence has undoubtedly affected the dipole-dipole field data. Therefore, the complexity found in the dipole-dipole vertical electrical soundings stems from combined effects of lateral inhomogeneities and of a texture of stacked lenses, both of which are illustrated in Figures 8 and 9. Curve matching using theoretical curves derived by Elliot (1974) was not possible due to the complexity of the field data. It should be noted that Al'pin et al. (1966) did derive similar looking theoretical dipole-dipole curves for laterally inhomogeneous earths.

B. Horizontal Profile Interpretation

Two post-infiltration Wenner horizontal resistivity profiles were conducted along the a'-a south-north center line of the study area. The most interesting feature in both of these horizontal surveys is the two resistivity troughs illustrated in each graph (Figures 22 and 23). The northernmost of these troughs in both figures correspond approximately to the location of the infiltration area (Figure 24). Given the increased soil moisture content in this area due to induced infiltration, lower apparent resistivity values are not surprising. However, the low values of resistivity evident in the southern portions of both horizontal profiles can not be attributed to the infiltration area. These resistivity measurements were not collected directly over the infiltration area. Therefore, it would not be expected that the infiltration area would greatly affect these resistivity measurements. Rather, the low readings indicate an interval of low resistivity just south of the infiltration area. Both these horizontal profiles further illustrate the lack of lateral homogeneity found at the study area.

C. Dipole-Dipole Pseudosections

1. Pseudosection Modeling

Without a simplified horizontal geoelectrical model for either the pre- or post-infiltration portion of the experiment, the weight of resistivity modeling was placed on the Dey and Morrison (1979a) integrated finite-difference inversion technique. Because a complete lithologic column was available for the geometric center of the infiltration area (Figure 3), the a-a' center line (Figure 26) was the focus of the modeling effort. Unfortunately, the previously discussed factors of dipole-dipole sensitivity to lateral inhomogeneities, coupled with the inability of two-dimensional pseudosection modeling to account for heterogeneities in a direction normal to the section, combined to frustrate this effort.

During the numerical modeling of the a-a' dipole-dipole pseudosection over 75 different capacitance matrices were utilized in an attempt to simulate the field data. Table 3 is the "best fit" model found among these inversions. Although the fit is reasonable, it is highly complex and is not unique. Thus, there are no pseudosection inversions with which the author feels confident enough to use in a quantitative analysis.

2. Moisture Content vs Dipole-Dipole Pseudosections

Despite the lack of a good numerical inversion of the dipole-dipole pseudosection data, a comparison can be made between portions of the pseudosections and soil moisture information presented in Parsons (1988). These comparisons are illustrated in Tables 4 to 8.

Three general observations are apparent on review of the information presented in these tables. In the 4 to 6 foot depth interval, which will be referred to as the upper zone of the pseudosection, a slight increase in resistivity values is evident between the pre- and post-infiltration resistivity measurements. Further, in the 8 to 12 foot depth interval or middle zone of the pseudosections, a subtle but consistent drop in resistivity can be observed between the pre- and post-infiltration resistivity measurements. Finally, the 14 to 26 foot depth interval, which will be referred to as the lower zone of the pseudosection, exhibits a confusing picture of increasing and decreasing resistivity values where no clear trend is apparent.

a. Upper Zone

In Tables 4, 5, and 6 the pseudosection resistivity measurements show a slight rise in value between pre- and post infiltration. This subtle increase can be attributed to three factors: the construction at the site necessary to place the infiltration piping, the probable increase in pore water resistivity as a result of months of infiltration, and the almost static moisture content observed between the pre- and post-infiltration measurements in the upper zone. A second-order effect on post-infiltration resistivity measurements may have been their minor relocation.

With respect to the construction problem, much activity was necessary to place the plastic sheets, hay, and piping used to both reduce evapotranspiration and introduce water into the system. Thus, it is possible that the construction activity changed some of the

electrical properties of the soil in the upper (0-6 foot depth) zone of the site. Additionally, since the construction tended to remove the location markers used during the first phase of resistivity measurements, it is possible, for the measurements directly over the infiltration area, that the post-infiltration readings may have been offset up to one foot from the previous pre-infiltration locations. Both of these factors, the first-order changes in resistivity due to site construction and the second-order changes as a result of measurement relocations, become less of a problem with depth.

Given the over 5 months of infiltration between the pre- and post-infiltration resistivity measurements, it is not unreasonable to assume a change in pore water resistivity between these readings. In this case it would appear that the infiltration acted as a flushing mechanism, moving electrolytic salts to lower zones of the profile. This would result in a rise of recorded resistivity in the flushed zone of the profile. Thus, the subtle increases in this zone of the pseudosection can, in part, be attributed to a chemical factor.

The static moisture content in the upper zone of the profile can be considered a factor in that it probably did not play a major role in controlling resistivity changes between the pre- and post-infiltration event. Interestingly, at borehole 11-15 (Table 5) and borehole 19-15 (Table 6), the percent soil moisture was slightly reduced; however, these changes were so small that they did not counteract the increase in resistivity in the middle zone.

b. Middle Zone

The middle zone, or the 8 to 12 foot depth interval, exhibits a drop in resistivity between pre- and post-infiltration measurements in all the pseudosections. A contributing factor to this change is probably the great increase in moisture content. This is particularly evident in the a-a' pseudosection (Table 4). Pre-infiltration saturations were generally below 20% for the middle zone of the profile. Saturations this low will not result in much capillary water interconnection between pores. After 5 months of infiltration, the saturation had increased to over 30%. Consequently, it is not unlikely that capillary interconnection of pore water in this zone of the profile is prevalent. Thus, the subtle drop in resistivity values in this zone of the profiles can primarily be attributed to soil moisture increases.

Another contributing factor to the decrease in post-infiltration resistivity values, may be an increase in pore water conductivity. As a result of electrolytic salts being flushed out of the upper zone, salt concentrations in the middle zone pore water may have increased. These salts would lower the pore water resistivity which would result in lower post-infiltration resistivity values.

c. Lower Zone

Table 4 illustrates the relationship between moisture content and resistivity in the 14 to 26 foot depth interval (lower zone of the pseudosection). Unfortunately, the other boreholes in which neutron access tubes were placed are not deep enough to yield soil moisture data at these depths. Thus, location 15-15 (Figure 1), at the center of the

a-a' pseudosection, is the only boring with which a comparison between deep soil moisture readings and resistivity measurements can be made.

The most striking feature of the 14 to 26 foot depth interval was the difference between pre- and post-infiltration soil moisture readings. Before infiltration, with less than 20% of the pore space filled with water, high resistivity values were measured. This is not surprising since the tortuosity of the current paths would likely be great due to the lack of capillary wedge water interconnection. However, by the time the second set of resistivity measurements were taken, saturation ranged from 25 to 39%. If saturation was the only factor, these values would cause resistivity to decrease as the current found more direct paths through the pores. Inspection of the results presented in Table 4 does not bear this out. The underlying assumption here is that an average porosity is applicable within this depth interval. However, inspection of Figures 8 and 9 (geologic cross sections) reveals that the lithology within this depth interval ranges from medium sand to coarse sand and gravel. Consequently, the use of an average porosity in this zone of the profile may be inappropriate.

A better way to analyze this interesting variability in resistivity could be to evaluate the spatial changes in pore water resistivity in relation to physical processes occurring within the pores. As previously discussed, infiltration will flush salts through the soil profile. As these salts are flushed through the system, their concentration fronts may not be uniform. Frequently, these non-uniform fronts are a result of localized heterogeneities in the porous medium that can stimulate or inhibit unsaturated flow.

In unsaturated conditions, it often happens that flow is impeded as water moves from a finer grained to coarser grained material. The occurrence of a layer of coarse sand or gravel in a finer-textured profile, may actually impede unsaturated water movement until water accumulates above the sand or gravel and suction decreases sufficiently for water to enter the larger pores (Hillel, 1980b). This phenomenon must surely be occurring at the study site since lenses of fine and coarse grained materials interfinger throughout the infiltration area. Differential flow paths result in differential concentration fronts of electrolytic salts. The lack of any trends evident in the post-infiltration resistivity measurements for the lower zone may be a direct result of the variability in pore water resistivity.

3. Qualitative Analysis

Up to this point the discussion has focused on the problems associated with a quantitative analysis of this research. The results of this study will now be analyzed in a qualitative manner. To facilitate this qualitative analysis, the dipole-dipole resistivity measurements will be presented in a grouped interval format.

Figures 26 to 35 are the pre- and post-infiltration pseudosections for the five lines of dipole-dipole resistivity measurements in this study. The data in these figures have been grouped into six intervals: less than 200 ohm ft, 201-400 ohm ft, 401-600 ohm ft, 601-800 ohm ft, 801-1000 ohm ft, and greater than 1000 ohm ft (Figure 25). This grouping was designed in an effort to smooth the data so that qualitative changes within the two sets of data (pre- and post-infiltration) could be recognized. Since the highest pre- and post-

infiltration resistivity contrast was on the order of 200 ohm ft, this number was chosen as a suitable size for the intervals.

The d-d' (north boundary) and e-e' (south boundary) pseudosections, both of which were conducted from west to east, illustrate the Kean et al. (1987) assertion that "near-surface moisture changes can be defined by resistivity". The most significant contrast between these two sets of resistivity measurements occurs within their first 3 horizontal lines. Within these readings, a distinct reduction in resistivity is apparent between the pre- and post-infiltration resistivity measurements. A reduction in resistivity is also apparent deeper in the pseudosection (especially d-d'), particularly in the west side of the section. The deepest portion of these pseudosections (horizontal lines 7 and greater) did not exhibit a significant change in resistivity during the study.

When considering qualitative contrasts for the north-south oriented pseudosections (east boundary, c-c'; west boundary, b-b'; and center line, a-a') the a-a' pseudosection exhibits a clear contrast between pre- and post-infiltration resistivity measurements. This is particularly true in the middle portion of this section where a significant reduction in resistivity has occurred. The contrasts become less distinct deeper within the section.

For the c-c' and b-b' pseudosections, no distinct trends between resistivity measurements are apparent, although a general reduction in values can be inferred from the data. Interestingly, for the b-b' pseudosection, the qualitative groupings indicate a rise in values between pre- and post-infiltration resistivity measurements in the first 3 horizontal lines.

VIII. CONCLUSIONS

The purpose of this study was to apply earth resistivity techniques in the monitoring of water infiltration in the vadose zone. Because the terrain is so very heterogeneous, a quantitative relationship between moisture content and resistivity could not be developed. Thus, several conclusions have been reached concerning this work.

The study area exhibits strong lateral inhomogeneity in three dimensions. These inhomogeneities interfere with the numerical modeling of resistivity pseudosections. Specifically, although lateral inhomogeneities along the survey line can be modeled, they can not be accounted for if they also exist perpendicular to the survey line.

Electrical resistivity measurements in the vadose zone must be considered in relation to saturation and pore water resistivity. Each of these factors is capable of changing independently, resulting at times in contrasting effects on resistivity. In this study, both of these elements have combined to cloud a quantitative comparison between pre- and post-infiltration resistivity measurements.

Construction over the infiltration area and small changes in the location of pre- and post-infiltration resistivity measurements appear to have adversely affected the shallower dipole-dipole readings in the pseudosections. Although these effects can be filtered out through grouping the data into intervals, they do not readily permit a comparison between pre- and post-infiltration resistivity measurements.

These problems became less of a factor as the dipole-dipole electrode spacings were increased.

Despite the problems encountered in this study, qualitative decreases in resistivity could be correlated with increases in moisture content in the shallower dipole-dipole resistivity measurements. However, for the deeper resistivity measurements in the pseudosections, no correlation between pre- and post-infiltration resistivity measurements was apparent. Because of this qualitative result, it is felt that in the absence of the problems encountered here, an empirical relationship between moisture content in the vadose zone and resistivity measurements may be possible for shallow resistivity measurements in the vadose zone.

IX. RECOMMENDATIONS

As previously addressed in this paper, a number of factors in this study have worked to confuse the results and make a quantitative analysis impossible. Hindsight has supplied this author with several ideas that may alleviate some of the problems encountered and permit a simpler, as well as more revealing picture of soil water infiltration monitoring by resistivity.

As can be seen in the preceding sections, because of the complexity of interpreting resistivity measurements in a partially saturated media, picking a study site that can be accurately modeled using resistivity techniques as a three- and four-layered earth would be beneficial. Such a study site would permit the development of a good pre-infiltration resistivity model which could then be compared with post-infiltration resistivity measurements and model. These two models could be compared with soil moisture information to determine the relationship between moisture content and resistivity in the vadose zone.

An important aspect in electrical resistivity surveys is the effect of observational and instrumental errors on the observed readings. These type of errors often inhibit the development of resistivity models of the earth. Two significant papers dealing with both observational and instrumental errors in relation to a Wenner electrical resistivity survey are Carpenter and Habberjam (1956) and Habberjam and Watkins (1967). Their special technique, which in addition to addressing these errors also quantifies lateral

inhomogeneities, is termed a "tri-potential method of resistivity prospecting".

In the "tri-potential method" the Wenner array is split into three configurations. The standard Wenner array, $C_1P_1P_2C_2$, is defined as α , while β is defined as $C_1C_2P_1P_2$, and γ is oriented $C_1P_1C_2P_2$ (where C is a current electrode and P represents a potential electrode).

Given that the distance between any two adjoining electrodes is equal (the traditional Wenner electrode spacing), we have the relationship

$$R_{\alpha}(a) = R_{\beta}(a) + R_{\gamma}(a)$$

where R are the measured resistances. Although slight departures from the above equation are to be expected, any significant deviations can be attributed either to instrumental or observational errors.

Observational errors are those errors that can be attributed to deviations from the common assumptions used in electrical resistivity surveying (no sources or sinks, lateral homogeneity, etc.). For example, if we take the $R_{\alpha}(a)$ reading, we can define the error as

$$R_{\alpha}(a) - R_{\beta}(a) - R_{\gamma}(a) = \epsilon$$

and correct the reading by

$$\bar{R}_{\alpha}(a) = R_{\alpha}(a) - \epsilon \left[R_{\alpha}(a) / (R_{\alpha}(a) + R_{\beta}(a) + R_{\gamma}(a)) \right].$$

Even more intriguing is the use by Habberjam and Watkins (1967) of a Lateral Inhomogeneity Index (L.I.I.). Briefly, it is necessary to take progressive readings at $2^n a$ and $3 \cdot 2^n a$ electrode spacings, where n is an increasing integer (i.e. $n=1,2,3\dots$) These readings can be used by the researcher to construct a "Ladder Network" in which lateral inhomogeneities in the readings can be singled out and corrected.

Given the complex pre-infiltration resistivity inversions encountered in this study, the "tri-potential method" of geophysical surveying appears to be a good technique to help select an area for a resistivity-based vadose zone infiltration study. Ideally, when geophysically possible, it should be applied by means of two Wenner VES surveys, centered at the same location, but whose axes are perpendicular. In this way, lateral information is gathered in four different directions. Thus, a site with a low LII, that could realistically be interpreted as a three- or four-layered earth, would provide a good basis from which later (post-infiltration) readings could be interpreted.

The most obvious remedy afforded by a study area with a low LII would be the absence of lithologic lateral effects on pre-infiltration resistivity measurements. With minimal lateral inhomogeneities present at a resistivity surveying site, both VES and pseudosection inversion techniques become easier to apply and interpret. Furthermore, the simplified VES model (three- or four-layered earth) can be used to construct the conductivity matrix used in the pre-infiltration pseudosection inversion.

Procedurally, once a good site is found, a simplified VES model could be produced by curve fitting with theoretical sets of published type curves (e.g. Mooney and Wetzel, 1956; or Elliot, 1974). Additionally, for three- or four-layered earth models not found with these sets of type curves, VES inversion techniques developed by Zohdy (1975) or Petrick et al., (1977) could be used. This initial interpretation, using the restrictive assumption of lateral homogeneity, is critical since this model will be used as the basis for the capacitance matrix of electrical conductivity values used in the numerical interpretations of the pre-infiltration dipole-dipole pseudosections. The pre-infiltration conductivity matrix is important because it is used as the basis from which the changes in the post-infiltration conductivity matrix are interpreted.

It is recognized, however, that because of the nonuniqueness principle, the "absence of lateral resistivity changes is not proven if a depth sounding curve matches with a calculated curve that is derived from a horizontal layer model," (Frohlich et al., 1988). Thus, it is probably prudent to apply an independent technique to verify the accuracy of the earth model derived from resistivity. Such techniques as electro-magnetic surveys using Geonics EM31 and EM33 induction equipment could help check the accuracy of the working model.

Once a good layered-earth model has been verified, the dipole-dipole pseudosections should be concentrated along the two perpendicular Wenner VES lines. In this way, the initial Wenner surveys can be used to fortify the pseudosection modeling. In addition, the vertical lines of the pseudosection, which can be considered dipole-dipole VES curves,

can also be utilized to check the Wenner VES modeling results as well as to construct the conductivity matrix used in the pseudosection inversion models.

Several complete pseudosections should be conducted, in a short time interval, along the two perpendicular lines. Consequently, the equipment as well as measuring and recording techniques used by Kean et al. (1987) appear most appropriate. A difficulty encountered in this study was the time-consuming and laborious process of resistivity surveying. Kean et al. (1987) used equipment that, after initial setup and measurement, could be kept in place for the duration of the study. The use of a central circuit board and data logger was significant in that it cut down on electrode movement. Obviously, not all resistivity equipment can be utilized in this fashion and it is recognized that even with instruments capable of this application, a proper resistivity survey is a laborious exercise. However, the need for numerous resistivity measurements can be the motivating force behind innovative measuring techniques and devices.

An important factor in pseudosection modeling is the choice of the dipole spacing in the dipole-dipole configuration (Figure 3). Optimally, this distance should be chosen to get the maximum amount of pseudosection grid points within the area of interest. Logically, the more points within the study area the greater is the chance of detecting the moisture front as it moves through the system. Additionally, numerous points along a vertical line in a pseudosection enable clearer dipole-dipole VES curves to be constructed. Since these curves are used as both a supplement and a verification for the conductivity matrix used

during the finite-difference modeling of the pseudosection, it is important that they be properly defined.

On the other hand, a finely meshed grid can cause problems in the numerical modeling of the system in question. As seen in this study, when the earth shows a large degree of electrical heterogeneity, the capacitance matrix used in the numerical simulation of the field data becomes complex. This problem manifests itself when a finely meshed pseudosection grid is used, since a dense grid will require a more complex conductivity matrix than a less dense grid. Thus, conflicting requirements exist with respect to the numerical modeling of resistivity pseudosections. On the one hand, the researcher must strive to maximize the number of points in the pseudosection; however, the denser the pseudosection grid, the harder it is to model the system numerically.

With these conflicting requirements in mind, the electrode spacing in the dipole-dipole configuration should be chosen such that the $n=6$ spacings penetrate the deepest zone of interest in the study area. The $n=6$ spacing is recommended by Edwards (1977) as the maximum spacing for a dipole-dipole pseudosection. The actual decision regarding the electrode spacing can be aided with the Roy and Apparao (1971) method of determining depth of investigation. They found, for a dipole-dipole array, that the depth of investigation is approximately 20% of the dipole separation. For example, in a study area with a water table at 30 feet, a pseudosection of $n=1$ through $n=6$ could be constructed with an electrode spacing of 20 feet. This would result in approximate depths of investigation of 8, 12, 16, 20, 24, and 28 feet for $n=1$ through 6, respectively.

Although the $n=1$ through 6 dipole-dipole measurements will be the only ones modeled numerically, deeper readings can be taken. With an adequate power supply - dipole-dipole has a large power requirement (Keller, 1966) - additional pseudosection measurements, from $n=7$ onward, can be taken until the signal becomes too weak to take accurate readings. These additional points can be used to construct the dipole-dipole VES curves. In this way, the researcher has a properly sized pseudosection (Edwards, 1977) and ample vertical readings to properly construct dipole-dipole VES curves.

X. REFERENCES

- Al'pin, L. M., M. S. Berdicherskii, G. A. Veclrintsev, and A. M. Zagarmistr, 1966. Dipole Methods for Measuring Earth Conductivity: Consultants Bureau, New York (Selected and translated from Russian by G. V. Keller).
- Anderholm, S. K., 1983. Hydrogeology of the Socorro and La Jencia Basins, Socorro County, New Mexico: New Mexico Geological Society Guidebook, 34th Field Conference, Socorro Region II, pp. 303-311.
- Archie, G. E., 1942. The Electrical Resistivity Log as an Aid in Determining Some Reservoir Characteristics. Trans. AIME, v.146, pp. 54-62.
- Barker, R. D. and P. F. Worthington, 1973. Some Hydrogeophysical Properties of the Banter Sandstone of Northwest England, Geoexploration, v.11, pp. 151-170.
- Chamberlin, R. M., 1980. Cenozoic stratigraphy and structure of the Socorro Peak volcanic center New Mexico: New Mexico Bureau of Mines and Mineral Resources Open-file Report 118. 2 vol.
- Carpenter, E. W., and G. M. Habberjam, 1956. A tri-potential method of resistivity prospecting: Geophysics, v.21, No.2, pp. 455-469.
- Dey, A., and H. F. Morrison, 1976. Resistivity modeling for arbitrarily shaped two-dimensional structures, Part II, Computer Program, Lawrence Berkeley Laboratory, University of California, Berkeley.
- Dey, A., and H. F. Morrison, 1979a. Resistivity modeling for arbitrarily shaped two-dimensional structures: Geophysical Prospecting, v.27, No. 1, pp. 106-136.
- Dey, A., and H. F. Morrison, 1979b. Resistivity modeling for arbitrarily shaped three-dimensional structures: Geophysics, V.44, No. 4, pp. 753-780.
- Edwards, L. S., 1977. A modified pseudosection for resistivity and IP: Geophysics, v.42 No. 5, pp. 1020-1036.
- Elliot, C., 1974 Theoretical Response of Three-Layered Earth. vol. 5, Dipole-Dipole Response. Elliot Geophysical Company, Mining Geophysical Engineers, Tuscon, Arizona.
- Frohlich, R. K., 1968. The influence of lateral inhomogeneities on the dipole methods: Geophysical Prospecting, v.16, No. 3, pp. 314-325.

- Frohlich, R. K., C. D. Parker, and W. F. Kelly, 1988. Discussion of "Monitoring Moisture Migration in the Vadose Zone with Resistivity" by Kean et al. (1987). Ground Water, v.26, No.3, pp. 361-363.
- Ghosh, D. P., 1971. Inverse filter coefficients for the computation of apparent resistivity standard curves for a horizontally stratified earth: Geophysical Prospecting, v.19 No.4, pp. 769-775.
- Habberjam, G. M., and G. E. Watkins, 1967. The reduction of lateral effects in resistivity probing: Geophysical Prospecting, v.15, No. 2, pp. 221-235.
- Hillel, D., 1980a. Applications of Soil Physics. Academic Press Inc., New York, 385p.
- Hillel, D., 1980b. Fundamentals of Soil Physics. Academic Press, Inc., New York, 413p.
- Hillel, D., V. D. Krentos, and Y. Stylianou, 1972. Procedure and test of an internal drainage method for measuring soil hydraulic characteristics in situ: Soil Science, v. 114, pp. 395-400.
- Kean, F. K., M. J. Waller, and H. R. Layson, 1987. Monitoring moisture migration in the vadose zone with resistivity: Ground Water, v.25, No. 5, pp. 562-571.
- Keller, G. V., 1966. Dipole method for deep resistivity studies: Geophysics, v.31, No. 6, pp. 1088-1104.
- Koefoed, O., 1970. A fast method for determining the layer distribution from the raised kernel function in geophysical sounding: Geophysical Prospecting, v.18, pp. 564-570.
- Machette, M. N., 1978. Geological map of the San Acacia quadrangle, Socorro County, New Mexico: U. S. Geological Survey Quadrangle Map GQ-1415, 1:24000.
- Matson, E., 1989. Independent Study, Hydrology Program, New Mexico Institute of Mining and Technology, Socorro, New Mexico.
- Mooney, H. M. and W. W. Wetzel, 1956. The Potentials About a Point Electrode and Apparent Resistivity Curves for a Two-, Three-, and Four-Layered Earth: Minneapolis, Univ. of Minnesota Press, 146p., and 243 loose sheets of reference curves.
- Parsons, A., 1988. Independent Study, Hydrology Program, New Mexico Institute of Mining and Technology, Socorro, New Mexico.
- Petrick, W. R., W. H. Pelton, and S. H. Ward, 1977. Ridge Regression Inversion Applied to Crustal Resistivity Sounding Data from South Africa, Geophysics, v.42, pp. 995-1005.

- Roy, A., and A. Apparao, 1971. Depth of investigation in direct current methods: Geophysics, v.36, No. 5, pp. 943-959.
- Sunde, E. D., 1949. Earth Conduction Effects in Transmission Systems: Van Nostrand, New York, 370p.
- Telford, W. M., L. P. Geldart, R. E. Sheriff, and D. A. Keys, 1976. Applied Geophysics: Cambridge University Press, Cambridge, 860p.
- Urish, D. W., 1981. Electrical resistivity-hydraulic conductivity relationships in glacial outwash aquifers. Water Resources Research, v.17, No.5, pp.1401-1408.
- Watson, K. K. 1966. An instantaneous profile method for determining the hydraulic conductivity of unsaturated porous materials: Water Resources Research, v. 2, pp. 709-715.
- Zohdy, A. A. R., 1975. Automatic interpretation of Schlumberger sounding curves using modified Dar Zarrouk functions. U.S. Geological Survey Bulletin, 1313-E.
- Zohdy, A. A. R., and R. J. Bisdorf, 1975. Computer programs for the forward calculation and automatic inversion of Wenner sounding curves: National Technical Information Service, U.S. Dept. of Commerce, Report No. PB-247-265.
- Zohdy, A. A. R., G. P. Eaton, and D. R. Mabey, 1974. Application of surface geophysics to ground-water investigations. Techniques of Water-Resources Investigations of the United States Geological Survey. Book 2, Chapter D1, 116p.

XI. FIGURES

- Figure 1. Map of the Study Area.
- Figure 2. Lithologic Legend.
- Figure 3. Borehole Geologic Log Located at 15-15.
- Figure 4. Borehole Geologic Log Located at 11-15.
- Figure 5. Borehole Geologic Log Located at 19-15.
- Figure 6. Borehole Geologic Log Located at 15-19.
- Figure 7. Borehole Geologic Log Located at 15-11.
- Figure 8. Geologic Cross Section (South-North) of the Infiltration study area.
- Figure 9. Geologic Cross Section (West-East) of the infiltration study area.
- Figure 10. Water in an Unsaturated Coarse-Textured Soil.
- Figure 11. Wenner Electrode Configuration.
- Figure 12. Dipole-dipole Electrode Configuration and Pseudosection Format.
- Figure 13. Pre-infiltration Wenner Vertical Electrical Sounding Centered at 15-15.
- Figure 14. Post-infiltration Wenner Vertical Electrical Sounding Centered at 15-11.
- Figure 15. Geoelectric Section from Zohdy Inversion of Wenner VES Centered at 15-15.
- Figure 16. Geoelectric Section from Zohdy Inversion of Wenner VES Centerd at 15-11.
- Figure 17. Dipole-dipole VES Derived from the a-a' line, North-South Center Line.
- Figure 18. Dipole-dipole VES Derived from the a-a' line, North-South Center Line.
- Figure 19. Dipole-dipole VES Derived from the a-a' line, North-Souther Center Line.

- Figure 20. Dipole-dipole VES Derived from the a-a' line, North-South Center Line.
- Figure 21. Dipole-dipole VES Derived from the a-a' line, North-South Center Line.
- Figure 22. Post-infiltration Wenner Horizontal Resistivity Profile (Electrode Spacing = 30 feet).
- Figure 23. Post-infiltration Wenner Horizontal Resistivity Profile (Electrode Spacing = 50 feet).
- Figure 24. Map of the Study Area.
- Figure 25. Pseudosection Resistivity Legend.
- Figure 26. Pre-infiltration Pseudosection Conducted Along a-a' North-South Center Line.
- Figure 27. Post-infiltration Pseudosection Conducted Along a-a' North-South Center Line.
- Figure 28. Pre-infiltration Pseudosection Conducted Along b-b' Western Boundary of the Infiltration Area.
- Figure 29. Post-infiltration Pseudosection Conducted along b-b' Western Boundary of the Infiltration Area.
- Figure 30. Pre-infiltration Pseudosection Conducted Along c-c' Eastern Boundary of the Infiltration Area.
- Figure 31. Post-infiltration Pseudosection Conducted Along c-c' Eastern Boundary of the Infiltration Area.
- Figure 32. Pre-infiltration Pseudosection Conducted Along d-d' Northern Boundary of the Infiltration Area.
- Figure 33. Post-infiltration Pseudosection Conducted along d-d' Northern Boundary of the Infiltration Area.
- Figure 34. Pre-infiltration Pseudosection Conducted Along e-e' Southern Boundary of the Infiltration Area.
- Figure 35. Post-infiltration Pseudosection Conducted Along e-e' Southern Boundary of the Infiltration Area.

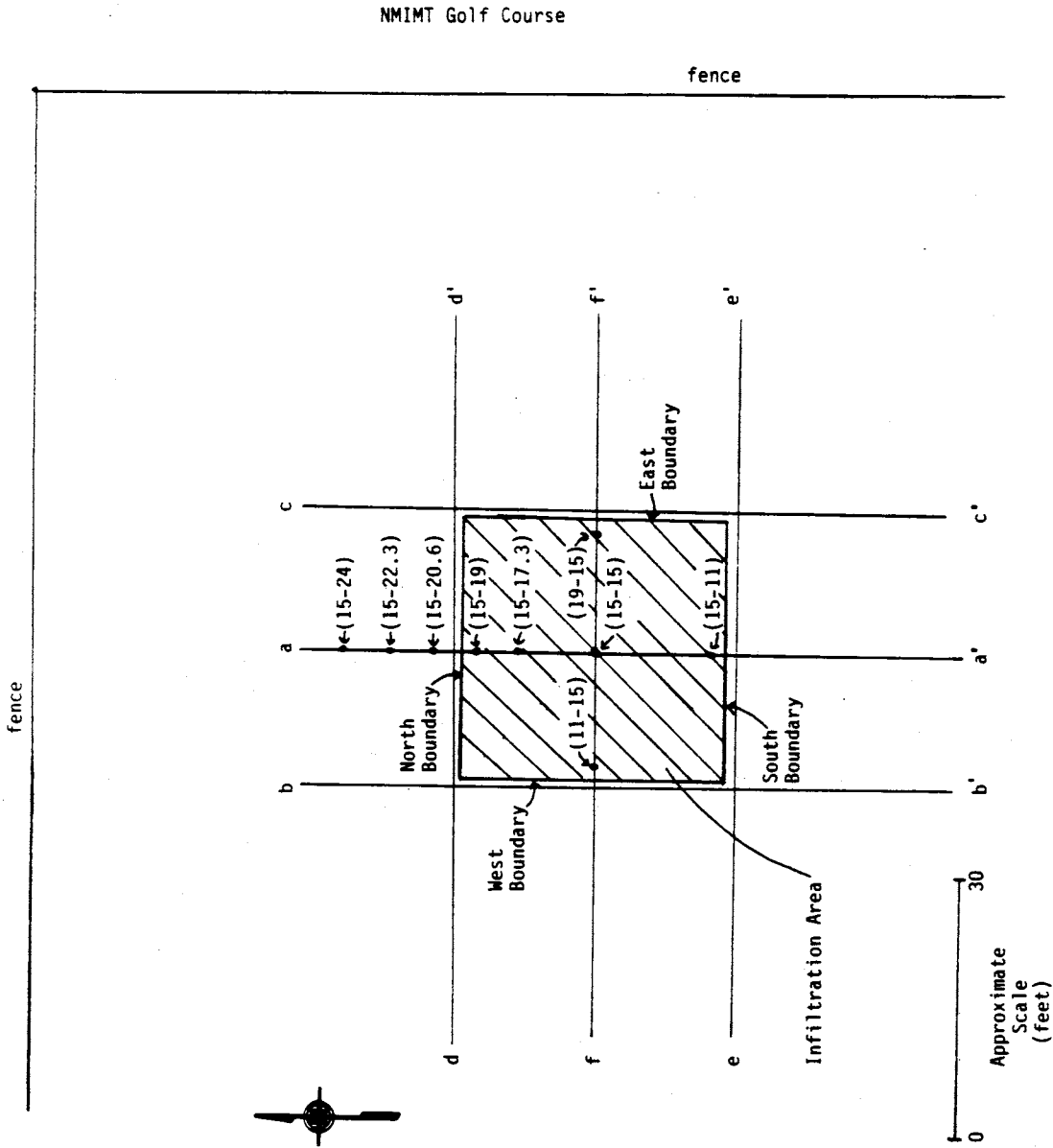


Figure 1 Map of the study area. Point locations on map are defined using the same system as Parsons (1988). Points 15-15, 11-15, 19-15, 15-19, and 15-11 are locations of boreholes illustrated in Figures 3, 4, 5, 6, and 7, respectively. Points 15-17.3, 15-19, 15-20.6, 15-22.3, and 15-24 are the center locations of dipole-dipole vertical electrical soundings illustrated in Figures 17, 18, 19, 20, and 21, respectively. Lines a - a' through e - e' represent orientations of resistivity pseudosections illustrated in Figures 26 through 35. Lines a' - a and f - f' represent orientations of geologic cross sections illustrated in Figures 8 and 9, respectively.

LITHOLOGIC LEGEND


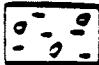










	Fine Sand, Silt
	Fine Sand, Silt, Pebbles
	Fine-Medium Sand, Silt
	Fine-Coarse Sand, Silt
	Fine-Coarse Sand, Silt, Pebbles
	Fine Sand
	Fine-Medium Sand
	Fine-Coarse Sand
	Fine-Coarse Sand, Pebbles
	Clay, Silt
	Clay, Silt, Fine Sand
	Cobbles

Figure 2 Legend of lithologic symbols for Figures 3 to 9 (adapted from Parsons (1988)).

BOREHOLE GEOLOGIC LOG

LOCATION: 15-15
 DATUM EL: 4650.65 feet
 GND SURFACE EL: 4647.83 feet

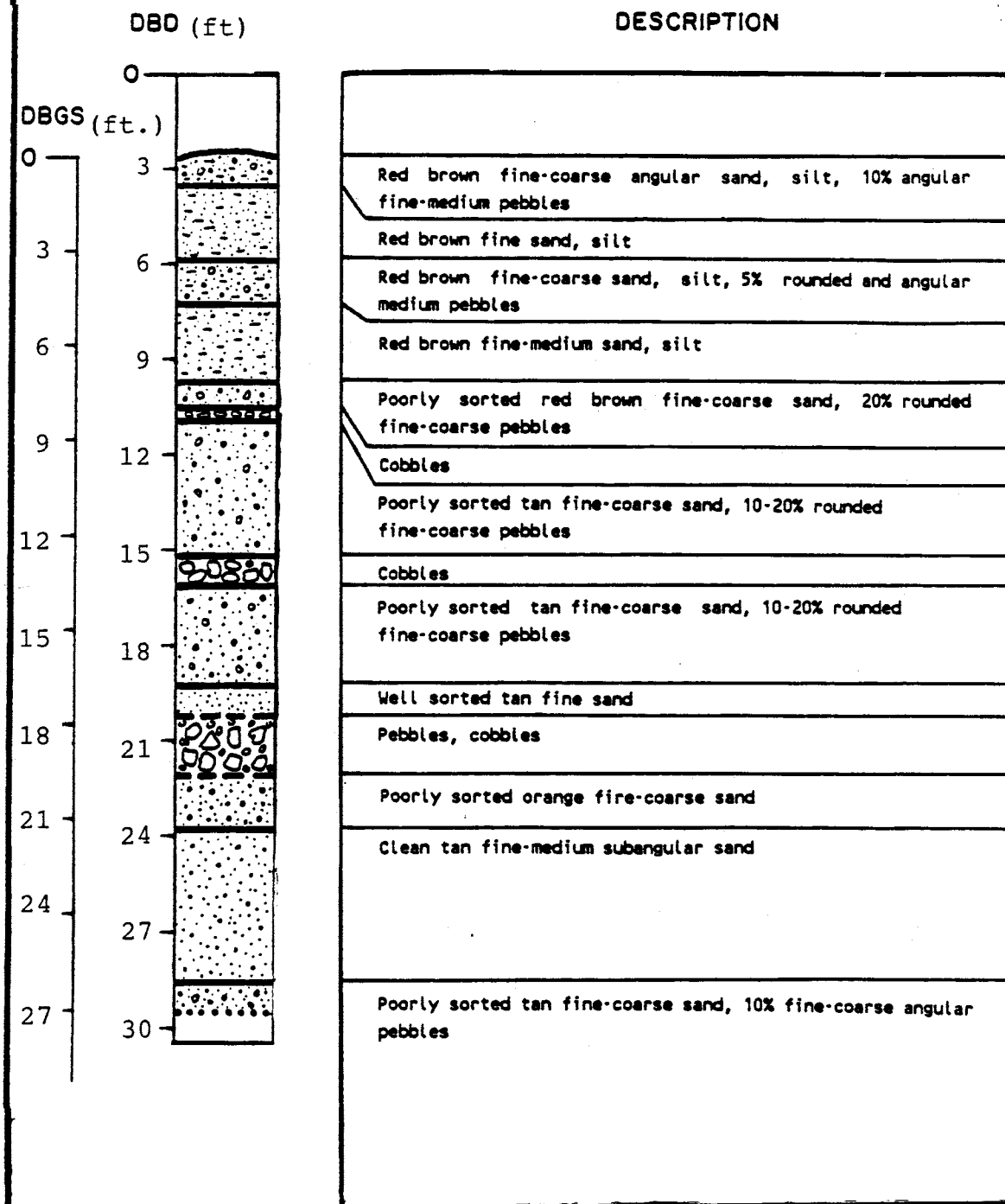


Figure 3 Borehole geologic log located at 15-15 (see Figure 1). DBD = depth below datum. DBGS = depth below ground surface. (adapted from Parsons (1988))

BOREHOLE GEOLOGIC LOG

LOCATION: 11-15
 DATUM EL: 4650.65 feet
 GND SURFACE EL: 4647.83 feet

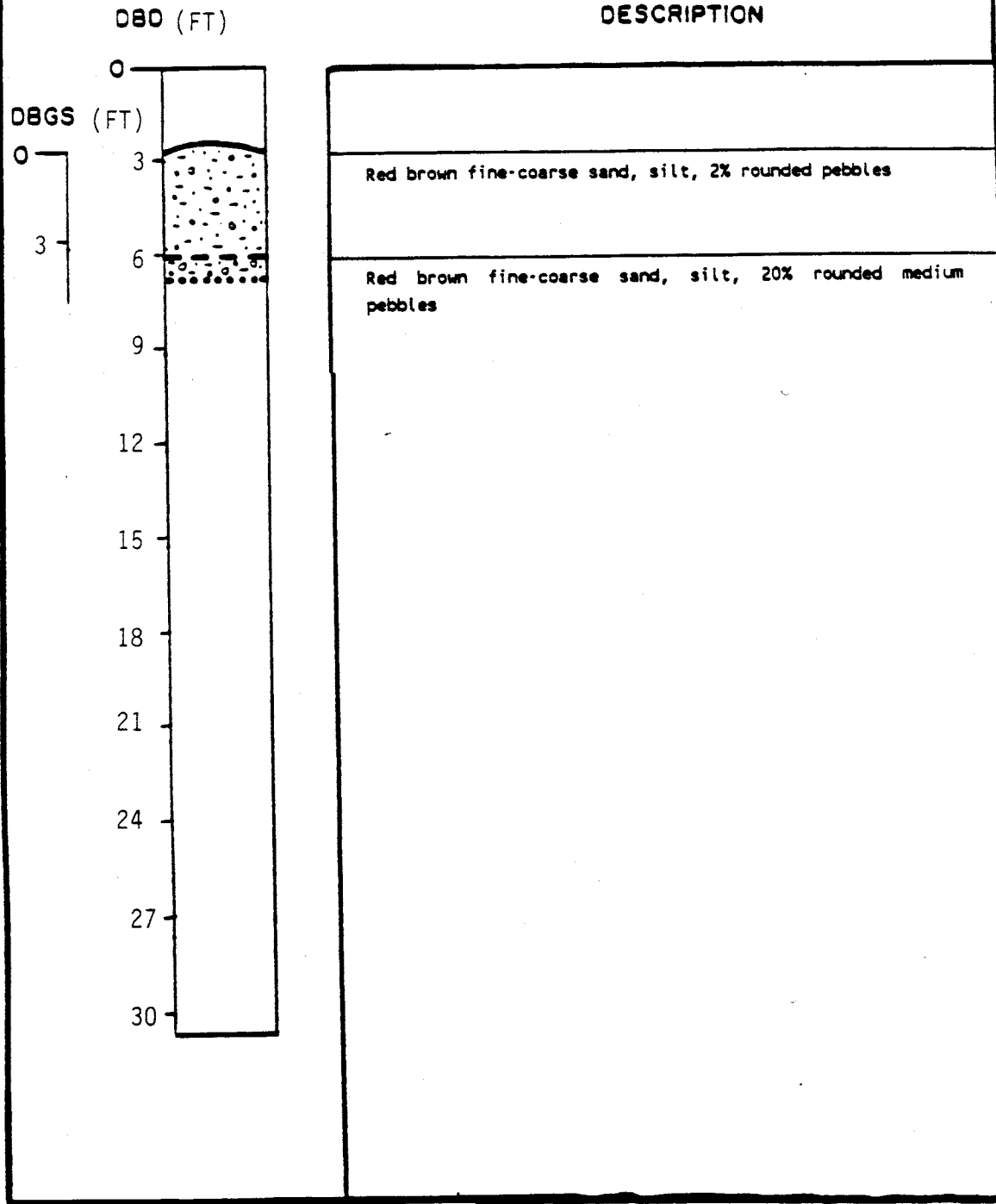


Figure 4 Borehole geologic log located at 11-15 (see Figure 1). DBD = depth below datum. DBGS = depth below ground-surface. (adapted from Parsons (1988))

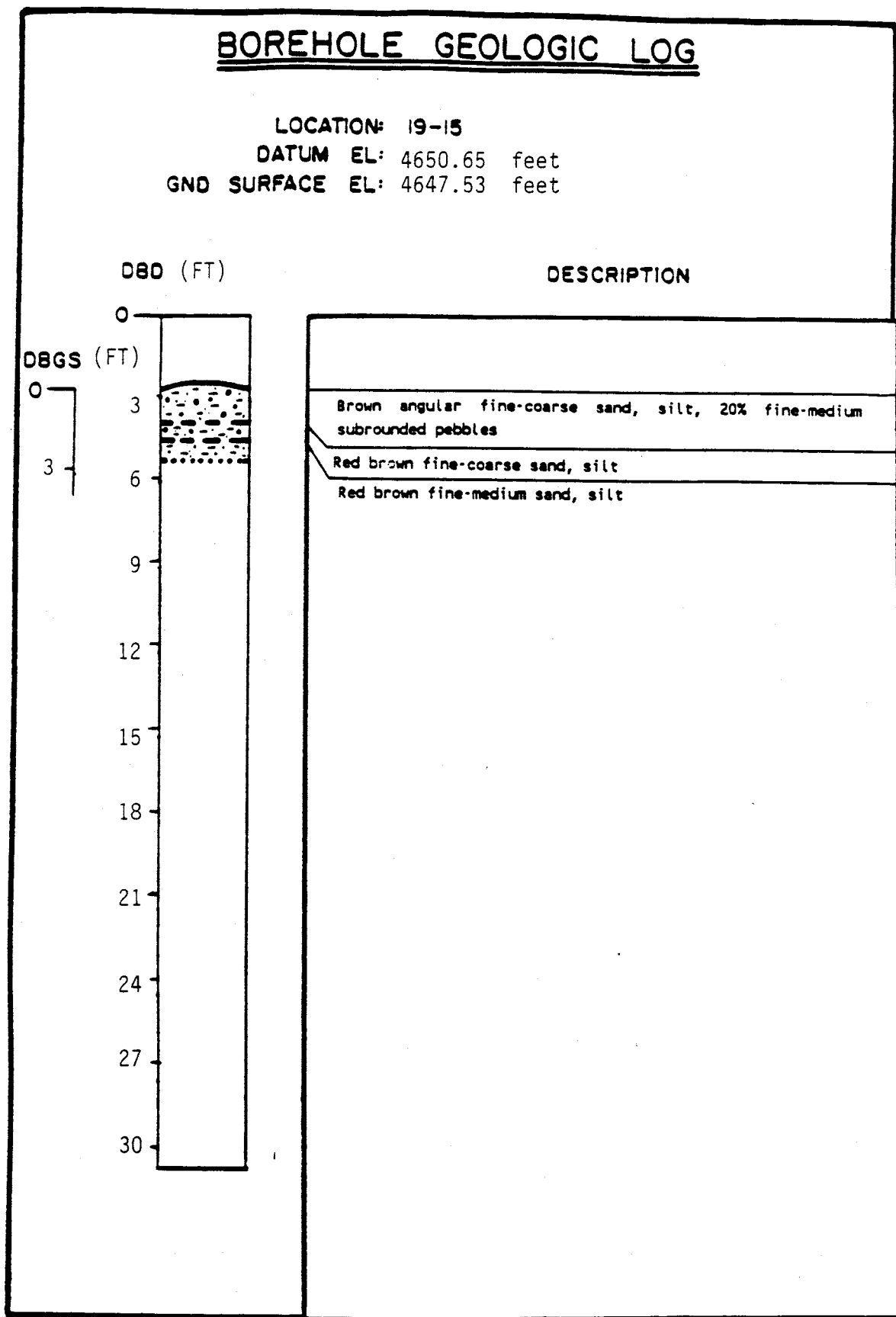


Figure 5 Borehole geologic log located at 19-15 (see Figure 1). DBD = depth below datum. DBGS = depth below ground surface. (adapted from Parsons (1988))

BOREHOLE GEOLOGIC LOG

LOCATION: 15-19
 DATUM EL: 4650.65 feet
 GND SURFACE EL: 4647.83 feet

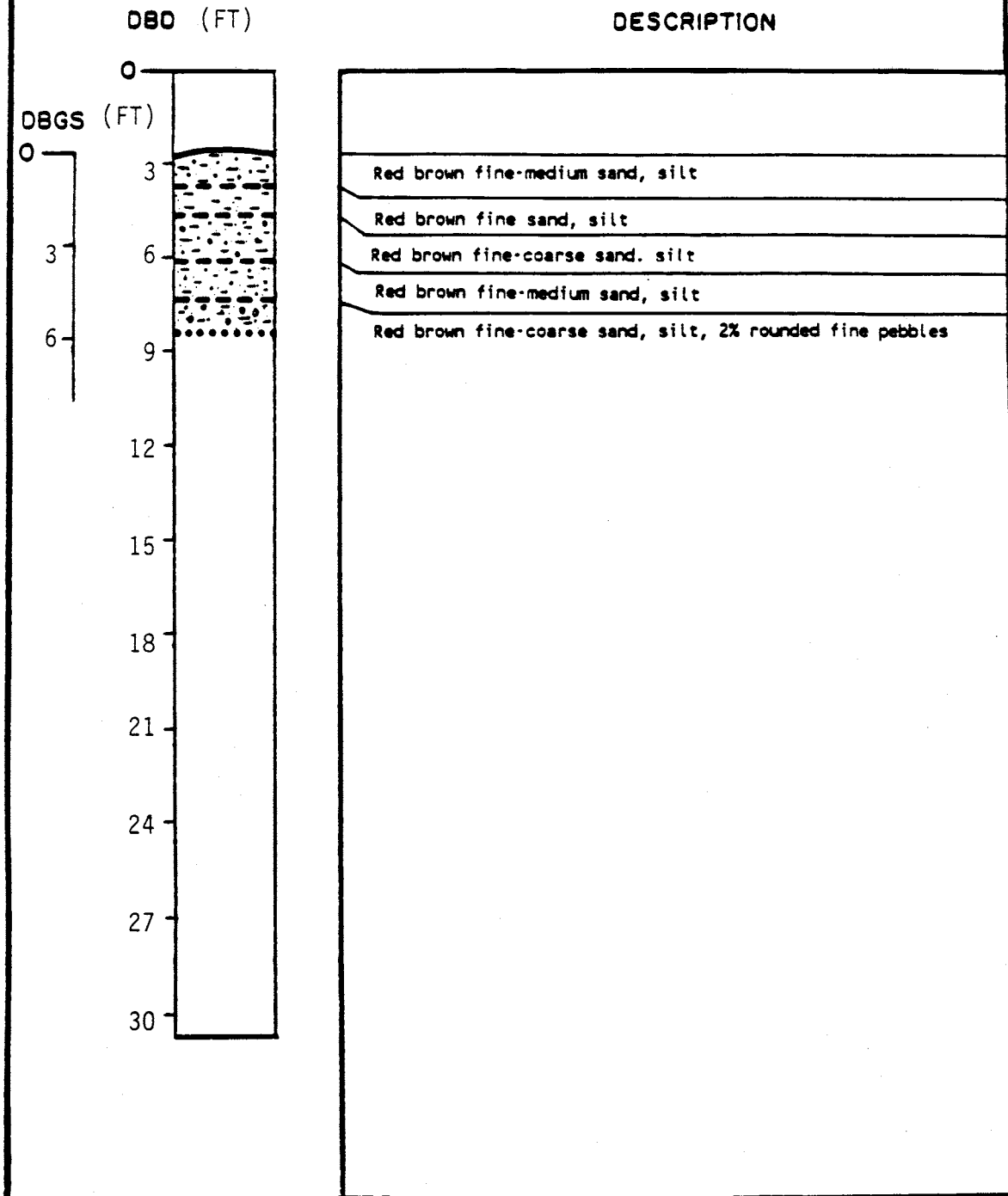


Figure 6 Borehole geologic log located at 15-19 (see Figure 1). DBD = depth below datum. DBGS = depth below ground surface. (adapted from Parsons (1988))

BOREHOLE GEOLOGIC LOG

LOCATION: 15-11
 DATUM EL: 4650.65 feet
 GND SURFACE EL: 4647.83 feet

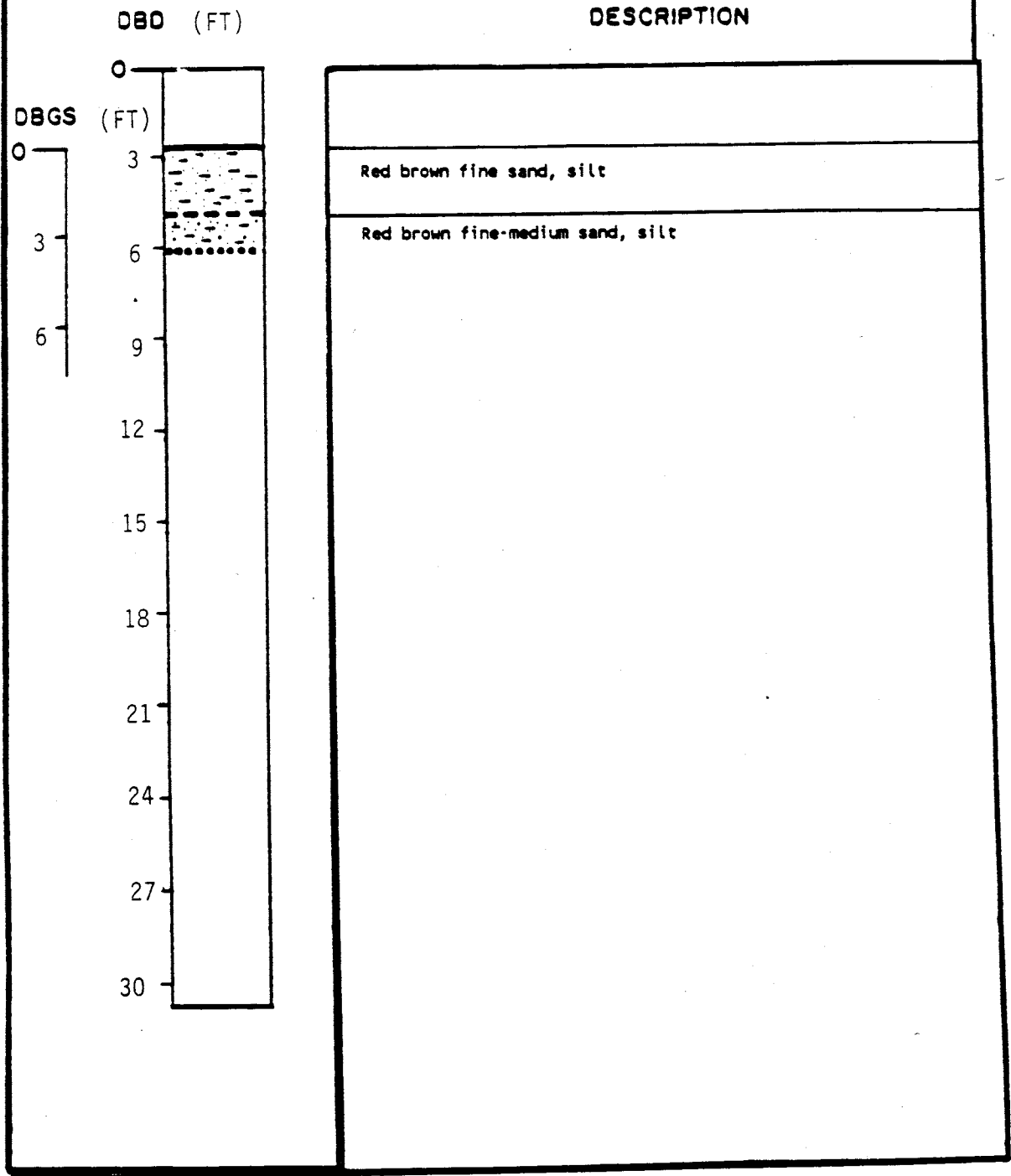


Figure 7 Borehole geologic log located at 15-11 (see Figure 1). DBD = depth below datum. DBGS = depth below ground surface. (adapted from Parsons (1988))

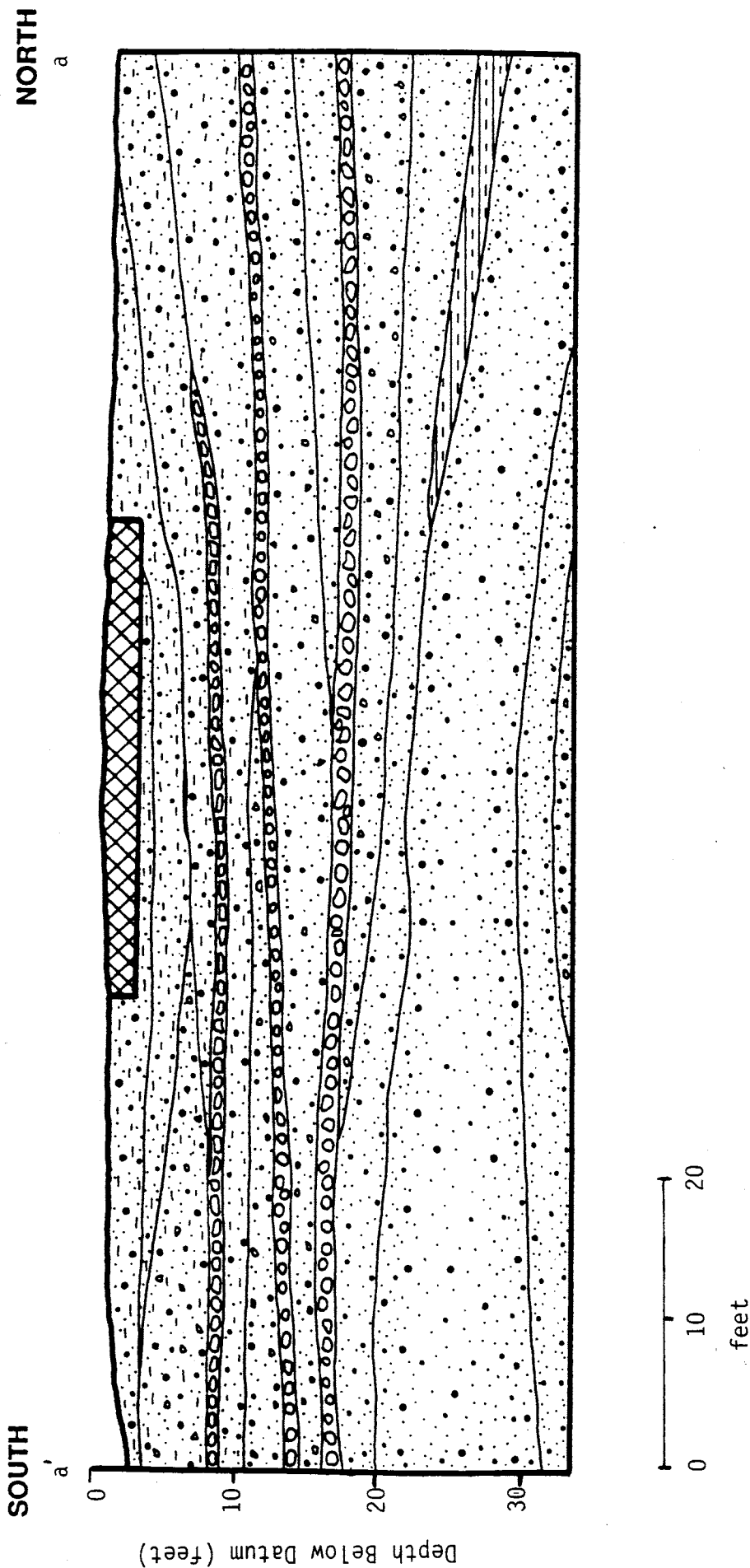


Figure 8 Geologic cross section of the infiltration study area. a - a', south-north orientation presented in Figure 1. (adapted from Parsons, 1988)

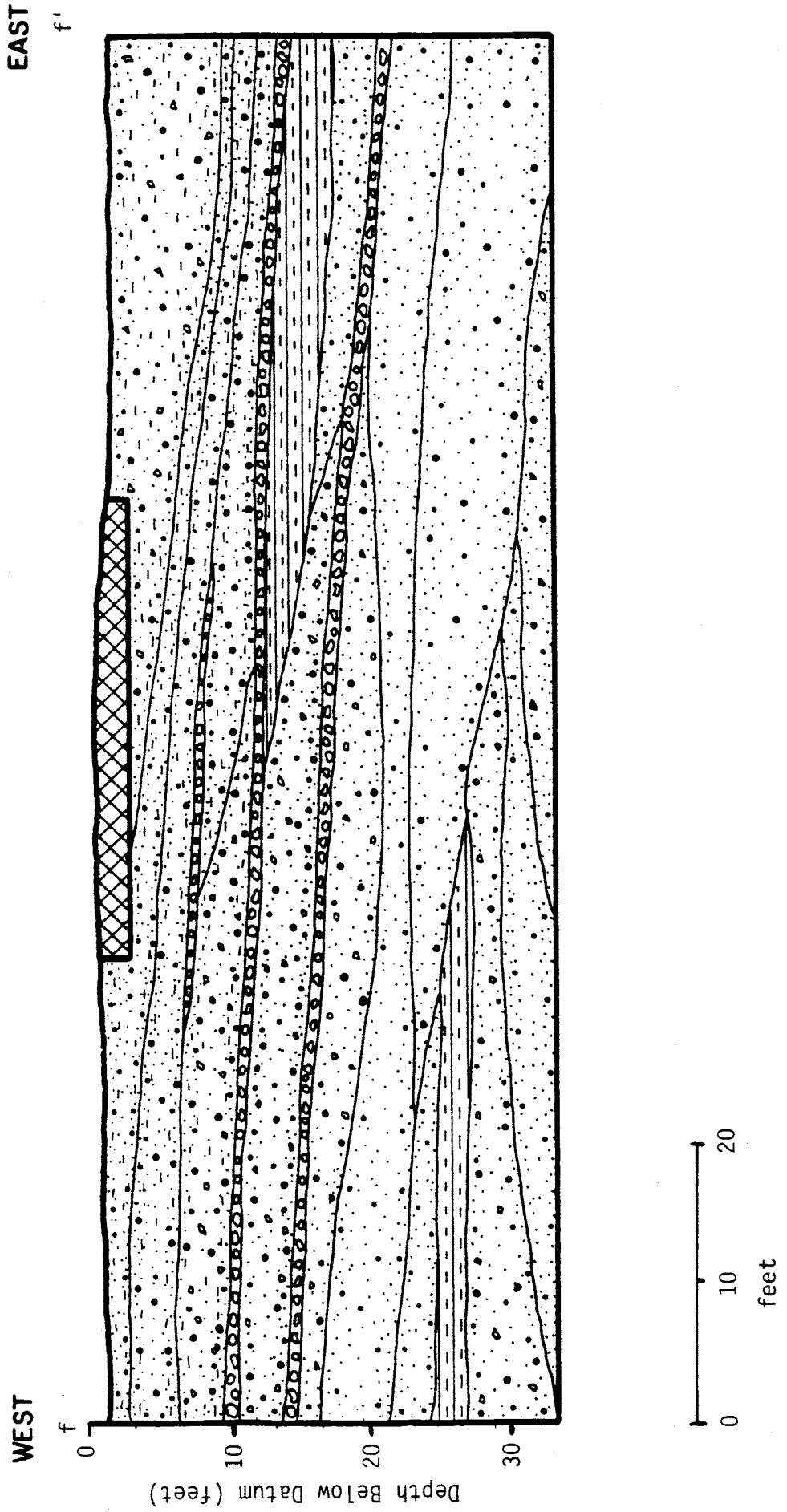


Figure 9 Geologic cross section of the infiltration area. f - f', west-east orientation presented in Figure 1. (adapted from Parsons, 1988)

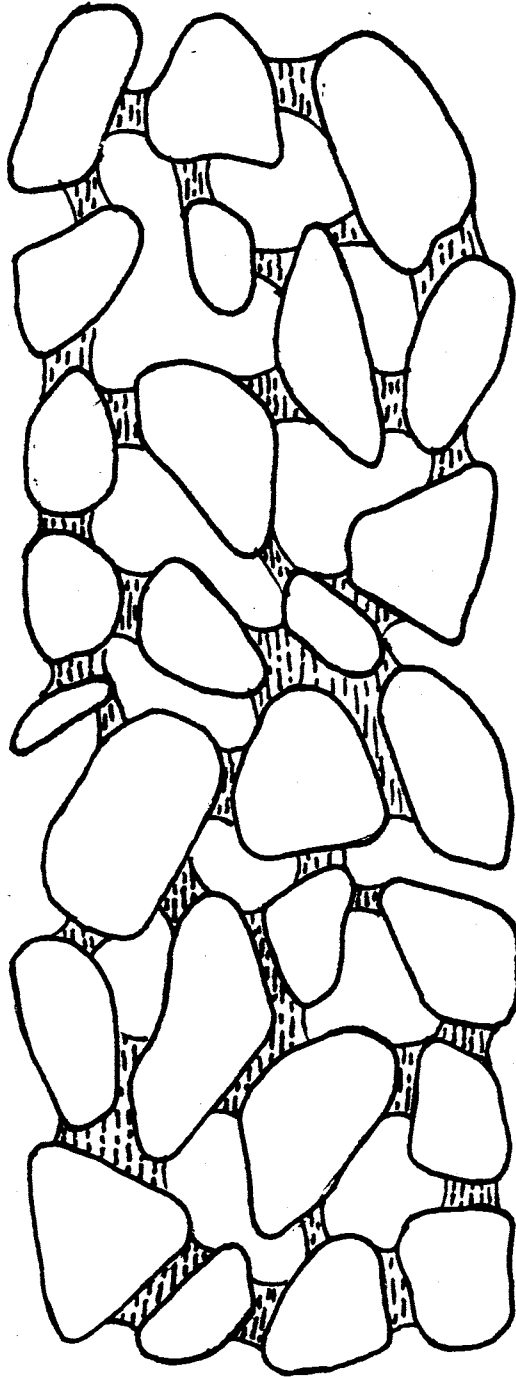


Figure 10 Water in an unsaturated coarse-textured soil (after Hillel, 1980a).

WENNER ELECTRODE CONFIGURATION

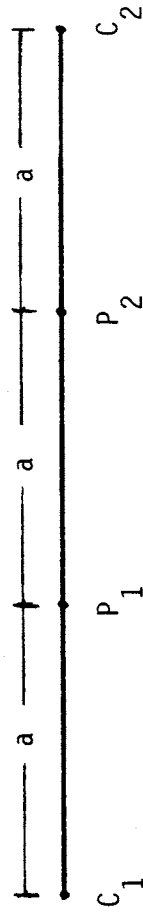


Figure 11 Wenner electrode array. C = current electrode, P = potential electrode, and a = electrode spacing.

DIPOLE-DIPOLE ELECTRODE CONFIGURATION and pseudosection format

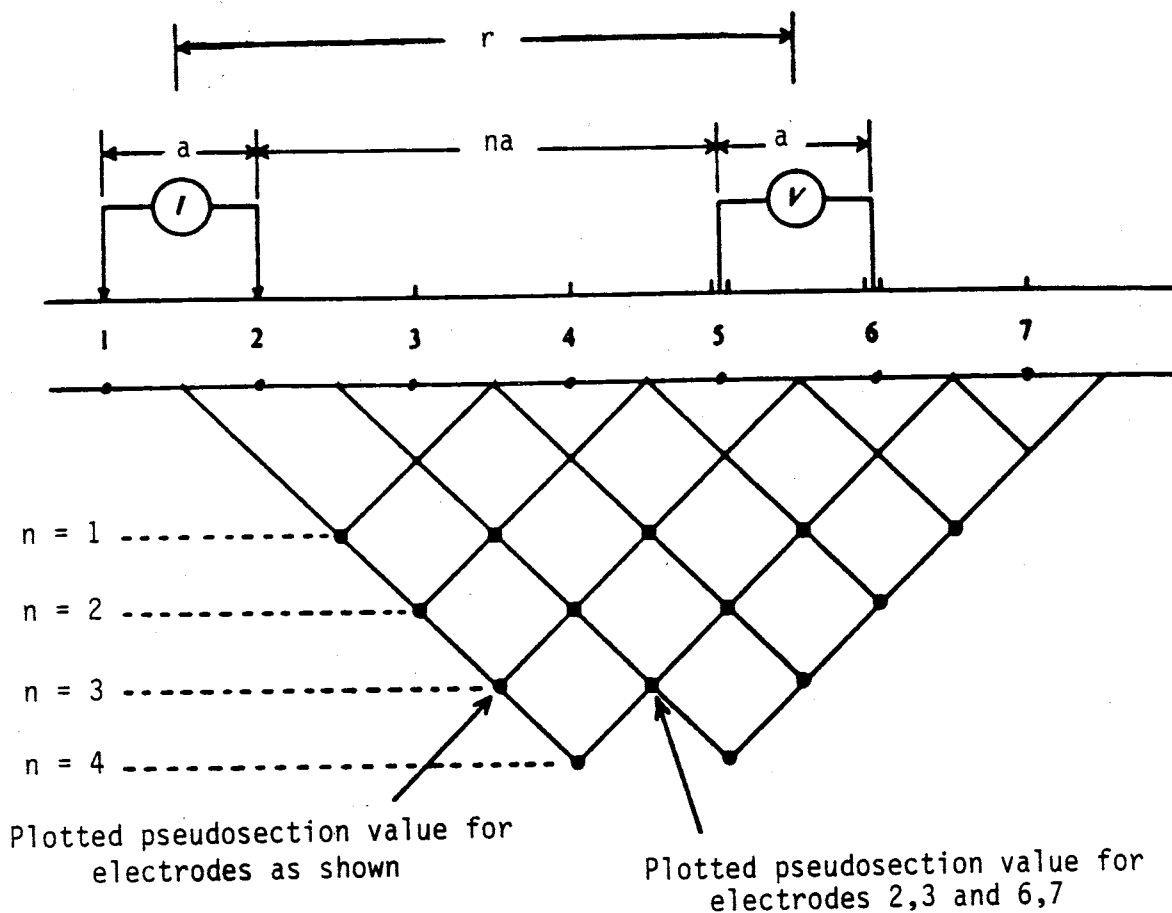


Figure 12 Dipole-dipole electrode configuration and graphical construction for locating data points in a pseudosection. I = current, V = potential (or measuring) dipole, a = dipole spacing, na = dipole separation, where n = integer multiple of dipole spacing (adapted from Telford et. al. (1976)), and r = dipole separation as defined by Roy and Apparao (1971).

Wenner vertical electrical sounding

Centered at borehole 15-15
Oriented east to west

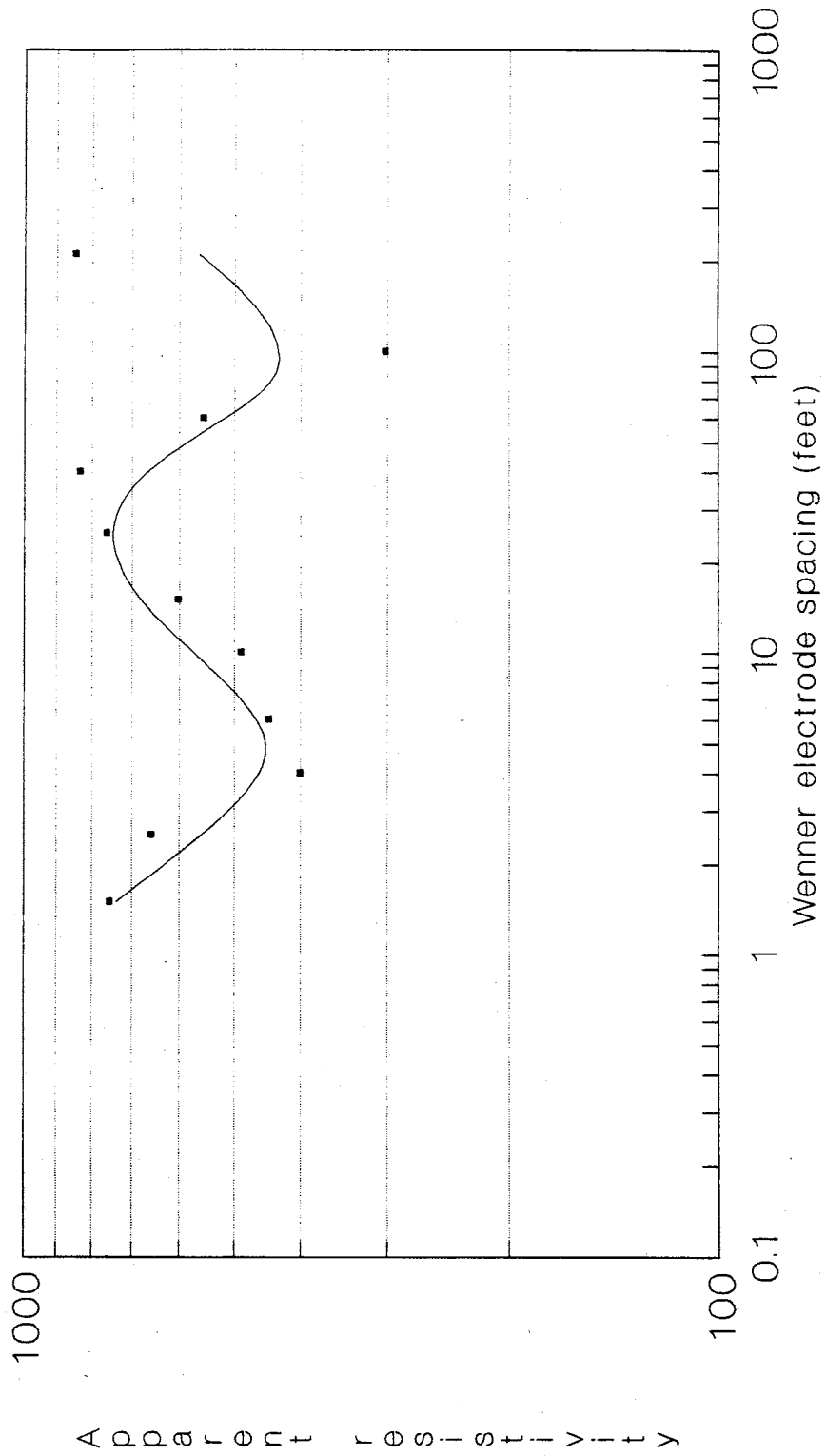


Figure 13 Pre-infiltration Wenner vertical electrical sounding conducted in Feb. 1986.

Wenner vertical electrical sounding

Centered at borehole 15-11
Oriented east to west

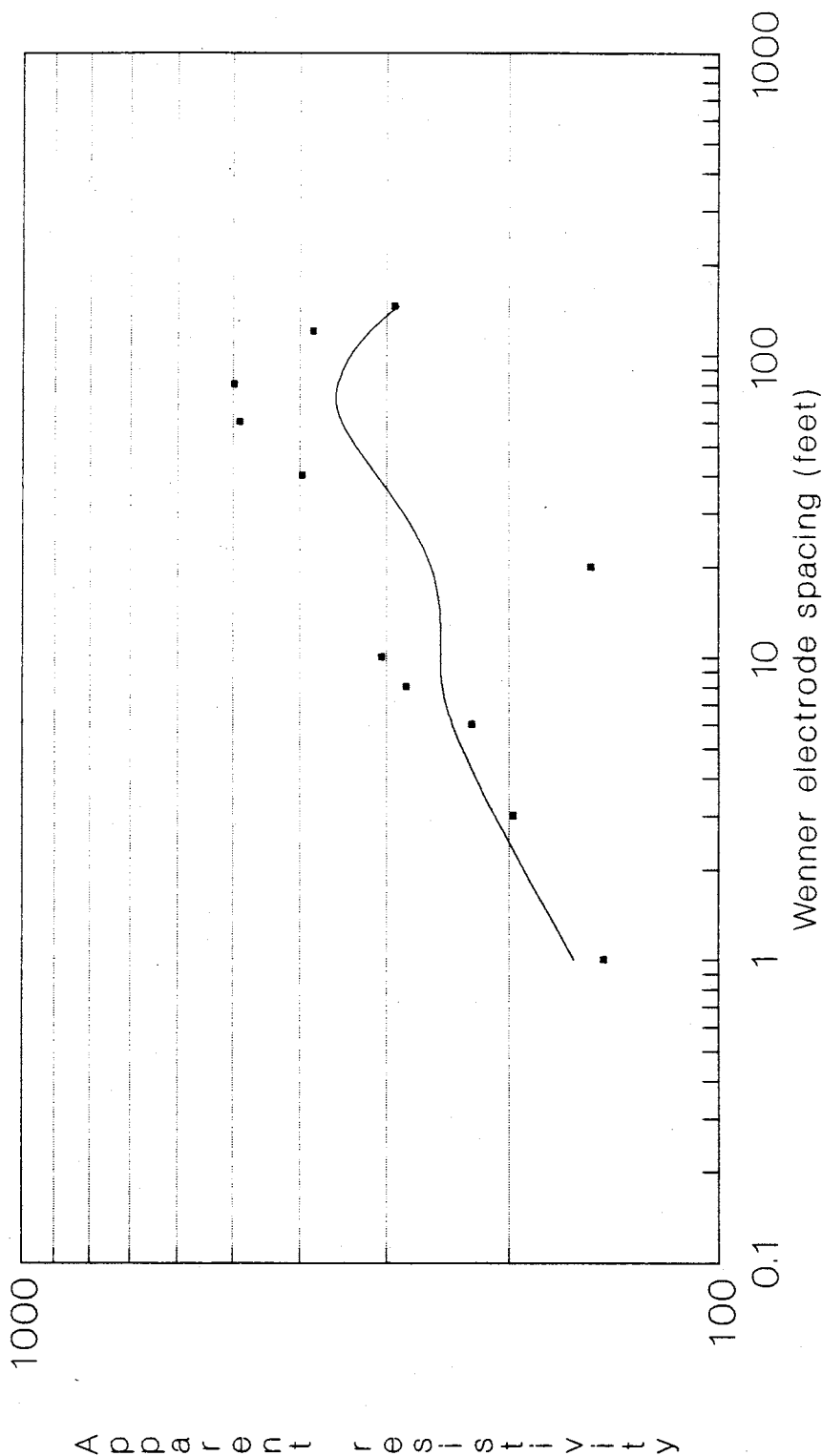


Figure 14 Post-infiltration Wenner vertical electrical sounding conducted in March 1987.

GEOELECTRICAL SECTION

Zohdy inversion of Wenner VES
centered at location 15-15

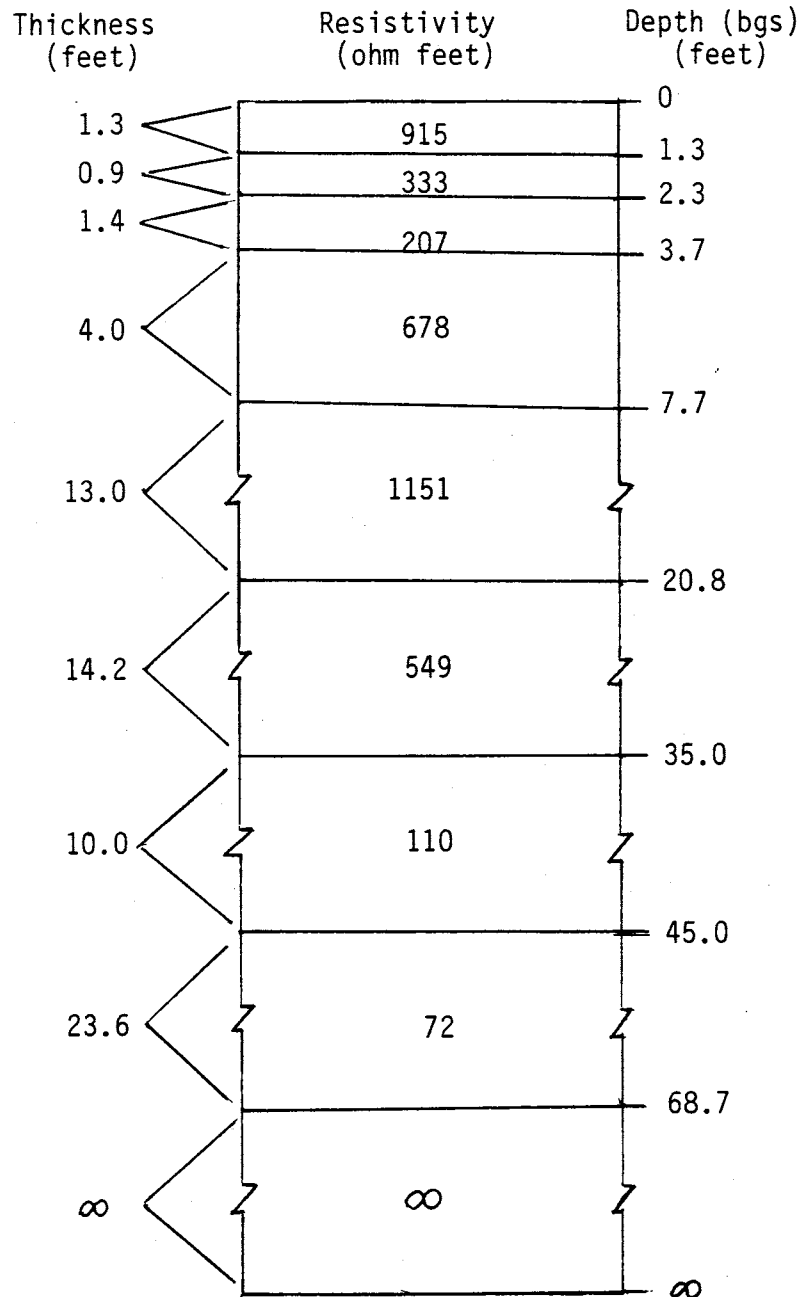


Figure 15 Geoelectrical section derived using Zohdy and Bisdorf (1975) numerical inversion of Wenner VES centered at borehole 15-15 (see Figure 1). Inverted model is also presented in Table 1. bgs = below ground surface

GEOELECTRICAL SECTION

Zohdy inversion of Wenner VES

centered at location 15-11

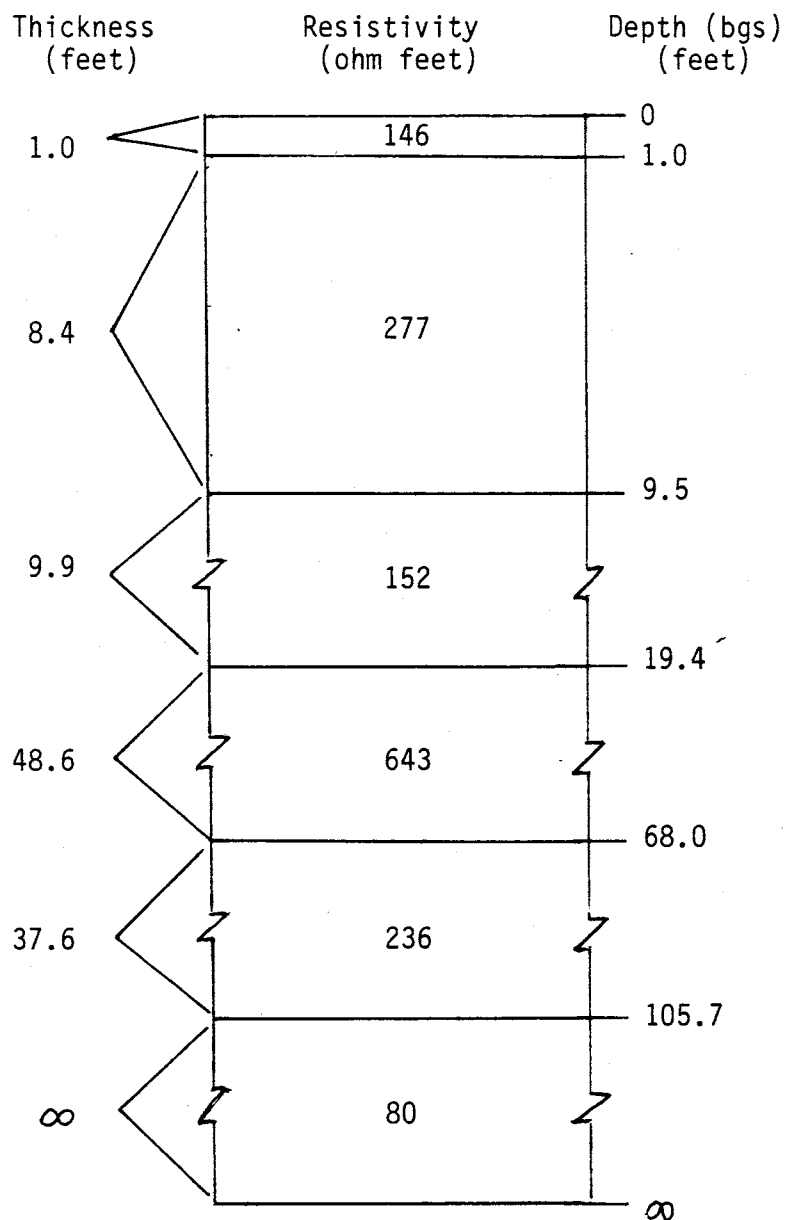


Figure 16 Geoelectrical section derived using Zohdy and Bisdorf (1975) numerical inversion of Wenner VES centered at borehole 15-11 (see Figure 1). Inverted model is also presented in Table 2. bgs = below ground surface

Dipole-Dipole VES

Centered at location 15-17.3
Dipole spacing = 10 feet

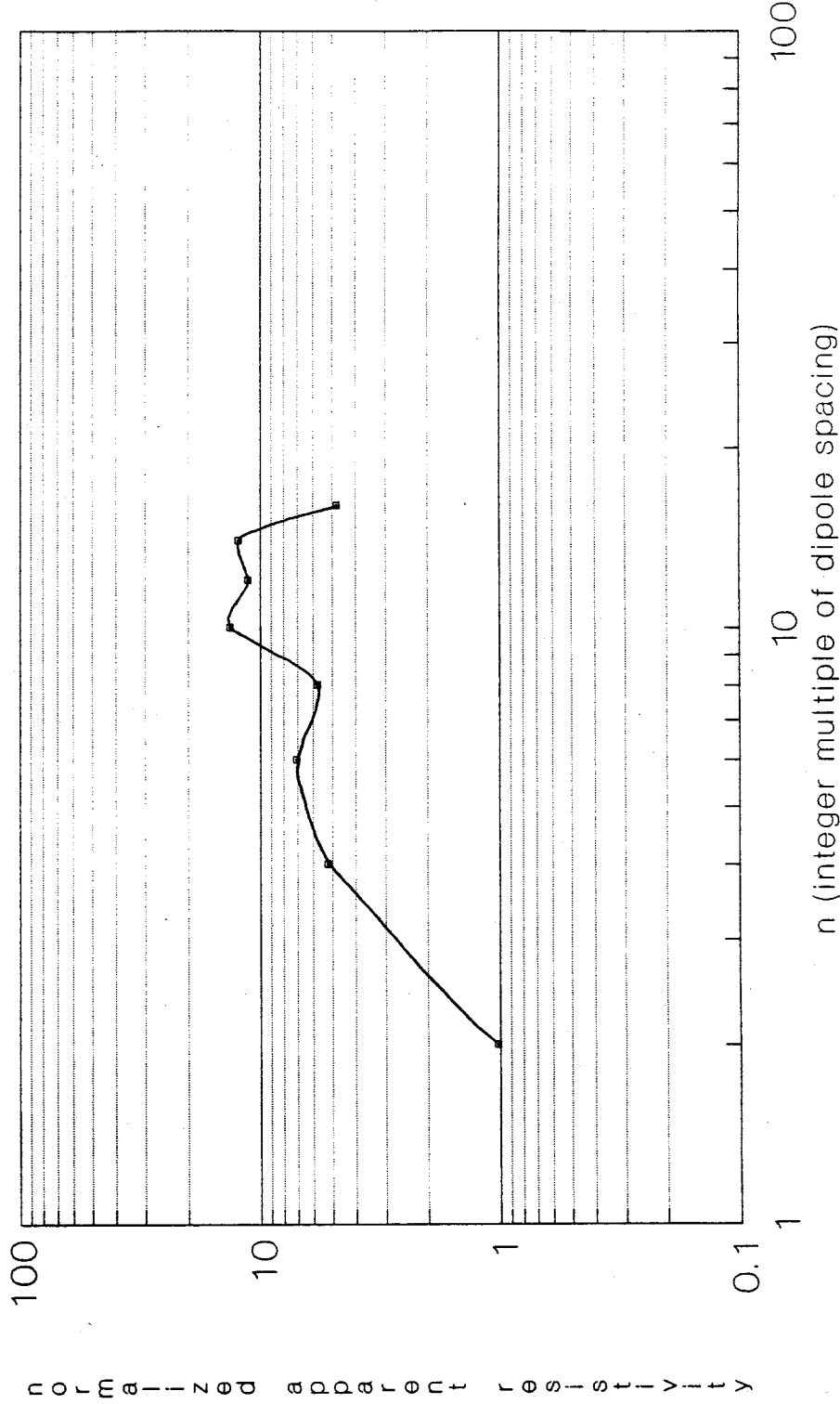


Figure 17 Dipole-dipole vertical electrical sounding (VES) derived from the a - a' pseudosection. VES centered at location 15-17.3 (see Figure 1). Normalized ordinate derived by dividing the field measurement by the n = 1 dipole-dipole resistivity measurement (average n = 1 resistivity measurement approximately 100 ohm feet), technique after Elliot (1974).

Dipole-Dipole VES
 Centered at borehole 15-19
 Dipole spacing = 10 feet

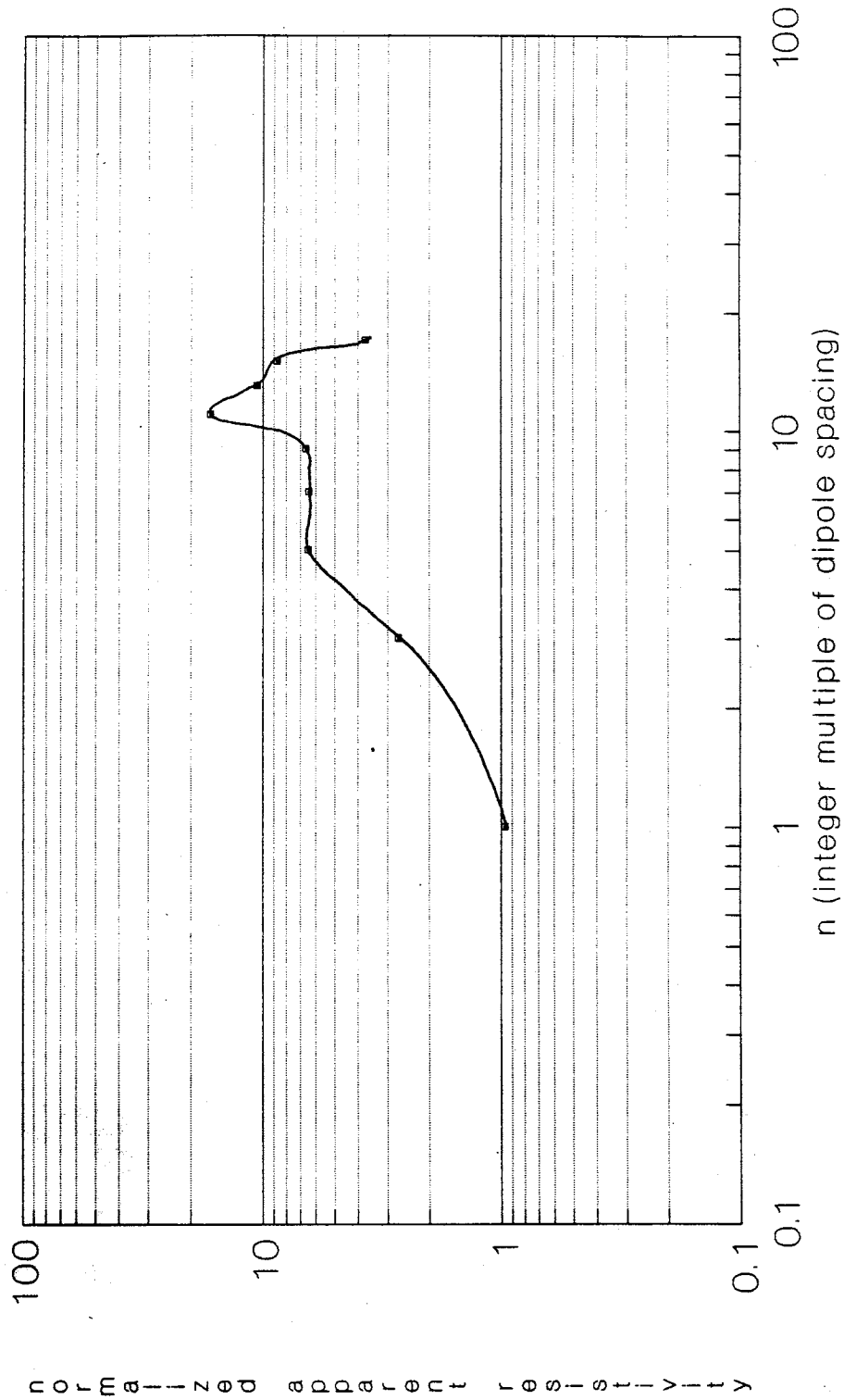


Figure 18 Dipole-dipole vertical electrical sounding (VES) derived from a - a' pseudosection. VES centered at location 15-19 (see Figure 1). Normalized ordinate derived by dividing the field measurement by the $n = 1$ dipole-dipole resistivity measurement (average $n = 1$ resistivity measurement approximately 100 ohm feet), technique after Elliot (1974).

Dipole-Dipole VES

Centered at location 15-20.6
Dipole spacing = 10 feet

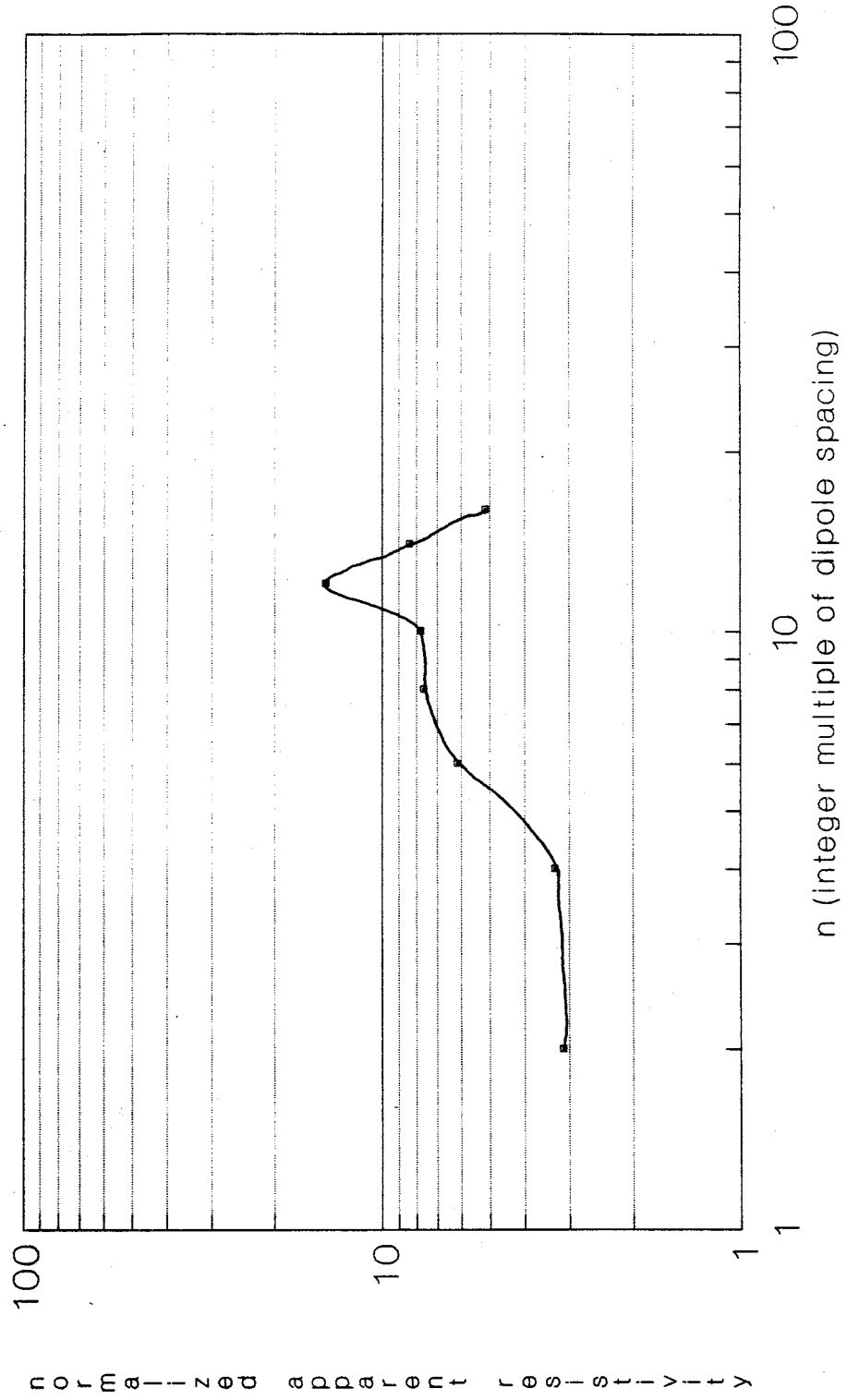


Figure 19 Dipole-dipole vertical electrical sounding (VES) derived from a 'a' pseudosection. VES centered at location 15-20.6 (see Figure 1). Normalized ordinate derived by dividing the field measurement by the $n = 1$ dipole-dipole resistivity measurement (average $n = 1$ resistivity measurement approximately 100 ohm feet), technique after Elliot (1974).

Dipole-Dipole VES

Centered at location 15-22.3
Dipole spacing = 10 feet

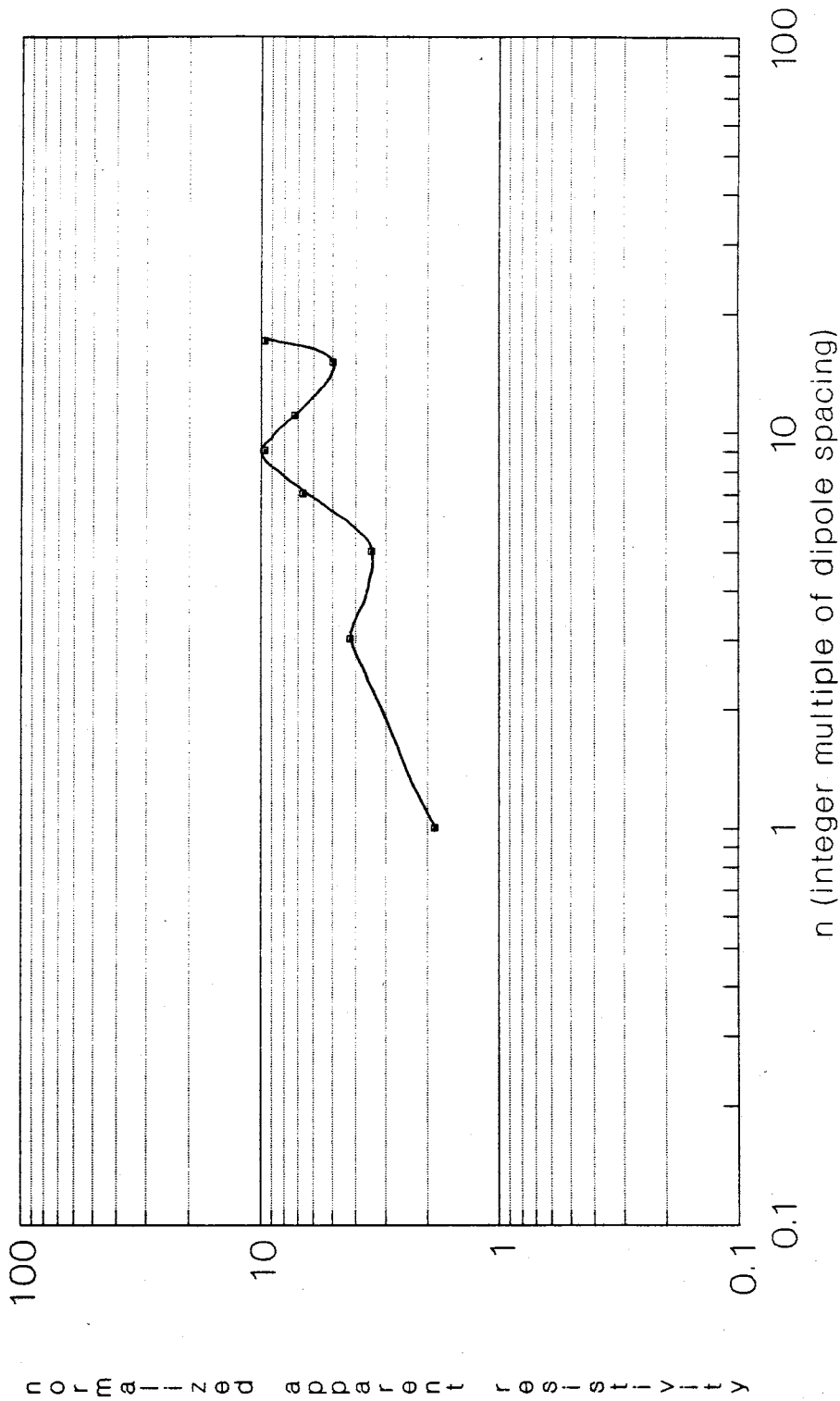


Figure 20 Dipole-dipole vertical electrical sounding (VES) derived from a - a' pseudosection. VES centered at location 15-22.3 (see Figure 1). Normalized ordinate derived by dividing the field measurement by the $n = 1$ dipole-dipole resistivity measurement (average $n = 1$ resistivity measurement approximately 100 ohm feet), technique after Elliot (1974).

Dipole-Dipole VES
 Centered at location 15-24
 Dipole spacing = 10 feet

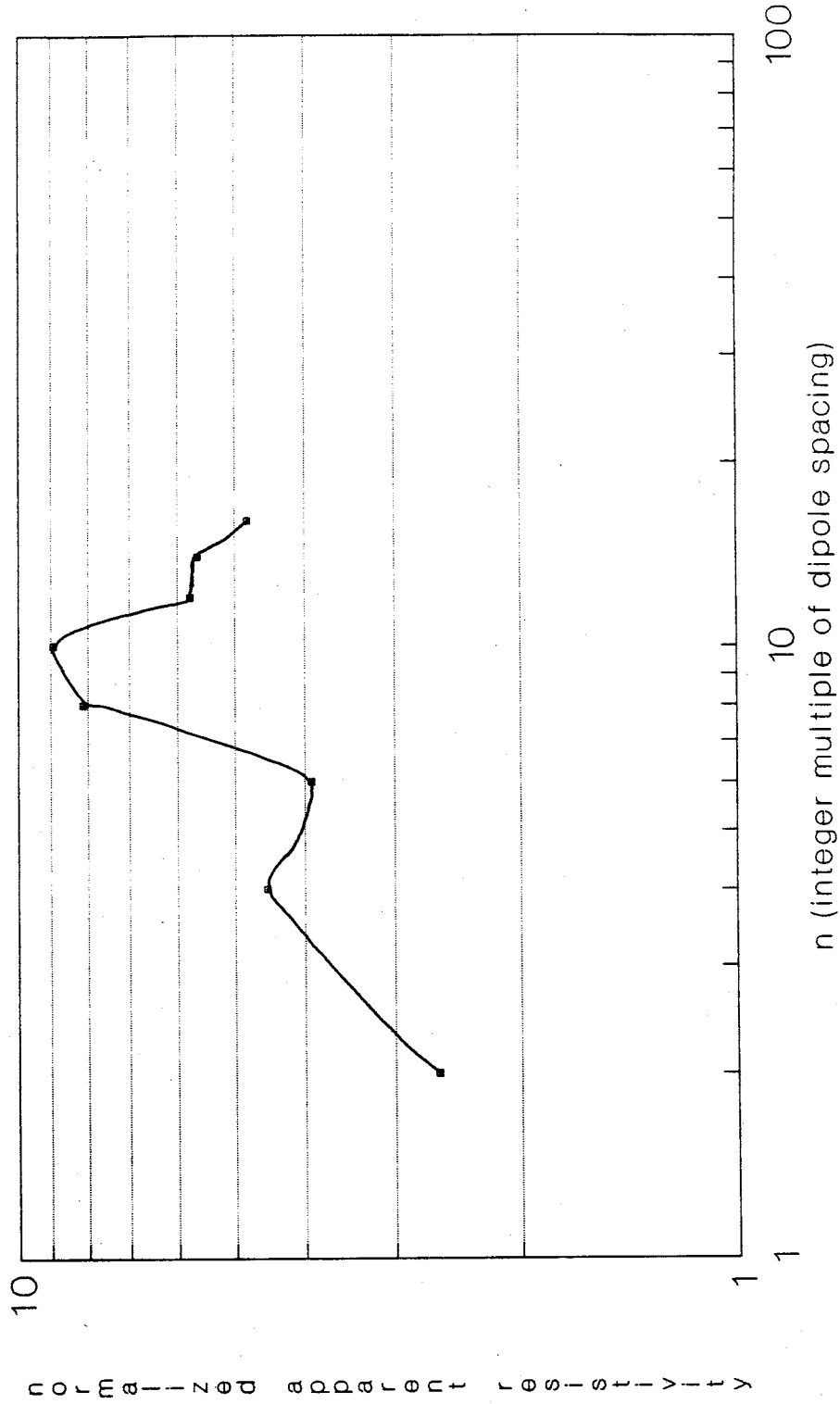


Figure 21 Dipole-dipole vertical electrical sounding (VES) derived from a - a' pseudosection. VES centered at location 15-24 (see Figure 1). Normalized ordinate derived by dividing the field measurement by the n = 1 dipole-dipole resistivity measurement (average n = 1 resistivity measurement approximately 100 ohm feet), technique after Elliot (1974).

Wenner horizontal resistivity profile

South-north center-line (a' - a)
Wenner electrode spacing = 30 feet

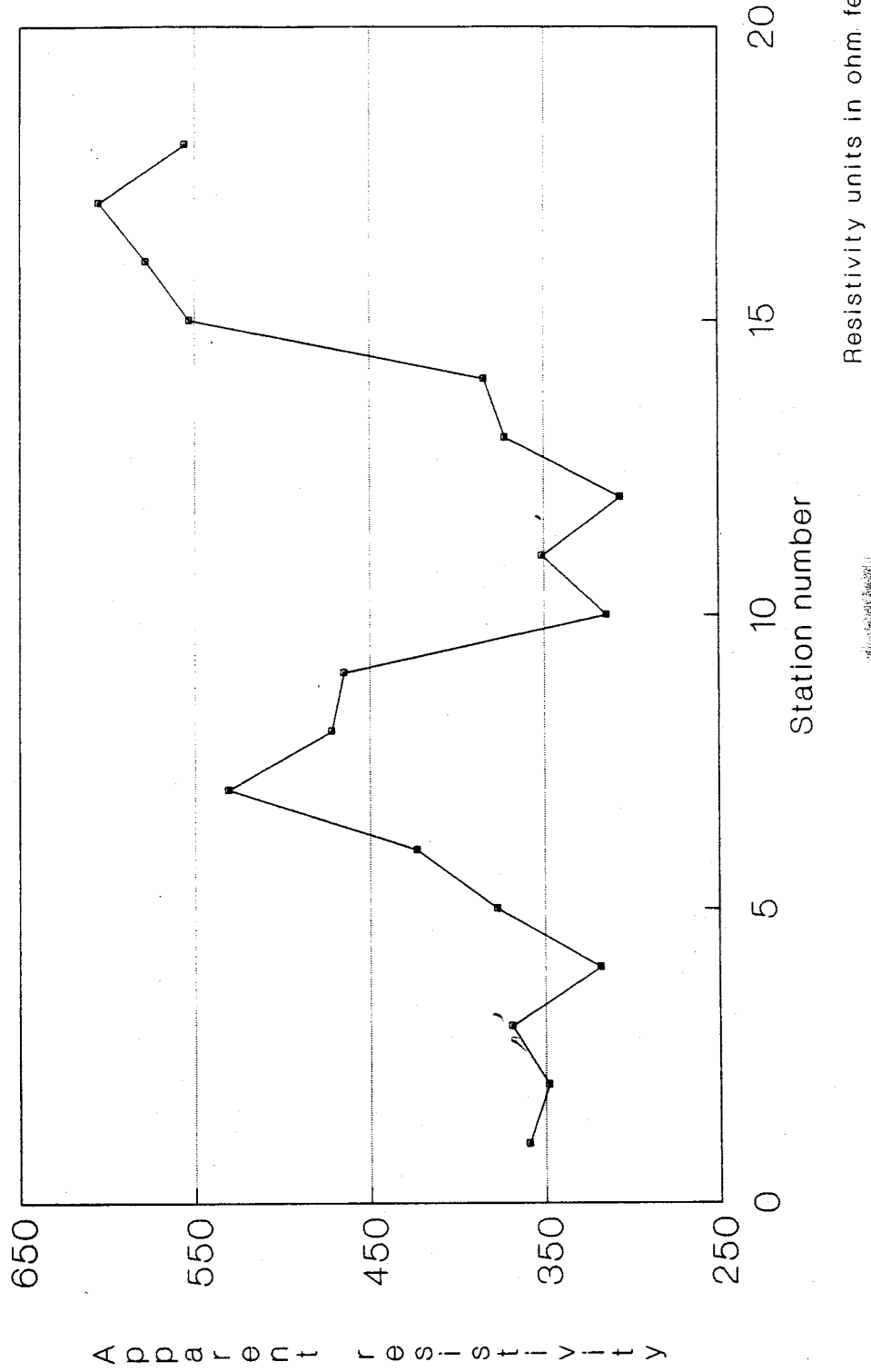


Figure 22 Post-infiltration Wenner horizontal resistivity profile conducted in May 1987.

Wenner horizontal resistivity profile

South-north center-line (a' - a)
Wenner electrode spacing = 50 feet

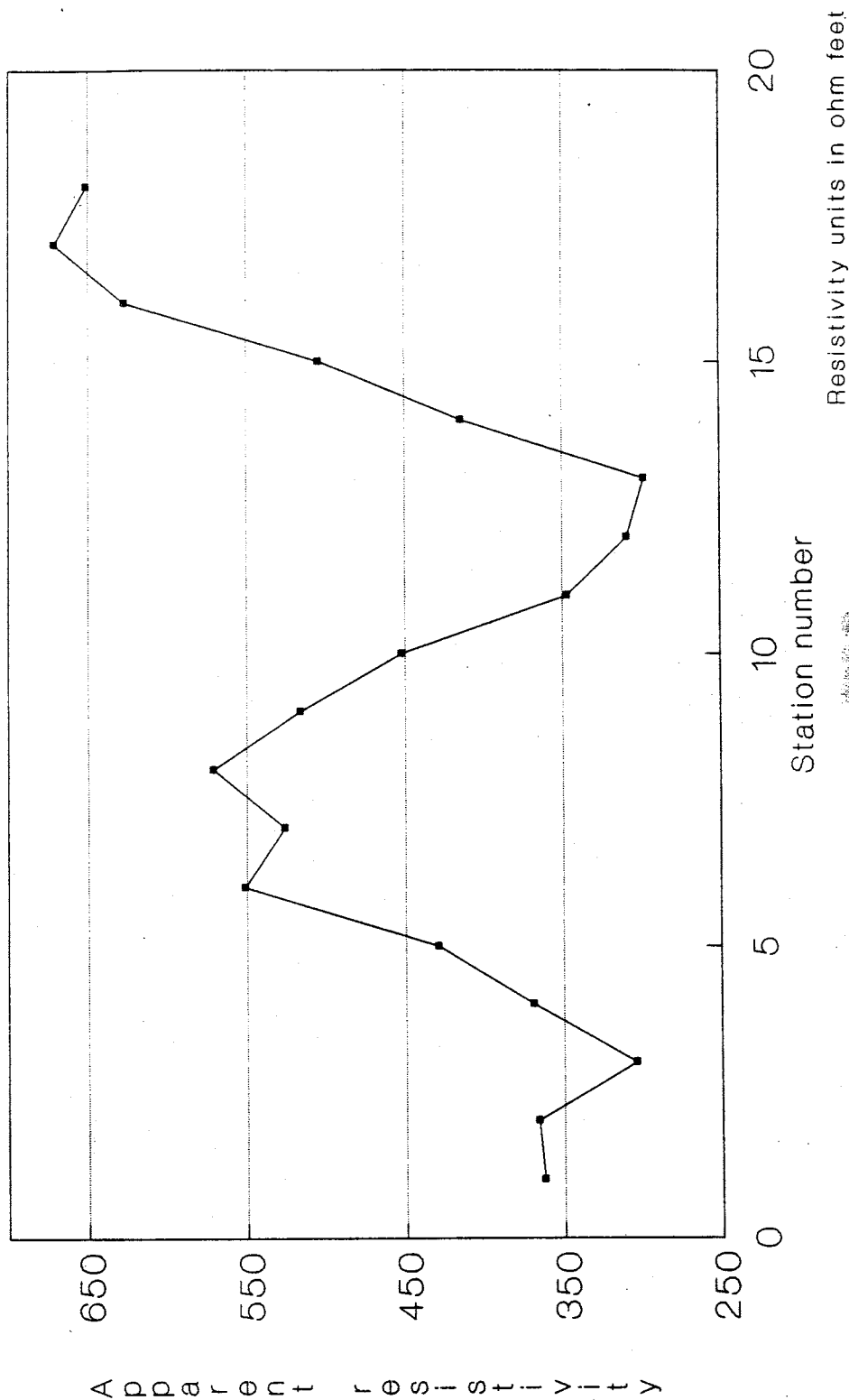


Figure 23 Post-infiltration Wenner horizontal resistivity profile conducted in May 1987.

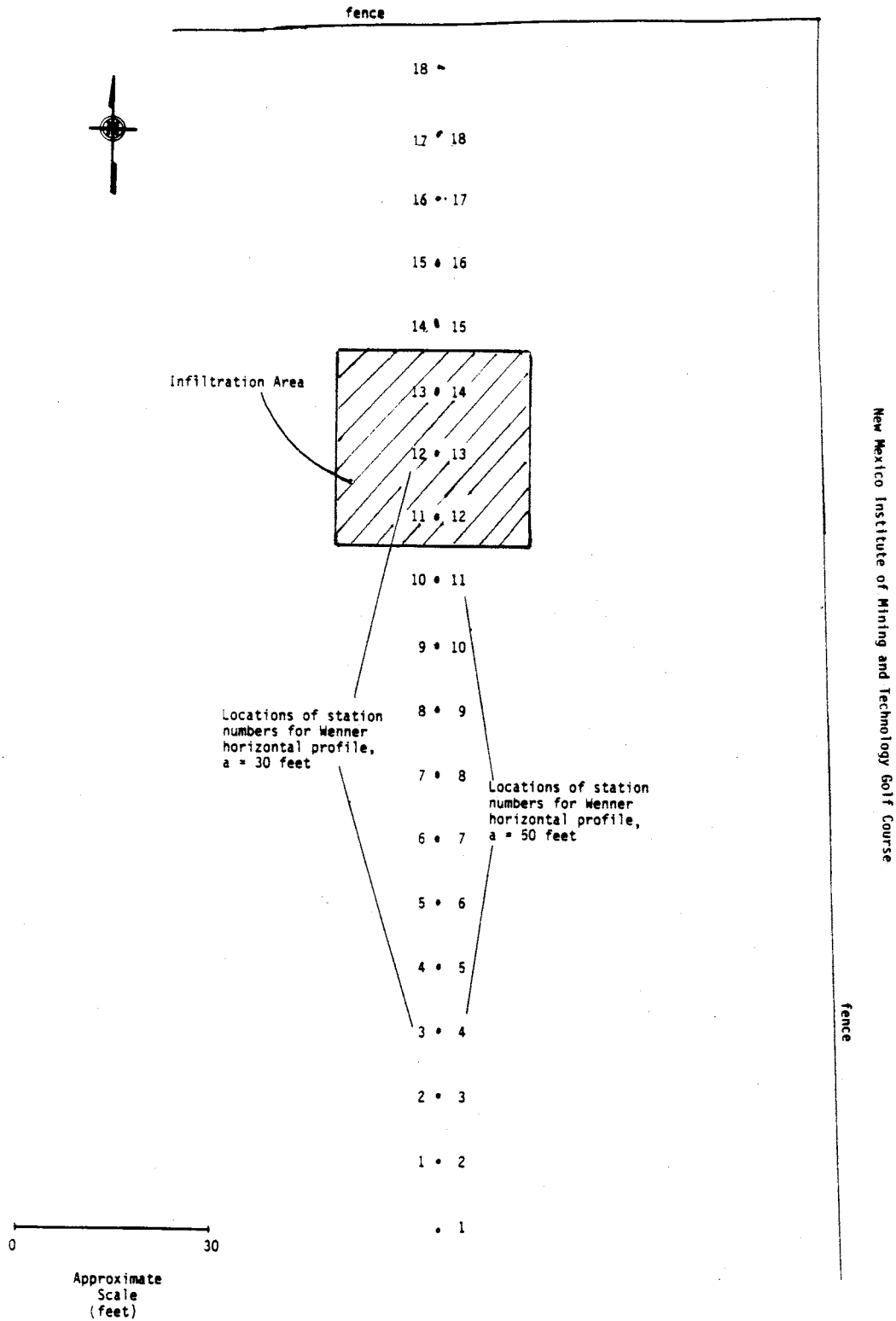


Figure 24 Map of study area. Numbered locations correspond to station numbers found on Figure 22 (Wenner horizontal profile, a = 30) and Figure 23 (Wenner horizontal profile, a = 50).

PSEUDOSECTION RESISTIVITY LEGEND

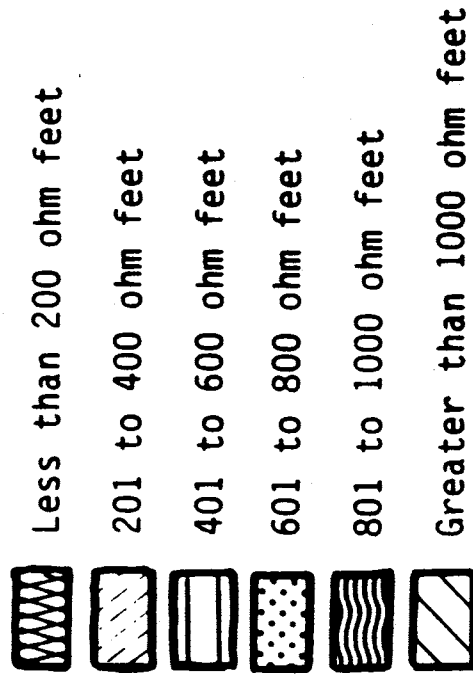


Figure 25 Legend of resistivity interval symbols for pseudosections presented in Figures 26 to 35.

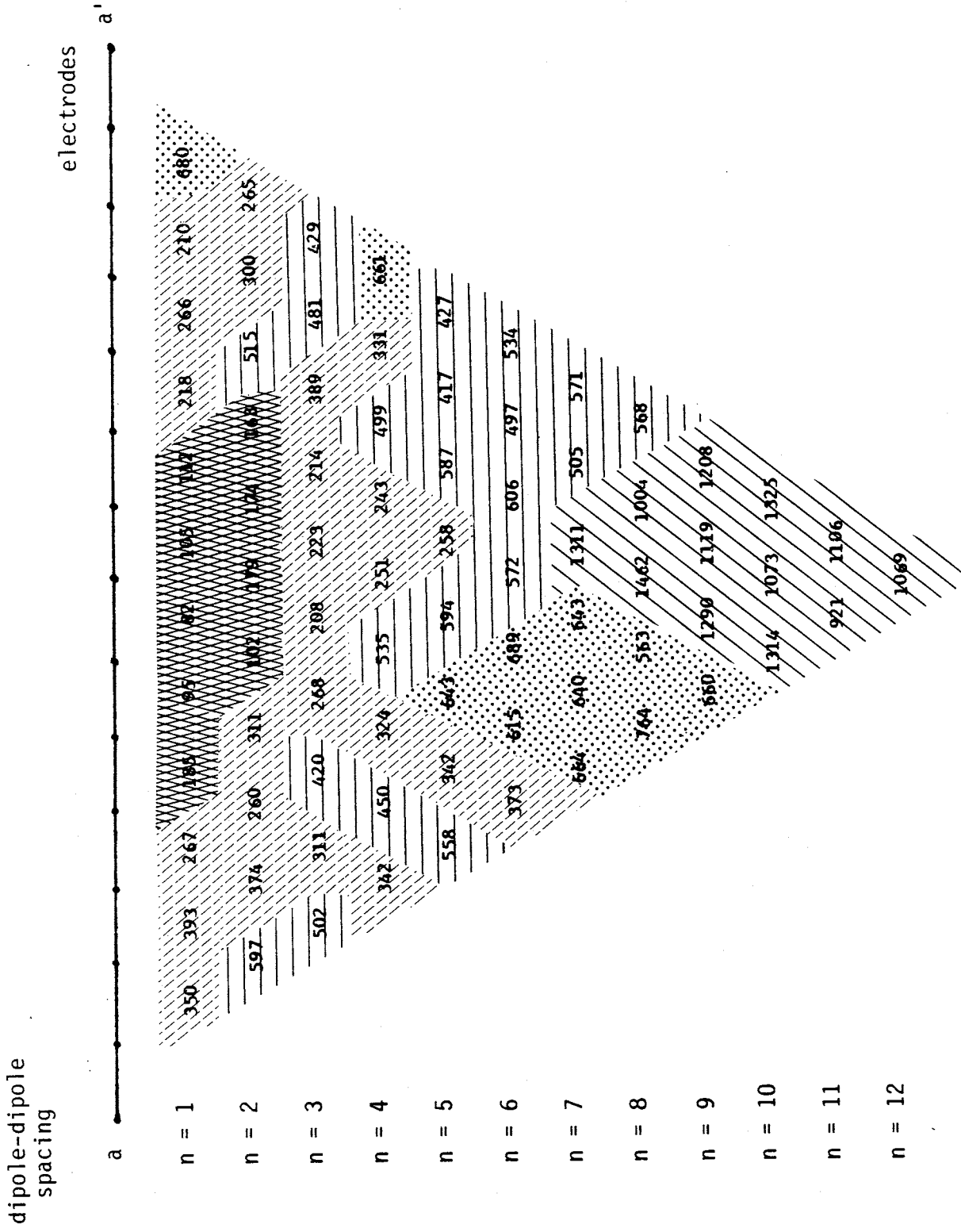


Figure 26 Pre-infiltration pseudosection conducted along the a - a' center line on 9/20/86. All resistivity values in ohm feet.

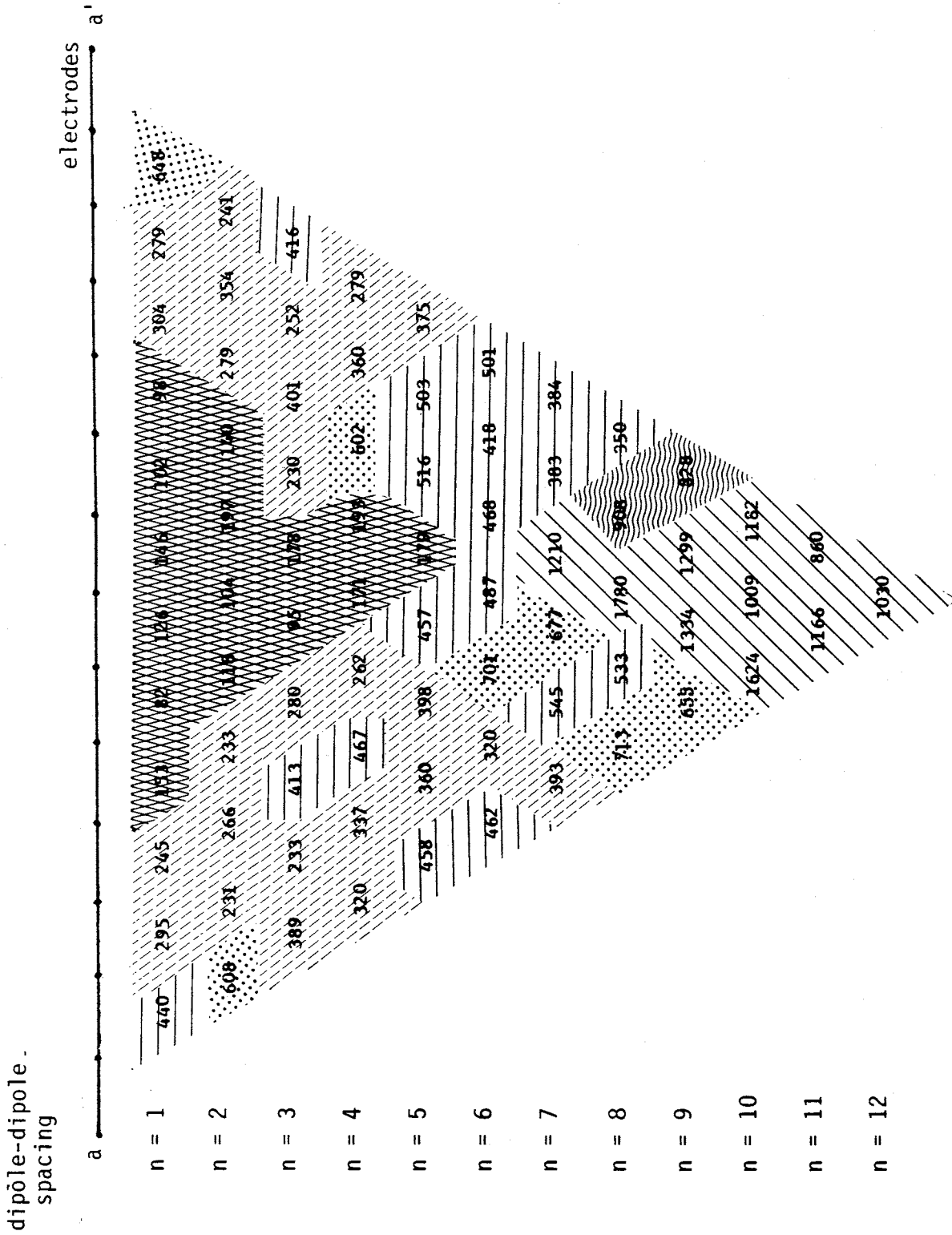


Figure 27 Post-infiltration pseudosection conducted along the a - a' center line on 6/8/87. All resistivity values are in ohm feet.

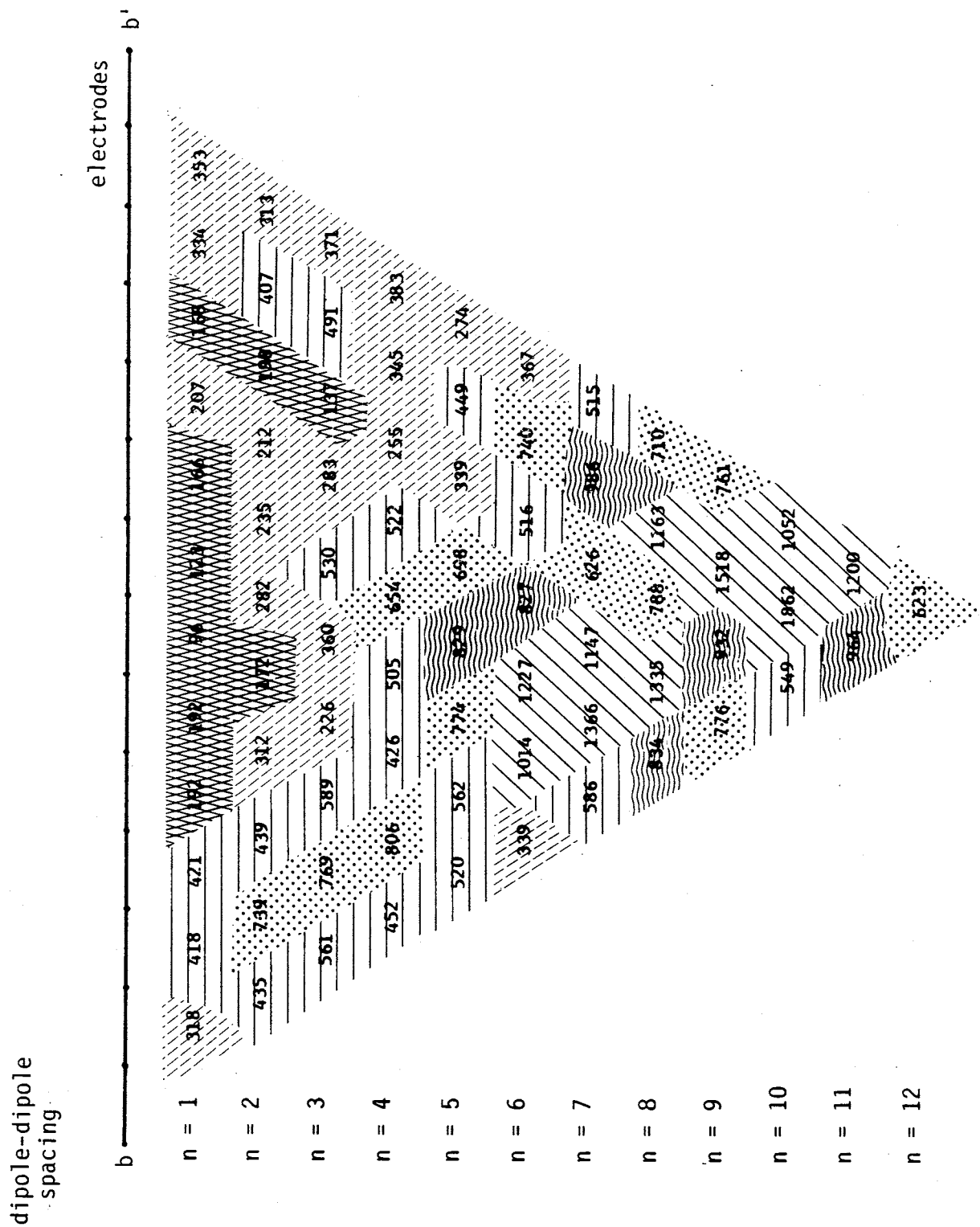


Figure 28 Pre-infiltration pseudosection conducted along the b - b' line, western boundary of the infiltration area on 7/2/86. All resistivity values are in ohm feet.

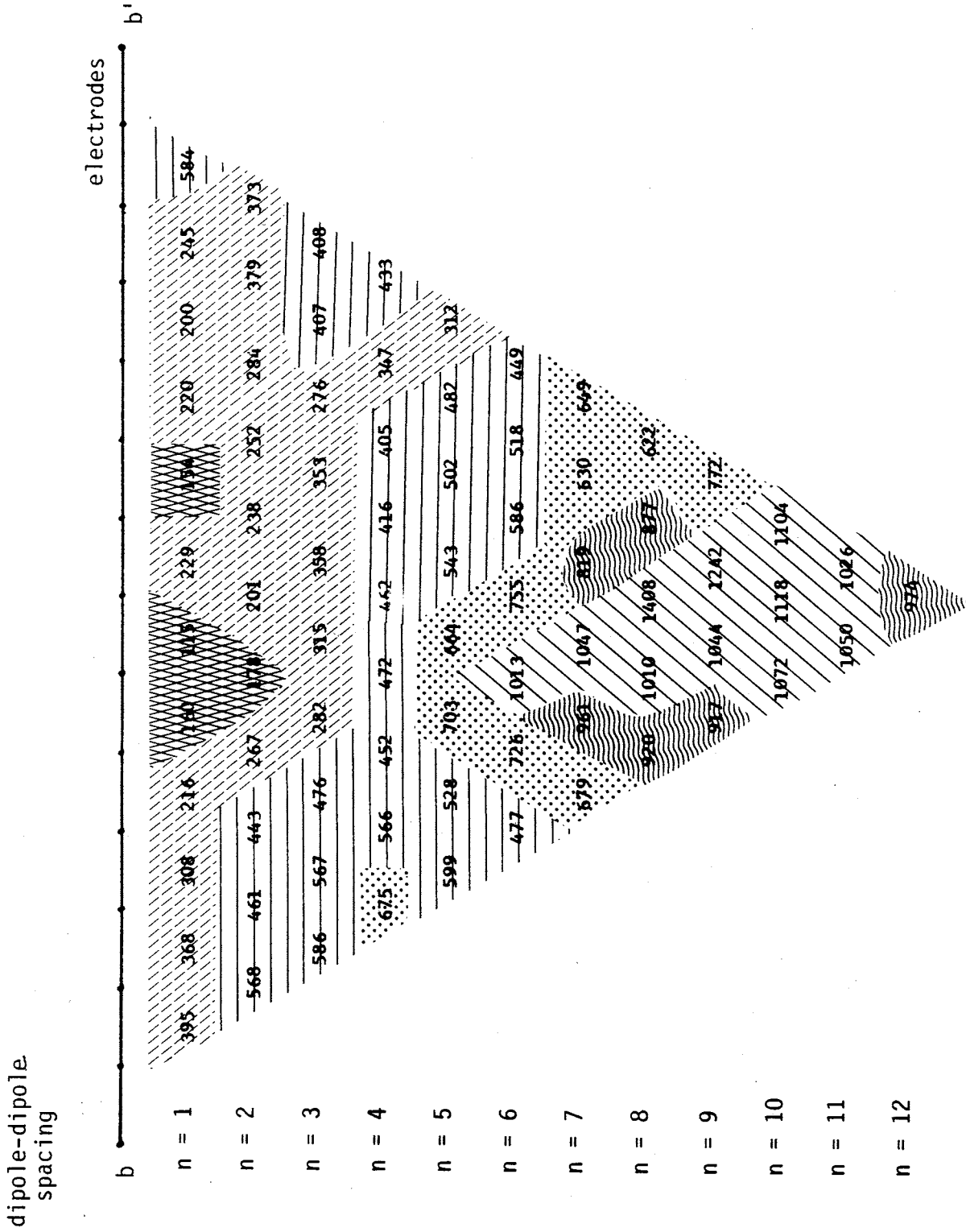


Figure 29 Post-infiltration pseudosection conducted along the b - b' line, western boundary of the infiltration area on 4/12/87. All resistivity values are in ohm feet.

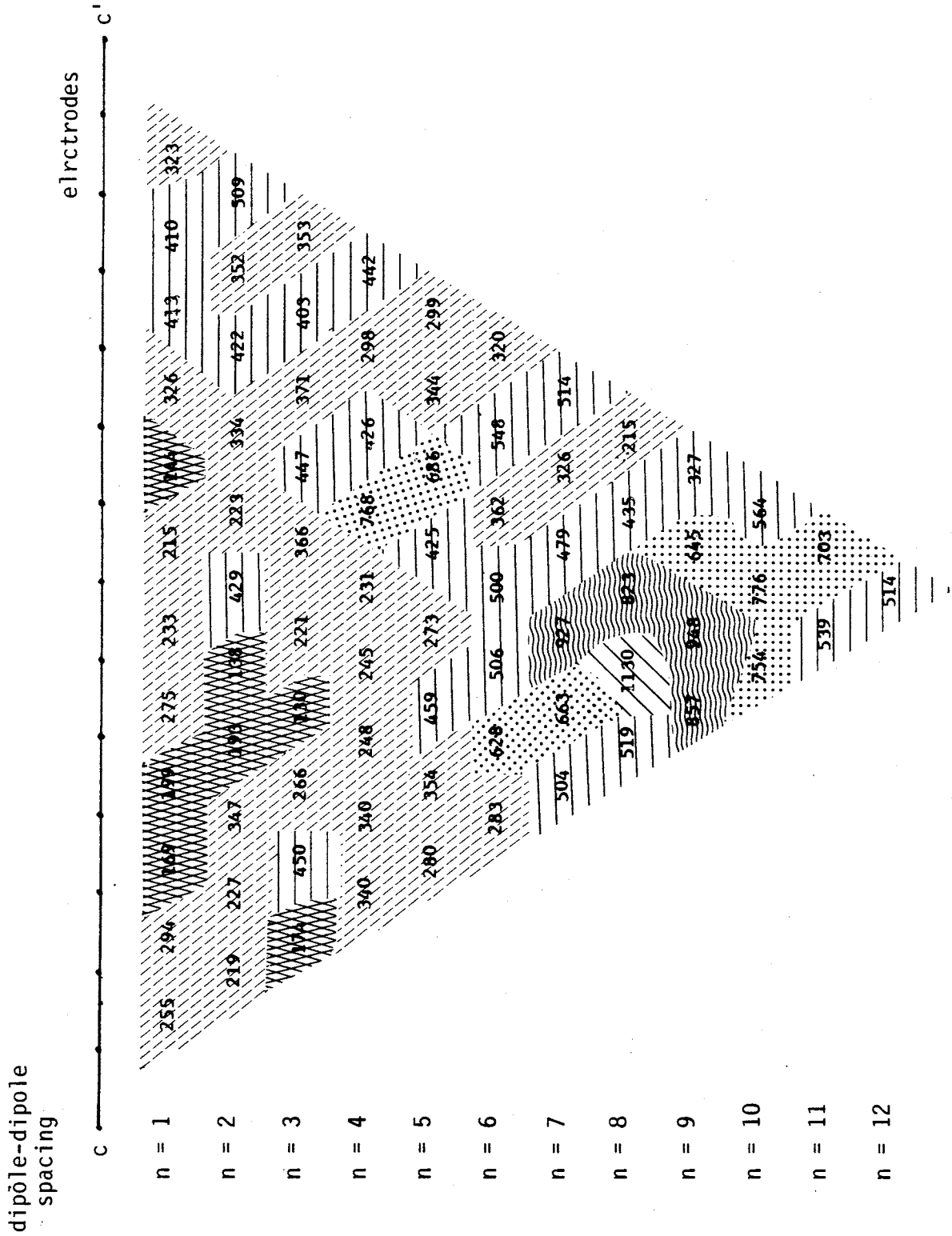


Figure 30 Pre-infiltration pseudosection conducted along the c - c' line, eastern boundary of the infiltration area on 7/5/86. All resistivity values are in ohm feet.

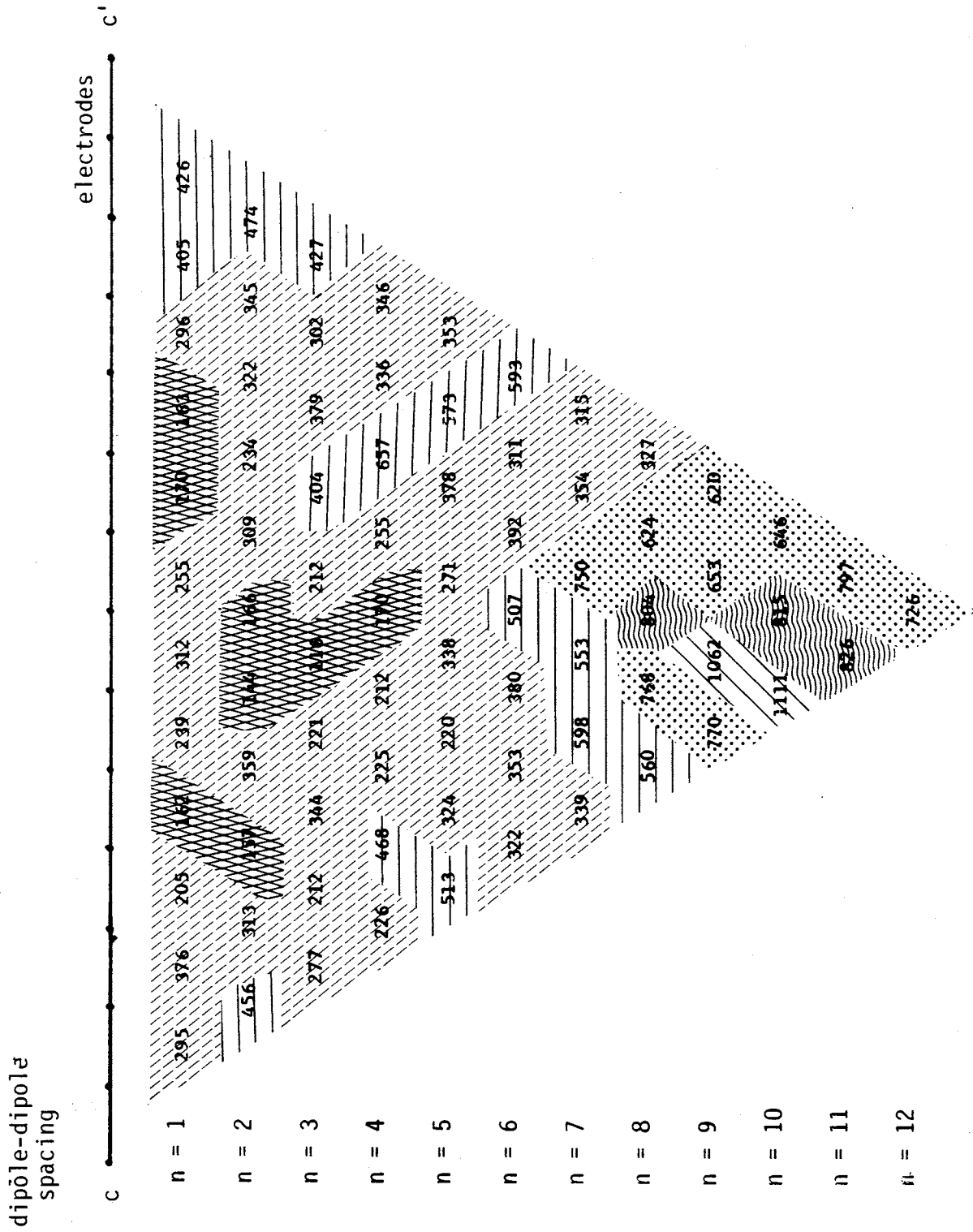


Figure 31 Post-infiltration pseudosection conducted along the c - c' line, eastern boundary of the infiltration area on 5/27/87. All resistivity values are in ohm feet.

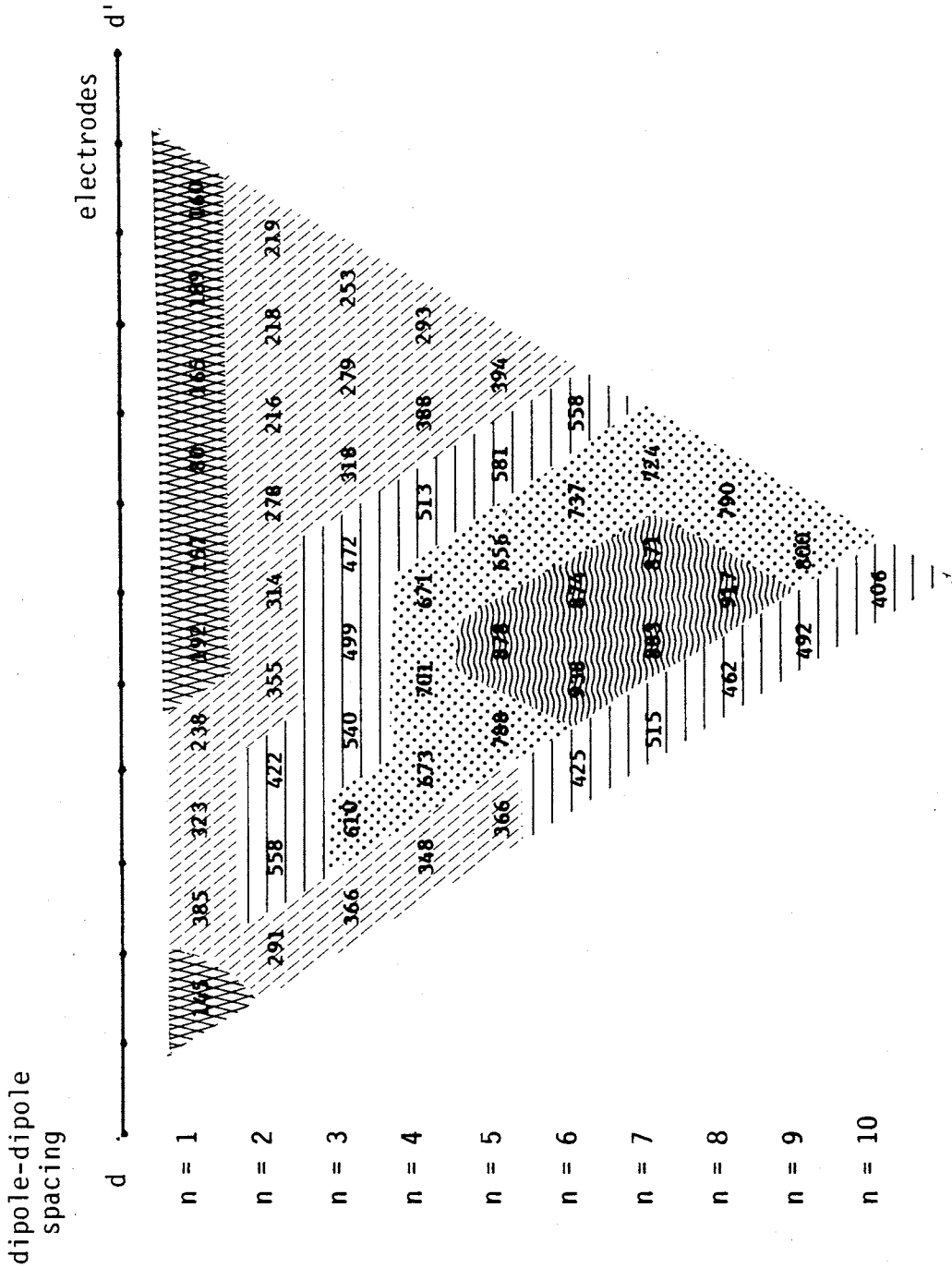


Figure 32 Pre-infiltration pseudosection conducted along the d - d' line, northern boundary of the infiltration area on 8/11/86. All resistivity values are in ohm feet.

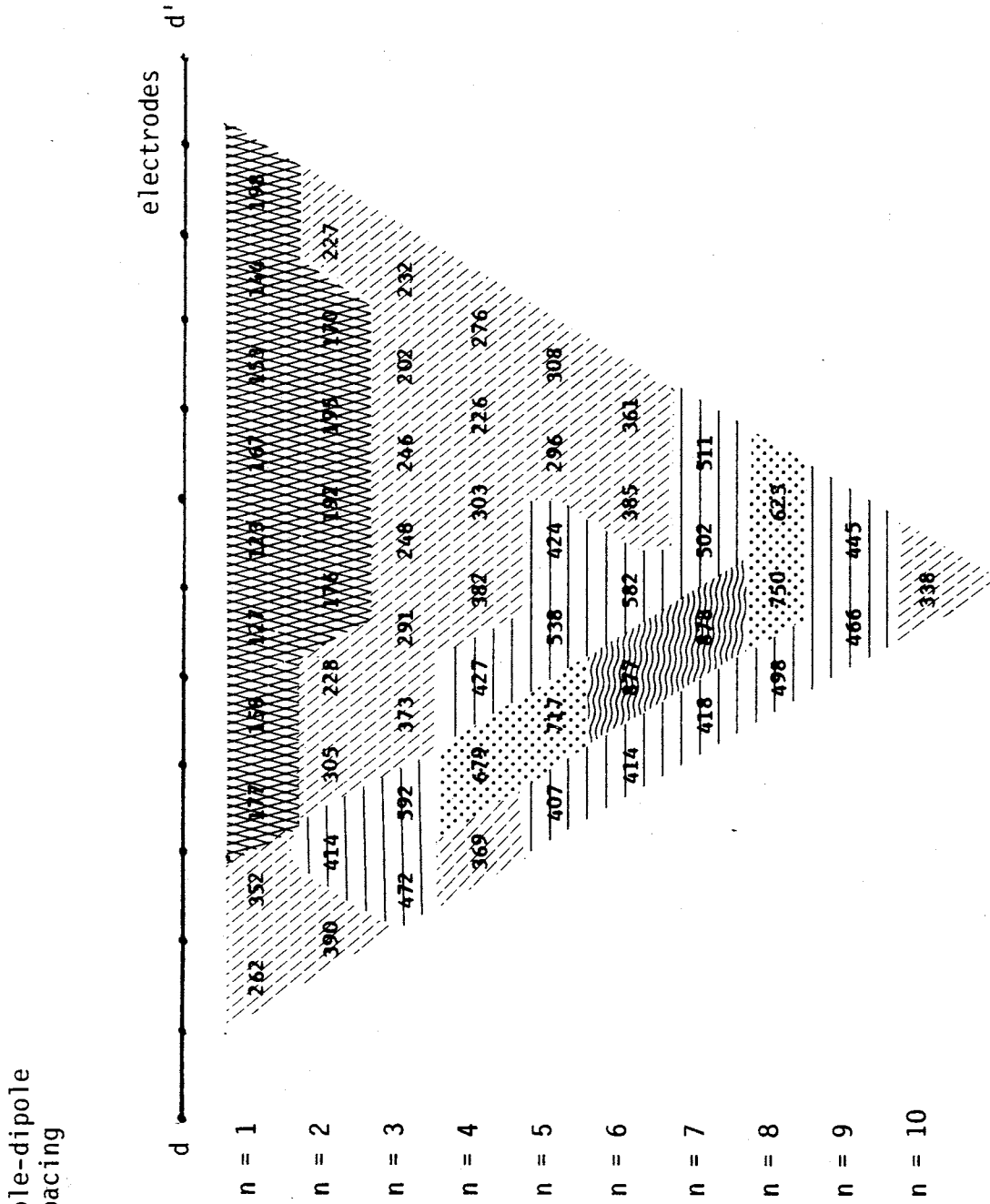


Figure 33 Post-infiltration pseudosection conducted along the d - d' line, northern boundary of the infiltration area on 5/6/87. All resistivity values are in ohm feet.

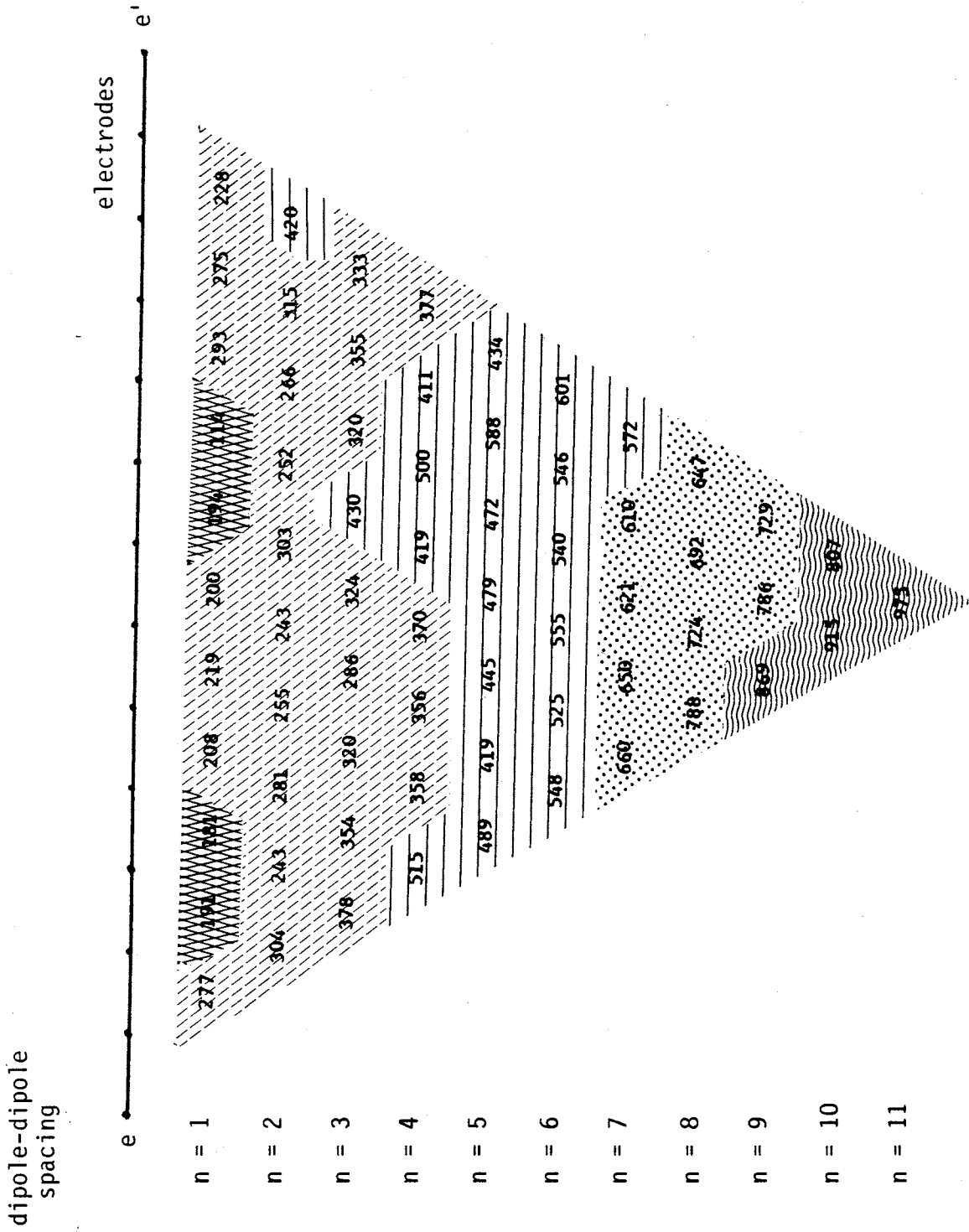


Figure 34 Pre-infiltration pseudosection conducted along the e - e' line, southern boundary of the infiltration area on 7/15/86. All resistivity values are in ohm feet.

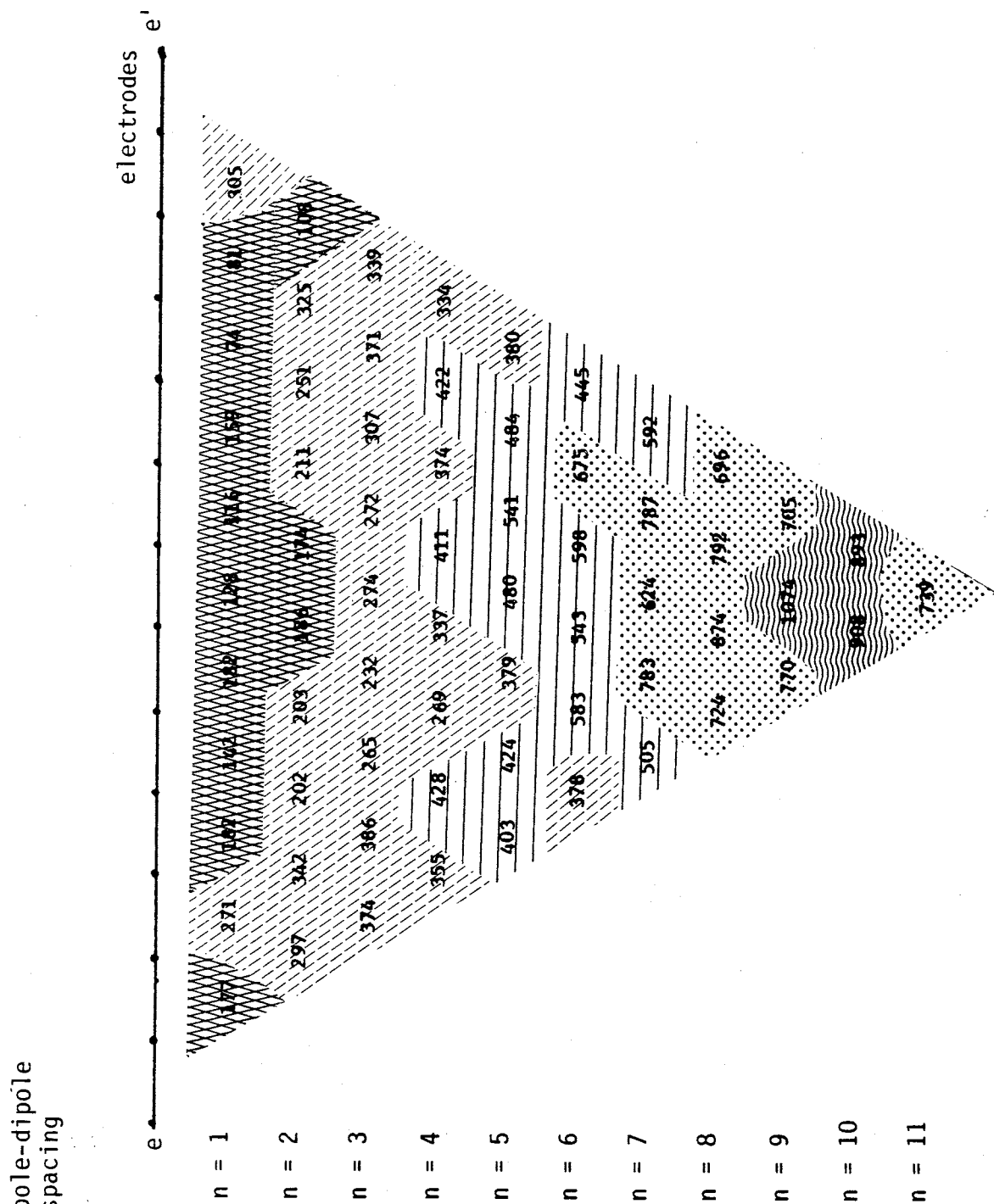
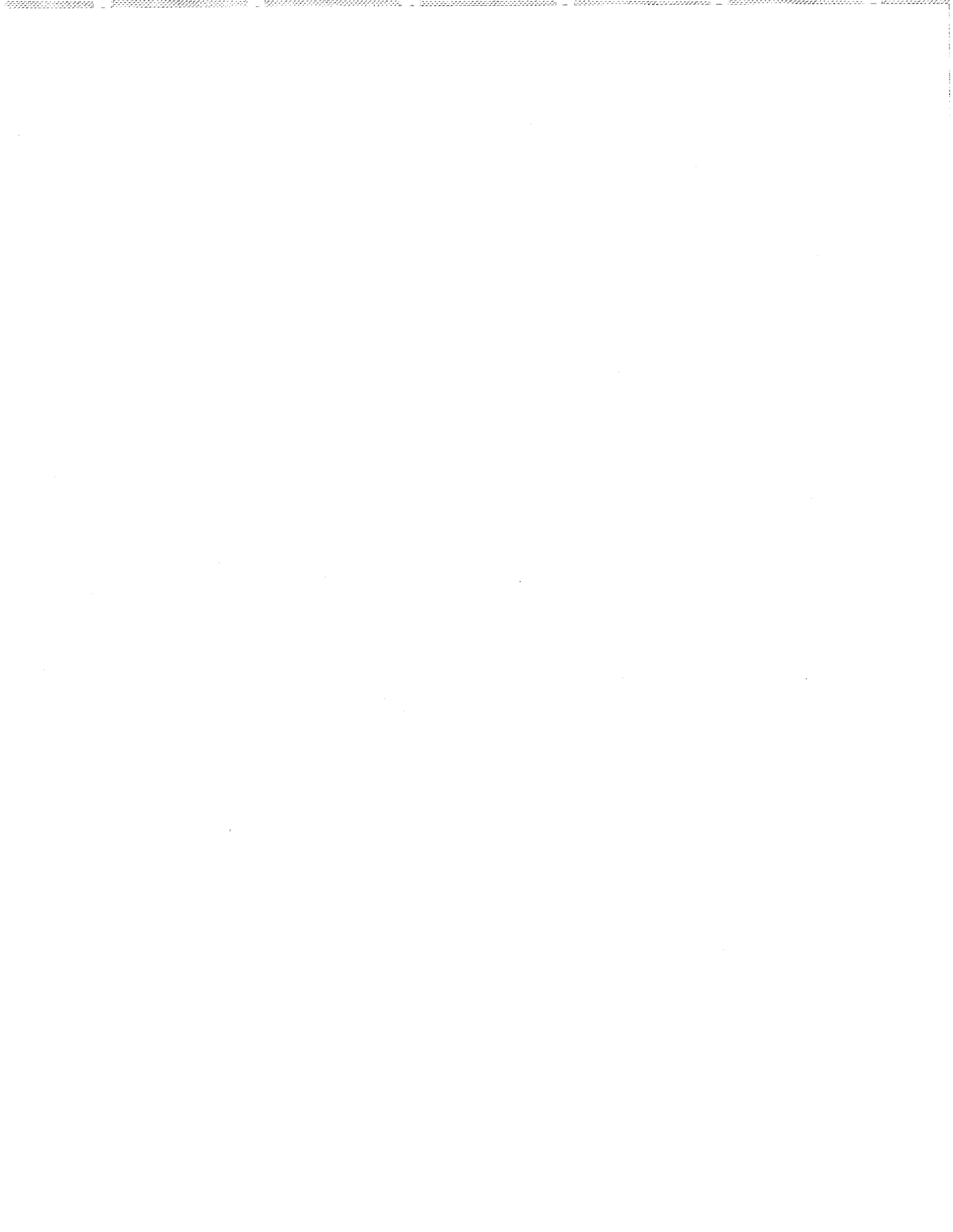


Figure 35 Post-infiltration pseudosection conducted along the e - e' line, southern boundary of the infiltration area on 5/12/87. All resistivity values are in ohm feet.



XII. TABLES

- Table 1. Sample computer output from Zohdy and Bisdorf (1975) vertical electrical sounding inversion computer code for the VES centered at 15-15.
- Table 2. Sample computer output from Zohdy and Bisdorf (1975) vertical electrical sounding inversion computer code from the VES centered at 15-11.
- Table 3. Computer program output from the Dey and Morrison (1976) finite difference computer code for the numerical model of the a-a', north-south center line pseudosection.
- Table 4. Comparison of pre- and post-infiltration moisture contents and resistivity measurements located at 15-15.
- Table 5. Comparison of pre- and post-infiltration moisture contents and resistivity measurements located at 11-15.
- Table 6. Comparison of pre- and post-infiltration moisture contents and resistivity measurements located at 19-15.
- Table 7. Comparison of pre- and post-infiltration moisture contents and resistivity measurements located at 15-19.
- Table 8. Comparison of pre- and post-infiltration moisture contents and resistivity measurements located at 15-11.



Vadose zone study

1.500000	2.500000	4.000000	6.000000	10.000000	15.000000	25.000000
40.000000	60.000000	100.000000	209.0000			
755.0000	658.0000	401.0000	445.0000	488.0000	602.0000	762.0000
833.0000	553.0000	302.0000	846.0000			

A OBS

1.500	755.000
2.500	658.000
4.000	401.000
6.000	445.000
10.000	488.000
15.000	602.000
25.000	762.000
40.000	833.000
60.000	553.000
100.000	302.000
209.000	846.000

WARNING.. SLOPE EXCEEDS +45 DEGREES

SOLUTION TO SMOOTHED VES CURVE FOLLOWS

THICKNESS	DEPTH	RESISTIVITY
0.1500	0.1500	923.2765
0.0702	0.2202	916.0632
0.1030	0.3232	916.9496
0.1512	0.4743	932.2213
0.2218	0.6962	951.6531
0.3257	1.0219	927.5509
0.4717	1.4936	722.9523
0.8534	2.3470	333.3961
1.2340	3.5810	207.1471
1.9998	5.5809	396.0750
2.9998	8.5807	1051.0790
2.9824	11.5631	1990.3113
8.9075	20.4706	1420.9041
14.1407	34.6113	549.5374
10.0480	44.6593	110.2031
23.6833	68.3426	72.1994
999999.0000	1000067.3100	11242.5830

KEY

$$\text{SUM T} = \sum_{i=1}^n h_i \rho_i = h_{1\rho_1} + h_{2\rho_2} + \dots + h_{n\rho_n}$$

the total transverse unit resistance

$$\text{SUM S} = \sum_{i=1}^n \frac{h_i}{\rho_i} = \frac{h_1}{\rho_1} + \frac{h_2}{\rho_2} + \dots + \frac{h_n}{\rho_n}$$

the total longitudinal unit conductance

where h_i = thickness and ρ_i = resistivity.

DZ DEPTH = Dar Zarrouk depth

DZ RESISTIVITY = Dar Zarrouk resistivity

Table 1 Sample computer output from Zohdy and Bisdorf (1975) numerical inversion of Wenner VES centered at borehole 15-15 (see Figure 1). Inverted geoelectrical model is presented under columns labeled reduced thickness, depth, and resistivity (see Figure 15). Inverted curve presented under columns A and smoothed VES (see Figure 13).

A	CALC. VES	SMOOTHED VES	DZ DEPTH	DZ RESISTIVITY	SUM T	SUM S
0.15000	922.45166	922.62451	0.15000	923.27649	138.49149	0.00016
0.22017	921.82098	922.24286	0.22017	920.97144	202.77039	0.00024
0.32317	920.27667	920.36194	0.32317	919.68774	297.21136	0.00035
0.47434	913.96338	913.05823	0.47434	923.66376	438.13248	0.00051
0.69624	892.30341	890.69318	0.69624	932.49213	649.23706	0.00075
1.02194	837.76318	837.82788	1.02194	930.91449	951.33765	0.00110
1.50000	735.48376	737.77063	1.50000	859.28980	1292.38245	0.00175
2.50000	551.59961	551.00848	2.50000	604.87073	1576.90417	0.00431
4.00000	439.58380	438.73584	4.00000	422.47107	1832.53149	0.01027
6.00000	451.80920	451.38541	6.00000	413.95557	2624.60962	0.01532
10.00000	577.61407	573.63934	10.00000	563.88733	5777.63525	0.01817
15.00000	695.94897	694.78754	15.00000	771.71063	11713.56738	0.01967
25.00000	769.57990	776.41693	25.00000	969.31219	24370.28906	0.02594
40.00000	686.62482	688.22321	40.00000	788.70032	32141.14844	0.05167
60.00000	520.19342	512.12970	60.00000	482.44794	33248.46875	0.14285
100.00000	380.09064	371.97528	100.00000	272.47314	34958.38672	0.47087
209.00000	574.74512	563.28259	209.00000	11212.96000	89.41831	
					11242606592.00000	

Table 1 cont.

REDUCED DZ RESISTIVITY

915.44550
604.87073
408.34164
517.50977
971.03687
788.70032
482.44794
272.47369
11242.58300

REDUCED RESISTIVITY

915.44550
333.39609
207.14714
678.01532
1511.18823
549.53735
110.20327
72.19923
11242.88090

REDUCED DZ DEPTH

1.38261
2.60701
4.59002
8.88120
25.05507
40.75204
68.91618
128.29999
1000000.00000

REDUCED THICKNESS

1.38261
0.93341
1.43566
4.01438
13.05812
14.21515
10.04801
23.68309
99997352.00000

REDUCED DEPTH

1.38261
2.31603
3.75168
7.76606
20.82419
35.03934
45.08734
68.77043
99997424.00000

SMOOTHED VES

922.62451
922.24286
920.36194
913.05823
890.69318
837.82788
737.77063
551.00848
438.73584
451.38541
573.63934
694.78754
776.41693
688.22321
512.12970
371.97528
563.28259

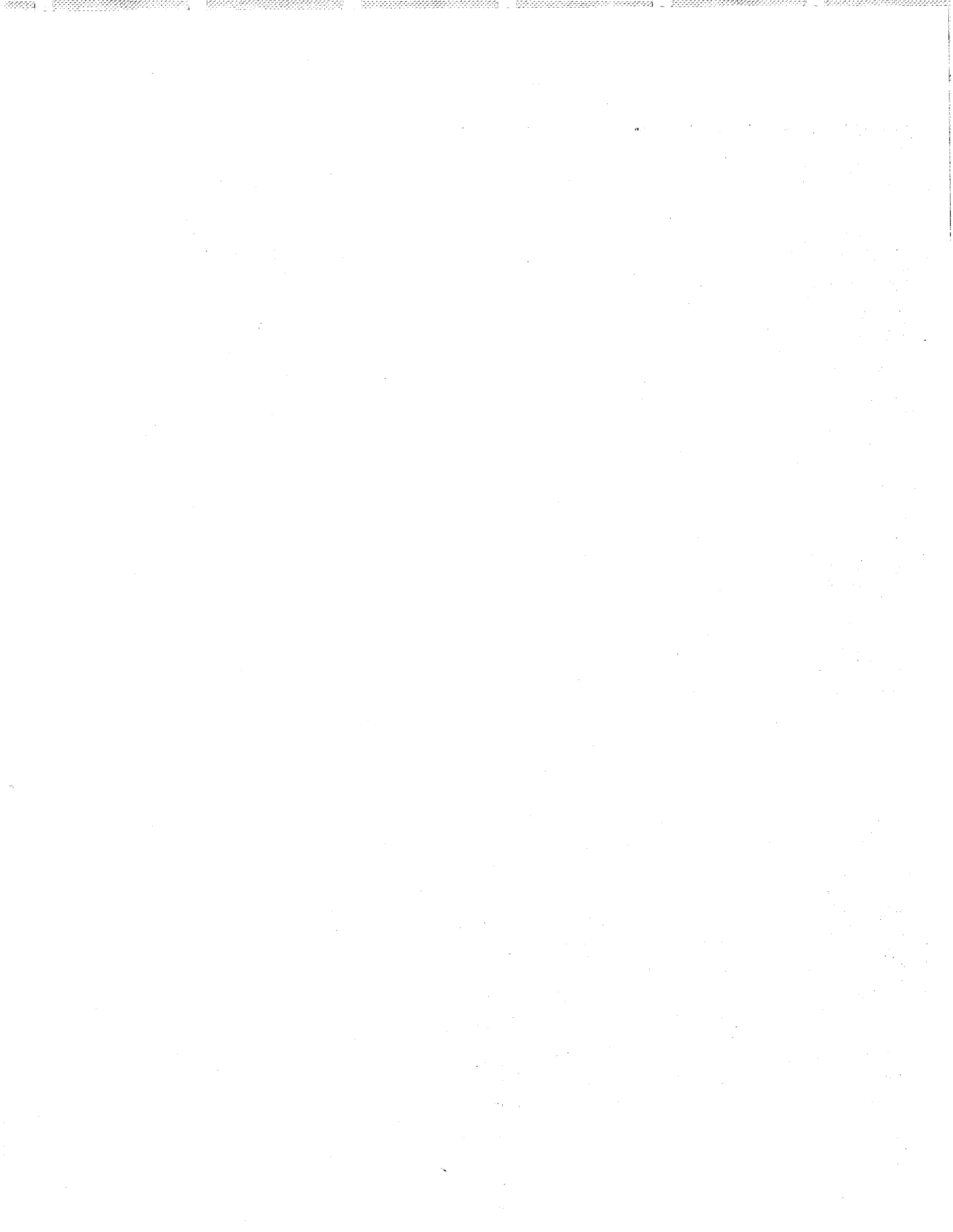
CALC. VES

915.39984
915.06909
913.38178
906.53314
885.50867
834.97040
738.75366
559.97546
451.18668
465.22134
586.31952
698.33826
767.82715
684.59271
518.81458
379.63000
574.76306

A

0.15000
0.22017
0.32317
0.47434
0.69624
1.02194
1.50000
2.50000
4.00000
6.00000
10.00000
15.00000
25.00000
40.00000
60.00000
100.00000
209.00000

Table 1 cont.



Vadose zone study

1.000000	3.000000	6.000000	8.000000	10.000000	20.000000	40.000000
60.000000	80.000000	120.000000	145.000000			
146.000000	197.000000	226.000000	281.000000	305.000000	152.000000	397.000000
448.000000	498.000000	383.000000	292.000000			

A OBS

1.000	146.000
3.000	197.000
6.000	226.000
8.000	281.000
10.000	305.000
20.000	152.000
40.000	397.000
60.000	448.000
80.000	498.000
120.000	383.000
145.000	292.000

WARNING.. SLOPE EXCEEDS +45 DEGREES

SOLUTION TO SMOOTHED VES CURVE FOLLOWS

THICKNESS	DEPTH	RESISTIVITY
0.1000	0.1000	145.9484
0.0468	0.1468	146.4527
0.0687	0.2154	146.4029
0.1008	0.3162	145.5580
0.1479	0.4642	144.1169
0.2171	0.6813	146.4470
0.3175	0.9988	161.6219
1.9377	2.9365	232.3602
2.8490	5.7855	315.2499
1.9760	7.7614	299.0345
1.9874	9.7489	227.5016
9.6069	19.3557	152.4194
15.3792	34.7349	541.3904
13.2145	47.9494	958.5333
19.5307	67.4802	533.9683
37.0088	104.4890	236.2800
999999.0000	1000103.5000	80.6989

KEY

$$\text{SUM T} = \sum_{i=1}^n h_i \rho_i = h_{1\rho_1} + h_{2\rho_2} + \dots + h_{n\rho_n}$$

the total transverse unit resistance

$$\text{SUM S} = \sum_{i=1}^n \frac{h_i}{\rho_i} = \frac{h_1}{\rho_1} + \frac{h_2}{\rho_2} + \dots + \frac{h_n}{\rho_n}$$

the total longitudinal unit conductance

where h_i = thickness and ρ_i = resistivity.

DZ DEPTH = Dar Zarrouk depth

DZ RESISTIVITY = Dar Zarrouk resistivity

Table 2 Sample computer output from Zohdy and Bisdorf (1975) numerical inversion of Wenner VES centered at borehole 15-11 (see Figure 1). Inverted geoelectrical model is presented under columns labeled reduced thickness, depth, and resistivity (see Figure 16). Inverted curve is presented under columns A and smoothed VES (see Figure 14).

A	CALC. VES	SMOOTHED VES	DZ RESISTIVITY	SUM T	SUM S
0.10000	146.01253	146.00406	145.94836	14.59484	0.00069
0.14678	146.06941	146.03206	146.10892	21.44586	0.00100
0.21544	146.20755	146.17368	146.20256	31.49839	0.00147
0.31623	146.71997	146.74802	145.99683	46.16826	0.00217
0.46416	148.42612	148.51788	145.39505	67.48659	0.00319
0.68129	152.83685	152.91753	145.72951	99.28453	0.00468
1.00000	161.79558	161.84911	150.60695	150.60713	0.00664
3.00000	211.72034	211.07512	200.28174	600.84540	0.01498
6.00000	242.46288	243.06729	249.83179	1498.99084	0.02402
8.00000	248.62408	250.53908	261.23358	2089.86865	0.03062
10.00000	249.77443	251.71555	254.13374	2542.00586	0.03936
20.00000	253.34773	249.42856	197.80814	4006.28003	0.10239
40.00000	310.77585	310.48364	307.06290	12332.42090	0.13080
60.00000	349.97806	353.07117	415.81876	24998.98047	0.14458
80.00000	357.98883	361.33197	442.22424	35427.77734	0.18116
120.00000	323.29242	324.10248	361.61917	44172.21875	0.33779
145.00000	289.35214	288.30481	80.71987	80742976.00000	12392.07031
DZ DEPTH					
0.10000					
0.14678					
0.21544					
0.31623					
0.46416					
0.68129					
1.00000					
3.00000					
6.00000					
8.00000					
10.00000					
20.00000					
40.00000					
60.00000					
80.00000					
120.00000					
145.00000					

Table 2 cont.

REDUCED DZ RESISTIVITY

146.56041
 257.67117
 197.55072
 444.43237
 361.59711
 80.69888

REDUCED DZ DEPTH

1.07844
 9.71646
 20.35733
 79.40022
 122.16975
 10000000.00000

REDUCED RESISTIVITY

146.56041
 277.99960
 152.41939
 643.07105
 236.28003
 80.69867

REDUCED DEPTH

1.07844
 9.51584
 19.47491
 68.09538
 105.71263
 99999816.00000

REDUCED THICKNESS

1.07844
 8.43740
 9.95907
 48.62047
 37.61724
 99999712.00000

SMOOTHED VES

146.00406
 146.03206
 146.17368
 146.74802
 148.51788
 152.91753
 161.84911
 211.07512
 243.06729
 250.53908
 251.71555
 249.42856
 310.48364
 353.07117
 361.33197
 324.10248
 288.30481

CALC. VES

146.56207
 146.57841
 146.67230
 147.09892
 148.59267
 152.66092
 161.73022
 218.33641
 245.85921
 249.42548
 249.28435
 253.97179
 313.00848
 350.97144
 357.95535
 322.56552
 288.62384

A

0.10000
 0.14678
 0.21544
 0.31623
 0.46416
 0.68129
 1.00000
 3.00000
 6.00000
 8.00000
 10.00000
 20.00000
 40.00000
 60.00000
 80.00000
 120.00000
 145.00000

Table 2 cont.



```

RESISTIVITY MODEL      (model input)
33333333333300000000000000111111111155555555555555
55555555555544400000000000111111111155555555555
44444444444444440022222222222222222222222222555
3333333444444444444400222222222222222222222222555
333333333444444444444444444400000055555522222227777
333333344444444444444444444444440088888877777777777
444444444444444444444444444444444444444444444444
7777777776666666666666666666666666666666666666666
7777777777666666666666666666666666666666666666666
7777777777766666666666666666666666666666666666666
8888888888888888888888888888888888888888888888888
8888888888888888888888888888888888888888888888888
8888888888888888888888888888888888888888888888888
8888888888888888888888888888888888888888888888888
8888888888888888888888888888888888888888888888888

```

resistivity key

```

0= 100.0  1= 200.0  2= 300.0  3= 250.0  4= 400.0
5= 850.0  6=2000.0  7=6000.0  8=*****  9= 50.0

```

Table 3 Sample computer program input and output from the Dey and Morrison (1976) finite difference computer code for the numerical model of the a - a' pre-infiltration pseudosection. Resistivity model is a coded capacitance matrix of inputted resistivity values (ohm feet). Resistivity key correlates number code to resistivity values (number 8 = 10000 ohm feet). The resulting numerically generated pseudosection corresponds to inputted capacitance matrix. (See p. 98).

CASE	(model pseudosection output)	DIPOLE-DIPOLE CONFIGURATION OF ELECTRODES										
1	440.1	472.3	291.7	193.2	121.4	117.1	145.3	189.0	210.0	304.7	264.6	642.7
2	484.6	316.1	274.0	238.4	127.5	166.0	228.5	194.6	350.7	396.6	362.3	
3	309.5	278.1	299.2	243.5	192.7	235.0	211.1	325.2	514.4	598.0		
4	276.8	299.0	298.9	381.5	266.3	202.9	342.5	465.0	764.3			
5	303.5	308.3	473.0	516.8	226.4	327.1	479.2	670.9				
6	321.4	492.8	617.9	430.0	369.0	450.6	676.2					
7	516.0	627.0	500.0	705.3	509.2	630.0						
8	643.2	497.4	813.7	972.4	715.8							
9	502.7	806.1	1110.1	1369.5								
10		813.7	1091.9	1552.2								
11		1097.2	1519.5									
12			1531.5									

Depth from surface (ft)	Dipole spacing	10/3/86		10/3/86		Resistivity with st dv (ohm ft)	Percent moisture content by volume of rock	Percent saturation	Resistivity with st dv (ohm ft)	6/10/87	6/10/87	Resistivity with st dv (ohm ft)	6/8/87
		Percent moisture content by volume of rock	Percent saturation	Percent moisture content by volume of rock	Percent saturation								
1		18.6	42.8										
2		15.4	35.4										
3		15.4	35.4										
4	n = 1	13.7	31.5	82+/-3	105+/-1		20.2	46.5				126+/-3	146+/-5
5		13.1	30.1										
6	n = 2	13.5	31.1	102+/-3	179+/-4	174+/-5	16.1	37.0	118+/-3	104+/-4			197+/-4
7		14.2	32.9										
8	n = 3	13.0	29.9	208+/-4	223+/-2		13.8	31.7	95+/-2			178+/-6	
9		9.7	22.3										
10	n = 4	6.8	15.6	535+/-20	251+/-2	243+/-7	16.8	38.7	262+/-8	171+/-4			193+/-9
11		6.2	14.3										
12	n = 5	6.6	15.2	594+/-4	258+/-8		14.9	34.3	457+/-10			179+/-3	
13		5.6	15.5										
14	n = 6	5.0	13.8	689+/-14	572+/-9	606+/-3	14.2	39.4	701+/-15	487+/-19			468+/-9
15		6.4	17.7										
16	n = 7	5.2	14.4	643+/-9	1311+/-39		12.9	35.8	677+/-13	1210+/-29			
17		6.1	16.9										
18	n = 8	5.2	14.4	563+/-15	1462+/-24	1004+/-30	12.5	34.7	533+/-8	1780+/-6			908+/-18
19		3.8	10.5										
20	n = 9	3.4	9.4	1290+/-22	1119+/-32		10.5	29.1	1334+/-14	1299+/-48			
21		4.0	11.1										
22	n = 10	4.1	11.3	1314+/-18	1073+/-29	1325+/-33	8.9	24.7	1624+/-17	1009+/-63			1182+/-45
23		3.4	9.4										
24	n = 11	4.4	12.2	921+/-47	1106+/-64		10.4	28.8	1166+/-52	860+/-42			
25		3.2	8.8										
26	n = 12			1069+/-79			9.6	26.6	1030+/-12				

Table 4 Comparison of pre- and post-infiltration moisture contents and resistivity measurements at borehole 15-15 (see Figure 1). Depth from surface corresponds to actual depth for percent moisture content and depth of investigation for resistivity measurements. (st dv = standard deviation)



Depth from surface (ft)	Dipole-dipole spacing	Percent moisture content by volume of rock	Resistivity with st dv (ohm ft)	Percent moisture content by volume of rock	Resistivity with st dv (ohm ft)	Percent moisture saturation	Resistivity with st dv (ohm ft)
1							
1.5							
2							
2.5							
3							
3.5							
4	n = 1	25.2	96+/-0	19.2	115+/-7	44.2	229+/-6
4.5		27.0		25.2		58.0	
5		24.9		26.7		61.5	
5.5		23.9		24.6		56.6	
6	n = 2	22.5	172+/-5	23.9	178+/-2	55.0	201+/-8
6.5		20.3	282+/-6	22.2		51.1	
7		20.5		21.0		48.3	238+/-32
7.5							
8	n = 3		360+/-17		530+/-10		315+/-4
8.5							358+/-12
9							
9.5	n = 4		505+/-8		522+/-17		462+/-23
10			654+/-38			472+/-38	416+/-14

100

Table 5 Comparison of pre- and post-infiltration moisture contents and resistivity measurements at borehole 11-15 (see Figure 1). Depth from surface corresponds to actual depth for percent moisture content and depth of investigation for resistivity measurements. (st dv = standard deviation)



Depth from surface (ft)	Dipole-dipole spacing	Percent moisture content by volume of rock	Percent moisture saturation	Resistivity with st dv (ohm ft)	Percent moisture content by volume of rock	Percent moisture saturation	Resistivity with st dv (ohm ft)
1							
1.5							
2							
2.5							
3		15.3	35.2		15.9	36.6	
3.5		17.6	40.5		18.4	42.3	
4	n = 1	19.3	44.4	233+/-5	18.5	42.6	312+/-6
4.5					16.8	38.7	
5							
5.5							
6	n = 2			429+/-76			166+/-3
6.5							
7							
7.5							
8	n = 3			221+/-26			116+/-4
8.5							
9							
9.5							
10	n = 4			245+/-3	768+/-47		170+/-4
							212+/-7
							255+/-3

Table 6 Comparison of pre- and post-infiltration moisture contents and resistivity measurements at borehole 19-15 (see Figure 1). Depth from surface corresponds to actual depth for percent moisture content and depth of investigation for resistivity measurements. (st dv = standard deviation).

Depth from surface (ft)	Dipole-dipole spacing	Percent moisture content by volume of rock	Percent saturation	Resistivity with st dv (ohm ft)	Percent moisture content by volume of rock	Percent saturation	Resistivity with st dv (ohm ft)
1							
1.5							
2							
2.5							
3							
3.5							
4	n = 1	21.5	49.5	192+/-3	157+/-2		123+/-0
4.5		22.5	51.8				
5		19.6	45.1				
5.5		18.1	41.7				
6	n = 2	19.9	45.8	355+/-1	278+/-4	228+/-2	176+/-11
6.5		19.8	45.3				
7		19.7	45.3				
7.5		18.2	41.9				
8	n = 3	18.5	42.6	499+/-9	472+/-16	291+/-18	248+/-19
8.5		21.9	50.4				
9							
9.5							
10	n = 4			701+/-23	671+/-15	513+/-3	382+/-4
						427+/-8	303+/-6

Table 7 Comparison of pre- and post-infiltration moisture contents and resistivity measurements at borehole 15-19 (see Figure 1). Depth from surface corresponds to actual depth for percent moisture content and depth of investigation for resistivity measurements. (st dv = standard deviation).

Depth from surface (ft)	Dipole-dipole spacing	Percent moisture content by volume of rock	Percent moisture saturation	Resistivity with st dv (ohm ft)	Percent moisture content by volume of rock	Percent moisture saturation	Resistivity with st dv (ohm ft)
1							
1.5							
2							
2.5							
3		18.2	41.9		23.7	54.6	
3.5		21.7	50.0		24.1	55.5	
4	n = 1	19.6	45.1	219+/-3	22.1	50.9	182+/-6
4.5		19.5	44.9		20.4	47.0	116+/-1
5		17.7	40.7		19.3	44.4	
5.5	n = 2	16.1	37.0				
6				243+/-3			186+/-3
6.5							
7							
7.5							
8	n = 3			286+/-6			274+/-9
8.5							272+/-9
9							
9.5	n = 4			370+/-2			441+/-9
10							

Table 8 Comparison of pre- and post-infiltration moisture contents and resistivity measurements at borehole 15-11 (see Figure 1). Depth from surface corresponds to actual depth for percent moisture content and depth of investigation for resistivity measurements. (st dv = standard deviation).



Appendix A



Pre-infiltration a - a' pseudosection continued

Row 9

Location	Resistivity (ohm ft)	Standard Deviation (ohm ft)	Location	Resistivity (ohm ft)	Standard Deviation (ohm ft)
1	660.00	16.20	1	1314.00	18.00
2	1290.75	22.02	2	1073.00	29.00
3	1119.25	31.99	3	1325.00	33.00
4	1208.00	32.22			

Row 10

Location	Resistivity (ohm ft)	Standard Deviation (ohm ft)	Location	Resistivity (ohm ft)	Standard Deviation (ohm ft)
1	921.00	47.00	1	1069.00	79.00
2	1106.00	64.00			

Row 11

Location	Resistivity (ohm ft)	Standard Deviation (ohm ft)
1	921.00	47.00
2	1106.00	64.00

Row 12

Location	Resistivity (ohm ft)	Standard Deviation (ohm ft)
1	1069.00	79.00

Post-infiltration a - a' pseudosection continued

Row 9

Location	Resistivity (ohm ft)	Standard Deviation (ohm ft)	Location	Resistivity (ohm ft)	Standard Deviation (ohm ft)
1	655.50	28.27	1	1624.00	16.67
2	1334.50	13.81	2	1009.00	62.74
3	1299.25	48.05	3	1181.50	45.28
4	828.00	32.01			

Row 10

Row 11

Location	Resistivity (ohm ft)	Standard Deviation (ohm ft)	Location	Resistivity (ohm ft)	Standard Deviation (ohm ft)
1	1165.50	51.69	1	1030.00	12.26
2	859.50	42.08			

Row 12

Pre-infiltration b - b' pseudosection
 Conducted along the western boundary of the infiltration area
 7/2/86

Row 1	Row 2	Row 3	Row 4
Location	Location	Location	Location
Resistivity (ohm ft)	Resistivity (ohm ft)	Resistivity (ohm ft)	Resistivity (ohm ft)
Standard Deviation (ohm ft)	Standard Deviation (ohm ft)	Standard Deviation (ohm ft)	Standard Deviation (ohm ft)
1 318.50	1 435.50	1 560.00	1 452.00
2 418.50	2 739.25	2 769.00	2 806.00
3 421.25	3 438.75	3 588.75	3 426.00
4 192.00	4 311.50	4 226.25	4 505.00
5 192.00	5 172.25	5 359.75	5 654.50
6 96.00	6 281.50	6 530.00	6 522.00
7 123.00	7 235.00	7 283.00	7 254.00
8 165.50	8 212.50	8 183.00	8 345.00
9 207.00	9 198.50	9 490.00	9 383.00
10 168.50	10 407.00	10 370.00	
11 333.00			
12 353.00			

Row 5	Row 6	Row 7	Row 8
Location	Location	Location	Location
Resistivity (ohm ft)	Resistivity (ohm ft)	Resistivity (ohm ft)	Resistivity (ohm ft)
Standard Deviation (ohm ft)	Standard Deviation (ohm ft)	Standard Deviation (ohm ft)	Standard Deviation (ohm ft)
1 519.00	1 338.75	1 586.00	1 834.00
2 562.00	2 1012.00	2 1368.00	2 1334.75
3 774.00	3 1226.75	3 1147.00	3 787.00
4 828.00	4 827.00	4 625.00	4 1163.00
5 698.00	5 516.00	5 986.00	5 710.00
6 399.00	6 739.75	6 515.00	
7 449.00			
8 274.00			

Pre-infiltration b - b' pseudosection continued

Row 9				Row 10				
Location	Resistivity (ohm ft)	Standard Deviation (ohm ft)	Location	Resistivity (ohm ft)	Standard Deviation (ohm ft)	Location	Resistivity (ohm ft)	Standard Deviation (ohm ft)
1	777.00	57.60	1	549.00	49.90			
2	933.00	58.00	2	1862.00	66.31			
3	1518.50	53.11	3	1052.50	22.68			
4	762.00	9.52						

Row 11				Row 12				
Location	Resistivity (ohm ft)	Standard Deviation (ohm ft)	Location	Resistivity (ohm ft)	Standard Deviation (ohm ft)	Location	Resistivity (ohm ft)	Standard Deviation (ohm ft)
1	964.00	30.90	1	623.00	29.92			
2	1200.00	58.72						

Post-infiltration b - b' pseudosection
 Conducted along the western boundary of the infiltration area
 4/12/87

ROW 1				ROW 2				ROW 3				ROW 4			
Location	Resistivity (ohm ft)	Standard Deviation (ohm ft)	Location	Resistivity (ohm ft)	Standard Deviation (ohm ft)	Location	Resistivity (ohm ft)	Standard Deviation (ohm ft)	Location	Resistivity (ohm ft)	Standard Deviation (ohm ft)	Location	Resistivity (ohm ft)	Standard Deviation (ohm ft)	
1	395.00	6.42	1	567.50	7.88	1	586.00	12.87	1	675.00	9.66	2	566.00	19.45	
2	368.00	7.49	2	460.75	10.40	2	567.00	3.76	2	566.00	19.45	3	451.50	12.69	
3	308.00	11.43	3	443.00	5.93	3	475.00	12.53	3	451.50	12.69	4	472.75	38.16	
4	216.00	3.20	4	266.00	8.34	4	281.50	13.68	4	472.75	38.16	5	462.00	22.87	
5	160.50	2.06	5	178.00	1.65	5	315.00	4.26	5	462.00	22.87	6	416.00	13.53	
6	115.00	7.15	6	200.75	7.94	6	358.00	12.42	6	416.00	13.53	7	405.00	9.93	
7	229.00	6.20	7	238.00	32.00	7	353.00	17.38	7	405.00	9.93	8	346.00	10.82	
8	154.00	3.67	8	251.00	7.76	8	275.00	15.36	8	346.00	10.82	9	433.00	10.08	
9	220.00	11.41	9	284.00	9.78	9	407.00	14.53	9	433.00	10.08				
10	200.00	4.96	10	379.00	10.52	10	408.00	27.21							
11	245.00	7.69	11	312.00	18.22										
12	584.00	14.31													

ROW 5				ROW 6				ROW 7				ROW 8			
Location	Resistivity (ohm ft)	Standard Deviation (ohm ft)	Location	Resistivity (ohm ft)	Standard Deviation (ohm ft)	Location	Resistivity (ohm ft)	Standard Deviation (ohm ft)	Location	Resistivity (ohm ft)	Standard Deviation (ohm ft)	Location	Resistivity (ohm ft)	Standard Deviation (ohm ft)	
1	599.00	4.20	1	477.00	6.13	1	678.75	10.91	1	919.75	5.76	2	1010.00	63.75	
2	528.00	42.39	2	726.00	48.20	2	960.75	16.51	2	1010.00	63.75	3	1155.00	24.50	
3	703.00	32.82	3	977.00	53.30	3	1047.00	10.87	3	1155.00	24.50	4	876.00	14.53	
4	664.00	8.03	4	754.00	24.00	4	819.00	18.50	4	876.00	14.53	5	622.00	12.85	
5	543.00	7.46	5	585.50	17.67	5	629.00	31.24	5	622.00	12.85				
6	501.00	23.90	6	518.00	47.60	6	643.00	55.30							
7	481.75	22.81	7	449.00	10.19										
8	331.50	8.87													

Post-infiltration b - b' pseudosection continued

Row 9				Row 10			
Location	Resistivity (ohm ft)	Standard Deviation (ohm ft)	Location	Resistivity (ohm ft)	Standard Deviation (ohm ft)	Location	Resistivity (ohm ft)
1	917.00	10.65	1	1071.75	24.23		
2	1043.50	16.19	2	1118.25	13.51		
3	1242.25	37.37	3	1104.25	39.65		
4							

Row 11				Row 12			
Location	Resistivity (ohm ft)	Standard Deviation (ohm ft)	Location	Resistivity (ohm ft)	Standard Deviation (ohm ft)	Location	Resistivity (ohm ft)
1	1050.25	51.87	1	974.25	77.93		
2	1026.00	21.80					

Pre-infiltration c - c' pseudosection
 Conducted along the eastern boundary of the infiltration area
 7/5/86

ROW 1	ROW 2	ROW 3	ROW 4
Location	Location	Location	Location
Resistivity (ohm ft)	Resistivity (ohm ft)	Resistivity (ohm ft)	Resistivity (ohm ft)
Standard Deviation (ohm ft)	Standard Deviation (ohm ft)	Standard Deviation (ohm ft)	Standard Deviation (ohm ft)
1 254.50	1 219.00	1 174.25	1 339.75
2 293.75	2 226.50	2 449.75	2 339.75
3 169.25	3 347.25	3 266.33	3 248.25
4 198.50	4 193.50	4 130.25	4 245.25
5 275.00	5 137.50	5 221.25	5 231.50
6 233.25	6 429.00	6 365.75	6 768.00
7 214.75	7 223.50	7 447.50	7 425.75
8 143.75	8 334.00	8 370.75	8 297.50
9 325.50	9 422.00	9 403.00	9 441.75
10 413.00	10 351.75		
11 410.25	11 509.25		
12 323.50			

ROW 5	ROW 6	ROW 7	ROW 8
Location	Location	Location	Location
Resistivity (ohm ft)	Resistivity (ohm ft)	Resistivity (ohm ft)	Resistivity (ohm ft)
Standard Deviation (ohm ft)	Standard Deviation (ohm ft)	Standard Deviation (ohm ft)	Standard Deviation (ohm ft)
1 279.00	1 282.75	1 504.00	1 519.00
2 354.00	2 628.00	2 663.00	2 1129.00
3 458.00	3 506.00	3 927.00	3 823.00
4 273.00	4 499.75	4 479.00	4 435.00
5 425.00	5 362.00	5 325.75	5 214.00
6 686.00	6 547.00	6 514.00	
7 343.75	7 321.00		
8 299.00			

Pre-infiltration c - c' pseudosection continued

Row 9				Row 10			
Location	Resistivity (ohm ft)	Standard Deviation (ohm ft)	Location	Resistivity (ohm ft)	Standard Deviation (ohm ft)	Location	Resistivity (ohm ft)
1	857.00	23.66	1	754.00	11.64		
2	948.00	19.59	2	776.00	19.29		
3	645.00	50.11	3	564.00	34.80		
4	327.00	46.02					

Row 11				Row 12			
Location	Resistivity (ohm ft)	Standard Deviation (ohm ft)	Location	Resistivity (ohm ft)	Standard Deviation (ohm ft)	Location	Resistivity (ohm ft)
1	539.00	41.28	1	514.00	15.72		
2	703.00	37.80					

Post-infiltration c. c' pseudosection
 Conducted along the eastern boundary of the infiltration area
 5/27/87

ROW 1		ROW 2		ROW 3		ROW 4		
Location	Resistivity (ohm ft)	Standard Deviation (ohm ft)	Location	Resistivity (ohm ft)	Standard Deviation (ohm ft)	Location	Resistivity (ohm ft)	Standard Deviation (ohm ft)
1	294.75	17.54	1	456.25	35.75	1	276.75	8.34
2	375.75	4.32	2	313.00	12.26	2	211.75	3.11
3	204.75	2.94	3	157.25	6.83	3	344.50	11.80
4	162.50	5.72	4	358.50	6.57	4	221.00	4.52
5	239.00	6.12	5	143.50	8.90	5	115.50	3.84
6	312.00	5.78	6	166.25	3.03	6	212.50	5.12
7	255.50	3.04	7	309.75	27.39	7	404.25	14.39
8	169.75	1.63	8	234.00	0.70	8	379.00	3.67
9	163.00	3.31	9	321.75	1.92	9	302.00	6.67
10	296.25	3.11	10	345.75	6.49	10	427.50	2.59
11	404.75	1.29						
12	426.25	1.92						

ROW 5		ROW 6		ROW 7		ROW 8		
Location	Resistivity (ohm ft)	Standard Deviation (ohm ft)	Location	Resistivity (ohm ft)	Standard Deviation (ohm ft)	Location	Resistivity (ohm ft)	Standard Deviation (ohm ft)
1	513.50	24.17	1	322.25	13.86	1	339.00	4.30
2	324.00	15.92	2	353.00	3.90	2	598.00	18.49
3	220.00	3.04	3	380.00	17.16	3	553.00	18.95
4	338.50	3.19	4	507.00	9.01	4	750.00	8.98
5	271.25	15.00	5	392.00	9.62	5	354.00	18.74
6	378.00	9.27	6	311.00	14.54	6	315.00	6.06
7	573.00	8.07	7	593.25	2.04			
8	353.00	10.19						

Post-infiltration c - c' pseudosection continued

Row 9				Row 10			
Location	Resistivity (ohm ft)	Standard Deviation (ohm ft)	Location	Resistivity (ohm ft)	Standard Deviation (ohm ft)	Location	Resistivity (ohm ft)
1	770.25	22.43	1	1110.75	53.01		
2	1062.00	73.06	2	815.25	50.64		
3	653.00	19.68	3	646.00	17.12		
4	620.00	46.24					

Row 11				Row 12			
Location	Resistivity (ohm ft)	Standard Deviation (ohm ft)	Location	Resistivity (ohm ft)	Standard Deviation (ohm ft)	Location	Resistivity (ohm ft)
1	825.75	63.01	1	725.50	67.50		
2	797.00	67.53					

Pre-infiltration d - d' pseudosection continued

Row 9		Row 10			
Location	Resistivity (ohm ft)	Standard Deviation (ohm ft)	Location	Resistivity (ohm ft)	Standard Deviation (ohm ft)
1	492.25	23.94	1	406.50	11.94
2	799.75	25.41			

Post-infiltration d - d' pseudosection
 Conducted along the northern boundary of the infiltration area
 5/6/87

Row 1				Row 2				Row 3				Row 4			
Location	Resistivity (ohm ft)	Standard Deviation (ohm ft)	Location	Resistivity (ohm ft)	Standard Deviation (ohm ft)	Location	Resistivity (ohm ft)	Standard Deviation (ohm ft)	Location	Resistivity (ohm ft)	Standard Deviation (ohm ft)	Location	Resistivity (ohm ft)	Standard Deviation (ohm ft)	
1	261.75	5.80	1	389.75	21.11	1	472.00	12.74	1	368.75	4.65	1	497.00	9.55	
2	352.00	10.42	2	414.00	36.22	2	591.75	14.82	2	679.00	11.37	2	750.00	20.50	
3	177.00	7.38	3	304.75	4.81	3	373.00	22.11	3	427.00	7.82	3	622.75	19.82	
4	157.75	2.38	4	228.00	1.92	4	290.75	18.23	4	382.00	4.43	4			
5	127.00	2.91	5	176.00	10.56	5	247.75	18.59	5	303.0	6.18	5			
6	123.00	0.00	6	192.00	3.60	6	246.00	12.07	6	226.00	7.01	6			
7	167.00	3.53	7	195.00	2.06	7	202.00	5.80	7	275.75	9.49	7			
8	153.00	1.22	8	170.00	0.70	8	232.00								
9	144.00	2.48	9	226.75	9.41										
10	198.00	4.84													

Row 5				Row 6				Row 7				Row 8			
Location	Resistivity (ohm ft)	Standard Deviation (ohm ft)	Location	Resistivity (ohm ft)	Standard Deviation (ohm ft)	Location	Resistivity (ohm ft)	Standard Deviation (ohm ft)	Location	Resistivity (ohm ft)	Standard Deviation (ohm ft)	Location	Resistivity (ohm ft)	Standard Deviation (ohm ft)	
1	407.00	9.69	1	414.00	33.50	1	418.00	8.34	1	497.00	9.55	1	497.00	9.55	
2	717.00	5.80	2	877.50	17.16	2	878.00	15.73	2	750.00	20.50	2	750.00	20.50	
3	538.00	16.43	3	581.50	14.22	3	502.00	18.82	3	622.75	19.82	3	622.75	19.82	
4	423.75	9.57	4	385.00	12.42	4	511.00	15.22	4			4			
5	296.00	6.89	5	361.00	5.24										
6	308.00	12.42													

Row 9				Row 10				
Location	Resistivity (ohm ft)	Standard Deviation (ohm ft)	Location	Resistivity (ohm ft)	Standard Deviation (ohm ft)	Location	Resistivity (ohm ft)	Standard Deviation (ohm ft)
1	465.50	12.50	1	338.25	1.78			
2	944.75	12.87						

Pre-infiltration e - e' pseudosection continued

Row 9			Row 10			Row 11		
Location	Resistivity (ohm ft)	Standard Deviation (ohm ft)	Location	Resistivity (ohm ft)	Standard Deviation (ohm ft)	Location	Resistivity (ohm ft)	Standard Deviation (ohm ft)
1	869.50	17.72	1	915.00	22.30	1	975.50	10.59
2	786.50	16.37	2	807.00	30.95			
3	729.50	8.32						

Post-infiltration e - e' pseudosection continued

Row 9			Row 10			Row 11		
Location	Resistivity (ohm ft)	Standard Deviation (ohm ft)	Location	Resistivity (ohm ft)	Standard Deviation (ohm ft)	Location	Resistivity (ohm ft)	Standard Deviation (ohm ft)
1	770.25	9.80	1	907.75	12.04	1	738.50	27.29
2	1074.25	41.99	2	892.50	10.13			
3	705.00	5.78						



Appendix B



COMPUTER PROGRAMS FOR THE FORWARD CALCULATION AND
AUTOMATIC INVERSION OF WENNER SOUNDING CURVES

BY A. A. R. ZOHDY AND R. J. BISDORF

THIS ALGORITHM UTILIZES MODIFIED DAR ZARROUK FUNCTIONS IN AN
ITERATIVE FASHION TO INVERT FIELD DATA

INTEGER DD,XDD,NN
CHARACTER TITLE*50
DIMENSION ALMF(50),DF(50),A(50),D(2),HF(50),PF(50)
DIMENSION PMF(50),HFF(50),DPF(50),PFF(50)
DIMENSION AL(50),P(50),H(50),DP(50),SLOPE(50),SZ(50)
DIMENSION E(10,50),PA(10,50),VESX(10,50),VESS(50)
DIMENSION VESF(50),NERR(50)
DIMENSION XAMDA(100),VV(100),PS(19),PPS(50)
DIMENSION DZD(50),DZR(50),SS(50),TS(50)
DIMENSION SUMLSQ(50,50),SMLSFF(50)
DIMENSION NERMIN(10),VESFF(50),HFINAL(50),DFINAL(50),PFINAL(50)
DOUBLE PRECISION VV,XRATIO,XAMDA,TS,SS,XMIN,XMAX

INPUT FILE = inweni, OUTPUT FILE = outweni

OPEN(99,FILE='inweni')
REWIND(99)
OPEN(25,FILE='outweni')
D(1)=0.0
D(2)=0.0
100 DO 50 I=1,50
 A(I)=0.0
 PS(I)=0.0
50 CONTINUE

MAXLYR = MAXIMUM NUMBER OF LAYERS IN THE REDUCED MODEL.
PROGRAM WILL ATTEMPT 3 TIMES TO REDUCE THE NUMBER OF
LAYERS IN THE DETAILED MODEL. IF UNSPECIFIED MAXLYR=10.
RHOMIN = THE MINIMUM VALUE FOR THE TRUE RESISTIVITY OF ANY LAYER
IN THE DETAILED MODEL. IF UNSPECIFIED RHOMIN=0 WHICH
GUARANTEES THE GENERATION OF LAYERS ONLY WITH POSITIVE
RESISTIVITIES. RHOMIN SHOULD NOT BE GREATER THEN ONE-HALF
THE VALUE OF THE MINIMUM APPARENT RESISTIVITY.
IFORCE = IF IFORCE=0, THEN THE PROGRAM WILL REJECT HIGHLY
DISTORTED CURVES. IF IFORCE=1, THEN INTERPRETATION WILL
BE COMPLETED REGARDLESS OF THE DISTORTION.

MAXLYR=10
KLM=1
RHOMIN=0.0
IFORCE=0

```

C
C      ITYPE = IF ITYPE=1 THEN INPUT FORMAT AS FOLLOWS
C              NN=NUMBER OF LOGARITHMICALLY SPACED POINTS (SEE BELOW)
C              TITLE=TITLE OF STUDY
C              RADMIN=SMALLEST ELECTRODE SPACING
C              RADMAX=LARGEST ELECTRODE SPACING
C              PS(1,NN)=SUCESSIVE DIGITIZED (6 LOGARITHMICALLY EQUALLY
C              SPACED POINTS PER DECADE) APPARENT RESISTIVITY VALUES FROM
C              RADMIN TO RADMAX
C              = IF ITYPE=0 THEN INPUT FORMAT AS FOLLOWS
C              NN=NUMBER OF FIELD MEASUREMENTS
C              TITLE=TITLE OF STUDY
C              A(1,NN)=WENNER ELECTRODE SPACINGS USED IN THE STUDY
C              PS(1,NN)=APPARENT RESISTIVITY CORRESPONDING TO EACH A(1,NN)

      READ(99,*)ITYPE
      READ(99,*) NN
      READ(99,8) TITLE
8      FORMAT(A50)
      IF(ITYPE.EQ.1)THEN
          READ(99,*)RADMIN,RADMAX
      ENDIF
      IF(ITYPE.EQ.0)THEN
          READ(99,*)(A(I),I=1,NN)
      ENDIF
      READ(99,*)(PS(I),I=1,NN)
      WRITE(25,545) TITLE
545      FORMAT(A20)
C
      IF(A(1).EQ.0.0) GO TO 5005
      WRITE(6,*)
      WRITE(6,*) TITLE
      WRITE(6,*)
      WRITE(6,*)(A(I),I=1,NN)
      WRITE(6,*)
      WRITE(6,*)(PS(I),I=1,NN)
      WRITE(25,*)
      WRITE(25,*)(A(I),I=1,NN)
      WRITE(25,*)
      WRITE(25,*)(PS(I),I=1,NN)
C
      IF(A(1).EQ.0.0) GO TO 5005
      CALL NPTS(PS,NP)
      CALL NPTS(A,NA)
      IF(NA.EQ.NP) GO TO 1111
      WRITE(6,55)
55      FORMAT(/,10X,'NUMBER OF DIGITIZED POINTS IS WRONG')
      N=NP
      IF(NA.GT.NP) N=NA
      CALL LDAT(A,PS,N)
      GO TO 100
1111     CALL LDAT(A,PS,NA)
      NRADII=NP
      LAYERS=NP
      N=NP
      DO 2222 I=1,NRADII
          AL(I)=A(I)
2222     CONTINUE
      XRATIO=DEXP(DLOG(10.0D0)/3.0D0)
      GO TO 5002

```



```

C
C      COMPUTE ELECTRODE SPACINGS
C
5005  AL(1)=RADMIN
      XRATIO=DEXP(DLOG(10.0D0)/6.0D0)
      EPSLON=0.02*RADMAX
      I=2
180   AL(I)=XRATIO*AL(I-1)
      IF(ABS(RADMAX-AL(I)).LT.EPSLON) GO TO 200
190   I=I+1
      GO TO 180
200   NRADII=I
      N=NRADII
      LAYERS=N
      IF(KLM.GT.1) GO TO 301
      CALL NPTS(PS,NP)
52    IF(NP.EQ.N) GO TO 53
      IF(N.LT.(I-1)) N=I-1
      WRITE(6,55)
      CALL LDAT(AL,PS,N)
      GO TO 100
53    CALL LDAT(AL,PS,N)
C
C      COMPUTE KERNEL FUNCTION SPACINGS
C
301   XMIN=(RADMIN/XRATIO**16.0)*1.36
      XMAX=(RADMAX*XRATIO**2.0)*1.36
      XAMDA(1)=XMIN
      I=2
1180  XAMDA(I)=XRATIO*XAMDA(I-1)
      IF(XMAX-XAMDA(I)) 1200,1200,1190
1190  I=I+1
      GO TO 1180
1200  NRAD=I
      IF(KLM.EQ.1) GO TO 5002
      CALL KERNEL(LYR,XAMDA,HFINAL,PFINAL,VV,NRAD)
      CALL CONVES(AL,VV,VESS,NRAD,NRADII)
      DO 5006 I=1,N
          PS(I)=VESS(I)
5006  CONTINUE
C
C      COMPUTE SLOPES AND FITTING TOLERANCE SZ ON OBSERVED VES
C
5002  SZ(1)=5.0
      DO 21 I=2,N
          SLOPE(I)=ALOG(PS(I)/PS(I-1))/ALOG(AL(I)/AL(I-1))
          IF(SLOPE(I).LE.1.0) GO TO 23
          WRITE(25,24)
24    FORMAT(10X,'WARNING.. SLOPE EXCEEDS +45 DEGREES',//)
          IF(SLOPE(I).LE.1.4) GO TO 23
          IF(IFORCE.EQ.1) GO TO 23
          WRITE(25,25)
25    FORMAT(10X,'SLOPE EXCEEDS +1.4, CURVE DISTORTED: LATERAL EFFECT,
+OR DIGITIZING ERROR',//)
          GO TO 100
23    SZ(I)=2.0+(SLOPE(I)*SLOPE(I))
21    CONTINUE
C
C      COMPUTE LAYERING WITH MDZ FROM VES
C

```

```

ITERAT=0
XZ=1.0
IK=0
IKK=0
YZ=0.20
L=1

```

```

          DO 201 I=1,N
                PPS(I)=PS(I)
201      CONTINUE
          GO TO 202
          40    CONTINUE
          110   IK=IK+1
                XZ=XZ-0.1
                IF(IK.GT.9) GO TO 600
                IF(IKK.EQ.1) GO TO 600
                IF(ITERAT.GT.50) GO TO 600
                DO 203 I=1,N
                        PS(I)=PPS(I)
203      CONTINUE
202      ID=0
          J=1
          9    IF(J.GT.10) GO TO 20

```

C
C
C

THIS MEANS ITERATION STOPS AFTER A MAXIMUM OF 10 ITERATIONS

```

P(1)=PS(1)
H(1)=AL(1)*XZ
DO 1 I=2,N
IF(PS(I).LT.PS(I-1)) GO TO 3
F=AL(I)*PS(I)-AL(I-1)*PS(I-1)
Q=AL(I)/PS(I)-AL(I-1)/PS(I-1)
IF(Q.LE.0.0) GO TO 90
P(I)=SQRT(F/Q)
H(I)=P(I)*Q*XZ
GO TO 98

```

C
C
C
C

USE MDZ-L AND REGULA FALSI METHOD
TO UNDERESTIMATE WE LET P(I)=RHOMIN

```

3    X=0.6
      P(I)=RHOMIN
      Q=AL(I)/PS(I)-AL(I-1)/PS(I-1)
      A1=((AL(I-1)+P(I)*Q)/AL(I))*((AL(I-1)+P(I)*Q)/AL(I))
      B1=AL(I-1)*PS(I-1)+(P(I)*P(I))*Q
      C1=AL(I)/PS(I)
      D1=(AL(I-1)+P(I)*Q)
      D1=D1*D1
33   AAL=(A1*(B1*C1/D1)**X)-1.0
      IF(AAL.LT.0.0) GO TO 5
      X=X-YZ
      IF(X.LT.0.0) GO TO 20
      GO TO 33
5    CONTINUE

```

C
C
C

TO OVERESTIMATE WE LET P(I)=PS(I)

```

P(I)=PS(I)
A1=((AL(I-1)+P(I)*Q)/AL(I))*((AL(I-1)+P(I)*Q)/AL(I))
B1=AL(I-1)*PS(I-1)+(P(I)*P(I))*Q
C1=AL(I)/PS(I)

```

```

D1=(AL(I-1)+P(I)*Q)
D1=D1*D1
BB=(AL*(B1*C1/D1)**X)-1
Y1=0.0
P(I)=(BB*Y1-AA1*P(I))/(BB-AA1)
DD=0

```

6

```

CONTINUE
AL=((AL(I-1)+P(I)*Q)/AL(I))*((AL(I-1)+P(I)*Q)/AL(I))
B1=AL(I-1)*PS(I-1)+(P(I)*P(I))*Q
C1=AL(I)/PS(I)
D1=(AL(I-1)+P(I)*Q)
D1=D1*D1
CC=(AL*(B1*C1/D1)**X)-1
IF(CC.GT.-1.0E-03) GO TO 7
P(I)=(CC*PS(I)-BB*P(I))/(CC-BB)
IF(DD.GT.15) GO TO 108

```

THE NUMBER 15 IN ABOVE STATEMENT DESIGNATES A MAXIMUM
OF 15 REGULA FALSI ITERATIONS

```

DD=DD+1
GO TO 6
108 CONTINUE
7 CONTINUE
H(I)=P(I)*Q*XZ
GO TO 98

```

USE MDZ-T

90 XX=0.9

TO OVERESTIMATE WE USE $P(I)=50*PS(I)$

```

P(I)=50.0*PS(I)
XA=(AL(I-1)+F/P(I))*(AL(I-1)+F/P(I))
XB=PS(I)*(AL(I-1)/PS(I-1)+F/(P(I)*P(I)))*AL(I)
99 XC=(XA/XB)**XX
XBB=((AL(I)*AL(I))/XA)*XC)-1.0
IF(XBB.GT.0.0) GO TO 92
XX=XX-0.1
IF(XX.LT.0.0) GO TO 20
GO TO 99
92 CONTINUE

```

TO UNDERESTIMATE WE USE $P(I)=PS(I)$

```

XA=(AL(I-1)+F/PS(I))*(AL(I-1)+F/PS(I))
XB=PS(I)*(AL(I-1)/PS(I-1)+F/(PS(I)*PS(I)))*AL(I)
XC=(XA/XB)**XX
XAA=((AL(I)*AL(I))/XA)*XC)-1.0
P(I)=(XBB*PS(I)-XAA*P(I))/(XBB-XAA)
XDD=0
96 CONTINUE
XA=(AL(I-1)+F/P(I))*(AL(I-1)+F/P(I))
XB=PS(I)*(AL(I-1)/PS(I-1)+F/(P(I)*P(I)))*AL(I)
XC=(XA/XB)**XX
XCC=((AL(I)*AL(I))/XA)*XC)-1.0
IF(XCC.LT.0.001) GO TO 97
P(I)=(XCC*PS(I)-XAA*P(I))/(XCC-XAA)
IF(XDD.GT.100) GO TO 106

```

```

XDD=XDD+1
GO TO 96
106 CONTINUE
97 CONTINUE
H(I)=(F/P(I))*XZ
98 CONTINUE
1 CONTINUE
H(N)=999999
SUMH=0.0
      DO 28 I=1,N
          SUMH=SUMH+H(I)
          DP(I)=SUMH
28 CONTINUE
C
ITERAT=ITERAT+1
IF(A(1).GT.0.0) GO TO 3001
CALL KERNEL(LAYERS,XAMDA,H,P,VV,NRAD)
CALL CONVES(AL,VV,VESS,NRAD,NRADII)
GO TO 4001
3001 CALL CONVLV(AL,XRATIO,LAYERS,H,P,VESS,VV,NRADII)
C
C ADJUST MDZ AND ITERATE
C
4001 NERR(J)=0
      DO 10 I=1,N
          VESX(J,I)=VESS(I)
          E(J,I)=((PPS(I)-VESX(J,I))/PPS(I))*100.0
          Z=ABS(E(J,I))
          IF(Z-SZ(I)) 10,10,41
41 NERR(J)=NERR(J)+1
10 CONTINUE
      IF(VESX(J,1).LE.0.0) GO TO 777
      SUMLSQ(J,1)=(ALOG10(PPS(1))-ALOG10(VESX(J,1)))*2.0
      DO 60 I=2,N
          IF(VESX(J,I).LE.0.0) GO TO 777
          SUMLSQ(J,I)=(ALOG10(PPS(I))-ALOG10(VESX(J,I)))*2.0+SUMLSQ(J,I-1)
60 CONTINUE
      GO TO 776
777 WRITE(25,778)
778 FORMAT(///10X,'GHOSH COEFFICIENTS RESULT IN NEGATIVE APPARENT
+ RESISTIVITIES...PROBLEM CANNOT BE SOLVED BY CONVOLUTION')
      GO TO 100
776 SMLS=SUMLSQ(J,N)
C WRITE(25,61) SMLS
C 61 FORMAT(10X,'SUM OF SQUARED RESIDUALS=',F10.5)
      WRITE(6,*)'NERR(J) =',NERR(J)
      IF(NERR(J)-1) 534,12,12
12 IF(J.GT.1) GO TO 17
          DO 11 I=1,N
              VESF(I)=VESX(J,I)
              HFF(I)=H(I)
              DPF(I)=DP(I)
              PFF(I)=P(I)
              PA(J,I)=PPS(I)*2.0/VESX(J,I)
              PS(I)=PA(J,I)
11 CONTINUE
      NERRF=NERR(J)
      SMLSQF=SMLS
      J=J+1
      GO TO 9

```

```

17      KK=1
604     IF(SUMLSQ(J,N).LE.SUMLSQ(J-KK,N)) GO TO 605
        GO TO 15
605     KK=KK+1
        IF(KK.EQ.J) GO TO 18
        GO TO 604
18      DO 19 I=1,N
            VESF(I)=VESX(J,I)
            HFF(I)=H(I)
            DPF(I)=DP(I)
            PFF(I)=P(I)
19      CONTINUE
        NERRF=NERR(J)
        SMLSQF=SUMLSQ(J,N)
        GO TO 26
15      ID=ID+1
        IF(ID.GT.5) GO TO 20
26      DO 16 I=1,N
        PA(J,I)=(PPS(I)*PA(J-1,I))/VESX(J,I)
        PS(I)=PA(J,I)
16      CONTINUE
        J=J+1
        GO TO 9
20      NERMIN(L)=NERRF
        SMLSFF(L)=SMLSQF
        IF(L.GT.1) GO TO 801
        MERF=NERMIN(L)
        SLSQ=SMLSFF(L)
            DO 881 I=1,N
                VESFF(I)=VESF(I)
                HFINAL(I)=HFF(I)
                DFINAL(I)=DPF(I)
                PFINAL(I)=PFF(I)
881     CONTINUE
        L=L+1
        GO TO 40
801     LL=1
802     IF(SMLSFF(L).LE.SMLSFF(L-LL)) GO TO 803
        L=L+1
        IKK=IKK+1
        GO TO 40
803     LL=LL+1
        IF(LL.EQ.L) GO TO 181
        GO TO 802
181     DO 804 I=1,N
            VESFF(I)=VESF(I)
            HFINAL(I)=HFF(I)
            DFINAL(I)=DPF(I)
            PFINAL(I)=PFF(I)
804     CONTINUE
        MERF=NERMIN(L)
        SLSQ=SMLSFF(L)
        L=L+1
        GO TO 40
534     DO 603 I=1,N
            VESFF(I)=VESX(J,I)
            HFINAL(I)=H(I)
            DFINAL(I)=DP(I)
            PFINAL(I)=P(I)
603     CONTINUE

```

```

600   IF(KLM.EQ.1) GO TO 5001
5050  WRITE(25,532)
      WRITE(25,533) (HFINAL(I),DFINAL(I),PFINAL(I),I=1,N)
333   WRITE(25,1301)
334   WRITE(25,1201) (AL(I),VESFF(I),PPS(I),I=1,N)
1301  FORMAT(/21X,'A',14X,'CALC. VES',10X,'SMOOTHED VES'//)
532   FORMAT(13X,'THICKNESS',7X,'DEPTH',4X,'RESISTIVITY'//)
533   FORMAT(10X,3F12.4)
1201  FORMAT(5X,3F20.5)
1202  CALL DZ(HFINAL,PFINAL,N,DZR,DZD,TS,SS)
      AD=2.0
4000  CALL DZSMTH(DZD,DZR,TS,SS,N,ALMF,PMF,NBR,AD)
      CALL LAYER(ALMF,PMF,HF,PF,NBR,DF,ITEST)
      IF(ITEST.GT.0) GO TO 100
      IF(A(1).GT.0.0) GO TO 5100
      CALL KERNEL(NBR,XAMDA,HF,PF,VV,NRAD)
      CALL CONVES(AL,VV,VESS,NRAD,NRADII)
      GO TO 6001
5100  CALL CONVLV(AL,XRATIO,NBR,HF,PF,VESS,VV,NRADII)
6001  WRITE(25,1301)
      WRITE(25,1201) (AL(I),VESS(I),PPS(I),I=1,N)
      IF(NBR.LE.MAXLYR) GO TO 5000
      AD=AD*2.0
      IF(AD.GT.8.0) GO TO 5000
      GO TO 4000
5000  DO 68 I=1,N
68    DZR(I)=DZR(I)/10.0
      DO 66 I=1,NBR
66    PMF(I)=PMF(I)/10.0
      GO TO 100
5001  IF(KLM.GT.1) GO TO 100
      KLM=KLM+1
      WRITE(25,5003)
5003  FORMAT(/10X,'SOLUTION TO SMOOTHED VES CURVE FOLLOWS'//)
      IF(A(1).GT.0.0) GO TO 7001
      RADMIN=RADMIN/10.0
      LYR=LAYERS
      GO TO 5005
7001  AL(1)=A(1)/10.0
      DO 8001 I=2,6
          AL(I)=AL(I-1)*EXP(ALOG(10.0)/6.0)
8001  CONTINUE
      DO 9001 I=7,NRADII+6
          AL(I)=A(I-6)
9001  CONTINUE
      NRADII=NRADII+6
      LYR=LAYERS
      CALL CONVLV(AL,XRATIO,LYR,HFINAL,PFINAL,VESS,VV,NRADII)
      N=NRADII
      LAYERS=NRADII
      DO 1166 I=1,NRADII
          PS(I)=VESS(I)
1166  CONTINUE
      GO TO 5002
500   STOP
      END
C
C
C
C
*****SUBROUTINE KERNEL*****
CALCULATES THE TKF (TOTAL KERNEL FUNCTION) CURVE FROM THE

```

```

XK(1)=-0.0067D 00
XK(2)= 0.0179D 00
XK(3)=-0.0258D 00
XK(4)= 0.0416D 00
XK(5)=-0.0935D 00
XK(6)= 0.3473D 00
XK(7)=-1.3341D 00
XK(8)= 1.5662D 00
XK(9)= 0.4582D 00
XK(10)= 0.0284D 00

```

```

C
C VV1=KERNEL FUNCTION FOR FIRST STEP
C VV2=KERNEL FUNCTION FOR SECOND SET, WHICH IS DISPLACED TO THE
C RIGHT OF THE FIRST SET BT (EXP OF LN10/6)
C

```

```

WRITE(6,*)'IN CONVES'
DO 5 I=1,100
VV1(I)=0.0
VV2(I)=0.0
5 CONTINUE
NODD=0
NEVEN=0

```

```

C
C TEST TO FIND IF NRAD IS EVEN OR ODD
C

```

```

IF(MOD(NRAD,2).EQ.0) GO TO 15
NODD=NRAD
NN=(NODD+1)/2
GO TO 16
15 NEVEN=NRAD
NN=NEVEN/2
GO TO 18
16 DO 20 J=1,NN
VV1(J)=VV(2*J-1)
20 CONTINUE
MM=NN-1
17 DO 22 J=1,MM
VV2(J)=VV(2*J)
22 CONTINUE
GO TO 24
18 DO 23 J=1,NN
VV1(J)=VV(2*J-1)
VV2(J)=VV(2*J)
23 CONTINUE
24 CONTINUE
M=0
L=1
LL=10
11 DO 9 J=L,LL
XVES1(J)=VV1(J)*XK(J-M)
XVES2(J)=VV2(J)*XK(J-M)
9 CONTINUE
SMVES1=0.0
SMVES2=0.0
DO 10 J=L,LL
SMVES1=XVES1(J)+SMVES1
SMVES2=XVES2(J)+SMVES2
10 CONTINUE
VES1(L)=SMVES1
VES2(L)=SMVES2

```

```

CONTINUE
L=L+1
LL=LL+1
M=M+1
IF(LL.GT.NRAD) GO TO 12
GO TO 11
12 IF(NRAD.EQ.NODD) GO TO 14
GO TO 13
14 DO 31 J=1,NN
VES(2*J-1)=SNGL(VES1(J))
31 CONTINUE
DO 32 J=1,MM
VES(2*J)=SNGL(VES2(J))
32 CONTINUE
GO TO 34
13 DO 33 J=1,NN
VES(2*J-1)=SNGL(VES1(J))
VES(2*J)=SNGL(VES2(J))
33 CONTINUE
34 CONTINUE
C WRITE(25,200)
C200 FORMAT(19X,'AB/2',20X,'VES'//)
C WRITE(25,201)
C201 FORMAT(5X,2F20.5)
500 RETURN
END

```

```

C
C *****SUBROUTINE DZ*****
C
C CALCULATES THE FUNDAMENTAL POINTS (POINTS DESIGNATING THE END OF
C ONE AND THE BEGINNINGS OF ANOTHER LAYER) ON A DZ (DAR ZARROUK) CURVE,
C FROM LAYER THICKNESSES AND RESISTIVITIES.
C

```

```

SUBROUTINE DZ(TH,RE,N,R,AL,TS,SS)
DIMENSION AL(50),R(50),TH(50),RE(50),SS(50),TS(50)
DOUBLE PRECISION TS,SS
WRITE(6,*)'IN DZ'
SUMS=0.0
SUMT=0.0
DO 100 I=1,N
SUMS=SUMS+TH(I)/RE(I)
SS(I)=DBLE(SUMS)
SUMT=SUMT+TH(I)*RE(I)
TS(I)=DBLE(SUMT)
R(I)=SQRT(SUMT/SUMS)
AL(I)=SQRT(SUMT*SUMS)
100 CONTINUE
WRITE(25,96)
96 FORMAT(/16X,'DZ DEPTH',10X,'DZ RESISTIVITY',9X,'SUM T',17X,
+'SUM S'/)
WRITE(25,97)(AL(I),R(I),TS(I),SS(I),I=1,N)
97 FORMAT(5X,4F20.5)
RETURN
END

```

```

C
C *****SUBROUTINE LAYER*****
C
C CALCULATES LAYER THICKNESSES AND RESISTIVITIES FROM COORDINATES
C OF POINTS ON A DZ CURVE.
C

```


C

```

SUBROUTINE LAYER(LZF,PMF,H,P,LS,D,ITEST)
REAL LZF(100)
DIMENSION PMF(100),H(100),D(100),P(100)
DIMENSION T(100),S(100),TS(100),SS(100)
DOUBLE PRECISION TS,SS,T,S
WRITE(6,*) 'IN LAYER'
ITEST=0
P(1)=PMF(1)
H(1)=LZF(1)
TS(1)=DBLE(P(1))*DBLE(H(1))
SS(1)=DBLE(H(1))/DBLE(P(1))
DO 1 I=2,LS
TS(I)=DBLE(LZF(I))*DBLE(PM(F(I)))
SS(I)=DBLE(LZF(I))/DBLE(PM(F(I)))
T(I)=TS(I)-TS(I-1)
S(I)=SS(I)-SS(I-1)
RATIO=T(I)/S(I)
IF(RATIO.LE.0.0) GO TO 2
P(I)=SNGL(DSQRT(T(I)/S(I)))
H(I)=SNGL(S(I)*DBLE(P(I)))
D(1)=H(1)
D(I)=D(I-1)+H(I)
1 CONTINUE
WRITE(25,10)
10 FORMAT(//20X,'REDUCED THICKNESS',20X,'REDUCED DEPTH',
+ 10X,'REDUCED RESISTIVITY')
WRITE(25,20)(H(I),D(I),P(I),I=1,LS)
20 FORMAT(10X,F25.5,10X,F25.5,F25.5)
GO TO 3
2 ITEST=ITEST+1
3 RETURN
END

```

C
C
C
C
C
C

*****SUBROUTINE DZSMTH*****

SMOOTHES DZ CURVE FOR DETAILED MODEL, TO REDUCE NUMBER OF LAYERS.

C
C
C

```

SUBROUTINE DZSMTH(ALM,PM,TS,SS,N,ALMFF,PMFF,NBR,AD)
DIMENSION SLP(50),ALM(50),PM(50),TS(50),SS(50),PMA(50)
DIMENSION SUMTS(50),SUMSS(50),SUMS2(50),SMTSSS(50)
DIMENSION P(50),SSA(50),TSA(50),ALMEPS(50),ALMSPE(50)
DIMENSION PMAEPS(50),PMASPE(50),A0(50),A1(50)
DIMENSION A0F(50),A1F(50),PF(50),ALMFF(50),PMFF(50)
EQUIVALENCE(NP1,NAP1)
DOUBLE PRECISION TS,SS,SUMTS,SUMSS,SUMS2,SMTSSS

COMPUTE FITTING TOLERANCE FOR THE FIRST DZ BRANCH

WRITE(6,*) 'IN DZSMTH'
EPSLON=1.02
AZ=1.5**(0.20)
101 DO 100 I=1,N
100 FT(I)=AZ
NBR=1
NTAP=1
SUMLOG(1)=ALOG(PM(1))
PMA(1)=PM(1)
NAP1=2

```

```

      I=2
1    SUMLOG(NAP1)=ALOG(PM(I))+SUMLOG(NAP1-1)
      ASUM=SUMLOG(NAP1)/NAP1
      PMA(NAP1)=EXP(ASUM)
C
      I=1
4    DIVIAT(I)=PM(I)/PMA(NAP1)
      IF(DIVIAT(I).GT.FT(I)) GO TO 3
      IF(DIVIAT(I).LT.1/FT(I)) GO TO 3
      IF(I.EQ.NAP1) GO TO 2
      I=I+1
      GO TO 4
C
2    NTAP=NTAP+1
      IF(NTAP.EQ.N) GO TO 6
      I=I+1
      NAP1=NAP1+1
      GO TO 1
C
6    PMFF(1)=PMA(NTAP)
      ALMFF(1)=99999999.
      WRITE(25,200)
200  FORMAT(10X,'PROBLEM REDUCED TO SEMI-INFINITE MEDIUM
+ WITH RESISTIVITY OF')
      WRITE(25,201) PMF(1)
201  FORMAT(/10X,1F10.5)
      GO TO 600
C
3    PMFF(1)=PMA(NTAP)
      PF(1)=PMA(NTAP)
      AOF(NBR)=0.0
      ALF(NBR)=PMFF(1)**2.0
      NRP=N-NTAP
22   IF(NRP.EQ.1) GO TO 8
      GO TO 7
8    NBR=NBR+1
      PF(NBR)=SNGL(DSQRT((TS(N)-TS(N-1))/(SS(N)-SS(N-1))))
      RATIO=PF(NBR)/PF(NBR-1)
      IF(RATIO.GE.1.1) GO TO 340
      IF(RATIO.LE.0.9) GO TO 340
      NBR=NBR-1
      PMFF(NBR)=PF(NBR)
      ALMFF(NBR)=99999999.
      GO TO 500
340  ALF(NBR)=PF(NBR)**2.0
      AOF(NBR)=SNGL(TS(N)-((DBLE(PF(NBR)**2.0))*SS(N)))
C
      AT INTERSECTION OF NBR AND NBR-1 BRANCHES
C
      SSA(NBR-1)=(AOF(NBR)-AOF(NBR-1))/(ALF(NBR-1)-ALF(NBR))
      TSA(NBR-1)=AOF(NBR-1)+ALF(NBR-1)*SSA(NBR-1)
      PMFF(NBR-1)=SQRT(TSA(NBR-1)/SSA(NBR-1))
      ALMFF(NBR-1)=SQRT(TSA(NBR-1)*SSA(NBR-1))
      ALMFF(NBR)=99999999.
      PMFF(NBR)=PF(NBR)
      GO TO 500
7    I=NTAP
      NAP1=1
      SUMTS(NAP1)=TS(I)
      SUMSS(NAP1)=SS(I)

```

```

SUMS2(NAP1)=SS(I)**2.0
SMTSSS(NAP1)=TS(I)*SS(I)
GO TO 21
40 IF(NAP1.GT.2) GO TO 17
   TS(NTAP)=DBLE(ALM(NTAP))*DBLE(PMA(NTAP))
   SS(NTAP)=DBLE(ALM(NTAP))/DBLE(PMA(NTAP))
   GO TO 7
21 NAP1=NAP1+1
   NAP=NAP1+NTAP
   I=I+1
   SUMTS(NAP1)=TS(I)+SUMTS(NAP1-1)
   SUMSS(NAP1)=SS(I)+SUMSS(NAP1-1)
   SUMS2(NAP1)=SS(I)**2.0+SUMS2(NAP1-1)
   SMTSSS(NAP1)=(TS(I)*SS(I))+SMTSSS(NAP1-1)
   AA=SNGL(NAP1*SMTSSS(NAP1)-SUMTS(NAP1)*SUMSS(NAP1))
   BB=SNGL(NAP1*SUMS2(NAP1)-SUMSS(NAP1)**2.0)
   IF(BB.LE.0.0) GO TO 19
   A1(NAP1)=AA/BB
   A0(NAP1)=SNGL((SUMTS(NAP1)-DBLE(A1(NAP1))*SUMSS(NAP1))/NAP1)
   IF(A1(NAP1).LE.0.0) GO TO 19
   P(NAP1)=SQRT(A1(NAP1))

C
C
C   AT INTERSECTION
202 SSA(NBR)=(A0(NAP1)-A0F(NBR))/(ALF(NBR)-A1(NAP1))
    TSA(NBR)=A0F(NBR)+ALF(NBR)*SSA(NBR)
    TSASSA=TSA(NBR)*SSA(NBR)
    IF(TSASSA.LE.0.0) GO TO 17
    ALMF(NPAl)=SQRT(TSA(NBR)*SSA(NBR))
    PMF(NPAl)=SQRT(TSA(NBR)/SSA(NBR))
    IF(ALMF(NAP1).GT.AL(M(I))) GO TO 40
    GO TO 203
19  IF(NAP1.GT.2) GO TO 17
    ALMF(NAP1)=ALM(I-1)
    PMF(NAP1)=PMA(I-1)
    IF(PM(I).GT.PM(I-1)) GO TO 20
    P(NAP1)=PMF(NAP1)/50.0
    GO TO 203
20  P(NAP1)=PMF(NAP1)*50.0
203 CONTINUE
31  IF(NAP1.GT.2) GO TO 32
    GO TO 21
32  IF(ALMF(NAP1)/ALM(NTAP).LE.1.0) GO TO 33
    IF(ALMF(NAP1).GE.AL(M(NTAP+1)) GO TO 17
38  I=NTAP+1
    NAP=NAP1+NTAP-1
    GO TO 14
33  IF(NTAP.EQ.1) GO TO 38
    IF(ALMF(NAP1).LT.AL(M(NTAP-1)) GO TO 17
    IF(ALM(NTAP)/ALMF(NAP1).GT.EPSLON) GO TO 34
    GO TO 38
34  I=NTAP
    NAP=NAP1+NTAP-1

C
C
C   COMPUTE SLOPES OF DZ AND FITTING TOLERANCES
14  ALMEPS(I)=ALM(I)*EPSLON
    ALMSPE(I)=ALM(I)/EPSLON
    Z1=-ALMF(NAP1)*(P(NAP1)**2.0-PMF(NAP1)**2.0)
    Z2=(-Z1)**2.0

```

```

ZEPS=4.0*((ALMEPS(I)*PMF(NAP1)*P(NAP1))**2.0)
PMAEPS(I)=(Z1+SQRT(Z2+ZEPS))/(2.0*ALMEPS(I)*PMF(NAP1))
ZSPE=4.0*((ALMSPE(I)*PMF(NAP1)*P(NAP1))**2.0)
PMASPE(I)=(Z1+SQRT(Z2+ZSPE))/(2.0*ALMSPE(I)*PMF(NAP1))
Z=4.0*((ALM(I)*PMF(NAP1)*P(NAP1))**2.0)
PMA(I)=(Z1+SQRT(Z2+Z))/(2.0*ALM(I)*PMF(NAP1))
SLP(I)=ALOG10(PMAEPS(I)/PMASPE(I))/ALOG10(ALMEPS(I)/ALMSPE(I))
B1=1.5707963*SLP(I)
B2=COS(B1)
B3=((2.0+SLP(I))*B2)/10.0
FT(I)=AD**B3
DIVIAT(I)=PM(I)/PMA(I)
IF(DIVIAT(I).GT.FT(I)) GO TO 15
IF(DIVIAT(I).LT.1.0/FT(I)) GO TO 15
IF(I.EQ.NAP) GO TO 11
I=I+1
GO TO 14
11 IF(NAP.EQ.N) GO TO 16
GO TO 21
17 IF(NAP.EQ.(NAP1+NTAP-1)) GO TO 10
NAP=NAP1+NTAP-2
GO TO 10
15 NAP=NAP-1
10 NAP1=NAP1-1
NTAP=NAP
18 ALMFF(NBR)=ALMF(NAP1)
PMFF(NBR)=PMF(NAP1)
12 NBR=NBR+1
PF(NBR)=P(NAP1)
AOF(NBR)=AO(NAP1)
ALF(NBR)=AL(NAP1)
NRP=N-NTAP
GO TO 22
16 NBR=NBR+1
PF(NBR)=P(NAP1)
PMFF(NBR-1)=PMF(NAP1)
ALMFF(NBR-1)=ALMF(NAP1)
ALMFF(NBR)=99999999.0
PMFF(NBR)=PF(NBR)
500 WRITE(25,501)
501 FORMAT(/20X,'REDUCED DZ DEPTH',5X,'REDUCED DZ RESISTIVITY')
WRITE(25,502) (ALMFF(I),PMFF(I),I=1,NBR)
502 FORMAT(10X,F20.5,5X,F20.5)
600 RETURN
END

```

```

C
C ***** SUBROUTINE NPTS *****
C

```

```

POINT COUNTER FOR ARRAY X

```

```

SUBROUTINE NPTS(X,N)
DIMENSION X(50)
DO 33 I=1,50
    IF(X(I).EQ.0.0) GO TO 2
33 CONTINUE
I=I+1
2 N=N-1
RETURN
END

```

```

C

```

***** SUBROUTINE LDAT *****

OUTPUT CHECK OF A (ELECTRODE SPACINGS) AND P (APPARENT RESISTIVITIES)

```

SUBROUTINE LDAT(A,P,N)
DIMENSION A(50),P(50)
WRITE(25,31)
WRITE(25,32)(A(I),P(I),I=1,N)
FORMAT(/,6X,'A',9X,'OBS',/)
FORMAT(1X,F9.3,2X,F9.3)
RETURN
END

```

31
32

***** SUBROUTINE CONVLV*****

CALCULATES THE APPARENT RESISTIVITIES ON A VES CURVE BY TWICE
CONVOLVING GHOSH'S INVERSE FILTER COEFFICIENTS (GHOSH GEOPHYS.
PROSP., V.19, NO.4, PP.769-775) WITH THE TKF CURVE WHICH IS
CALCULATED BY SUBROUTINE KERNEL.
NOTE: RESULTS IN A WENNER SOUNDING CURVE THAT IS CALCULATED
AT ANY PRESCRIBED WENNER ELECTRODE SPACINGS.

```

SUBROUTINE CONVLV(AB,XRATIO,LAYERS,THICK,RESIST,VES,VV,NRADII)
DIMENSION AB(50),THICK(50),RESIST(50),VV(100),VES(50),
          XK(10),XAMDA(100),XVES(100)
DOUBLE PRECISION XMIN,XAMDA,XRATIO,VV

```

```

XK(1)=-0.0067D 00
XK(2)= 0.0179D 00
XK(3)=-0.0253D 00
XK(4)= 0.0416D 00
XK(5)=-0.0935D 00
XK(6)= 0.3473D 00
XK(7)=-1.3341D 00
XK(8)= 1.5662D 00
XK(9)= 0.4582D 00
XK(10)=0.0284D 00

```

KERNEL FUNCTION SPACINGS

```

WRITE(6,*)'IN CONVLV'
K=1
I=1

```

```

410 XMIN=(AB(I)/XRATIO**8.0D 00)*1.36D 00
XAMDA(1)=XMIN
I=2

```

```

405 IF(I.GT.10) GO TO 406
XAMDA(I)=XAMDA(I-1)*XRATIO
I=I+1
GO TO 405

```

```

406 NRAD=10
CALL KERNEL(LAYERS,XAMDA,THICK,RESIST,VV,NRAD)
SUMVES=0.0
DO 1 J=1,10
  XVES(J)=VV(J)*XK(J)
  SUMVES=XVES(J)+SUMVES

```

```

1 CONTINUE
VES(K)=SUMVES
K=K+1
I=K
IF(I.LE.NRADII) GO TO 410

```

C
C
C
C

C
C
C
C
C
C
C
C

C
C
C

CONTINUE
RETURN
END

PROGRAM RESIS2

author - Abhijit Dey Engineering Geoscience
University of California, Berkeley

INTEGER OPTPUN

DIMENSION A(1808,17),RS(1808,23),UL(1808,17)

DIMENSION VKY(5,23,23),V(23,23)

DIMENSION X(113),Z(16),YKY(5),ITXP(23),IRXP(23),

1 YSHIFT(1),ZSHIFT(1),ZRSHIF(1),ICODE(16,113),RESIS(10),

2 PFE(10),IXS(23),IZS(23),COND(113,16),DX(112),

3 DZ(15),ICONFG(1),NSOURC(23)

DIMENSION XMAT(1808)

character title(18)

COMMON /PACK1/ INCLIN,ISHIFT,NRLIM

COMMON /GANG1/ OPTPUN,THETA,IPRINT

***** input data files *****

OPEN(31,FILE='for31')

OPEN(32,FILE='for32')

***** output data files *****

OPEN(87,FILE='for87')

OPEN(88,FILE='for88')

***** input parameters *****

nnodx-number of nodes in x-direction

nnodz-number of nodes in z-direction

nky-number of discrete (Fourier) Ky values

nxbeg-in x-direction, the first node to be defined

ie. all nodes to the left of nxbeg are assigned the same value
as nxbeg

nxend-in x-direction, the last node to be defined

ie. all nodes to the right of nxend are assigned the same value
as nxend

narray-number of resistivity survey configurations

xscal-scale factor in x-direction of mesh

zscal-scale factor in z-direction of mesh

unit-scaling factor of the mesh distances in terms of the unit length
for the electrode configuration

dx-separation of nodes in x-direction

dz-separation of nodes in z-direction

yky-array of discrete (Fourier) Ky values

iconfg-array of code numbers for various electrode configurations

1=collinear dipole-dipole and pole-dipole

2=reconnaissance bipole-dipole

```

C ntx-number of transmitting electrode nodes (projected at z=0)
C nzsft-number of surface and subsurface layers of transmitter
C electrodes
C nrx-number of receiver electrode nodes (projected at z=0)
C nysft-number of lines shifted along strike where receiver
C electrodes are located (including y=0 line)
C nzrsft-number of surface and subsurface layers of receiver
C electrodes
C itxp-array of node numbers of the receiver electrodes
C irxp-array of node numbers of the transmitter electrodes
C zshift-array of depths of the layers of transmitting electrodes
C zrshif-array of depths of layers of receiver electrodes
C yshift-array of values of y-shifts for various receiver lines
C (in terms of unit)
C ipkey 0=if only resistivity response is sought
C 0>if resistivity as well as percent frequency effects
C responses are sought
C resis-array of intrinsic resistivity values (0-9)
C pfe-array of intrinsic percent frequency effect values (0-9)
C icode-array of coded resistivity distribution in the lower
C x-z plane in terms of symbols 0-9

```

```

*****

```

```

C READ(31,*) NNODX, NNODZ, NKY, NXBEG, NXEND, NARRAY, XSCAL, ZSCAL, UNIT
C NELX=NNODX-1
C NELZ=NNODZ-1
C READ(31,*) (DX(I), I=1, NELX)
C READ(31,*) (DZ(J), J=1, NELZ)
C READ(31,*) (YKY(K), K=1, NKY)
C READ(31,*) (ICONFG(I), I=1, NARRAY)
C READ(31,*) NTX, NZSFT, NRX, NYSFT, NZRSFT
C READ(31,*) (ITXP(I), I=1, NTX)
C READ(31,*) (IRXP(J), J=1, NRX)
C READ(31,*) (ZSHIFT(I), I=1, NZSFT)
C READ(31,*) (ZRSHIF(I), I=1, NZRSFT)
C READ(31,*) (YSHIFT(K), K=1, NYSFT)
888 READ(31,*) IPKEY
C READ(32,*) (RESIS(I), I=1, 10)
C READ(32,*) (PFE(I), I=1, 10)
C DO 103 I=1, NNODZ
C READ(32,2) (ICODE(I,J), J=NXBEG, NXEND)
103 CONTINUE
C 2 FORMAT(2X, 58(I1))

```

```

***** READ IN THE SPECIAL INPUT DATA FOR CERTAIN ARRAYS *****

```

```

C IF(NARRAY.EQ.1.AND.ICONFG(1).EQ.1)THEN
C READ(32,*) OPTPUN, IPRINT, THETA
C ENDIF
C IF(NARRAY.EQ.1.AND.ICONFG(1).EQ.2)THEN
C READ(32,*) INCLIN, ISHIFT, NRLIM
C ENDIF
C READ(32,*) MORE

```

```

***** PRINT IMAGES OF THE INPUT DATA *****

```

```

C WRITE(87,99)
99 FORMAT(1H1,///,25X, 'IMAGES OF THE INPUT DATA '///  

C IF(MORE.NE.0) GO TO 998

```



```

WRITE(87,*) NNODX,NNODZ,NKY,NXBEG,NXEND,NARRAY,XSCAL,ZSCAL,UNIT
WRITE(87,*) (DX(I),I=1,NELX)
WRITE(87,*) (DZ(J),J=1,NELZ)
WRITE(87,*) (YKY(K),K=1,NKY)
WRITE(87,*) (ICONFG(I),I=1,NARRAY)
WRITE(87,*) NTX,NZSFT,NRX,NYSFT,NZRSFT
WRITE(87,*) (ITXP(I),I=1,NTX)
WRITE(87,*) (IRXP(J),J=1,NRX)
WRITE(87,*) (ZSHIFT(I),I=1,NZSFT)
WRITE(87,*) (ZRSHIF(I),I=1,NZRSFT)
WRITE(87,*) (YSHIFT(K),K=1,NYSFT)
998 WRITE(87,*) IPKEY,(TITLE(I),I=1,3)
WRITE(87,*) (PFE(I),I=1,10)
WRITE(88,*)
WRITE(88,*) 'RESISTIVITY MODEL'
WRITE(88,*)
DO 133 I=1,NNODZ
      WRITE(88,28) (ICODE(I,J),J=NXBEG,NXEND)
133 continue
28  format(2x,58I1)
WRITE(88,*)
WRITE(88,*)
write(88,*) 'resistivity key'
WRITE(88,*)
write(88,29) RESIS(1),RESIS(2),RESIS(3),RESIS(4),RESIS(5)
write(88,30) RESIS(6),RESIS(7),RESIS(8),RESIS(9),RESIS(10)
29  FORMAT(1X,'0=',F6.1,2X,'1=',F6.1,2X,'2=',F6.1,2X,'3=',F6.1,2X,
1    '4=',f6.1)
30  FORMAT(1X,'5=',F6.1,2X,'6=',F6.1,2X,'7=',F6.1,2X,'8=',F9.1,2X,
1    '9=',f9.1)
WRITE(87,*) MORE
WRITE(87,*) OPTPUN,IPRINT,THETA
WRITE(87,*) INCLIN,ISHIFT,NRLIM
NTXTOT=NTX*NZSFT
NRXTIT=NRX*NZRSFT
NRXTOT=NRX*NZRSFT*NYSFT
ipcnt=0

C
C
C
C
*** SETTING UP THE SCALED DISTANCES AND ASSIGNED CONDUCTIVITY ***
      DISTRIBUTION AT EACH ELEMENT IN THE MESH

IF(MORE.NE.0) GO TO 1303
X(1)=0.00
Z(1)=0.00
      DO 104 IX=2,NNODX
104  X(IX)=X(IX-1)+(DX(IX-1)/XSCAL)
      DO 105 IZ=2,NNODZ
105  Z(IZ)=Z(IZ-1)+(DZ(IZ-1)/ZSCAL)
1303 CONTINUE
IPCNT=1
DO 106 IZ=1,NNODZ
      DO 106 IX=1,NNODX
      IF(IPCNT.NE.1) GO TO 107
      IF(IX.LT.NXBEG) ICODE(IZ,IX)=ICODE(IZ,NXBEG)
      IF(IX.GT.NXEND) ICODE(IZ,IX)=ICODE(IZ,NXEND)
      IRESX=ICODE(IZ,IX)+1
      COND(IX,IZ)=1.0/RESIS(IRESX)
      GO TO 106
107  IRESX=ICODE(IZ,IX)+1
      COND(IX,IZ)=(1.0+PFE(IRESX)/100.0)/RESIS(IRESX)

```

```

106      CONTINUE
        IF(MORE.NE.0.OR.IPCNT.NE.1) GO TO 1304
            DO 130 IX=1,NELX
130                DX(IX)=DX(IX)/XSCAL
            DO 135 IZ=1,NELZ
135                DZ(IZ)=DZ(IZ)/ZSCAL
        WRITE(87,1045)
1045     FORMAT(5X,'DISTANCES IN MESH UNITS FROM THE ORGIN LOCATED
1 AT THE TOP, LEFT HAND CORNER OF THE MESH',//)
        WRITE(87,1040) (IX,X(IX),DX(IX), IX=1,NNODX)
1040     FORMAT(2X,'IX=',I5,3X,'X(IX)=' ,F10.3,3X,'DX(IX)=' ,F10.3)
        WRITE(87,1050) (IZ,Z(IZ),DZ(IZ), IZ=1,NNODZ)
1050     FORMAT(2X,'IZ=',I5,3X,'Z(IZ)=' ,F10.3,3X,'DZ(IZ)=' ,F10.3)
1304     CONTINUE
        DO 111 IZTX=1,NZSFT
            ZSFT=ZSHIFT(IZTX)*UNIT
            DO 112 INDXZ=1,NNODZ
                IF(ZSFT.EQ.Z(INDXZ)) IZSQ=INDXZ
112             CONTINUE
            DO 114 IXTX=1,NTX
                NTXCNT=(IZTX-1)*NTX+IXTX
                IXS(NTXCNT)=ITXP(IXTX)
                IZS(NTXCNT)=IZSQ
114             CONTINUE
111     CONTINUE
        NNODE=NNODX*NNODZ
        NBAND=2*NNODZ+1
        NNTOT=NNODE*NTXCNT
        NLNA=NNODE*(NNODZ+1)
        NBAND2=NNODZ+1
        WRITE(87,1171) NLNA,NNTOT
1171     FORMAT(1H1,25X,'DIMENSION OF A SHOULD BE AT LEAST =',I20,
1 5X,/,24X,'DIMENSION OF RS SHOULD BE AT LEAST =',I20)
        DO 110 IKY=1,NKY
        YLAMDA=YKY(IKY)
C
C
C     ***** FINITE DIFFERENCE SOLUTION FOR EACH OF THE KY VALUES *****
C
        write(6,*) 'entering slvent #',iky
        CALL SLVENT(X,Z,COND,IXS,IZS,YLAMDA,DX,DZ,NNODX,NNODZ,IKY,
1 NTXCNT,NTX,ITXP,NRX,IRXP,NZRSFT,ZRSHIF,NKY,NTXTOT,NRXTIT,
2 NNTOT,NBAND,NBAND2,NNODE,NLNA,VKY,UNIT,A,RS,XMAT,UL,NSOURC)
110     CONTINUE
        write(6,*) 'out of slvent'
C
C
C     *** INVERSE TRANSFORMATION OF THE POTENTIALS IN (X,KY,Z) SPACE ***
C
        IOPT .EQ. 0      INTEGRATION BY SUBSECTION EXPONENTIAL FIT
        IOPT .NE. 0      INTEGRATION BY TRAPEZOIDAL RULE
        IOPT=0
C
        write(6,*) 'entering ytran'
        CALL YTRAN(NRX,NYSFT,NZRSFT,YSHIFT,NTX,NZSFT,NKY,NTXTOT,
1 NRXTOT,NRXTIT,YKY,VKY,V,IOPT,UNIT)
        write(6,*) 'leaving ytran'
C
C
C     ***** SORT OUT COMBINATIONS OF THE POINT SOURCE POTENTIALS *****
C
C
C     FOR VARIOUS ELECTRODE ARRAYS
C
        IF(IPKEY.EQ.0) IPINDX=0

```

```

IF(IPKEY.NE.0.AND.IPCNT.EQ.1)IPINDX=0
IF(IPKEY.NE.0.AND.IPCNT.EQ.2)IPINDX=1
write(6,*)'entering arrays'
CALL ARRAYS(X,Z,NARRAY,ICONFG,TITLE,NTXTOT,NRXTOT,NTX,NRX,
1     ITXP,IRXP,NZSFT,NYSFT,NZRSFT,ZSHIFT,YSHIFT,ZRSHIF,IPINDX,V,
2     NNODX,NNODZ,UNIT)
write(6,*)'leaving arrays'
STOP
END

```

```

***** SUBROUTINE SOLVENT *****

```

```

C
C
C
C
C
C
C
C
C
THIS SUBROUTINE IS CALLED BY THE MAIN PROGRAM AND IT SETS UP
AND SOLVES THE CAPACITANCE MATRIX EQUATIONS IN (X,KY,Z) SPACE
FOR ALL SPECIFIED TRANSMITTING NODES SIMULTANEOUSLY. THE SOLUTION
PROVIDES THE POTENTIAL DISTRIBUTION AT EACH NODE IN THE GRID AND
THEIR VALUES AT RELEVANT RECEIVER NODES ARE SELECTED AND STORED.

```

```

SUBROUTINE SLVENT(X,Z,COND,IXS,IZS,YLAMDA,DX,DZ,NNODX,
1 NNODZ,IKY,NTXCNT,NTX,ITXP,NRX,IRXP,NZRSFT,ZRSHIF,NKY,
1 NTXTOT,NRXTIT,NNTOT,NBAND,NBAND2,NNODE,NLNA,VKY,UNIT,
1 A,RS,XMAT,UL,NSOURC)
DIMENSION A(NNODE,NBAND2),RS(NNODE,NTXCNT),XMAT(NNODE),
1     VKY(NKY,NTXTOT,NRXTIT),UL(NNODE,NBANB2)
DIMENSION COND(113,16),DX(112),DZ(15),ITXP(NTX),IRXP(NRX),
1     X(113),Z(16),ZRSHIF(1),IXS(NTXTOT),IZS(NTXTOT),
1     C(33),NSOURC(NTX)
EXTERNAL AK0,AK1
DATA PI/3.141592853/
IPC=0
AMP=2.0*PI
XCENTR=(X(1)+X(NNODX))/2.0
NELX=NNODX-1
NELZ=NNODZ-1
DO 100 ITX=1,NTXCNT
IXSP=IXS(ITX)
IZSP=IZS(ITX)
NSOURC(ITX)=(IXSP-1)*NNODZ+IZSP
DO 100 IX=1,NNODX
DO 100 IZ=1,NNODZ
N=(IX-1)*NNODZ+IZ
RS(N,ITX)=0.00
IF(N.NE.NSOURC(ITX)) GO TO 100
RS(N,ITX)=AMP/2.00

```

```

100 CONTINUE

```

```

***** SET UP COEFFICIENT MATRIX FOR THE MESH *****

```

```

C
C
C
N1=1
NCENT=NBAND2
NMIDL=NBAND2-1
NMIDU=NBAND2+1
NEND=NBAND
DO 210 IX=1,NNODX
DO 220 IZ=1,NNODZ
N=(IX-1)*NNODZ+IZ
IF(IX.EQ.1.OR.IX.EQ.NNODX) GO TO 310
IF(IZ.EQ.NNODZ) GO TO 315
IF(IZ.EQ.1) GO TO 320

```

***** COEFFICIENTS FOR THE SELF ADJOINT EQUATION OF AN *****
 INTERIOR NODE

C
C
C

```

ARCON=(COND(IX-1,IZ-1)*DX(IX-1)*DZ(IZ-1)/4.0)+
1 (COND(IX,IZ-1)*DX(IX)*DZ(IZ-1)/4.0)+(COND(IX,IZ)*
1 DX(IX)*DZ(IZ)/4.0)+(COND(IX-1,IZ)*DX(IX-1)*DZ(IZ)/4.0)
400 DO 400 KC=1,NBAND
      C(KC)=0.0
C(N1)=-((DZ(IZ-1)*COND(IX-1,IZ-1)+DZ(IZ)*COND(IX-1,IZ))/
1 (2.0*DX(IX-1)))
C(NMIDL)=-((DX(IX-1)*COND(IX-1,IZ-1)+DX(IX)*COND(IX,IZ-1)
1 )/(2.0*DZ(IZ-1)))
C(NMIDU)=-((DX(IX-1)*COND(IX-1,IZ)+DX(IX)*COND(IX,IZ))/
1 (2.0*DZ(IZ)))
C(NEND)=-((DZ(IZ-1)*COND(IX,IZ-1)+DZ(IZ)*COND(IX,IZ))/
1 (2.0*DX(IX)))
1 C(NCENT)=-((C(N1)+C(NMIDL)+C(NMIDU)+C(NEND)-YLAMDA*YLAMDA
      *ARCON)
410 DO 410 KC=1,NBAND2
      A(N,KC)=C(KC)
GO TO 350
320 CONTINUE

```

C
C
C
C

***** COEFFICIENTS FOR THE SELF ADJOINT EQUATION OF A NODE *****
 LOCATED ON THE TOP SURFACE (Neumann type condition)

```

ARCON=(COND(IX-1,IZ)*DX(IX-1)*DZ(IZ)/4.0)+(COND(IX,IZ)
1 *DX(IX)*DZ(IZ)/4.0)
420 DO 420 KC=1,NBAND
      C(KC)=0.0
C(N1)=-DZ(IZ)*COND(IX-1,IZ)/(2.0*DX(IX-1))
C(NMIDL)=0.0
C(NMIDU)=-((DX(IX)*COND(IX,IZ)+DX(IX-1)*COND(IX-1,IZ))/
1 (2.0*DZ(IZ)))
C(NEND)=-DZ(IZ)*COND(IX,IZ)/(2.0*DX(IX))
1 C(NCENT)=-((C(N1)+C(NMIDL)+C(NMIDU)+C(NEND)-YLAMDA*YLAMDA
      *ARCON)
430 DO 430 KC=1,NBAND2
      A(N,KC)=C(KC)
GO TO 350
315 CONTINUE

```

C
C
C
C

***** COEFFICIENTS FOR THE SELF ADJOINT EQUATION OF A NODE *****
 LOCATED ON THE BOTTOM SURFACE (mixed boundary condition)

```

ARCON=(COND(IX-1,IZ-1)*DX(IX-1)*DZ(IZ-1)/4.0)+(COND(IX,IZ-1)
1 *DX(IX)*DZ(IZ-1)/4.0)
XTX=ABS(X(IX)-XCENTR)
R=SQRT(XTX*XTX+Z(IZ)*Z(IZ))
ARG=YLAMDA*R
ARG1=AK1(ARG)
ARG2=AK0(ARG)
IF(ARG1.LT.1.0E-30.AND.ARG2.LT.1.0E-30) ARG3=1.0
IF(ARG1.GE.1.0E-30.OR.ARG2.GE.1.0E-30) ARG3=ARG1/ARG2
THETA=ATAN(XTX/Z(IZ))
440 DO 440 KC=1,NBAND
      C(KC)=0.0
C(N1)=-DZ(IZ-1)*COND(IX-1,IZ-1)/(2.0*DX(IX-1))
1 C(NMIDL)=-((DX(IX)*COND(IX,IZ-1)+DX(IX-1)*COND(IX-1,IZ-1))/
      (2.0*DZ(IZ-1)))

```

```

C(NMIDU)=0.00
C(NEND)=-DZ(IZ-1)*COND(IX,IZ-1)/(2.0*DX(IX))
CADD=-C(NMIDL)*DZ(IZ-1)*YLAMDA*COS(THETA)*ARG3
C(NCENT)=-C(N1)+C(NMIDL)+C(NMIDU)+C(NEND)-YLAMDA*YLAMDA
1      *ARCON)+CADD
441    DO 441 KC=1,NBAND2
      A(N,KC)=C(KC)
310    GO TO 350
CONTINUE
IF(IX.EQ.NNODX) GO TO 330
      DO 450 KC=1,NBAND
450    C(KC)=0.00
IF(IZ.GT.1.AND.IZ.NE.NNODZ) GO TO 4501
IF(IZ.EQ.NNODZ) GO TO 4502

```

```

C
C
C
C
***** COEFFICIENTS FOR THE SELF ADJOINT EQUATION OF A NODE *****
          LOCATED AT THE TOP LEFT CORNER
          (Neumann on top, mixed on the left)

```

```

ARCON=COND(IX,IZ)*DX(IX)*DZ(IZ)/4.0
XTX=ABS(X(IX)-XCENETR)
R=XTX
ARG=YLAMDA*R
ARG1=AK1(ARG)
ARG2=AK0(ARG)
IF(ARG1.LT.1.0E-30.AND.ARG2.LT.1.0E-30) ARG3=1.0
IF(ARG1.GE.1.0E-30.OR.ARG2.GE.1.0E-30) ARG3=ARG1/ARG2
C(N1)=0.00
C(NMIDL)=0.00
C(NMIDU)=-DX(IX)*COND(IX,IZ)/(2.0*DZ(IZ))
C(NEND)=-DZ(IZ)*COND(IX,IZ)/(2.0*DX(IX))
CADD=-C(NEND)*DX(IX)*YLAMDA*ARG3
C(NCENT)=-C(N1)+C(NMIDL)+C(NMIDU)+C(NEND)-YLAMDA*YLAMDA
1      *ARCON)+CADD
GO TO 4503

```

```

C
C
C
C
***** COEFFICIENTS FOR THE SELF ADJOINT EQUATION OF A NODE *****
          LOCATED AT THE LEFT EDGE (mixed boundary condition)

```

```

4501  ARCON=(COND(IX,IZ-1)*DX(IX)*DZ(IZ-1)/4.0)+(COND(IX,IZ)
1      *DX(IX)*DZ(IZ)/4.0)
XTX=ABS(X(IX)-XCENETR)
R=SQRT(XTX*XTX+Z(IZ)*Z(IZ))
ARG=YLAMDA*R
ARG1=AK1(ARG)
ARG2=AK0(ARG)
IF(ARG1.LT.1.0E-30.AND.ARG2.LT.1.0E-30) ARG3=1.0
IF(ARG1.GE.1.0E-30.OR.ARG2.GE.1.0E-30) ARG3=ARG1/ARG2
THETA=ATAN(Z(IZ)/XTX)
C(N1)=0.0
C(NMIDL)=-DX(IX)*COND(IX,IZ-1)/(2.0*DZ(IZ-1))
C(NMIDU)=-DX(IX)*COND(IX,IZ)/(2.0*DZ(IZ))
C(NEND)=-((DZ(IZ)*COND(IX,IZ)+DZ(IZ-1)*COND(IX,IZ-1))
1      /(2.0*DX(IX)))
CADD=-C(NEND)*DX(IX)*YLAMDA*COS(THETA)*ARG3
C(NCENT)=-C(N1)+C(NMIDL)+C(NMIDU)+C(NEND)-YLAMDA*YLAMDA
1      *ARCON)+CADD
GO TO 4503

```

```

C
C
***** COEFFICIENTS FOR THE SELF ADJOINT EQUATION OF A NODE *****

```

C LOCATED AT THE BOTTOM LEFT CORNER (mixed boundary condition)

```

C
C
4502 ARCON=COND(IX,IZ-1)*DX(IX)*DZ(IZ-1)/4.0
      XTX=ABS(X(IX)-XCENTR)
      R=SQRT(XTX*XTX+Z(IZ)*Z(IZ))
      ARG=YLAMDA*R
      ARG1=AK1(ARG)
      ARG2=AK0(ARG)
      IF(ARG1.LT.1.0E-30.AND.ARG2.LT.1.0E-30) ARG3=1.0
      IF(ARG1.GE.1.0E-30.OR.ARG2.GE.1.0E-30) ARG3=ARG1/ARG2
      THETA1=ATAN(Z(IZ)/XTX)
      THETA2=ATAN(XTX/Z(IZ))
      C(N1)=0.0
      C(NMIDL)=-DX(IX)*COND(IX,IZ-1)/(2.0*DZ(IZ-1))
      C(NMIDU)=0.0
      C(NEND)=-DZ(IZ-1)*COND(IX,IZ-1)/(2.0*DX(IX))
      CADD=-(C(NMIDL)*DZ(IZ-1)*COS(THETA2)+C(NEND)*
1         DX(IX)*COS(THETA1))*ARG3*YLAMDA
      C(NCENT)=-C(N1)+C(NMIDL)+C(NMIDU)+C(NEND)-YLAMDA*YLAMDA
1         *ARCON)+CADD
4503 DO 4511 KC=1,NBAND2
4511 A(N,KC)=C(KC)
      GO TO 350
330 CONTINUE
      DO 460 KC=1,NBAND
460   C(KC)=0.0
      IF(IZ.GT.1.AND.IZ.NE.NNODZ) GO TO 4601
      IF(IZ.EQ.NNODZ) GO TO 4602

```

C ***** COEFFICIENTS FOR THE SELF ADJOINT EQUATION OF A NODE *****
 C LOCATED AT THE TOP RIGHT CORNER
 C (Neumann on top, mixed on the right)
 C

```

ARCON=COND(IX-1,IZ)*DX(IX-1)*DZ(IZ)/4.00
XTX=ABS(X(IX)-XCENTR)
R=XTX
ARG=YLAMDA*R
ARG1=AK1(ARG)
ARG2=AK0(ARG)
IF(ARG1.LT.1.0E-30.AND.ARG2.LT.1.0E-30) ARG3=1.00
IF(ARG1.GE.1.0E-30.OR.ARG2.GE.1.0E-30) ARG3=ARG1/ARG2
C(N1)=-DZ(IZ)*COND(IX-1,IZ)/(2.0*DX(IX-1))
C(NMIDL)=0.00
C(NMIDU)=-DX(IX-1)*COND(IX-1,IZ)/(2.0*DZ(IZ))
C(NEND)=0.00
CADD=-C(N1)*DX(IX-1)*YLAMDA*ARG3
1 C(NCENT)=-C(N1)+C(NMIDL)+C(NMIDU)+C(NEND)-YLAMDA*YLAMDA
   *ARCON)+CADD
GO TO 4603

```

C ***** COEFFICIENTS FOR THE SELF ADJOINT EQUATION OF A NODE *****
 C LOCATED AT THE RIGHT EDGE (mixed boundary condition)
 C

```

4601 ARCON=(COND(IX-1,IZ-1)*DX(IX-1)*DZ(IZ-1)/4.0)+(COND(
1   IX-1,IZ)*DX(IX-1)*DZ(IZ)/4.0)
      XTX=ABS(X(IX)-XCENTR)
      R=SQRT(XTX*XTX+Z(IZ)*Z(IZ))
      ARG=YLAMDA*R
      ARG1=AK1(ARG)
      ARG2=AK0(ARG)

```

```

IF(ARG1.LT.1.0E-30.AND.ARG2.LT.1.0E-30) ARG3=1.0
IF(ARG1.GE.1.0E-30.OR.ARG2.GE.1.0E-30) ARG3=ARG1/ARG2
THETA=ATAN(Z(IZ)/XTX)
C(N1)=- (DZ(IZ)*COND(IX-1,IZ)+DZ(IZ-1)*COND(IX-1,IZ-1))
1 / (2.0*DX(IX-1))
C(NMIDL)=-DX(IX-1)*COND(IX-1,IZ-1)/(2.0*DZ(IZ-1))
C(NMIDU)=-DX(IX-1)*COND(IX-1,IZ)/(2.0*DZ(IZ))
C(NEND)=0.00
CADD=-C(N1)*DX(IX-1)*YLAMDA*COS(THETA)*ARG3
C(NCENT)=- (C(N1)+C(NMIDL)+C(NMIDU)+C(NEND)-YLAMDA*YLAMDA
1 *ARCON)+CADD
GO TO 4603

C
C ***** COEFFICIENTS FOR THE SELF ADJOINT EQUATION OF A NODE *****
C LOCATED AT THE BOTTOM RIGHT CORNER (mixed boundary condition)
C
4602 ARCON=COND(IX-1,IZ-1)*DX(IX-1)*DZ(IZ-1)/4.0
XTX=ABS(X(IX)-XCENTR)
R=SQRT(XTX*XTX+Z(IZ)*Z(IZ))
ARG=YLAMDA*R
ARG1=AK1(ARG)
ARG2=AK0(ARG)
IF(ARG1.LT.1.0E-30.AND.ARG2.LT.1.0E-30) ARG3=1.0
IF(ARG1.GE.1.0E-30.OR.ARG2.GE.1.0E-30) ARG3=ARG1/ARG2
THETA2=ATAN(Z(IZ)/XTX)
THETA1=ATAN(XTX/Z(IZ))
C(N1)=-DZ(IZ-1)*COND(IX-1,IZ-1)/(2.0*DX(IX-1))
C(NMIDL)=-DX(IX-1)*COND(IX-1,IZ-1)/(2.0*DZ(IZ-1))
C(NMIDU)=0.00
C(NEND)=0.00
CADD=- (C(NMIDL)*DZ(IZ-1)*COS(THETA2)+C(N1)*DX(IX-1)*
1 COS(THETA1))*YLAMDA*ARG3
C(NCENT)=- (C(N1)+C(NMIDL)+C(NMIDU)+C(NEND)-YLAMDA*YLAMDA
1 *ARCON)+CADD
4603 DO 4611 KC=1,NBAND2
4611 A(N,KC)=C(KC)
350 CONTINUE
220 CONTINUE
210 CONTINUE

C
C ***** sending capacitance matrix to band-solver *****
C (symmetric Cholesky decomposition)
C
Write(6,*)'ENTERING BNDSYM'
CALL BNDSYM(A,NNODE,NNODZ,NNODE,RS,NNODE,NTXCNT,14,D1,D2,
1 NBAND2,XMAT,IER,UL)
WRITE(6,*)'LEAVING BNDSYM'

C
WRITE(87,910) IER
910 FORMAT(20X,'MATRIX SOLUTION ERROR INDEX = ',I5)
DO 1210 ITX=1,NTXCNT
DO 1220 IDWN=1,NZRSFT
ZRSFT=ZRSHTF(IDWN)*UNIT
DO 1230 INDXZ=1,NNODZ
1230 IF(ZRSFT.EQ.Z(INDXZ)) IZRS=INDXZ
DO 1240 IRX=1,NRX
IRXX=IRXP(IRX)
IRDWNX=IRX+(IDWN-1)*NRX
NRXCHK=(IRXX-1)*NNODZ+IZRS
VKY(IKY,ITX,IRDWNX)=RS(NRXCHK,ITX)

```

1240 CONTINUE
1220 CONTINUE
1210 CONTINUE
RETURN
END

150

```
C
C ***** LINEAR EQUATION SOLVER-SYMMETRIC BAND STORAGE MODE- *****
C           SPACE ECONOMIZER SOLUTION
C
C A-(INPUT) THE COEFFICIENT MATRIX OF THE EQUATION  $AX = B$ , WHERE A
C IS ASSUMED TO BE AN N BY N POSITIVE DEFINITE SYMMETRIC BAND MATRIX.
C A IS STORED IN SYMMETRIC BAND STORAGE MODE AND THEREFORE HAS
C DIMENSIONS N BY (NC+1)
C (OUTPUT) A IS REPLACED BY L WHERE  $A = L * L$ -TRANPOSE. L IS A LOWER
C BAND MATRIX STORED IN BAND FORM AND THEREFORE HAS DIMENSIONS
C N BY (NC+1). NOTE THAT THE DIAGONAL ELEMENTS OF L ARE STORED
C IN RECIPROCAL FORM
C N-ORDER OF THE MATRIX A AND NUMBER OF ROWS IN B.
C NC-NUMBER OF UPPER OR LOWER CO-DIAGONALS OF A.
C NBND-NC+1
C IA-ROW DIMENSION OD A AS SPECIFIED IN THE MAIN PROGRAM
C B-(INPUT) MATRIX OF DIMENSION N BY M CONTAINING THE M RIGHT-HAND
C SIDES OF THE EQUATION  $AX = B$ .
C (OUTPUT) THE N BY M SOLUTION MATRIX X REPLACES B.
C IB-ROW DIMENSION OF B AS SPECIFIED IN THE MAIN PROGRAM.
C M-NUMBER OF RIGHT HAND SIDES (COLUMNS IN B)
C D1,D2-COMPONENTS OF THE DETERMINANT OF A
C IER-ERROR PARAMETERS
C
C SUBROUTINE BNDSYM(A,N,NC,IA,B,IB,M,IDGT,D1,D2,NBND,X,IER,UL)
C DIMENSION A(IA,NBND),B(IB,M)
C DIMENSION X(N),UL(IA,NBND)
C IER=0
C
C SUBROUTINE LUDAPB - IMSL CALL
C LU DECOMPOSITION OF A POSITIVE DEFINITE SYMMETRIC BAND MATRIX
C - CHOLESKY DECOMPOSITION
C
C WRITE(6,*)'ENTERING LUDAPB'
C CALL LUDAPB(A,N,NC,IA,UL,IA,D1,D2,IER)
C WRITE(6,*)'LEAVING LUDAPB'
C IF(IER.NE.0)THEN
C     WRITE(6,*)'SHIT'
C     STOP
C ENDIF
C WRITE(6,*)'ENTERING SOLVE (BACK SUBSTITUTION)'
C DO 5 I=1,M
C
C           SOLUTION OF  $AX=B$ 
C
C     DO 51 IX=1,N
C     X(IX)=B(IX,I)
51 CALL SOLVE(UL,X,N,NC,IA,NBND)
C     DO 52 IX=1,N
52 B(IX,I)=X(IX)
C 5 CONTINUE
C WRITE(6,*)'LEAVING SOLVE'
```



```

9000 CONTINUE
      RETURN
      END

```

```

      ELIMINATION PORTION OF THE SOLUTION OF AX=B
      SYMMETRIC BAND STORAGE MODE

```

```

      UL-OUTPUT MATRIX L WHERE A = L*L-TRANPOSE. L IS STORED IN
      BAND STORAGE MODE. UL SHOULD BE AN ARRAY OF SIZE N BY NC+1
      NOTE THAT THE DIAGONAL OF UL CONTAINS THE RECIPROCAL OF
      THE ACTUAL DIAGONAL ELEMENTS.
      IU-ROW DIMENSION OF UL AS SPECIFIED IN THE MAIN PROGRAM.

```

```

      SUBROUTINE SOLVE(UL,X,N,NC,IA,NBND)
      DIMENSION UL(IA,NBND)
      DIMENSION X(N)

```

```

      SOLUTION LY=B

```

```

      NC1=NC+1
      IW=0
      L=0

```

```

      DO 15 I=1,N
          SUM=X(I)
          IF(NC.LE.0) GO TO 10
          IF(IW.EQ.0) GO TO 9
          L=L+1
          IF(L.GT.NC) L=NC
          K=NC1-L
          KL=I-L
          DO 5 J=K,NC
              SUM=SUM-X(KL)*UL(I,J)
              KL=KL+1

```

```

5          CONTINUE
          GO TO 10
9          IF(SUM.NE.0.0) IW=1
10         X(I)=SUM*UL(I,NC1)
15         CONTINUE

```

```

      SOLUTION UX = Y

```

```

20        X(N)=X(N)*UL(N,NC1)
          IF(N.LE.1) GO TO 40
          N1=N+1
          DO 35 I=2,N
              K=N1-I
              SUM=X(K)
              IF(NC.LE.0) GO TO 30
              KL=K+1
              K1=MIN0(N,K+NC)
              L=1
              DO 25 J=KL,K1
                  SUM=SUM-X(J)*UL(J,NC1-L)
                  L=L+1
25          CONTINUE
30          X(K)=SUM*UL(K,NC1)
35          CONTINUE
40          RETURN
          END

```

EVALUATES THE MODIFIED BESSEL FUNCTION OF ZEROETH
ORDER FOR ARGUMENT X

```

C
C
C
FUNCTION AK0(X)
IF(X.GE.2.0) GO TO 10
T=X/3.75
T=T*T
1 B1=1.0+T*(3.5156229+T*(3.0899424+T*(1.2067492+T*
  (0.2659732+T*(0.0360768+T*0.0045813))))))
T=0.5*X
Y=T*T
1 AK0=-ALOG(T)*B1-0.57721566+Y*(0.42278420+Y*(0.23069756+Y*
  (0.03488590+Y*(0.00262698+Y*(0.00018750+Y*0.00000740))))))
RETURN
10 T=2.00/X
F=EXP(-X)/SQRT(X)
1 AK0=F*(1.25331414+T*(-0.07832358+T*(0.02189568+T*(-0.01062446
  +T*(0.00587872+T*(-0.00251540+T*0.00053208))))))
RETURN
END

```

EVALUATES THE MODIFIED BESSEL FUNCTION OF ORDER 1
FOR AN ARGUMENT X

```

C
C
C
FUNCTION AK1(X)
IF(X.GE.2.00) GO TO 100
T=X/3.75
T2=T*T
T4=T2*T2
T6=T4*T2
T8=T4*T4
T10=T6*T4
T12=T8*T4
1 B=0.50+0.87890594*T2+0.51498869*T4+0.15084934*T6+
  0.02658733*T8+0.00301532*T10+0.00032411*T12
B11=X*B
T=X*0.5
T2=T*T
T4=T2*T2
T6=T4*T2
T8=T4*T4
T10=T6*T4
T12=T8*T4
1 AA=X*ALOG(T)*B11+1.00+0.15443144*T2-0.67278579*T4-0.18156897
  *T6-0.01919402*T8-0.0011040*T10-0.00004686*T12
AK1=AA/X
RETURN
100 T=2.0/X
T2=T*T
T3=T2*T
T4=T2*T2
T5=T3*T2
T6=T4*T2
1 BB=1.25331414+0.23498619*T-0.03655620*T2+0.01504268*T3-
  0.00780353*T4+0.00325614*T5-0.00068245*T6
AK1=BB*EXP(-X)/SQRT(X)
RETURN
END

```

C
C
C
C
C
C
C
SUBROUTINE YTRAN PERFORMS THE INVERSE FOURIER TRANSFORM
OF THE POTENTIALS IN (X-KY-Z) SPACE BACK TO (X-Y-Z) SPACE.
THE TRANSFORMATION INTEGRAL IS DETERMINED BY FITTING SUBSECTIONS
IN KY-SPACE BY EXPONENTIALS OR BY TRAPEZOIDAL RULE

1 SUBROUTINE YTRAN(NRX,NYSFT,NZRSFT,YSHIFT,NTX,NZSFT,NKY,NTXTOT,
NRXTOT,NRXTIT,YKY,VKY,V,INDEX,UNIT)
DIMENSION VKY(NKY,NTXTOT,NRXTIT),V(NTXTOT,NRXTOT)
DIMENSION YSHIFT(1),YKY(5)
DO 100 ID=1,NZSFT
DO 100 IE=1,NTX
ITX=(ID-1)*NTX+IE
IRX=0
DO 100 IA=1,NZRSFT
DO 100 IC=1,NYSFT
Y=YSHIFT(IC)*UNIT
DO 100 IB=1,NRX
IRXA=(IA-1)*NRX+IB
IRX=IRX+1
IF(INDEX.NE.0.AND.Y.EQ.0.00) GO TO 300

C
C
C
INTEGRATION BY SUBSECTIONAL EXPONENTIAL FITS

IF(Y.EQ.0.00) VA=VKY(1,ITX,IRXA)*YKY(1)
IF(Y.NE.0.00) VA=VKY(1,ITX,IRXA)*SIN(YKY(1)*Y)/Y
DO 200 IKY=2,NKY
IK1=IKY-1
XK1=YKY(IK1)
XK2=YKY(IKY)
Y1=VKY(IK1,ITX,IRXA)
Y2=VKY(IKY,ITX,IRXA)
IF(Y1.LT.1.0E-30.OR.Y2.LT.1.0E-30) GO TO 210
A=-ALOG(Y2/Y1)/(XK2-XK1)
GO TO 215
210 A=0.00
215 CONTINUE
IF(A.EQ.0.00.AND.Y.EQ.0.00) GO TO 220
VA=VA+(Y1*(A*COS(XK1*Y)-Y*SIN(XK1*Y))-Y2*(A*COS(XK2*Y)
-Y*SIN(XK2*Y)))/(A*A+Y*Y)
1 GO TO 225
220 VA=VA+Y1*(XK2-XK1)
225 CONTINUE
200 CONTINUE
GO TO 250
300 CONTINUE

C
C
C
INTEGRATION BY TRAPEZOIDAL RULE

VA=VKY(1,ITX,IRXA)*YKY(1)
DO 310 IKY=2,NKY
IK1=IKY-1
XK1=YKY(IK1)
XK2=YKY(IKY)
Y1=VKY(IK1,ITX,IRXA)
Y2=VKY(IKY,ITX,IRXA)
AA=(Y1+Y2)*0.50*(XK2-XK1)
310 VA=VA+AA
250 CONTINUE
V(ITX,IRX)=(VA*2.0/3.141592653)*UNIT

```

100 CONTINUE
    RETURN
    END

```

```

C
C THE THREE-DIMENSIONAL POTENTIAL DISTRIBUTION FOR ALL OF THE
C SELECTED RECEIVER NODES FOR THE PRESCRIBED TRANSMITTER NODES
C ARE USED, IN COMBINATION, TO EVALUATE THE APPARENT RESISTIVITY
C RESPONSE FOR ANY ARBITRARY ARRAY. THIS SUBROUTINE WILL SELECT
C THE SPECIFIC SUBROUTINE REQUIRED TO COMPUTE RESPONSES FOR ANY
C PARTICULAR CONFIGURATION.

```

```

SUBROUTINE ARRAYS(X,Z,NARRAY,ICONFG,TITLE,NTXTOT,NRXTOT,
1   NTX,NRX,ITXP,IRXP,NZSFT,NYSFT,NZRSFT,ZSHIFT,YSHIFT,
1   ZRSHIF,IPKEY,V,NNODX,NNODZ,UNIT)
DIMENSION V(NTXTOT,NRXTOT)
DIMENSION X(113),Z(16),ICONFG(1),ITXP(NTS),IRXP(NRX)
1   ,ZSHIFT(1),YSHIFT(1),ZRSHIF(1)
CHARACTER TITLE(18)
    DO 10 IX=1,NNODX
10   X(IX)=X(IX)/UNIT
    DO 15 IZ=1,NNODZ
15   Z(IZ)=Z(IZ)/UNIT
DO 100 I=1,NARRAY
INDEX=ICONFG(I)
write(6,*)'hi paul'
GO TO (1,2), INDEX
WRITE(6,*)'ENTERING CLINDP'
1 CALL CLINDP(X,Z,IPKEY,TITLE,NTXTOT,NRXTOT,NRX,IRXP,
1   NTX,ITXP,NYSFT,YSHIFT,V,NNODX,NNODZ)
WRITE(6,*)'LEAVING CLINDP'
GO TO 99
WRITE(6,*)'ENTERING RECN2D'
2 CALL RECN2D(X,Z,NTXTOT,NRXTOT,NTX,NRX,ITXP,IRXP,NYSFT,
1   YSHIFT,TITLE,V,NNODX,NNODZ)
WRITE(6,*)'LEAVING RECN2D'
99 CONTINUE
100 CONTINUE
DO 11 IX=1,NNODX
11 X(IX)=X(IX)*UNIT
DO 16 IZ=1,NNODZ
16 Z(IZ)=Z(IZ)*UNIT
RETURN
END

```

```

C
C THIS SUBROUTINES PURPOSE IS TO OBTAIN PROFILES OF APPARENT
C RESISTIVITY OVER INHOMOGENEITIES WITH DIPOLE-DIPOLE AND POLE-DIPOLE
C CONFIGURATION OF ELECTRODES. THE PROFILE LINES ARE INCLIND TO THE
C STRIKE OF THE INHOMOGENEITY.

```

```

SUBROUTINE CLINDP(X,Z,IPKEY,TITLE,NTXTOT,NRXTOT,NRX,IRXP,
1   NTX,ITXP,NYSFT,YSHIFT,V,NNODX,NNODZ)
INTEGER OPTPUN
COMMON /GANG1/ OPTPUN,THETA,IPRINT
DIMENSION V(NTXTOT,NRXTOT)
DIMENSION X(113),Z(16),IRXP(NRX),ITXP(NTX),YSHIFT(1)
1   DIMENSION NPTS(19),NRA(18),NRB(18),GEOMFD(18),GEOMFP(18),
1   APRES1(25),APRES2(25),APIP1(25,20),APIP2(25,20),
1   APRDC1(25,20),APRDC2(25,20),APMCFD(25,20),APMCFP(25,20),
1   TXA(50),TXB(50),RXP(50)

```

DIMENSION TXPOS(23),RXPOS(23),CRFD(19),CRFP(18)

CHARACTER TITLE(18)

DATA NTA/1/,NTB/2/

DATA NRA/1,2,3,4,5,6,7,8,9,10,11,12,13,14,15,16,17,18/

DATA NRB/2,3,4,5,6,7,8,9,10,11,12,13,14,15,16,17,18,19/

DATA NPTS/22,21,20,19,18,17,16,15,14,13,12,11,10,9,8,7,6,5,4/

1 DATA TXPOS/-12.0,-11.0,-10.0,-9.0,-8.0,-7.0,-6.0,-5.0,-4.0,
-3.0,-2.0,-1.0,0.0,1.0,2.0,3.0,4.0,5.0,6.0,7.0,8.0,9.0,10.0/

1 DATA RXPOS/-10.0,-9.0,-8.0,-7.0,-6.0,-5.0,-4.0,-3.0,-2.0,-1.0
0.0,1.0,2.0,3.0,4.0,5.0,6.0,7.0,8.0,9.0,10.0,11.0,12.0/

1 DATA GEOMFD/3.0,12.0,30.0,60.0,105.0,168.0,252.0,360.0,495.0,
660.0,858.0,1092.0,1365.0,1680.0,2040.0,2448.0,2907.0,3420.0/

1 DATA GEOMFP/2.0,6.0,12.0,20.0,30.0,42.0,56.0,72.0,90.0,110.0,
132.0,156.0,182.0,210.0,240.0,272.0,306.0,342.0/

C
C
C
C
C
C
C

THE ARRAYS CRFD AND CRFP CONSIST OF THE CORRECTION FACTORS
EMPLOYED TO THE DP-DP AND P-DP ARRAYS FOR DIFFERENT DIPOLE
SEPARATIONS. THESE FACTORS ARE BASED ON COMPARISONS WITH KNOWN
SOLUTIONS OVER TWO-DIMENSIONAL STRUCTURES (FOR A PRESCRIBED
SET OF KY VALUES USED)

1 DATA CRFD/0.945,0.96,0.965,0.96,0.96,0.96,0.96,0.96,0.96,
0.96,0.96,0.966,0.97,0.97,0.97,0.97,0.97,0.97,0.97/

1 DATA CRFP/0.99,1.00,1.00,1.01,1.01,1.02,1.03,1.03,1.04,
1.06,1.07,1.08,1.08,1.09,1.09,1.09,1.09,1.09/

XCENTR=(X(1)+X(NNODX))/2.0

THETAX=THETA/57.296

DO 16 NSEP=1,18

N1=NPTS(NSEP)

DO 15 I=1,N1

IA=NTA+I-1

IB=NTB+I-1

JC=NRA(NSEP)+I-1

JD=NRB(NSEP)+I-1

IF(THETA.EQ.90.00) GO TO 771

C
C
C

COORDINATES OF THE TX AND RX ELECTRODES ON THE INCLIND PROFILE

AX=TXPOS(IA)

BX=TXPOS(IB)

CX=RXPOS(JC)

DX=RXPOS(JD)

C
C
C

COORDINATES OF THE TX AND RX ELECTRODES ON THE X-Y PLANE

CC=SIN(THETAX)

SS=COS(THETAX)

XATX=(AX*CC)+XCENTR

XBTX=(BX*CC)+XCENTR

XCRX=(CX*CC)+XCENTR

XDRX=(DX*CC)+XCENTR

YATX=AX*SS

YBTX=BX*SS

YCRX=CX*SS

YDRX=DX*SS

NTPOSX=NTX-1

DO 12 IX1=1,NTPOSX

NX1=ITXP(IX1)

NX2=ITXP(IX1+1)

X1=X(NX1)

```

X2=X(NX2)
AA=ABS(X1-X2)
IF(XATX.LT.X2.AND.XATX.GE.X1) ITAX=IX1
IF(XBTX.LT.X2.AND.XBTX.GE.X1) ITBX=IX1
12 CONTINUE
NRPOSX=NRX-1
DO 13 IX2=1,NRPOSX
    NX1=IRXP(IX2)
    NX2=IRXP(IX2+1)
    X1=X(NX1)
    X2=X(NX2)
    IF(XCRX.LT.X2.AND.XCRX.GE.X1) IRCX=IX2
    IF(XDRX.LT.X2.AND.XDRX.GE.X1) IRDX=IX2
13 CONTINUE

```

C
C
C
DETERMINATION OF THE RELATIVE Y-SHIFT BETWEEN TX AND RX POLES

```

NRLINY=NYSFT-1
DO 14 IY1=1,NRLINY
Y1=YSHIFT(IY1)
Y2=YSHIFT(IY1+1)
IF(ABS(YATX-YCRX).LT.Y2.AND.ABS(YATX-YCRX).GE.Y1) IACY=IY1
IF(ABS(YATX-YDRX).LT.Y2.AND.ABS(YATX-YDRX).GE.Y1) IADY=IY1
IF(ABS(YBTX-YCRX).LT.Y2.AND.ABS(YBTX-YCRX).GE.Y1) IBCY=IY1
IF(ABS(YBTX-YDRX).LT.Y2.AND.ABS(YBTX-YDRX).GE.Y1) IBDY=IY1
14 CONTINUE

```

C
C
C
C
C
TWO-DIMENSIONAL INTERPOLATION OF V(RECEIVER) ASSUMING LINEAR
VARIATION ALONG THE EDGES OF A SQUARE GRID OF KNOWN CORNER VALUES
AA IS THE SIDE DIMENSION OF THE SQUARE GRID

```

KNXA=ITXP(ITAX)
DXA=ABS(X(KNXA)-XATX)
KNXC=IRXP(IRCX)
KRC1=(IACY-1)*NRX+IRCX
KRC2=KRC1+1
KRC3=KRC2+NRX
KRC4=KRC1+NRX
V1=V(ITAX,KRC1)-(DXA*(V(ITAX,KRC1)-V(ITAX+1,KRC1)))/AA
V2=V(ITAX,KRC2)-(DXA*(V(ITAX,KRC2)-V(ITAX+1,KRC2)))/AA
V3=V(ITAX,KRC3)-(DXA*(V(ITAX,KRC3)-V(ITAX+1,KRC3)))/AA
V4=V(ITAX,KRC4)-(DXA*(V(ITAX,KRC4)-V(ITAX+1,KRC4)))/AA
DXC=ABS(X(KNXC)-XCRX)
DYC=ABS(ABS(YATX-YCRX)-YSHIFT(IACY))
V(IA,JC)=V1+(DXC*(V2-V1)/AA)+(DYC*(V4-V1)/AA)+
1 (DXC*DYC*(V1-V2+V3-V4)/(AA*AA))
KNXD=IRXP(IRDX)
KRD1=(IADY-1)*NRX+IRDX
KRD2=KRD1+1
KRD3=KRD2+NRX
KRD4=KRD1+NRX
V1=V(ITAX,KRD1)-(DXA*(V(ITAX,KRD1)-V(ITAX+1,KRD1)))/AA
V2=V(ITAX,KRD2)-(DXA*(V(ITAX,KRD2)-V(ITAX+1,KRD2)))/AA
V3=V(ITAX,KRD3)-(DXA*(V(ITAX,KRD3)-V(ITAX+1,KRD3)))/AA
V4=V(ITAX,KRD4)-(DXA*(V(ITAX,KRD4)-V(ITAX+1,KRD4)))/AA
DXD=ABS(X(KNXD)-XDRX)
DYD=ABS(ABS(YATX-YDRX)-YSHIFT(IADY))
1 V(IA,JD)=V1+(DXD*(V2-V1)/AA)+(DYD*(V4-V1)/AA)+(DXD*DYD*
    (V1-V2+V3-V4)/(AA*AA))

```

C

```

KNXB=ITXP(ITBX)
DXB=ABS(X(KNXB)-XBTX)
KNXC=IRXP(IRCX)
KRC1=(IBCY-1)*NRX+IRCX
KRC2=KRC1+1
KRC3=KRC2+NRX
KRC4=KRC1+NRX
V1=V(ITBX,KRC1)-(DXB*(V(ITBX,KRC1)-V(ITBX+1,KRC1)))/AA)
V2=V(ITBX,KRC2)-(DXB*(V(ITBX,KRC2)-V(ITBX+1,KRC2)))/AA)
V3=V(ITBX,KRC3)-(DXB*(V(ITBX,KRC3)-V(ITBX+1,KRC3)))/AA)
V4=V(ITBX,KRC4)-(DXB*(V(ITBX,KRC4)-V(ITBX+1,KRC4)))/AA)
DXC=ABS(X(KNXC)-XCRX)
DYC=ABS(ABS(YBTX-YCRX)-YSHIFT(IBCY))
V(IB,JC)=V1+(DXC*(V2-V1)/AA)+(DYC*(V4-V1)/AA)+
1 (DXC*DYC*(V1-V2+V3-V4)/(AA*AA))
KNXD=IRXP(IRDY)
KRD1=(IBDY-1)*NRX+IRDY
KRD2=KRD1+1
KRD3=KRD2+NRX
KRD4=KRD1+NRX
V1=V(ITBX,KRD1)-(DXB*(V(ITBX,KRD1)-V(ITBX+1,KRD1)))/AA)
V2=V(ITBX,KRD2)-(DXB*(V(ITBX,KRD2)-V(ITBX+1,KRD2)))/AA)
V3=V(ITBX,KRD3)-(DXB*(V(ITBX,KRD3)-V(ITBX+1,KRD3)))/AA)
V4=V(ITBX,KRD4)-(DXB*(V(ITBX,KRD4)-V(ITBX+1,KRD4)))/AA)
DXD=ABS(X(KNXD)-XDRX)
DYD=ABS(ABS(YBTX-YDRX)-YSHIFT(IBDY))
V(IB,JD)=V1+(DXD*(V2-V1)/AA)+(DYD*(V4-V1)/AA)+(DXD*DYD*
1 (V1-V2+V3-V4)/(AA*AA))
771 CONTINUE

C
C
C

TXA(I)=TXPOS(IA)
TXB(I)=TXPOS(IB)
RXP(I)=(RXPOS(JC)+RXPOS(JD))/2.0
APRES1(I)=ABS((V(IB,JC)+V(IA,JD)-V(IA,JC)-V(IB,JD))*
1 GEOMFD(NSEP))*CRFD(NSEP)
APRES2(I)=ABS((V(IB,JC)-V(IB,JD))*GEOMFP(NSEP))*CRFP(NSEP)
IF(IPKEY) 11,10,11
11 APIP1(I,NSEP)=((APRDC1(I,NSEP)-APRES1(I))/APRES1(I))*100.0
APMCFD(I,NSEP)=APIP1(I,NSEP)*1000.0/APRDC1(I,NSEP)
APIP2(I,NSEP)=((APRDC2(I,NSEP)-APRES2(I))/APRES2(I))*100.0
APMCFP(I,NSEP)=APIP2(I,NSEP)*1000.0/APRDC2(I,NSEP)
GO TO 15
10 APRDC1(I,NSEP)=APRES1(I)
APRDC2(I,NSEP)=APRES2(I)
15 CONTINUE
IF(IPRINT.EQ.0) GO TO 991
WRITE(87,170) (TITLE(LL),LL=1,3)
170 FORMAT(1H1,////////,55X,'CASE',1X,3A4,////,50X,'DIPOLE-DIPOLE
1 CONFIGURATION OF ELECTRODES'//)
WRITE(87,171) THETA,NSEP
171 FORMAT(/20X,'THE PROFILE LINE IS INCLIND TO THE STRIKE
1 (+Y DIR) AT ',F10.3,'DEGREES',/,50X,'DIPOLE-SEPARATION=',I5//)
WRITE(87,172) (TXA(I),TXB(I),RXP(I),APRDC1(I,NSEP),
1 APIP1(I,NSEP),APMCFD(I,NSEP),I=1,N1)
172 FORMAT(1X,'CURRENT ELECTRODES AT',1X,F7.2,1X,'AND',1X,
1 F7.2,12X,'CENTER OF RECEIVER=',F7.2,1X,'APP. RES.=',
1 F8.2,2X,'APP. P.F.E.=',F7.3,2X,'APP. MCF =',F8.2)
WRITE(87,173) (TITLE(LL),LL=1,3)

```

```

173  FORMAT(1H1,////////,55X,'CASE',1X,3A4,////,50X,'POLE-DIPOLE
1    CONFIGURATION OF ELECTRODES'///)
      WRITE(87,171) THETA,NSEP
      WRITE(87,174) (TXB(I),RXP(I),APRDC2(I,NSEP),
1                APIP2(I,NSEP),APMCFP(I,NSEP),I=1,N1)
174  FORMAT(1X,'CURRENT ELECTRODES AT',1X,F7.2,1X,'AND',1X,
1      F7.2,12X,'CENTER OF RECEIVER=',F7.2,1X,'APP. RES.=',
1      F9.2,2X,'APP. P.F.E.=',F7.3,2X,'APP. MCF =',F9.3)
991  CONTINUE
      IF(OPTPUN.EQ.0) GO TO 998
C    WRITE(88,180) (RXP(I),I=1,N1)
C    WRITE(88,181) (APRDC1(I,NSEP),I=1,N1)
C    WRITE(88,182) (APRDC2(I,NSEP),I=1,N1)
C 180  FORMAT(8F10.4)
C 181  FORMAT(8F10.4)
C 182  FORMAT(8F10.4)
998  CONTINUE
16   continue
      IF(IPRINT.EQ.1) GO TO 9915
      write(88,*)
      write(88,*)
      WRITE(88,200) (TITLE(LL),LL=1,18)
200  FORMAT(1X,'CASE',1X,18A,/,50X,'DIPOLE-DIPOLE
1    CONFIGURATION OF ELECTRODES')
      WRITE(87,221)
221  FORMAT(/80X,'PSEUDO-SECTION OF THE APPARENT RESISTIVITY')
      WRITE(87,205) THETA
205  FORMAT(/45X,'THE PROFILE LINE IS INCLIND TO THE STRIKE
1    ( +Y DIR ) AT ',F4.1,'DEGREES')
      WRITE(88,*)
220  FORMAT(4X,'X...X...X...X...X...X...X...X...X...X...X...
1    X...X...X...X...X...X...X...X...X...X...X...X...X...
1    X')
      WRITE(88,231) (APRDC1(I, 1),I=6,17)
      WRITE(88,232) (APRDC1(I, 2),I=6,16)
      WRITE(88,233) (APRDC1(I, 3),I=6,15)
      WRITE(88,234) (APRDC1(I, 4),I=6,14)
      WRITE(88,235) (APRDC1(I, 5),I=6,13)
      WRITE(88,236) (APRDC1(I, 6),I=6,12)
      WRITE(88,237) (APRDC1(I, 7),I=6,11)
      WRITE(88,238) (APRDC1(I, 8),I=6,10)
      WRITE(88,239) (APRDC1(I, 9),I=6, 9)
      WRITE(88,240) (APRDC1(I,10),I=6, 8)
      WRITE(88,241) (APRDC1(I,11),I=6, 7)
      WRITE(88,242) APRDC1(6,12)
231  FORMAT(////////,3X,' 1',12(F6.1,3X))
232  FORMAT( //,3X,' 2', 4X,11(F6.1,3X))
233  FORMAT( //,3X,' 3', 8X,10(F6.1,3X))
234  FORMAT( //,3X,' 4',12X,10(F6.1,3X))
235  FORMAT( //,3X,' 5',16X, 9(F6.1,3X))
236  FORMAT( //,3X,' 6',20X, 9(F6.1,3X))
237  FORMAT( //,3X,' 7',24X, 8(F6.1,3X))
238  FORMAT( //,3X,' 8',28X, 8(F6.1,3X))
239  FORMAT( //,3X,' 9',32X, 7(F6.1,3X))
240  FORMAT( //,2X,'10',36X, 7(F6.1,3X))
241  FORMAT( //,2X,'11',40X, 6(F6.1,3X))
242  FORMAT( //,2X,'12',44X, 6(F6.1,3X))
      IF(IPKEY.EQ.0) RETURN
      WRITE(87,200) (TITLE(LL),LL=1,3)
      WRITE(87,222)

```



```

222  FORMAT(50X, 'PSEUDO-SECTION OF THE PERCENT FREQUENCY EFFECT')
      WRITE(87,205) THETA
      WRITE(87,220)
      WRITE(87,331) (APIP1(I, 1), I=1, 11)
      WRITE(87,332) (APIP1(I, 2), I=1, 11)
      WRITE(87,333) (APIP1(I, 3), I=1, 10)
      WRITE(87,334) (APIP1(I, 4), I=1, 10)
      WRITE(87,335) (APIP1(I, 5), I=1, 9)
      WRITE(87,336) (APIP1(I, 6), I=1, 9)
      WRITE(87,337) (APIP1(I, 7), I=1, 8)
      WRITE(87,338) (APIP1(I, 8), I=1, 8)
      WRITE(87,339) (APIP1(I, 9), I=1, 7)
      WRITE(87,340) (APIP1(I, 10), I=1, 7)
      WRITE(87,341) (APIP1(I, 11), I=1, 6)
      WRITE(87,342) (APIP1(I, 12), I=1, 6)
      WRITE(87,343) (APIP1(I, 13), I=1, 5)
      WRITE(87,344) (APIP1(I, 14), I=1, 5)
      WRITE(87,345) (APIP1(I, 15), I=1, 4)
331  FORMAT(//////, 4X, ' 1', 11(F6.1, 3X))
332  FORMAT( //, 3X, ' 2', 5X, 11(F6.1, 3X))
333  FORMAT( //, 3X, ' 3', 10X, 10(F6.1, 3X))
334  FORMAT( //, 3X, ' 4', 15X, 10(F6.1, 3X))
335  FORMAT( //, 3X, ' 5', 20X, 9(F6.1, 3X))
336  FORMAT( //, 3X, ' 6', 25X, 9(F6.1, 3X))
337  FORMAT( //, 3X, ' 7', 30X, 8(F6.1, 3X))
338  FORMAT( //, 3X, ' 8', 35X, 8(F6.1, 3X))
339  FORMAT( //, 3X, ' 9', 40X, 7(F6.1, 3X))
340  FORMAT( //, 3X, '10', 45X, 7(F6.1, 3X))
341  FORMAT( //, 3X, '11', 50X, 6(F7.1, 3X))
342  FORMAT( //, 3X, '12', 55X, 6(F7.1, 3X))
343  FORMAT( //, 3X, '13', 60X, 5(F7.1, 3X))
344  FORMAT( //, 3X, '14', 65X, 5(F7.1, 3X))
345  FORMAT( //, 3X, '15', 70X, 4(F7.1, 3X))
      WRITE(87,381) (APIP1(I, 1), I=12, 22)
      WRITE(87,382) (APIP1(I, 2), I=11, 21)
      WRITE(87,383) (APIP1(I, 3), I=11, 20)
      WRITE(87,384) (APIP1(I, 4), I=10, 19)
      WRITE(87,385) (APIP1(I, 5), I=10, 18)
      WRITE(87,386) (APIP1(I, 6), I=9, 17)
      WRITE(87,387) (APIP1(I, 7), I=9, 16)
      WRITE(87,388) (APIP1(I, 8), I=8, 15)
      WRITE(87,389) (APIP1(I, 9), I=8, 14)
      WRITE(87,390) (APIP1(I, 10), I=7, 13)
      WRITE(87,391) (APIP1(I, 11), I=7, 12)
      WRITE(87,392) (APIP1(I, 12), I=6, 11)
      WRITE(87,393) (APIP1(I, 13), I=6, 10)
      WRITE(87,394) (APIP1(I, 14), I=5, 9)
      WRITE(87,395) (APIP1(I, 15), I=5, 8)
381  FORMAT(//////, 10X, 11(F7.1, 3X), ' 1')
382  FORMAT( //, 5X, 11(F7.1, 3X), 5X, ' 2')
383  FORMAT( //, 10X, 10(F7.1, 3X), 10X, ' 3')
384  FORMAT( //, 5X, 10(F7.1, 3X), 15X, ' 4')
385  FORMAT( //, 10X, 9(F7.1, 3X), 20X, ' 5')
386  FORMAT( //, 5X, 9(F7.1, 3X), 25X, ' 6')
387  FORMAT( //, 10X, 8(F7.1, 3X), 30X, ' 7')
388  FORMAT( //, 5X, 8(F7.1, 3X), 35X, ' 8')
389  FORMAT( //, 10X, 7(F7.1, 3X), 40X, ' 9')
390  FORMAT( //, 5X, 7(F7.1, 3X), 45X, '10')
391  FORMAT( //, 10X, 6(F7.1, 3X), 50X, '11')
392  FORMAT( //, 5X, 6(F7.1, 3X), 55X, '12')

```

```

393  FORMAT( //,10X, 5(F7.1,3X),60X,'13')
394  FORMAT( //, 5X, 5(F7.1,3X),65X,'14')
395  FORMAT( //,10X, 4(F7.1,3X),70X,'15')
9915  CONTINUE
      RETURN
      END

```

```

C
C   THIS SUBROUTINE PRODUCES A MAP OF SEVERAL apparent resistivity
C   PARAMETERS ON THE X-Y PLANE OF THE GROUND SURFACE.  THE LENGTH
C   AND ORIENTATION OF THE TRANSMITTING DIPOLE WITH RESPECT TO THE
C   STRIKE-DIRECTION CAN BE MADE ARBITRARY, BY A PROPER SELECTION OF
C   THE GRID IN X-Z AND X-Y PLANES.
C

```

```

SUBROUTINE RECN2D(X,Z,NTXTOT,NRXTOT,NTX,NRX,ITXP,IRXP,
1  NYSFT,YSHIFT,TITLE,V,NNODX,NNODZ)
  DIMENSION X(113),Z(16),YSHIFT(1),IRXP(NRX),ITXP(NTX)
  DIMENSION V(NTXTOT,NRXTOT)
  DIMENSION RESKEL(50),CONKEL(50),RXP(50),THETA(50),APREST(50),
1  APRESX(50),APRESY(50),APRESP(50),CRFX(50),YSHIFX(50),
1  APRES1(50),APRES2(50),GMFX(50),GMFY(50),GMFP(50)
  DIMENSION CRF1(50),CRF2(50),GMF1(50),GMF2(50)
  CHARACTER TITLE(18)
  COMMON /PACK1/ INCLIN,ISHIFT,NRLIM
  DO 1333 III=1,50
    CRF1(III)=0.96
    CRF2(III)=0.96
1333  CONTINUE
  CRFX(III)=0.96
  PI=3.141592654
  XCENTR=(X(1)+X(95))/2.0
  XCENTR=(X(1)+X(NNODX))/2.0
  NTXX=NTX-1
  DO 100 ITX=1,NTXX
    IA=ITX
    IB=ITX+1
    NIA=ITXP(IA)
    NIB=ITXP(IB)
    TXA=X(NIA)-XCENTR
    TXB=X(NIB)-XCENTR
    CRF=1.00
    IF(INCLIN.NE.0) GO TO 500
    NRL=NRLIM
    ILX=0
    DO 200 I=1,NRL,2
C
C   DO 200 I=1,NRL
C
      ILX=ILX+1
      RYY=YSHIFT(I)
      YSHIFX(ILX)=RYY
      RYYD2=RYY+YSHIFT(2)
      NRP=NRX-2
      JRX=0
C
C   DO 300 J=1,NRP
C
      DO 300 J=2,NRP,2

```

```

JC=J+1
JD1=JC+1
JD2=JC-1
JE1=JD1
JE2=JC
JCC=JC+(I-1)*NRX
JDD1=JCC+NRX+1
JDD2=JCC+NRX-1
JEE1=JCC+1
JEE2=JDD1-1
NJC=IRXP(JC)
NJD1=IRXP(JD1)
NJD2=IRXP(JD2)

```

```

C
C
C
RXL=ABS(X(NJC)-X(NJD1))*1.4142

```

```

RXL=ABS(X(NJC)-X(NJD1))
TXLONG=ABS(X(NIB)-X(NIA))

```

```

C
C
C
CALCULATE RELEVANT DISTANCES

```

```

AC=X(NJC)-X(NIA)
BC=X(NJC)-X(NIB)
IF((AC+BC).EQ.0.0) GO TO 300
IF(ABS(AC).LT.1.10.OR.ABS(BC).LT.1.10) GO TO 300
JRX=JRX+1
RXP(JRX)=X(NJC)-XCENR
AE1=X(NJD1)-X(NIA)
BE1=X(NJD1)-X(NIB)
AD2=X(NJD2)-X(NIA)
BD2=X(NJD2)-X(NIB)
AE2=AC
BE2=BC
RAC=SQRT(AC*AC+RYY*RYY)
RBC=SQRT(BC*BC+RYY*RYY)
RAC3=1.0/RAC
RBC3=1.0/RBC
RAE1=1.0/SQRT(AE1*AE1+RYY*RYY)
RBE1=1.0/SQRT(BE1*BE1+RYY*RYY)
RAE2=1.0/SQRT(AE2*AE2+RYYD2*RYYD2)
RBE2=1.0/SQRT(BE2*BE2+RYYD2*RYYD2)
RAD1=1.0/SQRT(AE1*AE1+RYYD2*RYYD2)
RBD1=1.0/SQRT(BE1*BE1+RYYD2*RYYD2)
RAD2=1.0/SQRT(AD2*AD2+RYYD2*RYYD2)
RBD2=1.0/SQRT(BD2*BD2+RYYD2*RYYD2)

```

```

C
C
C
EVALUATE THE POTENTIAL DIFFERENCES OBSERVED AT THE TWO
      ORTHOGONAL RECEIVER DIPOLES

```

```

DELV1=(V(IA,JCC)-V(IB,JCC)-V(IA,JDD1)+V(IB,JDD1))
DELV2=(V(IA,JCC)-V(IB,JCC)-V(IA,JDD2)+V(IB,JDD2))
DELVX=(V(IA,JCC)-V(IB,JCC)-V(IA,JEE1)+V(IB,JEE1))
DELVY=(V(IA,JCC)-V(IB,JCC)-V(IA,JEE2)+V(IB,JEE2))
DELVP=(V(IA,JCC)-V(IB,JCC))

```

```

C
C
C
C
DELVX=DELVX*CRF1(JRX)
DELVY=DELVY*CRF2(JRX)

```

```

E1=DEL VX/RXL
E2=DEL VY/RXL
ETOT=SQRT(E1*E1+E2*E2)
COSDEL=(RBC*RBC+RAC*RAC-TXLONG*TXLONG)/(2.0*RAC*RBC)
DELTA=ACOS(COSDEL)

```

```

C
C
C
EVALUATE RESISTIVITY PARAMETERS A LA KELLER

```

```

DENOM1=RAC3-RBC3-RAD1+RBD1
DENOM2=RAC3-RBC3-RAD2+RBD2
DENOMX=RAC3-RBC3-RAE1+RBE1
DENOMY=RAC3-RBC3-RAE2+RBE2
DENOM=SQRT(1.0+((RAC*RAC*RAC*RAC)/(RBC*RBC*RBC*RBC))-
1      2.00*(RAC*RAC/(RBC*RBC))*COS(DELTA))

```

```

C
C
C
RESKEL(JRX)=ETOT*RAC*RAC*CRF/DENOM

```

```

DNUM=SQRT(1.0+(RAC*RAC/(RBC*RBC))-2.0*(RAC/RBC)*COS(DELTA))

```

```

C
C
C
CONKEL(JRX)=DNUM/(ETOT*RAC)

```

```

VTOT=SQRT(DEL VX*DEL VX+DEL VY*DEL VY)
RESKEL(JRX)=VTOT/(SQRT(DENOMX*DENOMX+DENOMY*DENOMY))
DNUMA=ALOG(RAC3)-ALOG(RBC3)-ALOG(RAE1)+ALOG(RBE1)
DNUMB=ALOG(RAC3)-ALOG(RBC3)-ALOG(RAE2)+ALOG(RBE2)
DUMNX=SQRT(DNUMA*DNUMA+DNUMB*DNUMB)
CONKEL(JRX)=DNUMX/VTOT

```

```

C
C
C
C
EVALUATE THE TOTAL APPARENT RESISTIVITY IN THE VECTOR
E-FIELD DIRECTION AT EACH OBSERVATION POINT

```

```

IF(DENOM1.EQ.0.00) GMF1(JRX)=0.00
IF(DENOM1.NE.0.00) GMF1(JRX)=1.00/DENOM1
IF(DENOM2.EQ.0.00) GMF2(JRX)=0.00
IF(DENOM2.NE.0.00) GMF2(JRX)=1.00/DENOM2
IF(DENOMX.EQ.0.00) GMFX(JRX)=0.00
IF(DENOMX.NE.0.00) GMFX(JRX)=1.00/DENOMX
IF(DENOMY.EQ.0.00) GMFY(JRX)=0.00
IF(DENOMY.NE.0.00) GMFY(JRX)=1.00/DENOMY
IF(RAC3.EQ.RBC3) GMFP(JRX)=0.00
IF(RAC3.NE.RBC3) GMFP(JRX)=1.00/(RAC3-RBC3)
APRES1(JRX)=ABS(DEL V1*GMF1(JRX))
APRES2(JRX)=ABS(DEL V2*GMF2(JRX))
APRESX(JRX)=ABS(DEL VX*GMFX(JRX))
APRESY(JRX)=ABS(DEL VY*GMFY(JRX))
APRESP(JRX)=ABS(DEL VP*GMFP(JRX))*CRFX(JRX)
RXRTL=RXL
DELVT=ETOT*RXRTL

```

```

C
C
C
C
C
ANGLE OF THE FIELD LINES ARE CALCULATED ON THE BASIS OF
THE MEASURED EX AND EY OVER THE LENGH OF THE ORTHOGONAL
RECEIVER

```

```

IF(E1.EQ.0.00) BETA=PI*0.50
IF(E1.NE.0.00) BETA=ATAN2(E2,E1)
DELX=RXRTL*COS(BETA)
DELY=RXRTL*SIN(BETA)
THETA1=BETA*57.296
RAD3=1.0/SQRT((AC+DELX)*(AC+DELX)+(RYY+DELY)*(RYY+DELY))
RBD3=1.0/SQRT((BC+DELX)*(BC+DELX)+(RYY+DELY)*(RYY+DELY))

```

```
GMF=1.0/(RAC3-RBC3-RAD3+RBD3)
APREST(JRX)=ABS(GMF*DELVT)*CRF
```

```
C
C
C   CALCULATE THE DEVIATION IN THE CURRENT LINES FROM THE
C   HOMOGENEOUS HALF SPACE SITUATION
```

```
HDELV1=RAC3-RBC3-RAE1+RBE1
HDELV2=RAC3-RBC3-RAE2+RBE2
IF(HDELV1.EQ.0.00) BETA=PI*0.50
IF(HDELV1.NE.0.00) BETA=ATAN2(HDELV2,HDELV1)
THETA2=BETA*57.296
THETA(JRX)=THETA2-THETA1
NJRX=JRX
```

```
300 CONTINUE
```

```
WRITE(87,310) (TITLE(LL),LL=1,3)
```

```
310 FORMAT(1H1,///,55X,'CASE',1X,3A4,///,40X,'TRANSMITTING
1 DIPOLE IS PERPENDICULAR TO THE STRIKE OF THE INHOMOGENEITY',/)
```

```
WRITE(87,311) TXA,TXB,RXL
```

```
311 FORMAT(/,30X,'CURRENT ELECTRODES ARE LOCATED AT ',F12.4,2X,
1 'AND',F12.4,/,35X,'LENGTH OF THE RECEIVER DIPOLES ARE ',
1 2X,F12.4)
```

```
WRITE(87,312) RYY
```

```
312 FORMAT(/,20X,'POINTS OF OBSERVATION ARE SITUATED ON THE LINE
1 SHIFTED ON Y-AXIS BY ',F12.4,/)
WRITE(87,1110)
```

```
1110 FORMAT(/,10X,'OBS.PT. ',5X,'GMFX',5X,'APRES(X)',5X,'GMFY',5X,
1 'APRES(Y)',5X,'GMFP',5X,'APRESP',5X,'RESKEL',5X,'CONKEL',5X,
1 'APREST',5X,'THETA',/)
```

```
WRITE(87,314) (RXP(JRX),GMFX(JRX),APRESX(JRX),GMFY(JRX),
1 APRESY(JRX),GMFP(JRX),APRESP(JRX),RESKEL(JRX),CONKEL(JRX),
1 APREST(JRX),THETA(JRX),JRX=1,NJRX)
```

```
314 FORMAT(7X,F8.2,4X,E10.3,2X,F8.2,2X,E10.3,2X,F8.2,2X,E10.3,2X,
1 F8.2,2X,F8.2,2X,F8.2,2X,F8.2,2X,F8.2)
```

```
NRLX=ILX
```

```
200 CONTINUE
```

```
GO TO 1500
```

```
500 CONTINUE
```

```
C
C
C   INCLIN=1 FOR THE CASE WITH TX AT AN ACUTE ANGLE TO X-AXIS
C   INCLIN=2 FOR THE CASE WITH TX AT AN OBTUSE ANGLE TO X-AXIS
```

```
AYA=0.00
```

```
AYB=0.00
```

```
NRL=2*NRLIM-1
```

```
RYT=YSHIFT(ISHIFT)
```

```
TXLONG=SQRT((X(NIA)-X(NIB))*(X(NIA)-X(NIB))+RYT*RYT)
```

```
ILX=0
```

```
C
C
C   DO 600 I=1,NRL
```

```
DO 600 I=1,NRL,2
```

```
ILX=ILX+1
```

```
IF(I.LE.NRLIM) RYY=YSHIFT(I)
```

```
IF(I.GT.NRLIM) RYY=YSHIFT(I-NRLIM+1)
```

```
YSHIFX(ILX)=RYY
```

```
RYYD2=RYY+YSHIFT(2)
```

```
NRP=NRX-2
```

```
JRX=0
```

```
C
C
C   DO 700 J=1,NRP
```

```

DO 700 J=2,NRP,2
JC=J+1
JD1=JC+1
JD2=JC-1
NJC=IRXP(JC)
NJD1=IRXP(JD1)
NJD2=IRXP(JD2)
AC=X(NJC)-X(NIA)
BC=X(NJC)-X(NIB)
IF(ABS(AC).LT.1.10.OR.ABS(BC).LT.1.10) GO TO 700
IF(RYT.EQ.0.00.AND.(AC+BC).EQ.0.00) GO TO 700
JRX=JRX+1
AEL=X(NJD1)-X(NIA)
IF(AEL.EQ.0.00) GO TO 700
BEL=X(NJD1)-X(NIB)
AD1=AEL
BD1=BEL
AE2=AC
BE2=BC
RXL=ABS(X(NJC)-X(NJD1))
AD2=X(NJD2)-X(NIA)
BD2=X(NJD2)-X(NIB)
RXP(JRX)=X(NJC)-XCENTR
IF(I.LE.NRLIM) GO TO 710
IF(I.GT.NRLIM) GO TO 720
710 NRY=IABS(ISHIFT-1)*NRX
JCC=JC+(I-1)*NRX
JDD1=JCC+NRX+1
JDD2=JCC+NRX-1
JEE1=JCC+1
JEE2=JCC+NRX
JCCX=JC+NRY
JEE1X=JCCX+1
IF(ISHIFT.LE.I) JDD1X=JC+NRY+NRX+1
IF(ISHIFT.GT.I) JDD1X=JC+NRY-NRX+1
JDD2X=JDD1X-2
JEE2X=JDD1X-1
IF(INCLIN.EQ.1) GO TO 715
IF(INCLIN.EQ.2) GO TO 716
715 RAC=SQRT(AC*AC+RYY*RYY)
RBC=SQRT(BC*BC+(RYY-RYT)*(RYY-RYT))
AYB=RYT
RAE1=1.00/SQRT(AEL*AEL+RYY*RYY)
RAD1=1.00/SQRT(AD1*AD1+RYY*RYY)
RBE1=1.00/SQRT(BEL*BEL+(RYY-RYT)*(RYY-RYT))
RBD1=1.00/SQRT(BD1*BD1+(RYY-RYT)*(RYY-RYT))
RAE2=1.00/SQRT(AE2*AE2+RYYD2*RYYD2)
RAD2=1.00/SQRT(AD2*AD2+RYYD2*RYYD2)
RBE2=1.00/SQRT(BE2*BE2+(RYYD2-RYT)*(RYYD2-RYT))
RBD2=1.00/SQRT(BD2*BD2+(RYYD2-RYT)*(RYYD2-RYT))
DELV1=(V(IA,JCC)-V(IA,JDD1)-V(IB,JCCX)+V(IB,JDD1X))
DELV2=(V(IA,JCC)-V(IA,JDD2)-V(IB,JCCX)+V(IB,JDD2X))
DELVX=(V(IA,JCC)-V(IA,JEE1)-V(IB,JCCX)+V(IB,JEE1X))
DELVY=(V(IA,JCC)-V(IA,JEE2)-V(IB,JCCX)+V(IB,JEE2X))
DELVP=(V(IA,JCC)-V(IB,JCCX))
RYTC=RYY-RYT
GO TO 745
716 RAC=SQRT(AC*AC+(RYY-RYT)*(RYY-RYT))
RBC=SQRT(BC*BC+RYY*RYY)
AYA=RYT

```

```

RAE1=1.00/SQRT(AE1*AE1+(RYY-RYT)*(RYY-RYT))
RAD1=1.00/SQRT(AD1*AD1+(RYY-RYT)*(RYY-RYT))
RBE1=1.00/SQRT(BE1*BE1+RYY*RYY)
RBD1=1.00/SQRT(BD1*BD1+RYY*RYY)
RAE2=1.00/SQRT(AE2*AE2+(RYYD2-RYT)*(RYYD2-RYT))
RAD2=1.00/SQRT(AD2*AD2+(RYYD2-RYT)*(RYYD2-RYT))
RBE2=1.00/SQRT(BE2*BE2+RYYD2*RYYD2)
RBD2=1.00/SQRT(BD2*BD2+RYYD2*RYYD2)
DELV1=(V(IA,JCCX)-V(IA,JDD1X)-V(IB,JCC)+V(IB,JDD1))
DELV2=(V(IA,JCCX)-V(IA,JDD2X)-V(IB,JCC)+V(IB,JDD2))
DELVX=(V(IA,JCCX)-V(IA,JEE1X)-V(IB,JCC)+V(IB,JEE1))
DELVY=(V(IA,JCCX)-V(IA,JEE2X)-V(IB,JCC)+V(IB,JEE2))
DELVP=(V(IA,JCCX)-V(IB,JCC))
RYTC=RYY-RYT
GO TO 745
720 NRY=IABS(ISHIFT+I-NRLIM-1)*NRX
JCC=JC+(I-NRLIM)*NRX
JDD1=JCC-NRX+1
JDD2=JCC-NRX-1
JEE1=JCC+1
JEE2=JCC-NRX
JCCX=JC+NRY
JDD1X=JCCX-NRX+1
JDD2X=JDD1X-2
JEE1X=JCCX+1
JEE2X=JDD1X-1
IF(INCLIN.EQ.1) GO TO 725
IF(INCLIN.EQ.2) GO TO 726
725 RAC=SQRT(AC*AC+RYY*RYY)
RBC=SQRT(BC*BC+(RYY-RYT)*(RYY-RYT))
RAE1=1.0/SQRT(AE1*AE1+RYY*RYY)
RAD1=1.0/SQRT(AD1*AD1+RYY*RYY)
RBE1=1.0/SQRT(BE1*BE1+(RYY-RYT)*(RYY-RYT))
RBD1=1.0/SQRT(BD1*BD1+(RYY-RYT)*(RYY-RYT))
RAE2=1.0/SQRT(AE2*AE2+RYYD2*RYYD2)
RAD2=1.0/SQRT(AD2*AD2+RYYD2*RYYD2)
RBE2=1.0/SQRT(BE2*BE2+(RYYD2-RYT)*(RYYD2-RYT))
RBD2=1.0/SQRT(BD2*BD2+(RYYD2-RYT)*(RYYD2-RYT))
DELV1=(V(IA,JCC)-V(IA,JDD1)-V(IB,JCCX)+V(IB,JDD1X))
DELV2=(V(IA,JCC)-V(IA,JDD2)-V(IB,JCCX)+V(IB,JDD2X))
DELVX=(V(IA,JCC)-V(IA,JEE1)-V(IB,JCCX)+V(IB,JEE1X))
DELVY=(V(IA,JCC)-V(IA,JEE2)-V(IB,JCCX)+V(IB,JEE2X))
DELVP=(V(IA,JCC)-V(IB,JCCX))
GO TO 745
726 RAC=SQRT(AC*AC+(RYY-RYT)*(RYY-RYT))
RBC=SQRT(BC*BC+RYY*RYY)
RAE1=1.0/SQRT(AE1*AE1+(RYY-RYT)*(RYY-RYT))
RAD1=1.0/SQRT(AD1*AD1+(RYY-RYT)*(RYY-RYT))
RBE1=1.0/SQRT(BE1*BE1+RYY*RYY)
RBD1=1.0/SQRT(BD1*BD1+RYY*RYY)
RAE2=1.0/SQRT(AE2*AE2+(RYYD2-RYT)*(RYYD2-RYT))
RAD2=1.0/SQRT(AD2*AD2+(RYYD2-RYT)*(RYYD2-RYT))
RBE2=1.0/SQRT(BE2*BE2+RYYD2*RYYD2)
RBD2=1.0/SQRT(BD2*BD2+RYYD2*RYYD2)
DELV1=(V(IA,JCCX)-V(IA,JDD1X)-V(IB,JCC)+V(IB,JDD1))
DELV2=(V(IA,JCCX)-V(IA,JDD2X)-V(IB,JCC)+V(IB,JDD2))
DELVX=(V(IA,JCCX)-V(IA,JEE1X)-V(IB,JCC)+V(IB,JEE1))
DELVY=(V(IA,JCCX)-V(IA,JEE2X)-V(IB,JCC)+V(IB,JEE2))
DELVP=(V(IA,JCCX)-V(IB,JCC))
745 CONTINUE

```

```

DELVX=DELVX*CRF1(JRX)
DELVY=DELVY*CRF2(JRX)
E1=DELVX/RXL
E2=DELVY/RXL
ETOT=SQRT(E1*E1+E2*E2)

```

```

EVALUATE THE RESISTIVITY PARAMETERS A LA KELLER

```

```

RAC3=1.0/RAC
RBC3=1.0/RBC
DENOMX=RAC3-RBC3-RAE1+RBE1
DENOM1=RAC3-RBC3-RAD1+RBD1
DENOMY=RAC3-RBC3-RAE2+RBE2
DENOM2=RAC3-RBC3-RAD2+RBD2
COSDEL=(RBC*RBC+RAC*RAC-TXLONG*TXLONG)/(2.0*RAC*RBC)
DELTA=ACOS(COSDEL)
DENOM=SQRT(1.0+((RAC*RAC*RAC*RAC)/(RBC*RBC*RBC*RBC))-
1      2.00*(RAC*RAC/(RBC*RBC))*COS(DELTA))

```

```

RESKEL(JRX)=ETOT*RAC*RAC*CRF/DENOM

```

```

DNUM=SQRT(1.0+(RAC/RBC)*(RAC/RBC)-2.0*(RAC/RBC)*COS(DELTA))

```

```

CONKEL(JRX)=DNUM/(ETOT*RAC)

```

```

VTOT=SQRT(DELVX*DELVX+DELVY*DELVY)
RESKEL(JRX)=VTOT/(SQRT(DENOMX*DENOMX+DENOMY*DENOMY))
DNUMA=ALOG(RAC3)-ALOG(RBC3)-ALOG(RAE1)+ALOG(RBE1)
DNUMB=ALOG(RAC3)-ALOG(RBC3)-ALOG(RAE2)+ALOG(RBE2)
DNUMX=SQRT(DNUMA*DNUMA+DNUMB*DNUMB)
CONKEL(JRX)=DNUMX/VTOT
IF(DENOM1.EQ.0.00) GMF1(JRX)=0.00
IF(DENOM1.NE.0.00) GMF1(JRX)=1.0/DENOM1
IF(DENOM2.EQ.0.00) GMF2(JRX)=0.00
IF(DENOM2.NE.0.00) GMF2(JRX)=1.0/DENOM2
IF(DENOMX.EQ.0.00) GMFX(JRX)=0.00
IF(DENOMX.NE.0.00) GMFX(JRX)=1.0/DENOMX
IF(DENOMY.EQ.0.00) GMFY(JRX)=0.00
IF(DENOMY.NE.0.00) GMFY(JRX)=1.0/DENOMY
IF(RAC3.EQ.RBC3) GMFP(JRX)=0.00
IF(RAC3.NE.RBC3) GMFP(JRX)=1.0/(RAC3-RBC3)

```

```

APRES1(JRX)=ABS(DELV1*GMF1(JRX))
APRES2(JRX)=ABS(DELV2*GMF2(JRX))
APRESX(JRX)=ABS(DELVX*GMFX(JRX))
APRESY(JRX)=ABS(DELVY*GMFY(JRX))
APRESP(JRX)=ABS(DELVP*GMFP(JRX))*CRFX(JRX)

```

```

EVALUATE THE TOTAL APPARENT RESISTIVITY IN THE VECTOR
E-FIELD DIRECTION

```

```

RXTL=RXL
DELVT=ETOT*RXTL

```

```

ANGLE OF THE FIELD LINES ARE CALCULATED ON THE BASIS OF
THE MEASURED EX AND EY OVER THE LENGHT OF THE ORTHOGONAL
RECEIVER DIPOLES

```



```

IF(E1.EQ.0.00) BETA=PI*0.50
IF(E1.NE.0.00) BETA=ATAN2(E2,E1)
DELX=RX*TL*COS(BETA)
DELY=RX*TL*SIN(BETA)
THETA1=BETA*57.296
IF(INCLIN.EQ.1) GO TO 810
IF(INCLIN.EQ.2) GO TO 820
810 RAD3=1.0/SQRT((AC+DELX)*(AC+DELX)+(RYY+DELY)*(RYY+DELY))
RBD3=1.0/SQRT((BC+DELX)*(BC+DELX)+(RYY-RYT+DELY)*
1 (RYY-RYT+DELY))
GO TO 845
820 RAD3=1.0/SQRT((AC+DELX)*(AC+DELX)+(RYY-RYT+DELY)
1 *(RYY-RYT+DELY))
RBD3=1.0/SQRT((BC+DELX)*(BC+DELX)+(RYY+DELY)*(RYY+DELY))
845 GMF=1.0/(RAC3-RBC3-RAD3+RBD3)
APREST(JRX)=ABS(GMF*DELVT)*CRF

C
C CALCULATE THE DEVIATION OF THE CURRENT LINES FROM THE
C HOMOGENEOUS HALF SPACE SITUATION
C

HDELV1=RAC3-RBC3-RAE1+RBE1
HDELV2=RAC3-RBC3-RAE2+RBE2
IF(HDELV1.EQ.0.00) BETA=PI*0.50
IF(HDELV1.NE.0.00) BETA=ATAN2(HDELV2,HDELV1)
THETA2=BETA*57.296
THETA(JRX)=THETA2-THETA1
NJRX=JRX

C
C TOTCON(JRX,ILX)=CONKEL(JRX)
C TOTRES(JRX,ILX)=RESKEL(JRX)
C

700 CONTINUE
WRITE(87,910) (TITLE(LL),LL=1,3)
910 FORMAT(1H1,///,50X,'CASE',1X,3A4,///,35X,'TRANSMITTING
1 DIPOLE IS INCLINED TO THE STRIKE OF THE INHOMOGENEITY'/)
WRITE(87,911) TXA,AYA,TXB,AYB,RXL
911 FORMAT(//25X,'CURRENT ELECTRODE POSITIONS ARE AT X1=',
1 F10.2,2X,'Y1=',F10.2,2X,'AND AT X2=',F10.2,2X,'Y2=',
1 F10.2,25X,'LENGTH OF THE RECEIVER DIPOLES ARE ',F10.3/)
WRITE(87,912) RYY
912 FORMAT(/20X,'POINTS OF OBSERVATION ARE SITUATED ON A LINE
1 SHIFTED ON Y-AXIS BY ',F12.4/)
WRITE(87,1110)
WRITE(87,914) (RXP(JRX),GMFX(JRX),APRESX(JRX),GMFY(JRX),
1 APRESY(JRX),GMFP(JRX),APRESP(JRX),RESKEL(JRX),
1 CONKEL(JRX),APREST(JRX),THETA(JRX),JRX=1,NJRX)
914 FORMAT(7X,F8.2,4X,E10.3,2X,F8.2,2X,E10.3,2X,F8.2,2X,E10.3,2X,
1 F8.2,2X,F8.2,2X,F8.2,2X,F8.2,2X,F8.2)

NRLX=ILX
600 CONTINUE
1500 CONTINUE
NJRXX=NJRX-1

C
C DO 1444 J=2,NJRXX
C DO 1444 I=1,NRL
C IF(APRESP(J).NE.0.00) GO TO 1444
C APRESP(J)=(APRESP(J-1)+APRESP(J+1))*0.50
C1444 CONTINUE
C WRITE(88,325) (TITLE(LL),LL=1,3)
C 325 FORMAT(3A5)

```

```
C      WRITE(88,321) (RXP(JRX),JRX=1,NRLX)
C 321  FORMAT(8F10.3)
C      WRITE(88,322) (YSHIFX(ILX),ILX=1,NRLX)
C 322  FORMAT(10F8.3)
C      WRITE(88,323) ((TOTRES(JRX,ILX),JRX=1,NJRX),ILX=1,NRLX)
C 323  FORMAT(8E10.3)
C      WRITE(88,324) ((TOTCON(JRX,ILX),JRX=1,NJRX),ILX=1,NRLX)
C 324  FORMAT(10F8.3)
100   CONTINUE
      RETURN
      END
```

Appendix C



A RESISTIVITY STUDY OF THE LA UNION

LOWER LANDFILL

by

Paul Michalak

and

Kim Edlund



ABSTRACT

An electrical resistivity survey was performed at the La Union, New Mexico lower (old) landfill. The study, conducted in conjunction with the Environmental Improvement Division of New Mexico, is part of an on going investigation of possible groundwater contamination in the region. The collected field data included horizontal resistivity profiles as well as a vertical electrical sounding (VES) using a Wenner electrode configuration. Examination of the field data revealed anomalously low resistivity readings in the southeastern corner of the landfill. The source of these irregular measurements can be attributed to either a change in pore-water resistivity (contamination) or a lithologic inhomogeneity. A conclusive interpretation was not possible without further data. As a result, it has been recommended that a test well be drilled in the vicinity of the anomalous resistivity area.

CONTENTS

Purpose of Work	1
Introduction	1
Presentation of Results	1
Discussion	3
Horizontal Profile	
Case I Uniform lithology	4
Case II Constant pore-water resistivity	8
Vertical electrical soundings	
Modeling procedure for Wenner VES	10
Inversion models of Wenner VES	10
Comparison and interpretation	12
Summary of Conclusions	13
Recommendations	14
List of References	16
Tables	19
Figures	25

LIST OF TABLES

- Table I. Relevant section of U.S.G.S. borehole #27S.2.13.333 (2 miles northwest and 300 feet above La Union, lower landfill).
- Table II. E.I.D. augered hole 6/11/87 (La Union, lower landfill).
- Table III. Inversion results from La Union, lower landfill. (Wenner VES, Petrick model)
- Table IV. Inversion results from La Union, lower landfill. (Wenner VES Zohdy model)

LIST OF FIGURES

- Figure 1. Relevant portion of La Union, New Mexico-Texas quadrangle showing location of lower landfill and U.S.G.S. borehole #27S.2.13.333
- Figure 2. (a) Wenner electrode configuration
 (b) Electrical current flow in the earth, plan view
 (c) Electrical current flow in the earth, vertical section
- Figure 3. Sketch of La Union, New Mexico lower landfill with locations of horizontal profiles and proposed test well.
- Figure 4. Horizontal profile F line, $a = 50$ feet.
- Figure 5. Horizontal profile F line, $a = 100$ feet.
- Figure 6. Horizontal profile D line, $a = 50$ feet.
- Figure 7. Horizontal profile D line, $a = 100$ feet.
- Figure 8. Horizontal profile X line, $a = 50$ feet.
- Figure 9. Horizontal profile X line, $a = 100$ feet.
- Figure 10. Theoretical horizontal resistivity profile across a perfectly conducting plate. (after Kunetz, 1966)
- Figure 11. Depth of investigation for Wenner $a = 50$ feet spacing. The abscissa is defined as depth, in percent of current-electrode separation or percent of 150 feet. The ordinate is the normalized depth of investigation. (Modeling data from Table III)
- Figure 12. Depth of investigation for Wenner $a = 100$ feet spacing. The abscissa is defined as depth, in percent of current-electrode separation or percent of 300 feet. The ordinate is the normalized depth of investigation. (Modeling data from Table III)
- Figure 13. Normalized plot of horizontal profile F line, $a = 50$ feet. The abscissa is marked x/a where x is the distance from the center of the anomaly and a is the Wenner electrode spacing. The ordinate is defined as ρ_a / ρ' where ρ_a is the measured resistivity and ρ' is taken as 170Ω feet.

- Figure 14. Normalized plot of horizontal profile F line, $a = 100$ feet. The abscissa is marked x/a where x is the distance from the center of the anomaly and a is the Wenner electrode spacing. The ordinate is defined as ρ_a / ρ' where ρ_a is the measured resistivity and ρ' is taken as 170Ω feet.)
- Figure 15. Normalized plot of horizontal profile D line, $a = 50$ feet. The abscissa is marked x/a where x is the distance from the center of the anomaly and a is the Wenner electrode spacing. The ordinate is defined as ρ_a / ρ' where ρ_a is the measured resistivity and ρ' is taken as 170Ω feet.
- Figure 16. Normalized plot of horizontal profile D line, $a = 100$ feet. The abscissa is marked x/a where x is the distance from the center of the anomaly and a is the Wenner electrode spacing. The ordinate is defined as ρ_a / ρ' where ρ_a is the measured resistivity and ρ' is taken as 170Ω feet.
- Figure 17. Theoretical horizontal resistivity profile across oblate hemispheroid, Wenner configuration, width at surface = $3a/2$, reflection coefficient = -0.7 . (after Van Nostrand and Cook, 1966)
- Figure 18. Theoretical horizontal resistivity profile across vertical dike, Wenner configuration, width = $a/2$, depth = infinite, reflection coefficient = -0.6 . (after Van Nostrand and Cook, 1966)
- Figure 19. Log-log plot of La Union lower landfill for Wenner VES using Petrick algorithm. (Data from table III)
- Figure 20. Log-log plot of La Union lower landfill for Wenner VES using Zohdy algorithm. (Data from table IV)
- Figure 21. Comparison of effect of soil type (gravel, sand, and silt) on Wenner VES. 3 layer model, 2nd layer saturated. (after Urish, 1983)

PURPOSE OF WORK

This report is the result of a resistivity profiling survey implemented at the La Union lower landfill. The survey was conducted in conjunction with the Environmental Improvement Division of New Mexico. After preliminary traverses of the landfill using Geonics EM-34-3 induction equipment, horizontal resistivity profiles were performed over areas found to be highly conductive. In addition, a vertical electrical sounding was executed to help improve interpretation. The purpose of these surveys was to perform a preliminary study of the anomalous resistivity areas with special attention paid to possible contamination of the subsurface.

INTRODUCTION

La Union, New Mexico is situated in Dona Ana County, approximately 30 miles south of Las Cruces on N.M. highway 28. The lower (old) landfill is located at T27S, R3E, Section 18.442, just outside the village of La Union (figure 1). Geologically the older landfill sits atop the Fort Hancock formation of the middle Santa Fe group. The Fort Hancock formation consists mainly of interbedded sand, silt, and clay with discontinuous zones of calcic cementation (Hawley and Lozinsky, 1986). Table I shows relevant sections of a U.S.G.S. borehole taken about 300 feet above and 2 miles northwest of the lower landfill (figure 1). Groundwater depth, as reported by Wilson *et. al.* (1981), is about 20 to 25 feet below the surface and its gradient is in the southeast direction indicating that the water is flowing toward the community.

PRESENTATION OF RESULTS

Using Soiltest's R-60 Earth Resistivity Meter (power unit and D.C. millivoltmeter) both horizontal and vertical soundings were conducted utilizing a Wenner array (figure 2). The equation for the apparent resistivity, when using a Wenner array is

$$\rho_a = 2 \pi a \frac{\Delta V}{I} \quad (1)$$

where a is the Wenner electrode spacing, ΔV is the potential difference and I is the current

In horizontal profiling the electrode separation is maintained at a constant value and the entire configuration is moved along a traverse. Readings along this traverse are taken at regular intervals. In theory, with array spacings held constant, any lateral inhomogeneity or anomaly will cause a rise or fall in observed readings. In this report, Wenner spacings of 50 and 100 feet were used. Readings were taken every 25 feet. Figure 3 is a map of the lower landfill vicinity showing approximate locations of the traverses. For the horizontal profiling data, apparent resistivities are plotted against the midpoint location of the Wenner configuration.

In vertical profiling, the center of the electrode configuration is fixed and measurements are made at various electrode spacings. Logically, we assume that wider electrode spacings produce greater current penetration which results in more information about deeper structures. In this report 10 data points were collected at spacings of 1 to 200 feet.

The actual resistivities reported in this paper are averages of two sets of readings. Specifically, a set is comprised of two measurements taken at the same current setting, where both the current and potential electrode poles are switched. This results in four resistivity readings, two at a normal polar orientation and two with the poles reversed.

Figures 4 through 9 are graphical representations of the horizontal profiling data collected at the La Union lower landfill. Electrode spacings of 50 and 100 feet were used. Both the D and X lines were oriented north-south while the F line was in the east-west direction. Inferred measurements are indicated by dashed lines. Profiles along the X line (figures 8 and 9) were taken for background resistivity information on the landfill. Although these profiles are clearly off any low resistivity areas, their location was situated on the landfill.

The vertical electrical sounding, represented in figures 19 and 20, was conducted along the F line approximately centered at location 14. Another VES, along the D line and centered at location 13, was attempted but surface objects impaired reasonable readings for small electrode spacings ($a=1$ through 10 ft.).

Finally, a dipole-dipole configuration was used in an attempt to collect a cross-sectional pseudo-section of resistivity values. Unlike the Wenner array, the dipole-dipole configuration requires a large current injection into the subsurface. This requirement is intensified as the dipole separation increases. Due to a highly conductive layer just under the surface (see vertical interpretation) and weakened batteries in our power unit the dipole-dipole array produced unsatisfactory results.

DISCUSSION

Electrical resistivity has proven itself a useful instrument in mapping geologic structures. Investigators such as Zohdy *et. al.* (1974), Petrick *et. al.* (1977) and a score of others have successfully applied this tool. Mapping groundwater contamination plumes is another excellent example of electrical resistivity application and can be seen in the works of Stollar and Roux (1975), Kelly (1976), and Urish (1983) among others. With these examples in mind it is easy to see how Cartwright and McComas (1968) concluded that, "resistivity is controlled by two factors - character of material and water quality".

Although the researchers cited above have had success with surface electrical methods these techniques cannot always distinguish between changing lithology of a rock and varying pore-water resistivity. As a result of this problem assumptions are necessary to interpret resistivity surveys. These assumptions narrow down the possible interpretations of collected field data. In electrical profiling one can assume the soil matrix is relatively uniform (Urish, 1983), then any variation in apparent resistivity would be due to a change in pore water resistivity. Since many contaminants cause an increase in total dissolved solids, as for instance landfill leachate, this could result in an increase in conductivity and produce a resistivity trough in the profile.

In the alternative, a variation in electrical profiling data can be a consequence of a lithological change. Specifically silt, shale, and clay will exhibit lower apparent resistivity values than gravel or sand. Klefstad *et. al.* (1975) found resistivity values quite sensitive to the thicknesses of silt and clay lenses. Thus, a drop in readings can be the product of a soil's physical characteristics. A hydrologic situation where both conditions exist can result in an ambiguous situation. Stollar and Roux (1975) found that extreme lateral variations in lithology overlying a contaminant plume can make interpretation difficult. Klefstad *et. al.* (1975) refer to natural "scatter" obscuring a decrease in resistivity due to contamination and limiting the usefulness of the technique.

As we can see, these two opposing premises, constant water quality or constant lithology, can lead to very different model interpretations. Adding to the difficulty is the fact that profiling curves derived from either of these assumptions can be quite similar. It can not be overemphasized that an integrated approach, using at least two independent geophysical techniques, can help reduce the ambiguities that are inherent in surface electrical resistivity studies. As a consequence of the above stated problem two separate interpretations will be posed below for the horizontal profiling data. In relation to the vertical electrical soundings, two different inversions of the field data, both fitting within geologic controls, will be presented.

HORIZONTAL PROFILE

CASE I UNIFORM LITHOLOGY

In this model we assume any change in profile readings a consequence of pore-water conductivity. As a rule, groundwater contamination by inorganic salts that ionize is usually indicated by anomalously low electrical resistivity. High conductivity anomalies associated with low pH and high concentrations of acidity, iron, sulfates, and trace metals have been described by Ladwig (1984). Although organic contaminants are usually poor conductors (Slaine *et. al.*, 1984) it has been reported that organics, accompanied by inorganic compounds in sufficient concentrations, can result in a low-resistivity anomaly (Bruehl 1984). Figure 10, adapted from Kunetz (1966), illustrates the general form of a

horizontal resistivity profile across a perfectly conducting plate. The diagnostic feature in this graph is its resistivity trough. In this theoretical example, the drop in resistivity is on an order of magnitude. A similar drop in resistivity was reported by Cartwright and McCamas (1968) who showed, in their study of a sanitary landfill, horizontal profiling data with a low of $8 \Omega \text{ m}$ and a high of $87 \Omega \text{ m}$. Clearly, in figures 4 through 7, although the drop is not quite as large as the theoretical model, it is sufficient to have been caused by a thin, highly conductive layer. As implied above, this layer could be the result of inorganic compounds in higher than normal concentrations.

A rough estimate for pore-water resistivity in a contaminated zone was presented by Urish (1983). It utilizes the formation factor formulas

$$F = \alpha \phi^{-m} \quad (2)$$

and

$$F = \frac{\rho_o}{\rho_w} \quad (3)$$

as well as the formula for specific conductance

$$\sigma_w [\mu\text{mhos/cm}] = \frac{10000}{\rho_w [\Omega \text{ m}]} \quad (4)$$

where α and m are empirical constants, ϕ is porosity, ρ_o and ρ_w are the resistivities of the rock and water respectively and σ_w is specific conductance. Reasonable values for α and m , derived by Wyllie and Gregory (1953) and utilized by Urish (1981), are 1 and 1.3 respectively. Uncertainties in these empirical constants are not serious and a variety of different numbers have been used. A much more serious limitation to the formation

factor stems from the assigned value for porosity. A sensitivity analysis of the formation factor formula shows an inverse relationship between porosity and equivalent salinity. As we increase porosity, we decrease the equivalent salinity. Equivalent salinity of a solution is defined as the salinity of a sodium chloride solution which would have the same resistivity as that of the particular solution for which the equivalent salinity is being expressed (Keller and Frischknecht, 1966). An obvious corollary is that as we decrease the equivalent salinity, we increase the pore-water resistivity. With this limitation in mind, a porosity can be derived using available water data. At the U.S.G.S. borehole cited earlier, a water analysis conducted by D. White found a native specific conductance of $\sigma_w = 838$ $\mu\text{mhos/cm}$ at an elevation comparable with that of the lower landfill. If we let $\rho_o = 95$ Ω feet = 31.16 Ω m (estimated background resistivity qualitatively derived from figures 8 and 9) and calculate ρ_w using the native specific conductance, we have, rearranging equation (3)

$$\rho_w = 10000 / 838 \mu\text{mhos/cm} = 11.93 \Omega \text{ m}$$

and

$$F = 31.16 \Omega \text{ m} / 11.93 \Omega \text{ m} = 2.61$$

Rearranging equation (2) we have

$$\phi = F^{-\frac{1}{1.3}} = 0.48$$

The low value for the formation factor and its correspondingly high porosity is consistent with the soil and rock types identified by the U.S.G.S. borehole data (table I) and the E.I.D. augered hole (table II). The equivalent salinity, using the calculated values above is 7.69 meq/liter.

The next step in the analysis is to use this derived porosity to calculate a specific conductance for the horizontal profiling resistivity troughs. We have, from our previous calcula-

tion $F = 2.61$. Rearranging equation (3), using the lowest recorded resistivity readings in the trough,

$$\rho_w = 25 \Omega \text{ feet} / 2.61 = 3.14 \Omega \text{ m} .$$

Employing the formula for the specific conductance (equation 4),

$$\sigma_w [\mu\text{mhos/cm}] = \frac{10000}{3.14 \Omega \text{ m}} = 3184 \mu\text{mhos/cm} .$$

The above calculations have resulted in $\rho_w = 11.93 \Omega \text{ m}$ for the background pore-water resistivity and $\rho_w = 3.14 \Omega \text{ m}$ for the area with low resistivity measurements. Although Keller and Frischknecht (1966) report a limiting range, for pore-water resistivities, between $10 \Omega \text{ m}$ and $0.1 \Omega \text{ m}$, the calculated pore-water resistivity for the background is not altogether surprising. In fine grained rocks, apparent pore-water resistivities are always much lower than would be expected on the basis of a chemical analysis of water extracted from the rock (Keller and Frischknecht, 1966). This is a result of the cation exchange capacity that exists between the pore-water and the rock. Obviously, this exchange capacity can not be accounted for once the water is removed from the rock. Unfortunately, a quantitative evaluation of the discrepancy between insitu and laboratory pore-water resistivities is not possible without knowledge of the cation exchange capacity of the rock. Since the background pore-water resistivity was calculated using a laboratory derived specific conductance, the above mentioned phenomena may explain the difference between this resistivity and Keller and Frischknecht's limiting values.

As indicated by Urish (1983), when the calculated specific conductance of the pore-water is substantially higher than the native water, it can be surmised that this discrepancy is due to the effect of contamination. As can be seen above, the native specific conductance is lower than the calculated one. Another limitations to this approach will be mentioned. It should be recognized that we have implicitly assumed that the apparent resis-

tivity (ρ_o) at its lowest value approaches the bulk resistivity of the saturated layer. Nevertheless, this approach can illustrate that a pore-water anomaly does exist.

Inorganic contaminants are not the only possible cause of a highly conductive layer. Visual inspection of the study area reveals buried metal near the surface. Although this will have some effect on the results we do not believe this metal is the sole reason for the anomalously low readings. Examination of depth of investigation (figures 11 and 12) for the Wenner array, given model parameters presented in table IV, reveal a probing depth of approximately 24 feet for a spacing of 100 feet, and of 16 feet for a spacing of 50 feet. Depth of investigation is defined as that depth at which a thin horizontal (parallel to the ground surface) layer of ground contributes the maximum amount to the total measured signal at the ground surface (Evjen, 1938; Roy and Apparao, 1971). It should be emphasized here that these depths are not absolute depths of targets since other layers contribute to the received signal. In addition, a simplified current penetration model (Van Nostrand and Cook, 1966), again using parameters from Table IV, reveals only 0.9% of the injected current is in the top layer for a spacing of 50 feet and 0.5% for a spacing of 100 feet. Thus, although there was visible metal at the surface, it does not appear this metal could cause the anomalous resistivity measurements.

CASE II CONSTANT PORE-WATER RESISTIVITY

For this interpretation we assert that a change in profile measurements originates in the lithology of the material. As discussed earlier, a model of this type assumes constant pore-water resistivity. Figures 13 through 16 are normalized plots of the F and D line profiles. The abscissa is marked x/a where x is the distance from the center of the anomaly and a is the Wenner electrode spacing. The ordinate is defined as ρ_a / ρ' where ρ_a is the measured resistivity and ρ' is taken as 170 Ω feet. This ρ' value is not arbitrary but derived from both of the VES inversions to be presented below. The normalized plot in figure 17 is a theoretical model adapted from Van Nostrand and Cook (1966) and is for an oblate hemispheroid. Distance between the two peaks, labeled A and B, minus the electrode spacing indicates the width of the body in question. Examination of figure 13

shows that the F line for $a = 50$ feet most closely matches the theoretical curve of figure 17. Calculation of the width of the geologic form using Van Nostrand's generalization indicates a structural diameter of approximately 300 feet. A graphical comparison for the F line $a = 100$ feet profile was not possible, but a logical extension of the theoretical graphs presented in Van Nostrand and Cook (p. 219) implies that the shape of the profile (figure 14, labeled C) should flatten as the a spacing becomes a bigger fraction of the structure diameter. In other words, we would expect the range of apparent resistivity measurements to become smaller as the electrode spacing increases. This would appear to be the trend for the F line as we increase the a spacing from 50 to 100 feet (figures 13 and 14).

It has been reported (Van Nostrand and Cook, 1966) that if the width of the sink is small in comparison with its length and depth, the edge effects are approximately those due to a vertical dike of finite length. With this in mind, we will assume that the F lines crossed over the length of the structure while the D lines crossed over its width. Using this assumption, it was found that the $a = 50$ feet D line (figure 15) closely resembles that of a theoretical profile (figure 18) for a vertical dike with $a/2 = 100$ feet width. This same model fits reasonably well for the $a = 100$ feet D line (figure 16) where, assuming a structural width of $a/4$, the expected theoretical curve would again have a flatter appearance (see Van Nostrand and Cook, 1966, p156). Thus, assuming constant pore-water resistivity, the structural dimensions of the geologic body causing the resistivity troughs in the horizontal profiling data can be defined as: width = 25 feet, length = 300 feet, and depth = 70 feet (from VES models).

It should be noted that all of the comparisons made with Van Nostrand and Cook theoretical curves are qualitative in nature. It can not be expected that the boundary conditions used to derive these curves were met in the field. Nonetheless, reasonable extensions can be applied if the above mentioned limitations are kept in mind.

VERTICAL ELECTRICAL SOUNDINGS (VES)

MODELING PROCEDURE FOR WENNER VES

The modeling of the La Union lower landfill VES data was conducted in 5 phases.

- 1) The initial Wenner VES data were plotted on log-log paper. This curve was matched to a theoretical curve using a set of curves published by Mooney and Wetzel (1956).
- 2) Parameters derived from curve matching were adjusted using the forward calculation portion of Fortran program SLUMB (Petrick *et. al.*, 1977, as modified by LaBrecque, 1987, unpublished)
- 3) Best forward fit was then inverted using SLUMB. During the inversions several different parameter combinations were held constant. The final result is the statistically best-fitting inverted model from this group.
- 4) An additional inversion using the Zohdy and Bisdorf (1975) method was applied.
- 5) Both models were compared to known geologic controls for verification and adjustment.

INVERSION MODELS OF WENNER VES

The 4-layered earth model used in this report (figure 19 and table III) is the result of a numerical inversion of the collected field data using the Fortran program SLUMB. SLUMB, which can be described as a simultaneous layered-earth plane wave and resistivity inversion program, was originally written by William Petrick and most recently revised by Doug LaBrecque of the University of Utah. SLUMB uses nonlinear weighted least squares inversion with Marquardt stabilization (sometimes called ridge regression).

In Petrick's algorithm, input includes: number of layers, layer thicknesses, and layer resistivities. In effect, the program user can control the complexity of the inverted model with respect to the input parameters. In this interpretation the 4-layer model was forced because it was felt that a more complicated case could not be rationalized with only 10 data points to invert.

Table III consists of the model parameters (resistivities and thicknesses) as well as several statistical parameters. The first section of the table, labeled observed apparent resistivity, essentially contains inputted field data along with the user calculated data weights. The data weighting is derived as follows: for each set of field data points a percent observation standard deviation is calculated. The actual weight is then $1/(\text{percent observation standard deviation})$. Underneath the inputted data are the initial and calculated layered-earth model parameters. In this example only two iterations after the initial guess were permitted. The resulting apparent resistivities, from the final iteration, are shown in the next section.

The remaining portions of Table III present relevant statistical parameters. The weighted residual is calculated as

$$\text{Weighted residual} = (\ln(\text{observ}) - \ln(\text{calc. rpsns})) * \text{Wt.}$$

where \ln is defined as the natural logarithm. The next section, labeled normalized derivatives, is essentially a sensitivity matrix. Each row corresponds to a particular electrode spacing, ordered from station 1 to station 10. The columns each correspond to the inverted geophysical parameters (resistivity or thickness). Normally, a four layered model would have 7 columns. Columns 1 through 4 would represent the resistivities of layers 1 through 4 while columns 5 through 7 would describe the thicknesses of layers 1 through 3 (layer 4 having infinite thickness). In table III, since the resistivities were held constant, columns 1 through 3 correspond to model thicknesses for layers 1 through 3. The normalized derivatives themselves represent contributions of a particular array separation (associated with a particular field observation and station) to the parameter (resistivity or thickness) represented by the column. Thus, each number represents the sensitivity of either a resistivity or thickness to a particular electrode spacing. The higher normalized derivatives indicate where the major contributions to the recorded signal lie. As expected, the greater contributions to the signal are associated with larger spacings.

The next section of table III is labeled estimated percent parameter standard deviations. General working experience with SLUMB has shown these percentages should

normally be below 30 to assure a good model fit. Finally, the covariance matrix represents the statistical relationship or correlation between any two parameters in the model.

The automatically inverted curve presented in figure 20 and table IV was derived using a different approach from that of the Petrick model. Zohdy and Bisdorf's algorithm utilizes modified Dar Zarrouk functions in an iterative fashion to calculate the proper model parameters. Table IV is an adjusted sample output from the Zohdy program. The column labeled adjusted reduction is the result of a visual qualitative reduction of model parameters. Zohdy recommends that manual smoothing of layers may be necessary to produce geologically acceptable results. As can be seen, the first three layers, with a total depth of 4.81 feet, can be considered an equivalent single layer with an approximate resistivity of 177 Ω feet. The resulting model is a much more manageable 5 layer case.

COMPARISON AND INTERPRETATION

Although both inversion codes use different approaches, the resulting models are not entirely different. Visual inspection confirms a better fit for the Zohdy model but it should be remembered that the Petrick inversion was forced to a simpler model and its statistical parameters are well within accepted ranges. If the Zohdy inversion were further reduced, as for example combining the third and fourth layers, it would be quite similar to the Petrick model.

Prior knowledge of geologic controls are essential for an accurate inversion of electrical resistivity data. For example, the lower landfill had a reported depth of 5 to 10 feet. This information matches the estimated thickness of the uppermost layer in both the Zohdy and Petrick inversion models. This permits interpretation of either model's top layer as that of the landfill itself. Another illustration showing the importance of prior knowledge of geologic controls is the gradual fall in resistivities between the second and third layers. Examination of both the Zohdy and Petrick inversions reveal that the drop in resistivity between the second and third layer is not particularly great. Without prior knowledge of the water table level (20-25 ft.), the boundary between the second and third layer could be misconstrued as something other than a water table boundary. It is

reassuring, given this prior knowledge, that the Zohdy model places an electrical layer at 24 feet and the Petrick model at 23 feet. Thus, we can interpret this electrical boundary as the top of the water table.

The above mentioned drop in resistivity values between the second and third layers is an important interpretation feature. Figure 21, an adaptation from Urish (1983), shows the contrasting VES graphs for gravel, sand, and silt as they move from unsaturated to saturated conditions. The gradual slope of the silt line, as opposed to those of gravel and sand, closely resembles those found in figures 19 and 20. This result is not surprising, given the borehole and augered data presented in tables I and II. Thus we can interpret the second and third layers as a silt or clay layer passing from unsaturated to saturated conditions.

It should be recognized that this implied silt layer may not be vertically continuous. The Wenner configuration, in general, has the tendency to average out thin contrasting layers. A perfect example of this phenomenon is the fact that neither model interpreted the one-foot gravel layer found during augering (table II). As stated by Zohdy *et. al.* (1974), "the detectability of a layer of given resistivity depends on its relative thickness, which is defined as the ratio of bed thickness to its depth of burial". In essence, the smaller the relative thickness, the smaller the chance of detecting it in an electrical sounding. Thus, since the relative thickness of the gravel layer is 0.06, neither VES model detected it.

SUMMARY OF CONCLUSIONS

Analysis of the field measurements resulted in two conflicting interpretations. Assuming constant lithology, it can be concluded that the low-resistivity readings are a result of a change in pore-water resistivity. This case is supported by an evaluation utilizing the formation factor and specific conductance of the native water. A second view, one in which the drop in resistivities is attributed to a change in lithology, is supported by a comparison with theoretical horizontal profiling curves presented in Van Nostrand and Cook (1966). In addition, an evaluation of the VES curve, using methods developed by

Petrick *et. al.* (1977) and Zohdy and Bisdorf (1975), supports the changing lithology interpretation.

Although a definitive model for the low-resistivity measurements was not possible, it was concluded, from an analysis of the depth of investigation and current penetration, that the cause of the anomalous readings was not within the first 5 to 7 feet (top layer).

RECOMMENDATIONS

This report has demonstrated that resistivity methods alone are not adequate to fully study a possible groundwater contaminant plume. Moreover, these techniques can not necessarily distinguish between a pollutant and a geologic body. As alluded to earlier, an integrated attack, one in which at least two independent geophysical or geological techniques are applied, is the preferred approach. Gilmer and Helbling (1984) combined electromagnetic and vertical electrical soundings with seismic refraction techniques to help develop a monitoring well system. Gilkeson *et. al.* (1984) used an approach which included electrical earth resistivity with shallow geothermic surveys to delineate contaminant pathways at an Illinois site. Finally, Benson *et. al.* (1984) give an excellent review of the integrated approach which includes comments on ground-penetrating radar, electromagnetics, resistivity, seismic refraction and reflection, metal detection, magnetometry, and organic vapor analysis.

Unfortunately, the two techniques applied at the La Union lower landfill, electromagnetics and resistivity, can not be considered independent of each other. Similar drawbacks to the ones discussed in this paper can inhibit interpretation of electromagnetic results. The two methods are, however, complementary in nature. For example, in a geological environment with a highly conductive top layer, electromagnetic methods may be of limited use as opposed to resistivity measurements (White *et. al.*, 1984). On the other hand, a thin highly resistive caliche layer that distorted resistivity data appeared transparent with respect to the Geonics EM-34-3 electromagnetic induction equipment (LeBrecque *et. al.*, 1984). In truth, the interpretation techniques (*ie.* inversion programming, type curves, etc.) are much more developed for resistivity methods. It is recog-

nized, however, that the ease with which electromagnetic surveys are conducted makes the technique a very powerful tool in the field.

A common denominator in almost all groundwater pollution investigations using either electrical resistivity or electromagnetic induction was the use of test wells to verify or adjust proposed earth models. Zohdy *et. al.* (1974) go as far as to recommend that parametric electrical soundings be made near test wells in order to determine the resistivity parameters of layers using accurately determined layer thicknesses. Thus, it is advised that a test well be drilled in the vicinity of the resistivity troughs reported in figures 4 through 9. Figure 3 shows the recommended location of the test well. This location is preferred because it is down gradient from the lowest resistivity readings recorded yet still within the high conductivity troughs. A well down-gradient from the investigation area will permit valuable water sampling both now and at a future date. In addition, since the location is still within the anomalously low resistivity area, lithologic study of the well borings can help confirm or dismiss either interpretation of the horizontal profiling data. Drilling on the landfill is not recommended because of the unknown nature of the possible contaminant source. Contaminant filled drums, under pressure, could rupture causing injury and possibly permitting pollutants to spread through uncontaminated portions of the system.

LIST OF REFERENCES

- Benson, R. C., R. A. Glaccum and M. R. Noel, 1984, Geophysical techniques for sensing buried wastes and waste migration: a applications review: *Proceedings of the NWWA/EPA conference on surface and borehole geophysical methods in ground water investigations, San Antonio Texas*, pp. 533-566
- Bruehl, D. H., 1984, Delineation of ground water contamination by electrical resistivity depth soundings: *Proceedings of the NWWA/EPA conference on surface and borehole geophysical methods in ground water investigations, San Antonio Texas*, pp. 403-412
- Cartwright, K., and M. R. McComas, 1968, Geophysical surveys in the vicinity of sanitary landfills in northeastern Illinois: *Ground Water*, v. 6, no. 5, pp. 23-30
- Evjen, H. M., 1938, Depth factor and resolving power of electrical measurements: *Geophysics*, v. 3, pp. 78-98
- Gilkeson, R. H., T. H. Larson, and P. C. Heigold, 1984, Definition of contaminant pathways: an integrated geophysical and geological study: *Proceedings of the NWWA/EPA conference on surface and borehole geophysical methods in ground water investigations, San Antonio Texas*, pp. 567-583
- Gilmer, T. H., and M. P. Helbling, 1984, Geophysical investigations of a hazardous waste site, Massachusetts: *Proceedings of the NWWA/EPA conference on surface and borehole geophysical methods in ground water investigations, San Antonio Texas*, pp. 618-636
- Hawley J. W., and R. P. Lozinsky, 1986, Progress report on: Hydrogeologic and geophysical framework of the Mesilla basin in southern New Mexico and western Texas. New Mexico Bureau of Mines and Mineral Resources
- Keller, G. V., and F. C. Frischknecht, 1966, *Electrical Methods in Geophysical Prospecting*: New York, Pergamon Press, 519 pp.
- Kelly, W. E., 1976, Geoelectrical sounding for delineating ground-water contamination: *Ground Water*, v. 14, no. 1, pp. 6-10
- Klefstad, G., L. V. A. Sendlein, and R. C. Palmquist, 1975, Limitations of the electrical resistivity method in landfill investigations: *Ground Water*, v. 13, no. 5, pp. 418-426
- Kunetz, G., 1966, *Principles of Direct Current Resistivity Prospecting*: Berlin, Gebrüder Borntraeger, 103 pp.

- Ladwig K.J., 1984, Use of surface geophysics to determine flow patterns in surface mine spoil: *Proceedings of the NWWA/EPA conference on surface and borehole geophysical methods in ground water investigations, San Antonio Texas*, pp. 455-471
- LaBrecque D. J., D. D. Weber, and R. B. Evans, 1984, Comparison of resistivity and electromagnetic methods over a contaminant plume using numerical methods: *Proceedings of the NWWA/EPA conference on surface and borehole geophysical methods in ground water investigations, San Antonio Texas*, pp. 316-333
- Mooney, H. M., and W. W. Wetzel, 1956, The potentials about a point electrode and apparent resistivity curves for a two-, three-, and four-layer earth: Minneapolis, Univ. Minnesota Press, p. 146 and 243 loose sheets of reference curves.
- Petrick, W. R., W. H. Pelton, and S. H. Ward, 1977, Ridge regression inversion applied to crustal resistivity sounding data from South Africa: *Geophysics*, v. 42, pp. 995-1005.
- Roy, A., and A. Apparao, 1971, Depth of investigation in direct current methods: *Geophysics*, v. 36, no. 5, pp. 943-959
- Slaine, D. D., P. K. Lee, and J. P. Phimister, 1984, A comparison of a geophysically and geochemically mapped contaminant plume: *Proceedings of the NWWA/EPA conference on surface and borehole geophysical methods in ground water investigations, San Antonio Texas*, pp. 383-402
- Stollar, R. L., and P. Roux, 1975, Earth resistivity surveys—a method for defining ground-water contamination: *Ground Water*, v. 13, no. 2, pp. 145-150
- Urish, D. W., 1981, Electrical resistivity-hydraulic conductivity relationships in glacial outwash aquifers: *Water Resources Research*, v. 17, no. 5, pp. 1401-1408
- Urish, D. W., 1983, The practical application of surface electrical resistivity to detection of Ground-water pollution: *Ground Water*, v. 21, no. 2, pp. 144-152
- Van Nostrand, R. G., and K. L. Cook, 1966, Interpretation of resistivity data: *U. S. Geol. Survey Prof. Paper 499*, 310 p.
- White, R. M., D. G. Miller, Jr., S. S. Bradwein, and A. F. Benson, 1984, Pitfalls of electrical surveys for ground water contamination investigations: *Proceedings of the NWWA/EPA conference on surface and borehole geophysical methods in ground water investigations, San Antonio Texas*, pp. 472-482
- Wilson, C. A., R. R. White, B. R. Orr, and R. G. Roybal, 1981, Water resources of the Rincon and Mesilla Valleys and Adjacent Areas, New Mexico: *N.M. State Engineer Technical Report no. 43*.

- Wyllie, M. R. J. and A. R. Gregory, 1953, Formation factors of unconsolidated porous media: influence of particle shape and effect of cementation: *Journal of Petroleum Technology*, v. 198, pp. 103-110.
- Zohdy, A. A. R., G. P. Eaton, and D. R. Mabey, 1974, Application of surface geophysics to Ground-water investigations: *Techniques of Water Resources Investigations of the U.S. Geological Survey. Book 2, Chap. D1* U.S. Government Printing office, Washington D.C.
- Zohdy, A. A. R., and R. J. Bisdorf, 1975, Computer programs for the forward calculation and automatic inversion of Wenner sounding curves: National Technical Information Service, U.S. Department of Commerce. Report no. PB-247-265

Table I U.S.G.S. borehole #27S.2.13.333

.....

Depth from surface (ft.)	Geologic description
300-325	silt and sandy silt interbeds
325-375	silt and sandy silt with minor clay
375-400	medium to fine sand
400-500	medium coarse sand with minor clay interbeds, moderately sorted
500-550	medium coarse sand with silt and clay interbeds

.....

Table II E.I.D. augered hole 6/11/87

Depth from surface (ft.)	Geologic description
0-6	pit
6-11	medium sand
11-15	hard, dry clay
15-16	gravel
16-22	clay
22.25-?	sandy clay (wet)

Table III - Wenner inversion program (Petrick)

La Union, lower landfill

OBSERVED APPARENT RESISTIVITY....WENNER

STATION	(3*A)/2	A	APP. RES.	WT
1	1.500E+00	1.000E+00	150.000	5.000
2	4.500E+00	3.000E+00	149.550	20.400
3	7.500E+00	5.000E+00	142.930	26.300
4	1.050E+01	7.000E+00	122.820	138.500
5	1.500E+01	1.000E+01	83.330	65.800
6	4.500E+01	3.000E+01	35.560	11.500
7	7.500E+01	5.000E+01	25.400	65.000
8	1.050E+02	7.000E+01	30.450	10.400
9	1.500E+02	1.000E+02	34.020	25.000
10	3.000E+02	2.000E+02	55.650	16.700

LAYERED EARTH MODEL PARAMETERS

LAYER 1	RESISTIVITY=	177.84	THICKNESS=	6.76
LAYER 2	RESISTIVITY=	27.54	THICKNESS=	14.12
LAYER 3	RESISTIVITY=	18.00	THICKNESS=	42.67
LAYER 4	RESISTIVITY=	96.80		

AFTER ITERATION 1 MQT PARAM IS 1.00E-03 THE SQUARE ERROR IS 1.50E+01

NEW PARAMETERS ARE

LAYER 1	RESISTIVITY=	177.84	THICKNESS=	5.91
LAYER 2	RESISTIVITY=	27.54	THICKNESS=	18.60
LAYER 3	RESISTIVITY=	18.00	THICKNESS=	41.36
LAYER 4	RESISTIVITY=	96.80		

AFTER ITERATION 2 MQT PARAM IS 1.00E-04 THE SQUARE ERROR IS 1.38E+01

NEW PARAMETERS ARE

LAYER 1	RESISTIVITY=	177.84	THICKNESS=	5.98
LAYER 2	RESISTIVITY=	27.54	THICKNESS=	16.92
LAYER 3	RESISTIVITY=	18.00	THICKNESS=	41.42
LAYER 4	RESISTIVITY=	96.80		

Table III - cont.

.....

APPARENT RESISTIVITY CALCULATED....WENNER

STATION	(3*A)/2	A	APP. RES.
1	1.500E+00	1.0000E+00	177.402
2	4.500E+00	3.0000E+00	168.735
3	7.500E+00	5.0000E+00	147.569
4	1.050E+01	7.0000E+00	121.286
5	1.500E+01	1.0000E+01	86.359
6	4.500E+01	3.0000E+01	27.356
7	7.500E+01	5.0000E+01	25.632
8	1.050E+02	7.0000E+01	28.449
9	1.500E+02	1.0000E+02	34.504
10	3.000E+02	2.0000E+02	51.810

.....

WEIGHTED RESIDUAL

-5.93E-01
-1.74E+00
-5.94E-01
1.23E+00
-1.66E+00
2.13E+00
-4.18E-01
5.00E-01
-2.50E-01
8.44E-01

.....

DERIVATIVE NORMALIZING FACTORS

1.19E-02 2.65E-02 2.73E-02

.....

Table III - cont.

.....

NORMALIZED DERIVATIVES

1.14E-05	0.00E-01	0.00E-01
3.82E-03	1.78E-04	0.00E-01
1.94E-02	1.78E-03	-5.70E-05
9.47E-01	1.56E-01	-4.74E-03
3.20E-01	1.23E-01	-4.99E-03
2.99E-03	5.90E-02	-9.40E-03
1.91E-02	9.50E-01	-9.61E-01
1.34E-04	-1.25E-02	-3.75E-02
-1.36E-05	-2.11E-01	-2.56E-01
-8.87E-05	-9.76E-02	-9.92E-02

.....

THE ESTIMATED PCT PARAMETER STD DEV IS

1.79E+00
7.55E+00
7.60E+00

.....

PARAMETER CORRELATION MATRIX

1.00E+00		
-3.52E-01	1.00E+00	
-2.92E-01	8.64E-01	1.00E+00

.....

Table IV - Wenner inversion program (Zohdy)

THICKNESS	DEPTH	RESISTIVITY	ADJUSTED REDUCTION
0.55260	0.55260	171.45830	-
0.39314	0.94574	94.92809	-
3.87386	4.81960	186.42143	177.00000
19.57811	24.39771	49.50846	49.50846
26.74222	51.13993	12.57237	12.57237
28.14887	79.28880	28.92520	28.92520
99999632.00000	99999712.00000	201.94412	201.94412

A	OBS.VES	CALC. VES	SMOOTHED VES
0.10000	-	171.38560	172.22380
0.14678	-	171.10847	172.03365
0.21544	-	170.12898	171.29735
0.31623	-	167.61008	169.16843
0.46416	-	162.51166	164.37317
0.68129	-	154.87502	156.12839
1.00000	150.0000	148.42145	146.66124
3.00000	149.5500	154.05205	151.81024
5.00000	142.9300	141.08444	143.62614
7.00000	122.8200	119.53151	121.03464
10.00000	83.3300	91.38408	91.25313
30.00000	35.5600	37.40022	36.66403
50.00000	25.4000	28.02647	27.32483
70.00000	30.4500	28.24363	28.25742
100.00000	34.0200	34.44092	34.17486
200.00000	55.6500	58.48822	58.23745

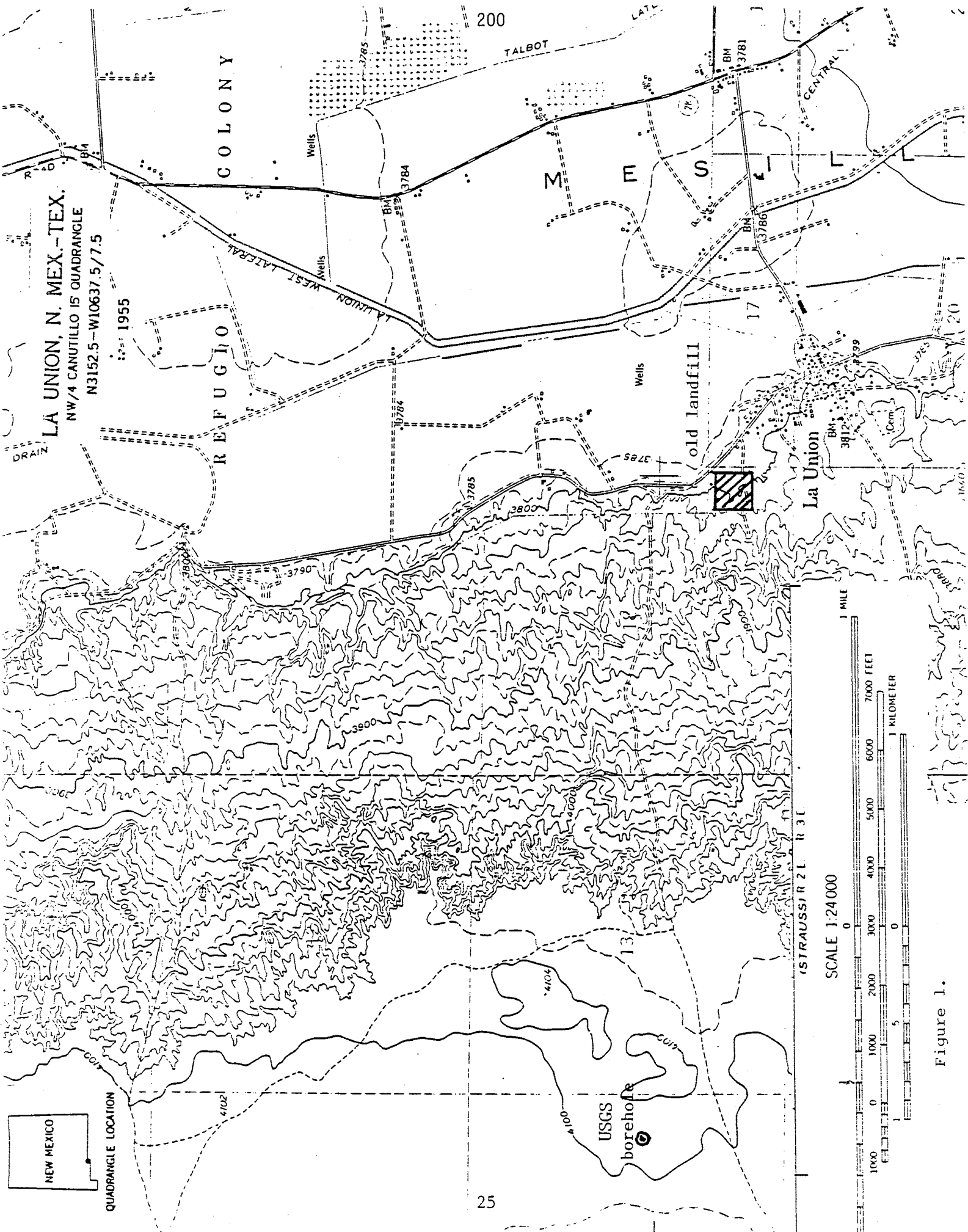


Figure 1.

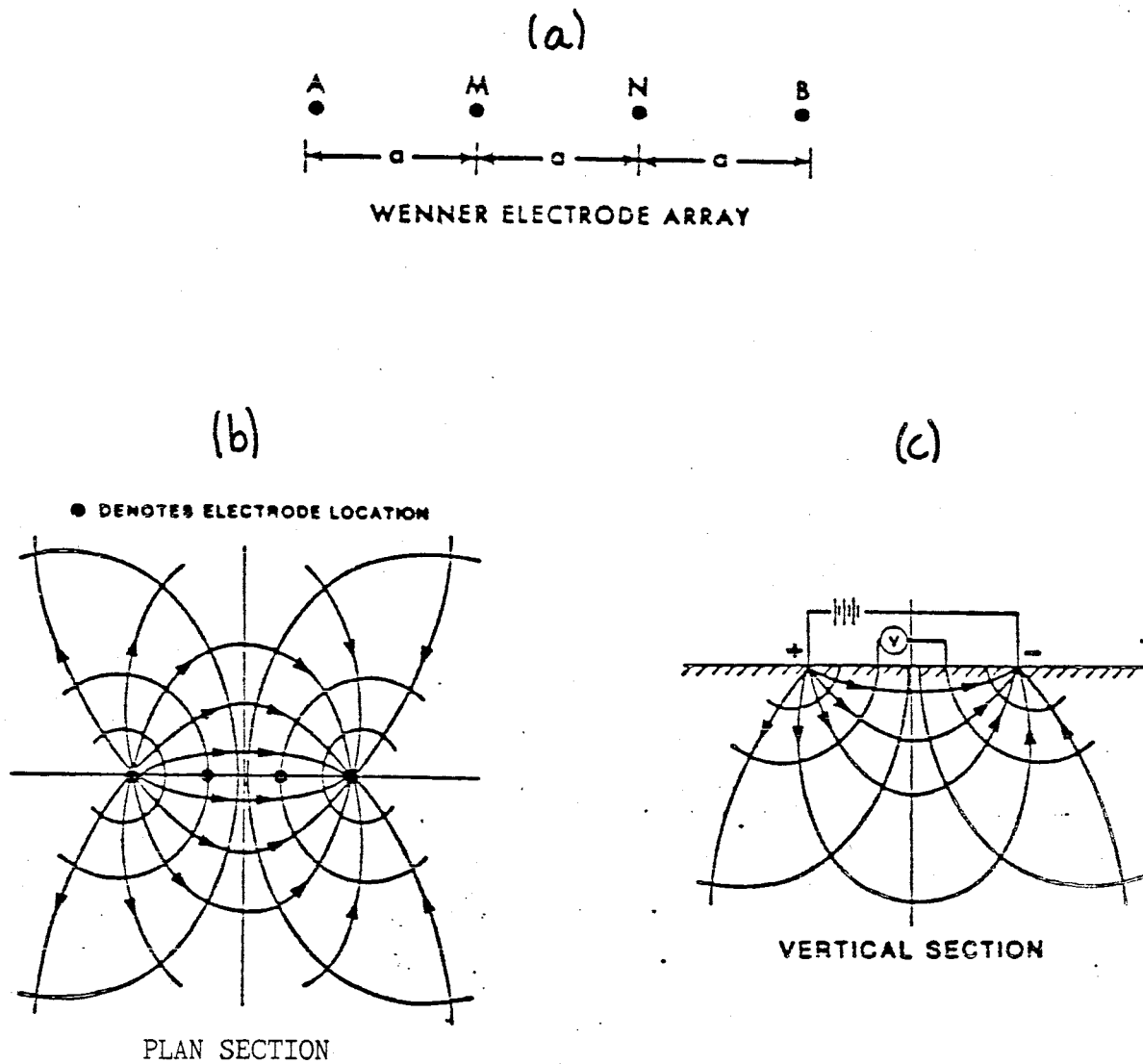
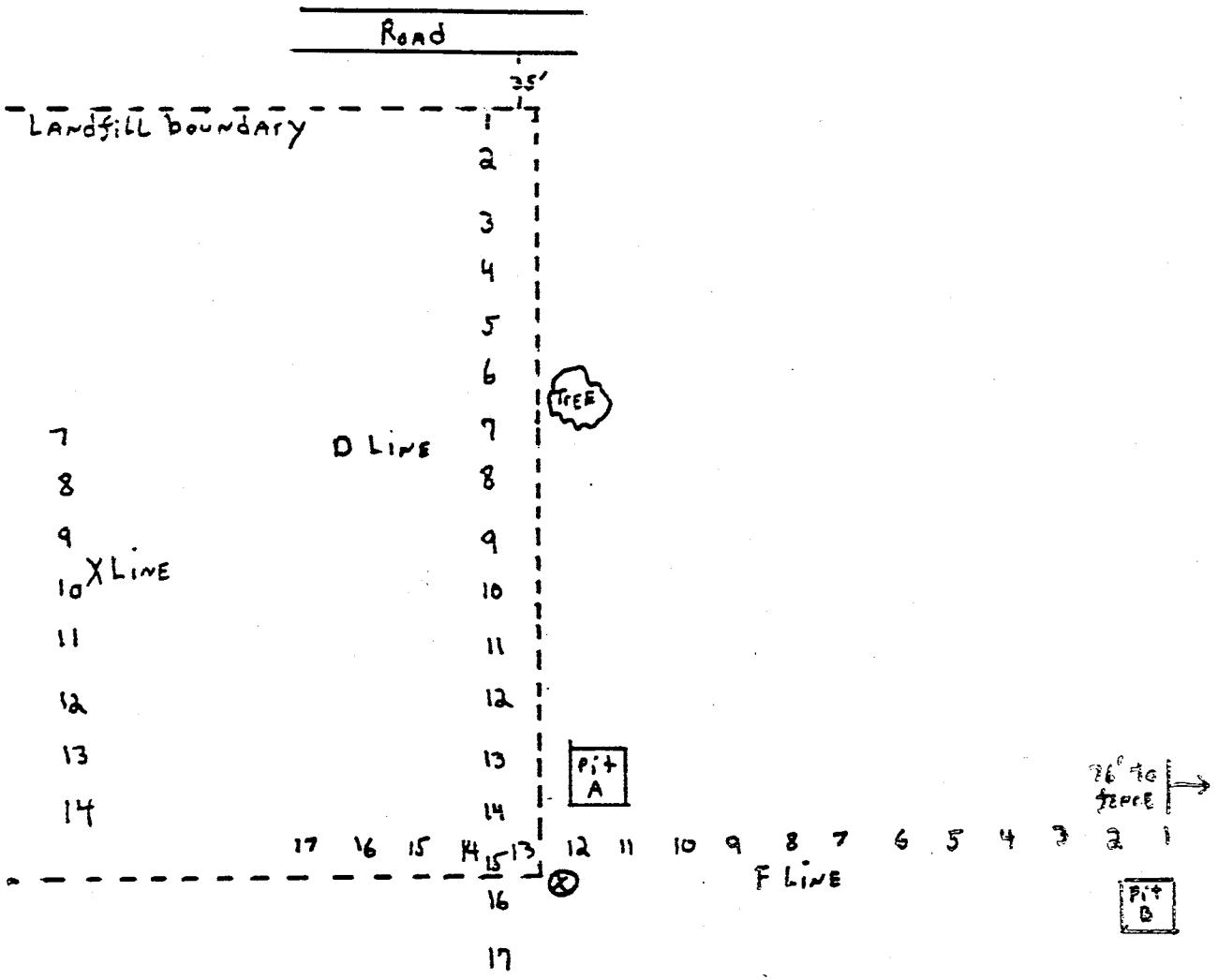


Figure 2. (a) Wenner electrode configuration
 (b) Electrical current flow in the earth (plan section)
 (c) Electrical current flow in the earth (vertical section)

SKETCH of SURVEY AREA LA UNION, NEW MEXICO



⊗ = proposed site of test well



SCALE (ft.)

Figure 3

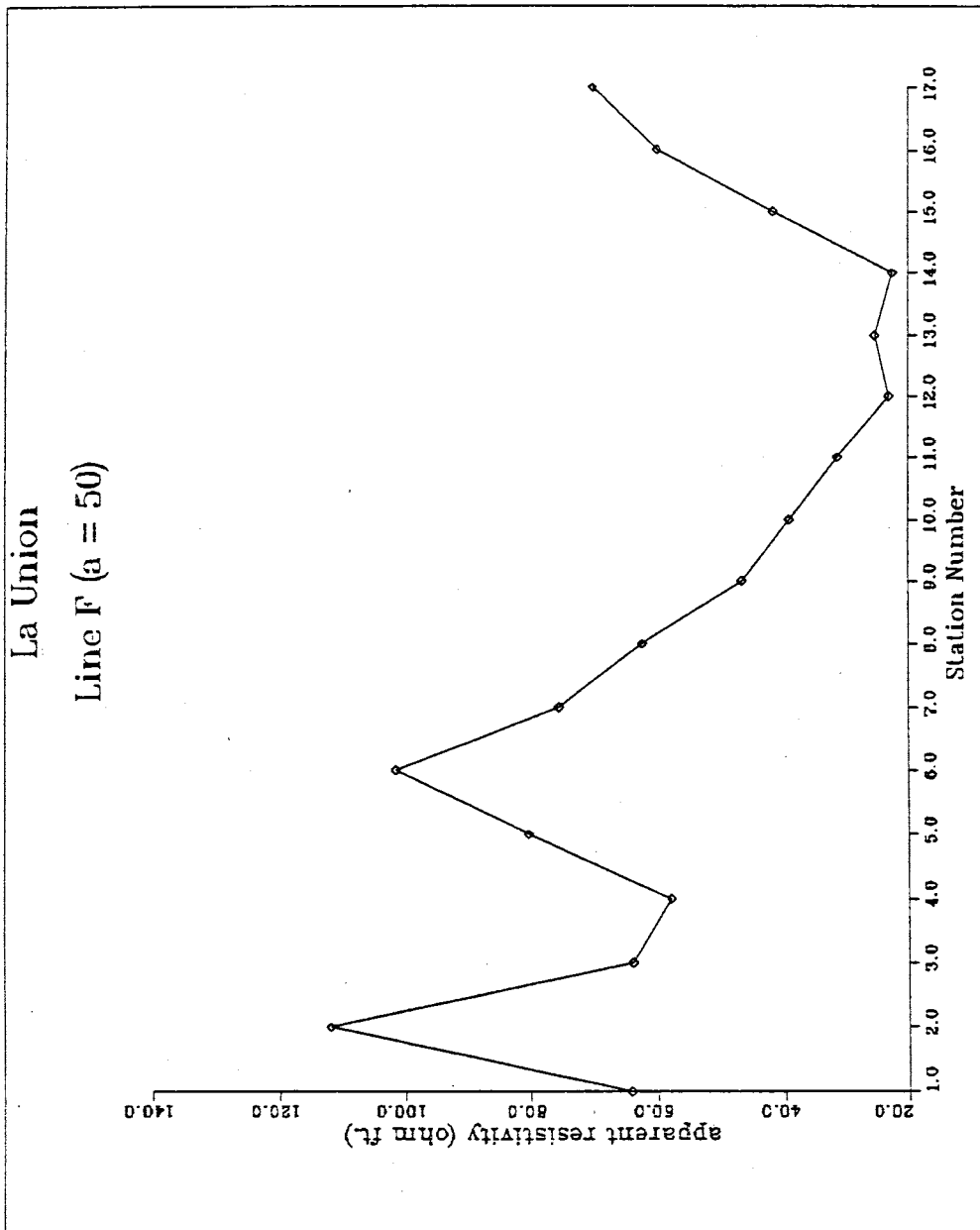


Figure 4. Horizontal resistivity profile, F line, a = 50 feet.

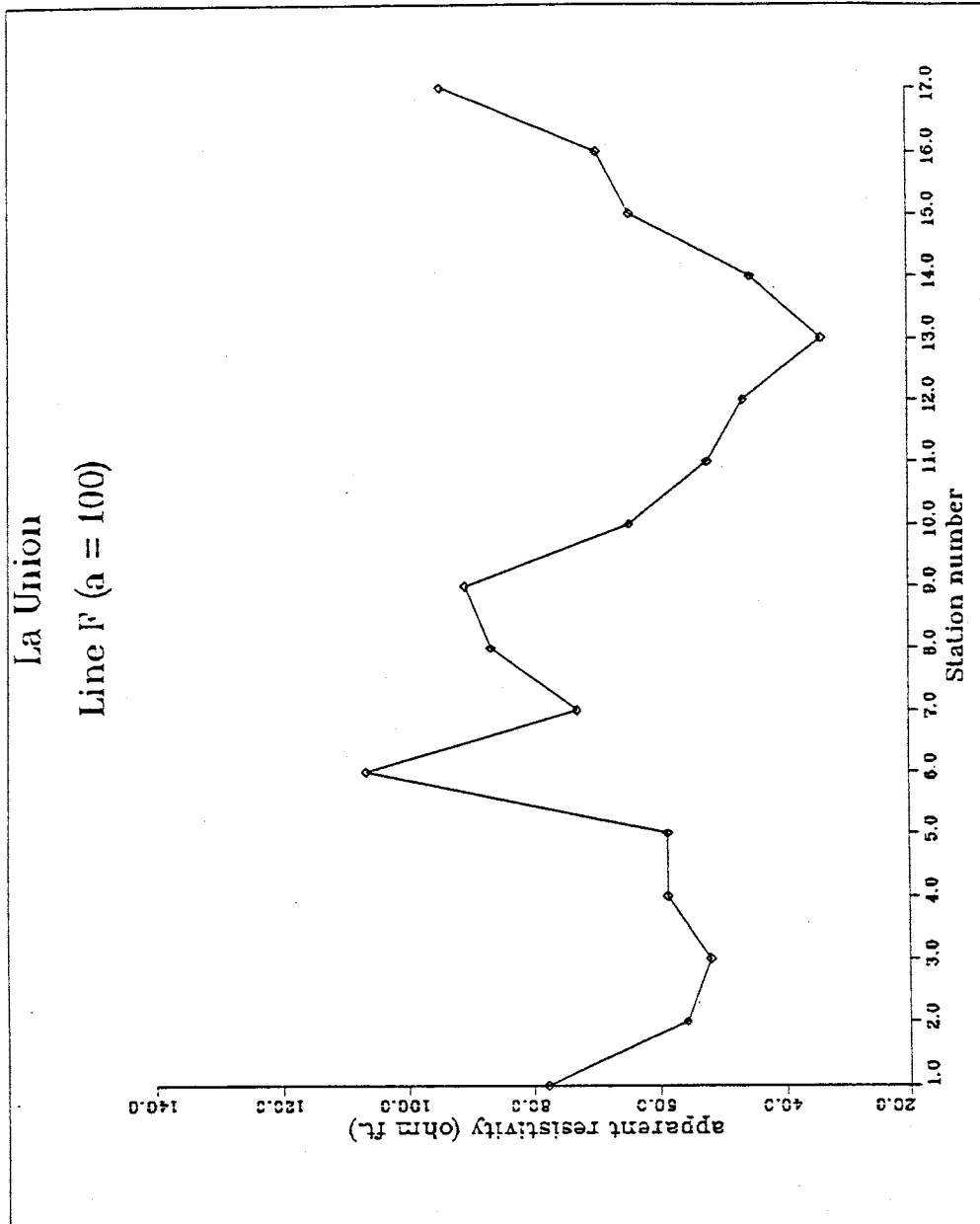


Figure 5. Horizontal resistivity profile, F line, a = 100 feet.

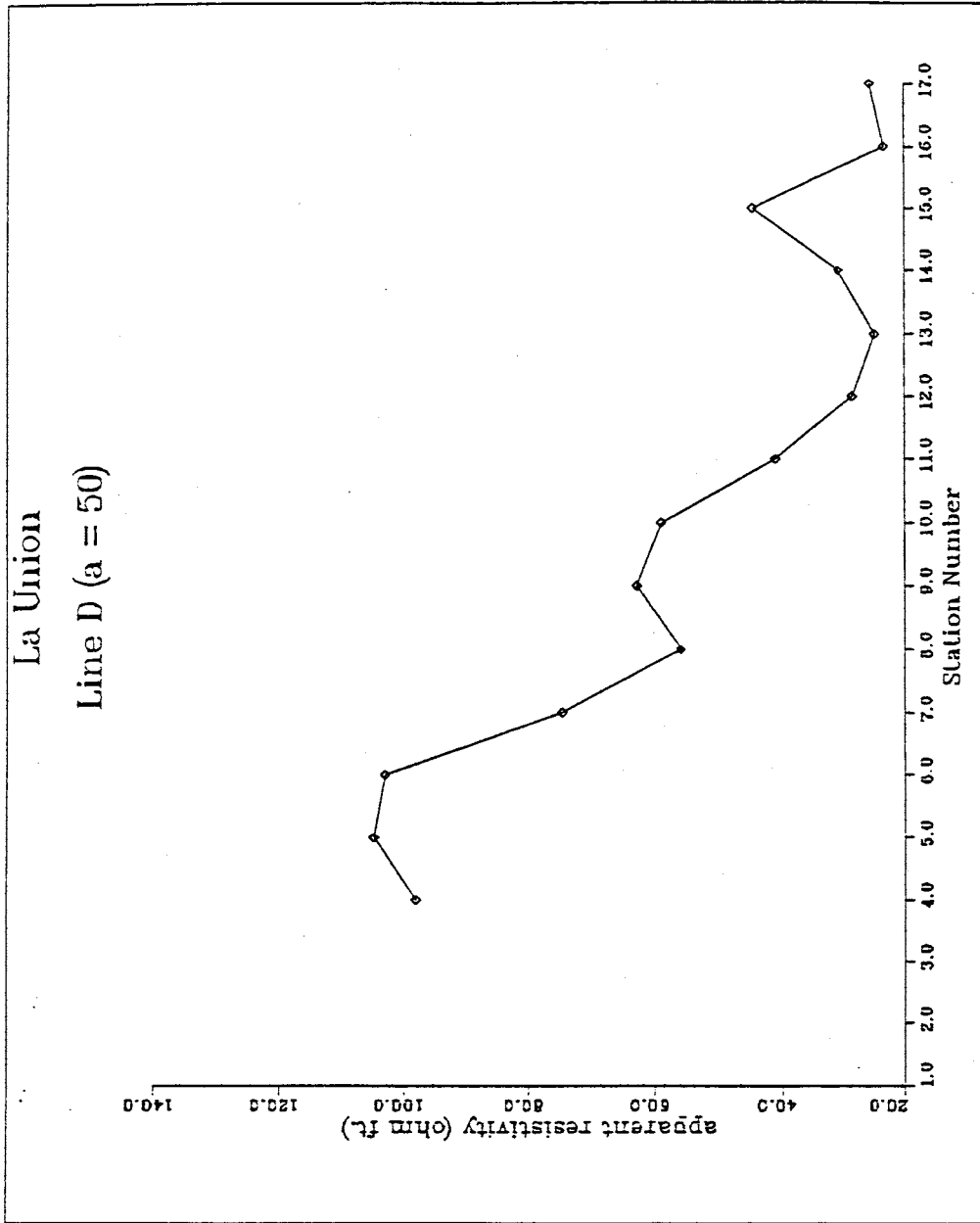


Figure 6. Horizontal resistivity profile, D line, a = 50 feet.

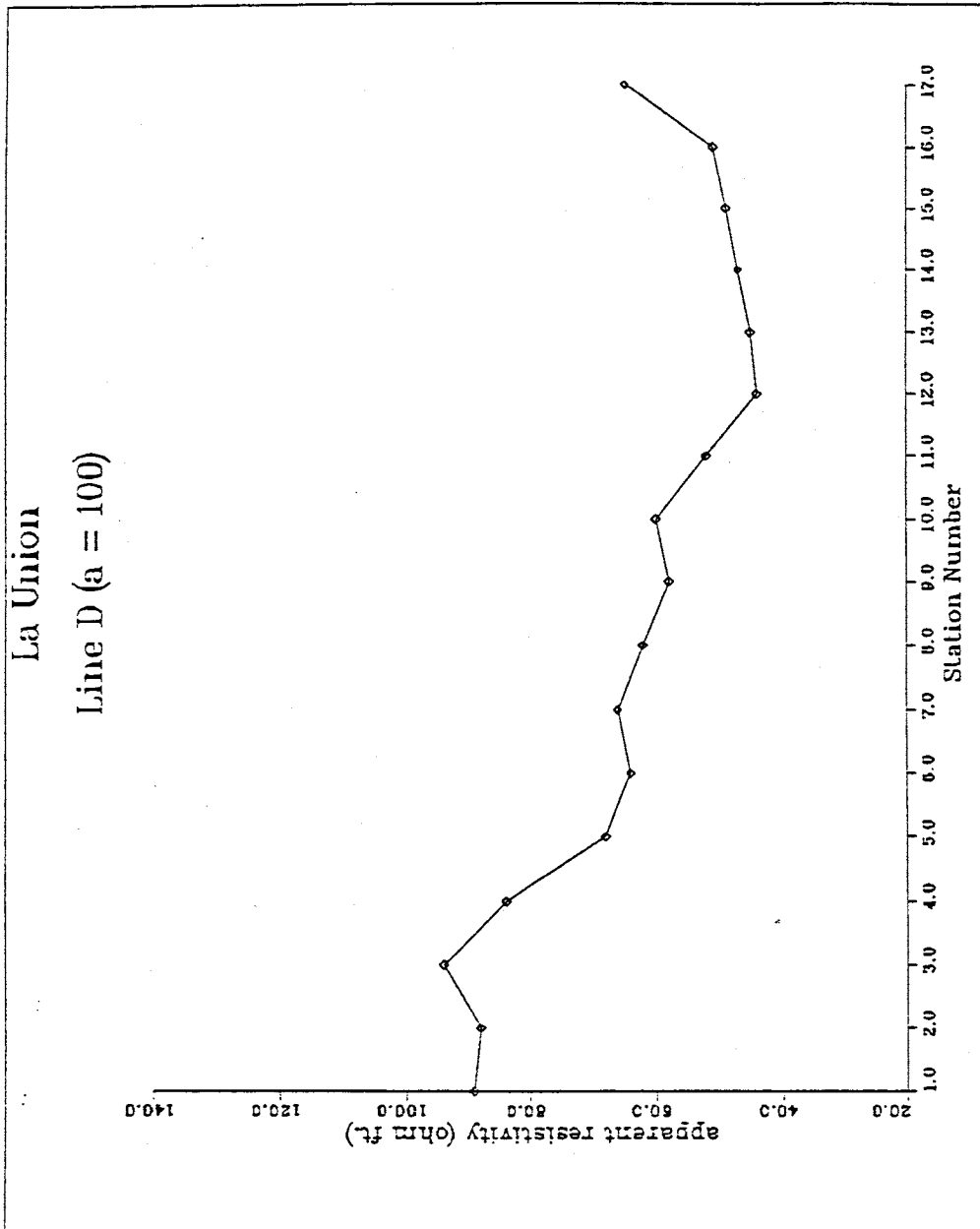


Figure 7. Horizontal resistivity profile, D line, a = 100 feet.

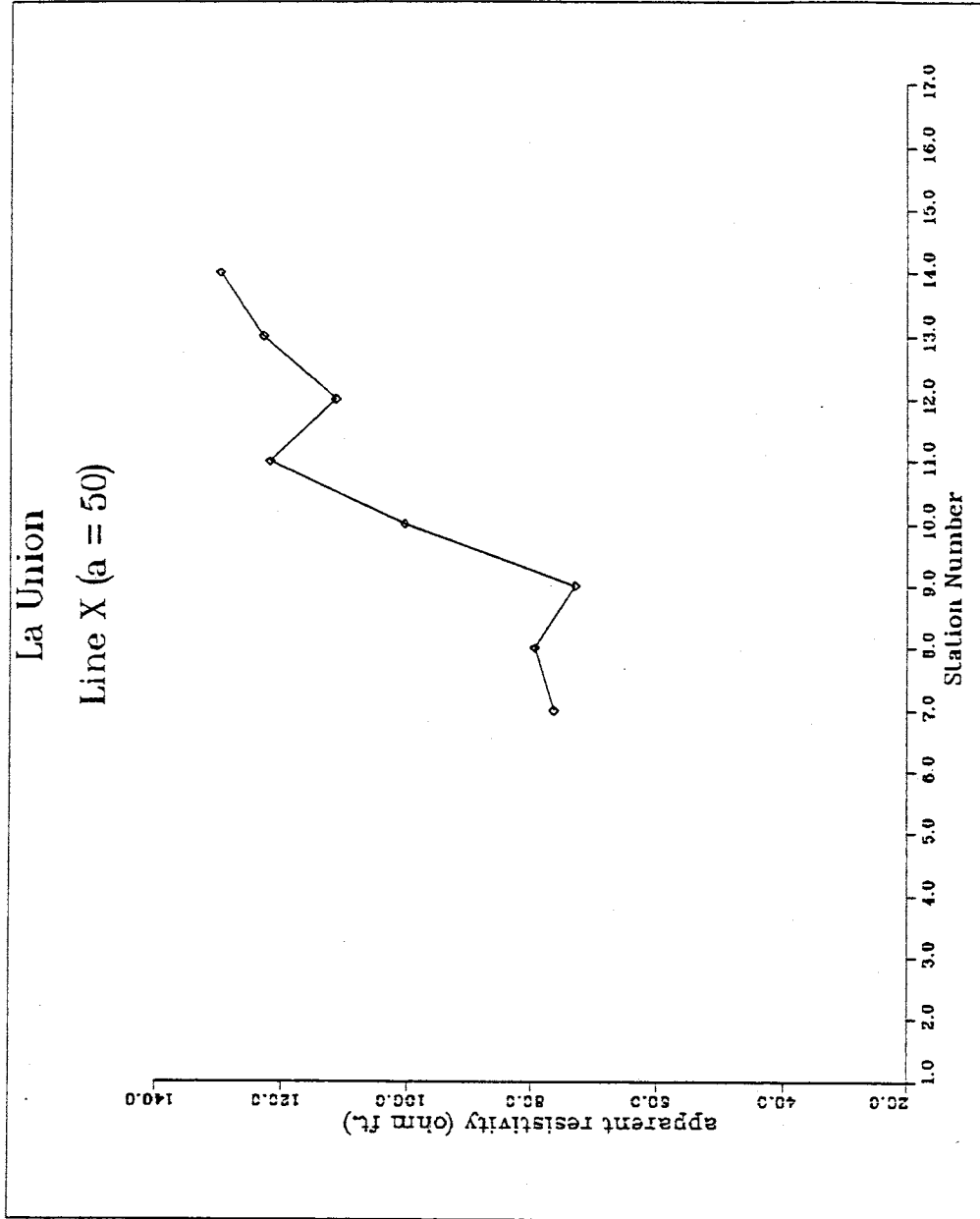


Figure 8. Horizontal resistivity profile, X line, a = 50 feet.

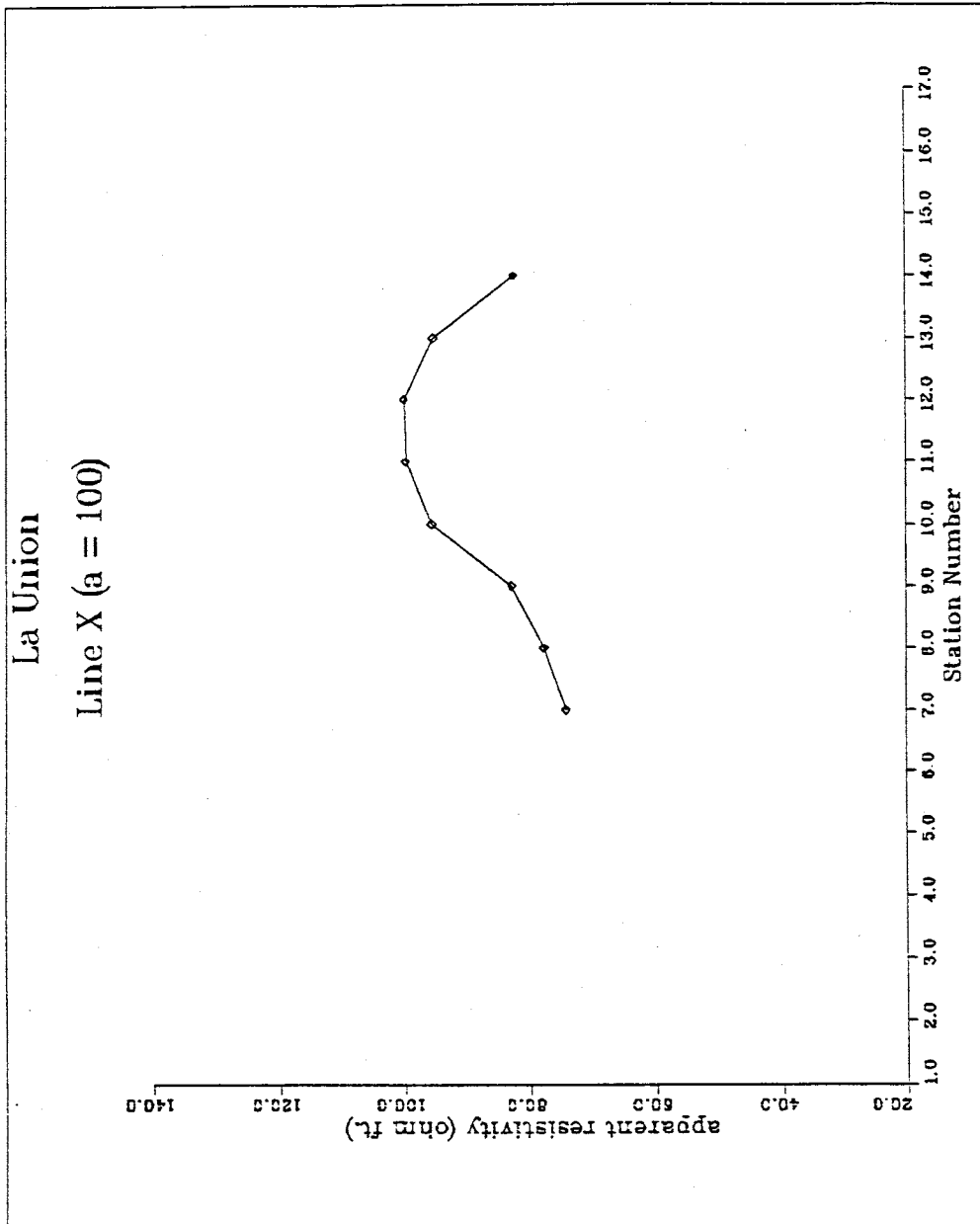


Figure 9. Horizontal resistivity profile, X line, a = 100 feet.

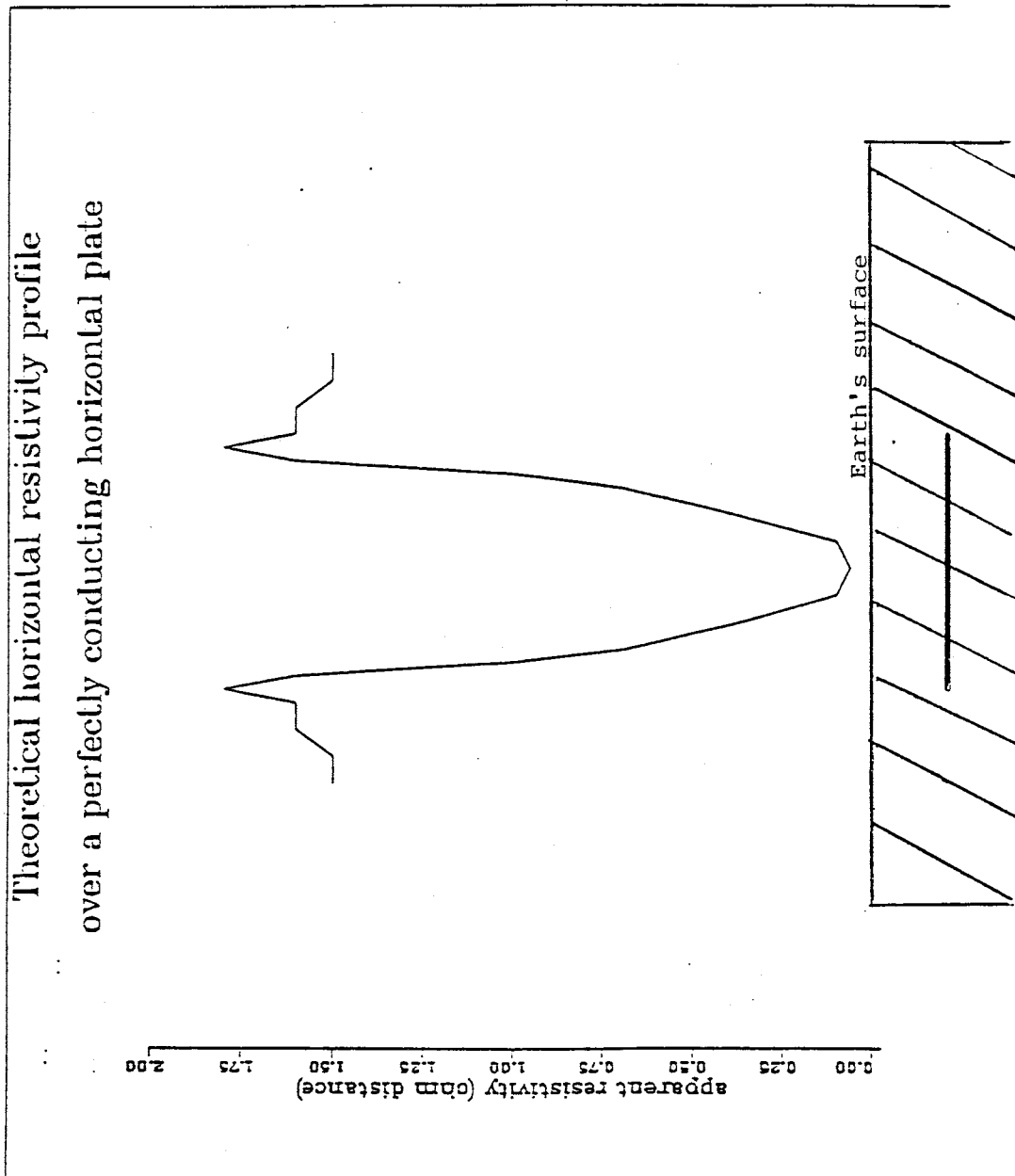


Figure 10. Theoretical horizontal resistivity profile over a buried, perfectly conducting horizontal plate. (after KUNETZ, 1966)

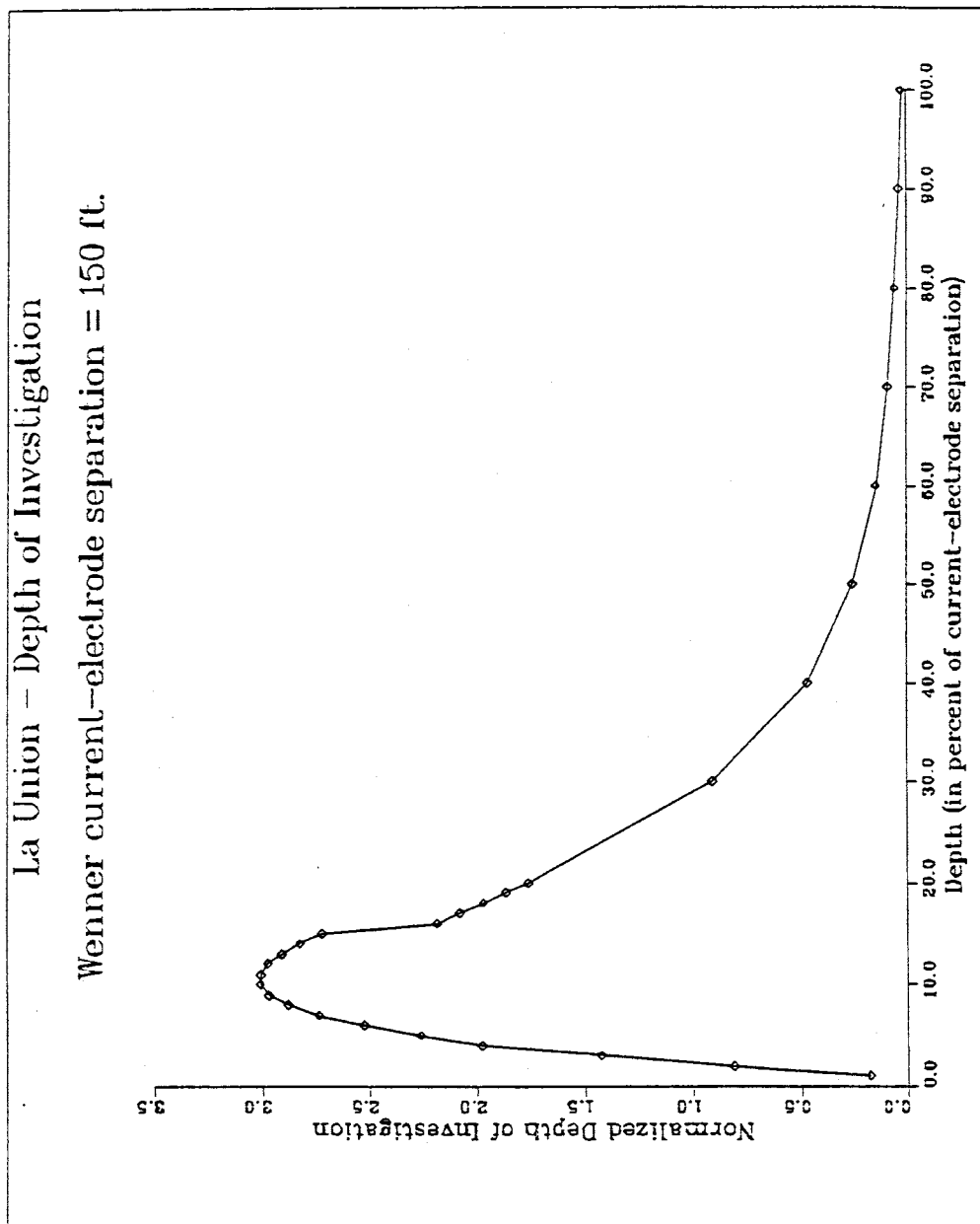


Figure 11. Depth of investigation for Wenner $a = 50$ feet. The abscissa is defined as depth, in percent of current-electrode separation or percent of 150 feet. The ordinate is the normalized depth of investigation. (Modeling data from Table III)

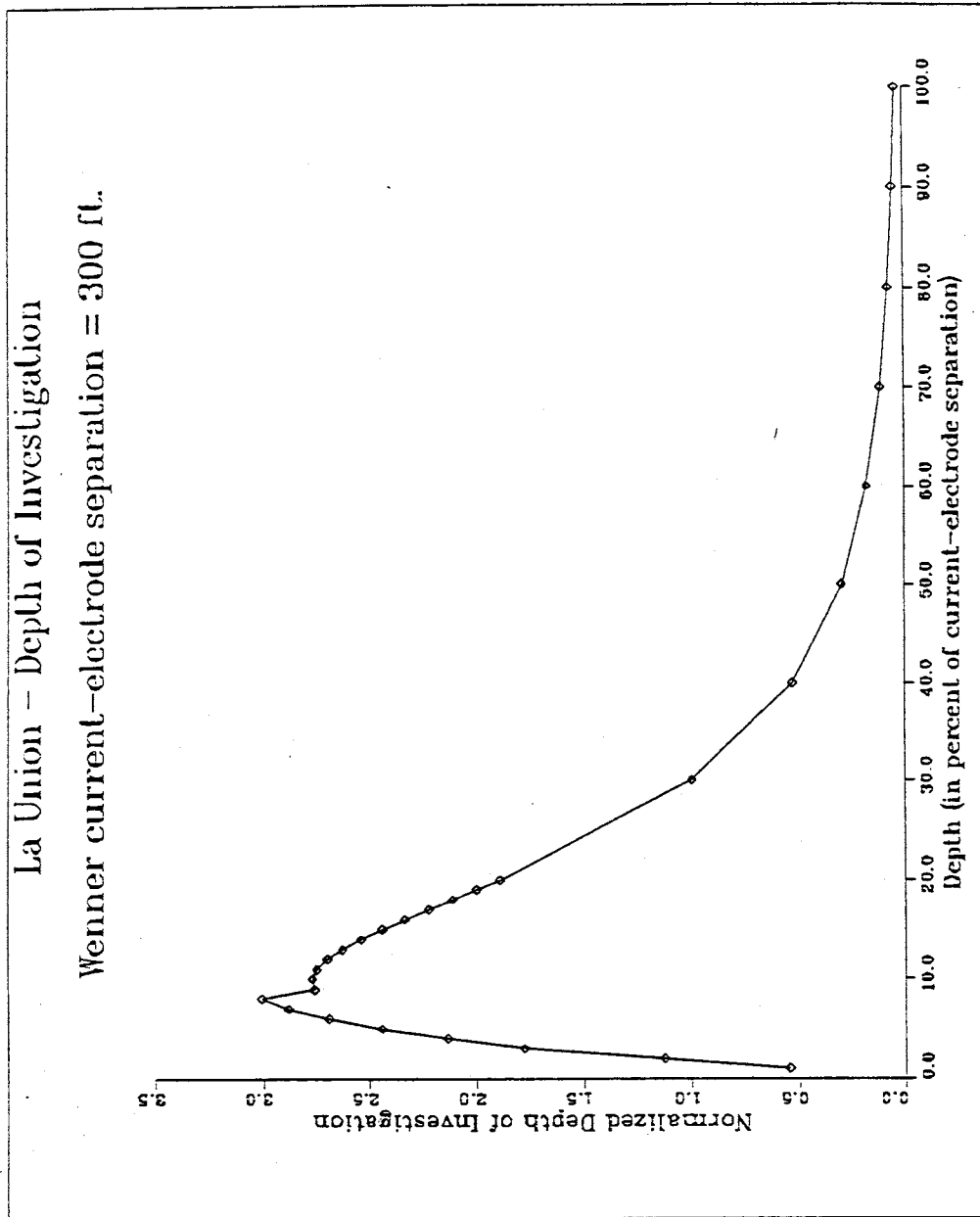


Figure 12. Depth of investigation for Wenner $a = 100$ feet. The abscissa is defined as depth, in percent of current-electrode separation or percent of 300 feet. The ordinate is the normalized depth of investigation. (Modeling data from Table III)

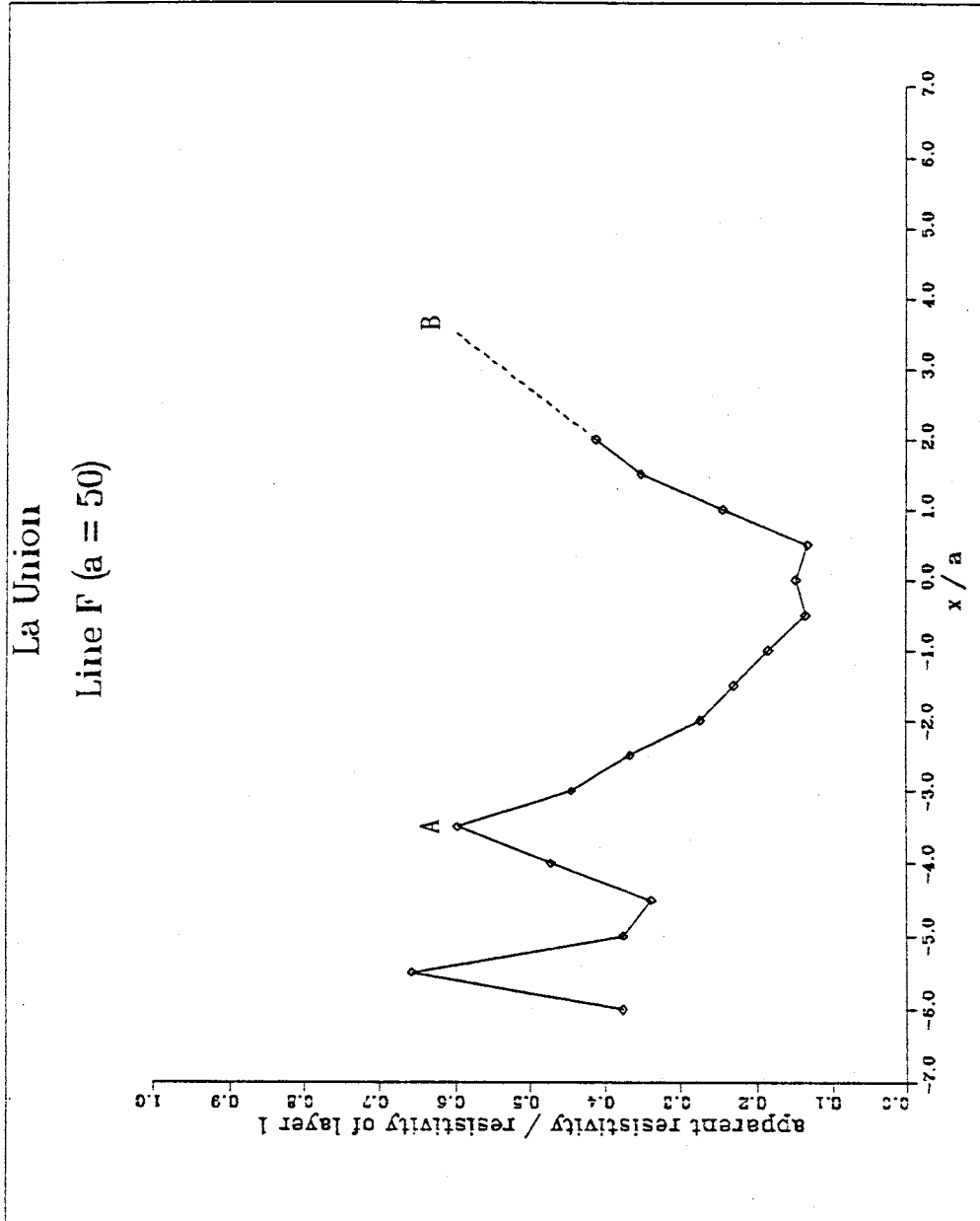


Figure 13. Normalized plot of horizontal resistivity profile, F line, a = 50 feet.
Resistivity of layer 1 = 170 ohm feet.

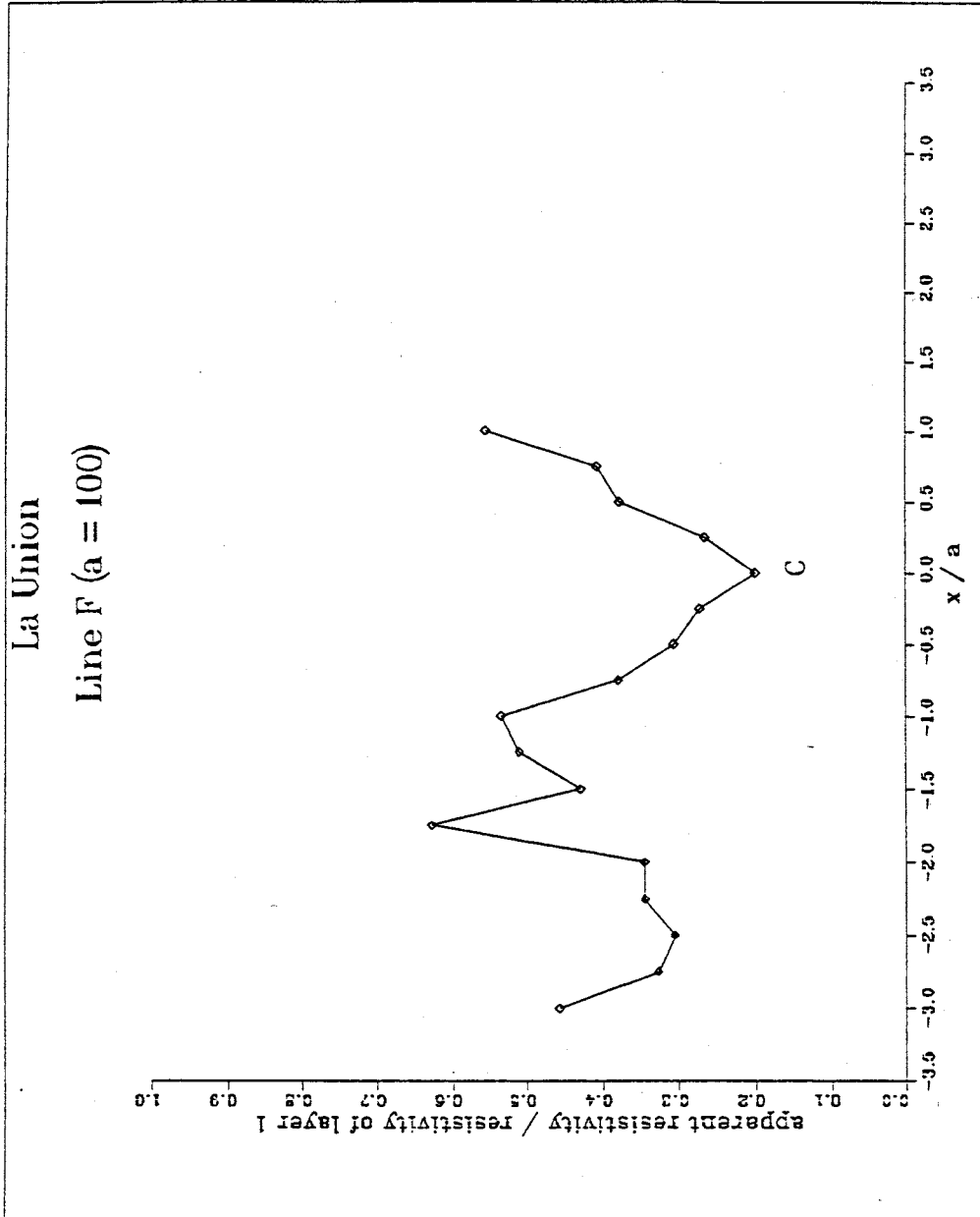


Figure 14. Normalized plot of horizontal resistivity profile, F line, a = 100 feet.
Resistivity of layer 1 = 170 ohm feet.

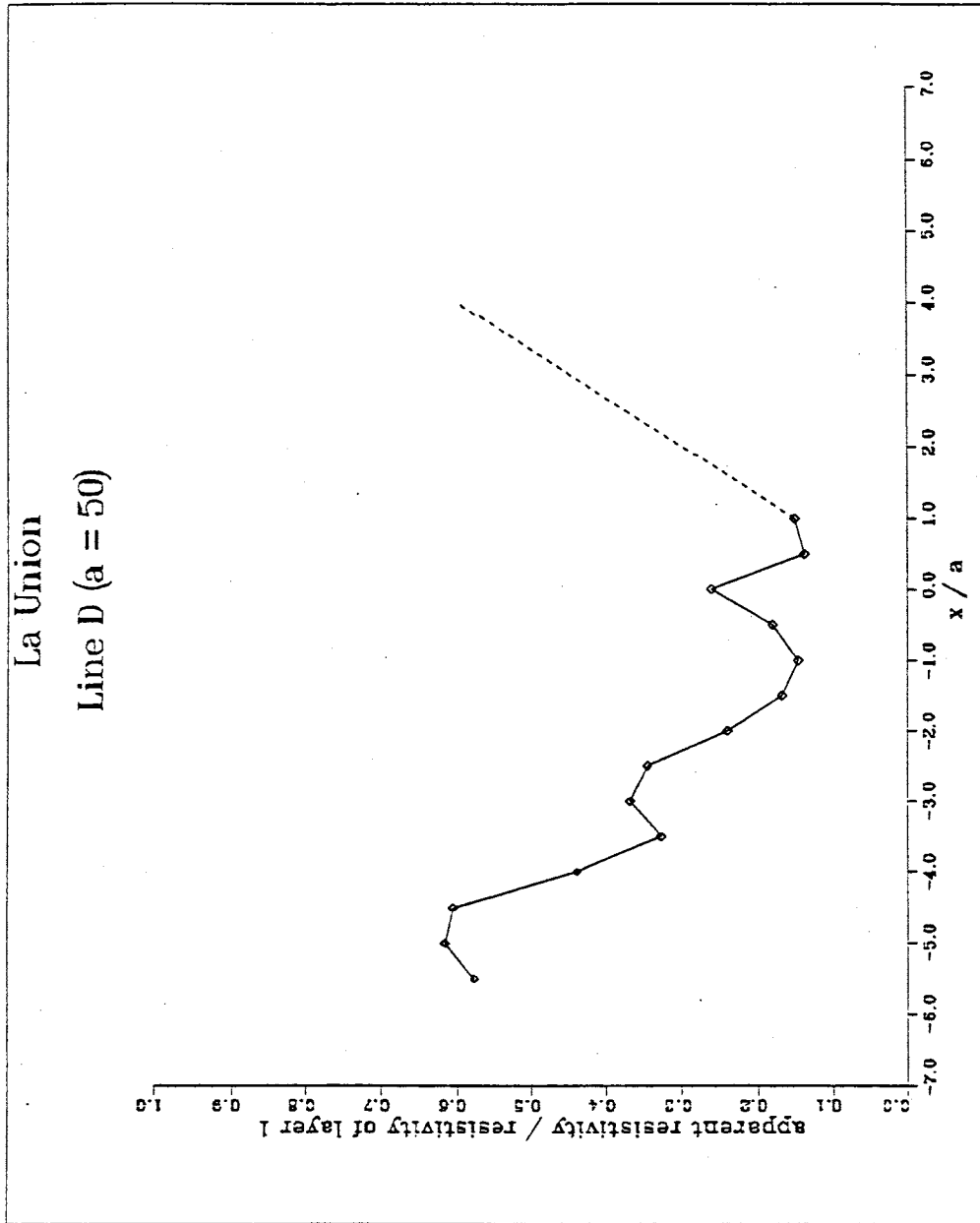


Figure 15. Normalized plot of horizontal resistivity profile, D line, a = 50 feet.
Resistivity of layer 1 = 170 ohm feet.

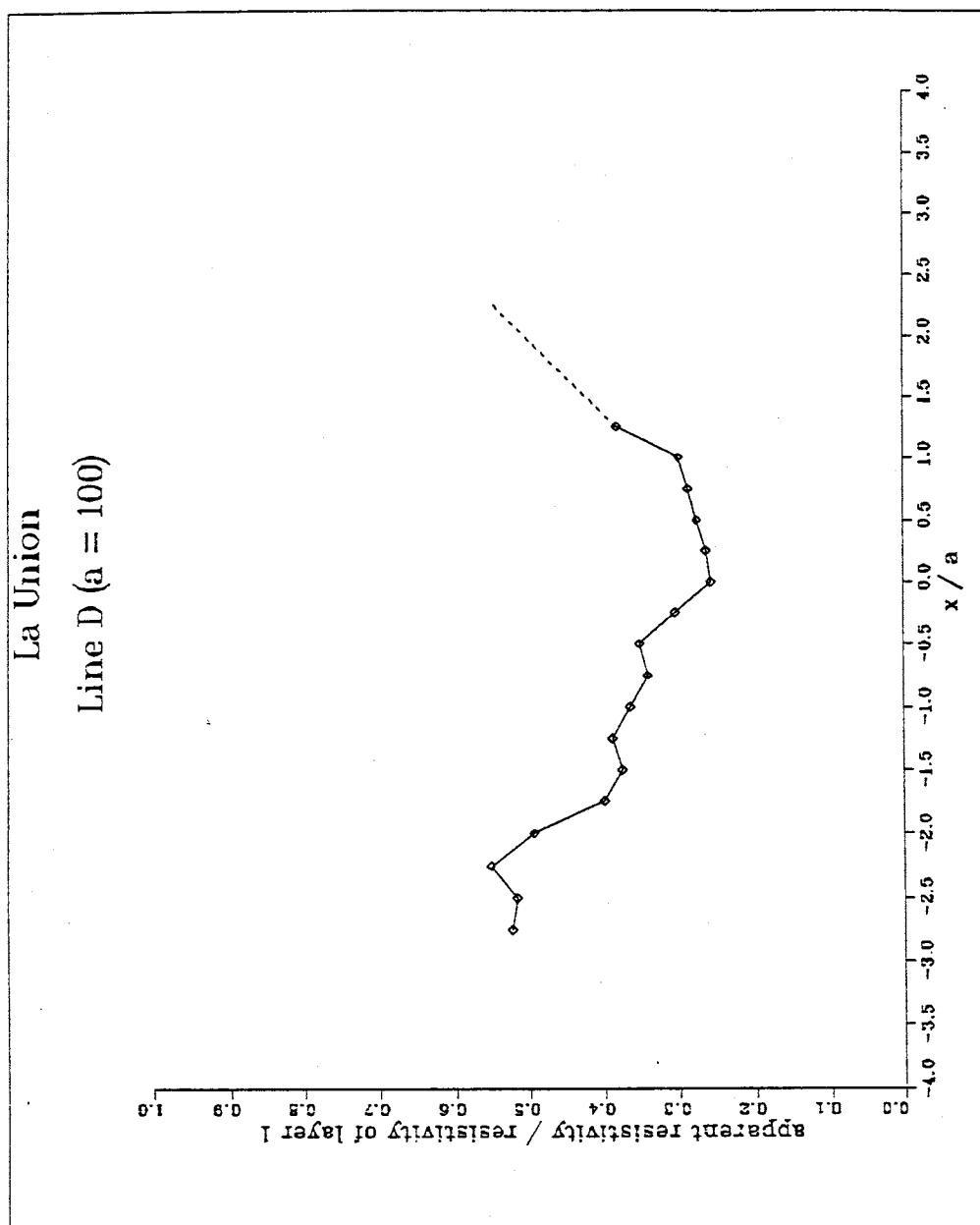


Figure 16. Normalized plot of horizontal resistivity profile, D line, a = 100 feet.
Resistivity of layer 1 = 170 ohm feet.

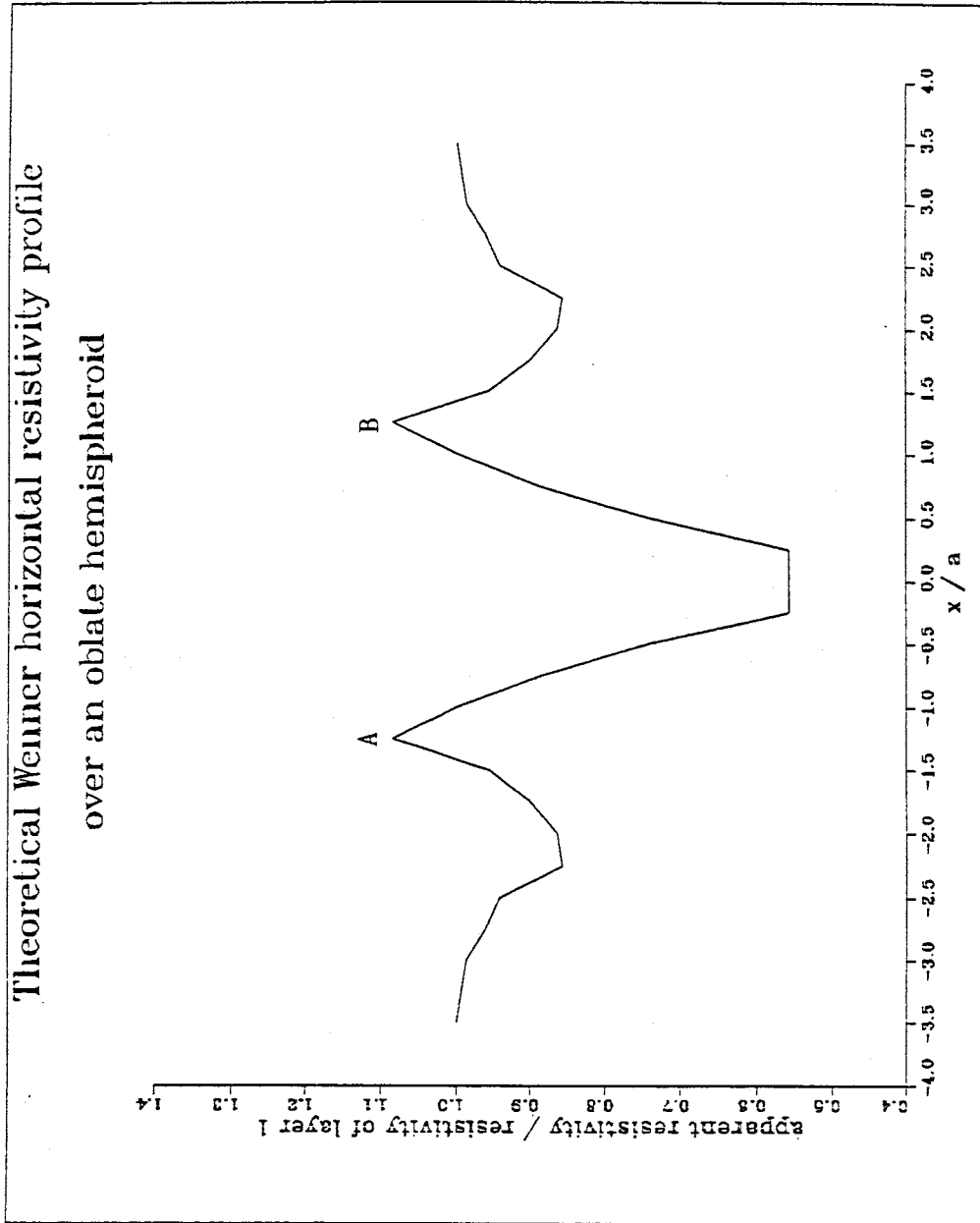


Figure 17. Theoretical horizontal resistivity profile over an oblate hemispheroid.
Wenner configuration, width at surface = $3a/2$, reflection coefficient
= -0.7 . (after Van Nostrand and Cook, 1966)

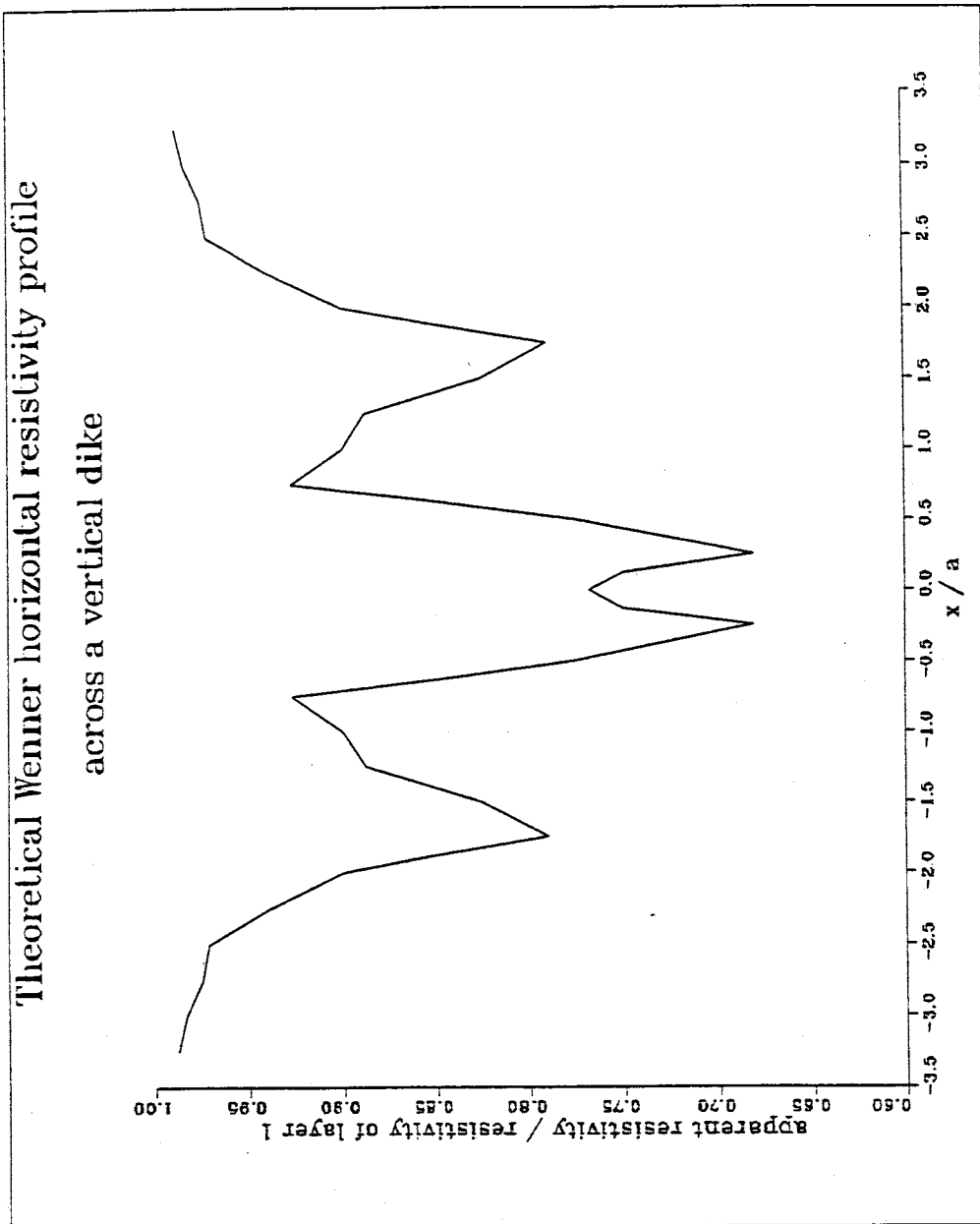


Figure 18. Theoretical horizontal resistivity profile across a vertical dike. Wenner configuration, width = $a/2$, depth = infinite, reflection coefficient = -0.6 . (after Van Nostrand and Cook, 1966)

Wenner VES Petrick Model

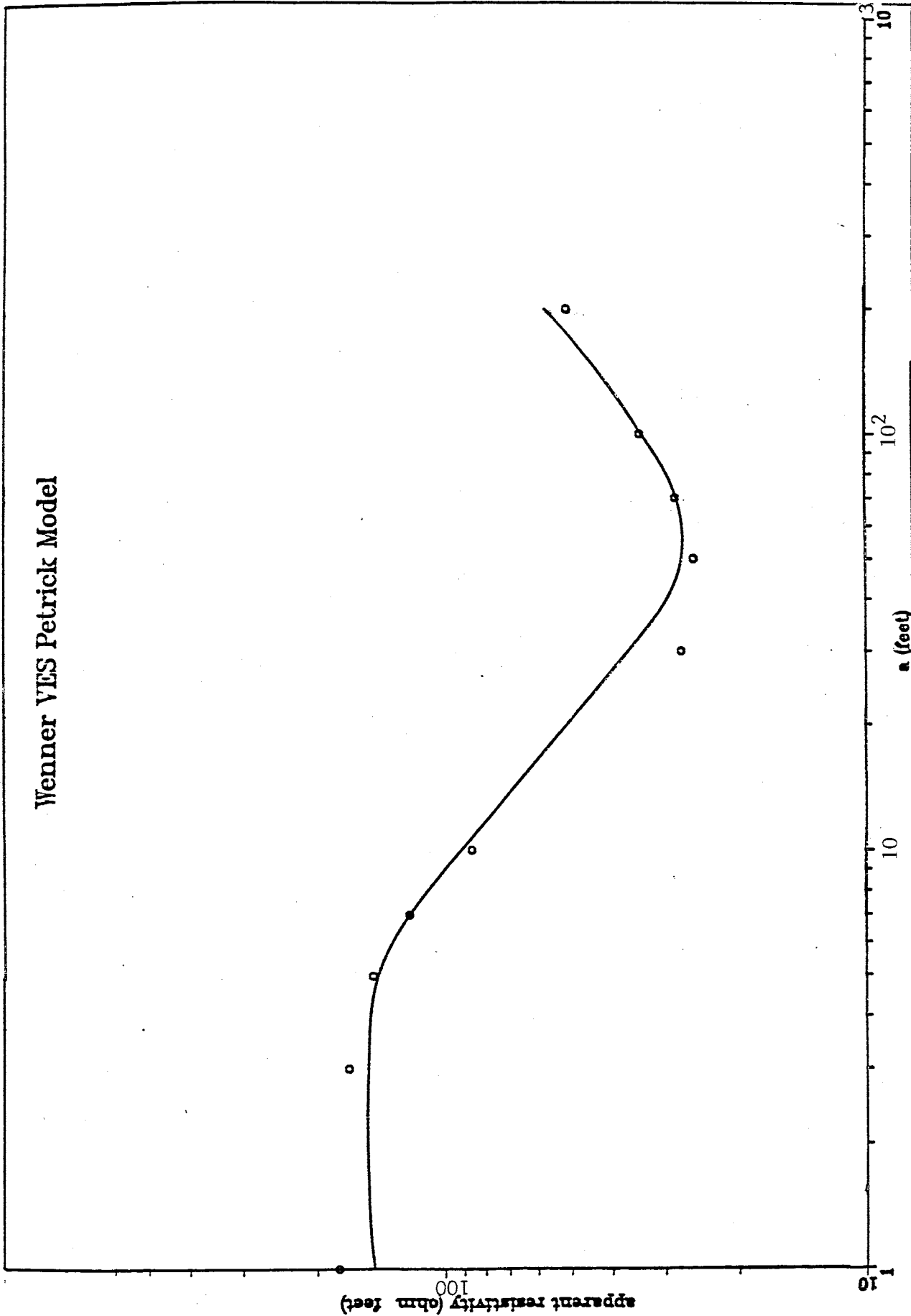


Figure 19. Log-log plot of La Union, lower landfill Wenner VES. Points = field measurements. Solid curve = model using Petrick inversion program.

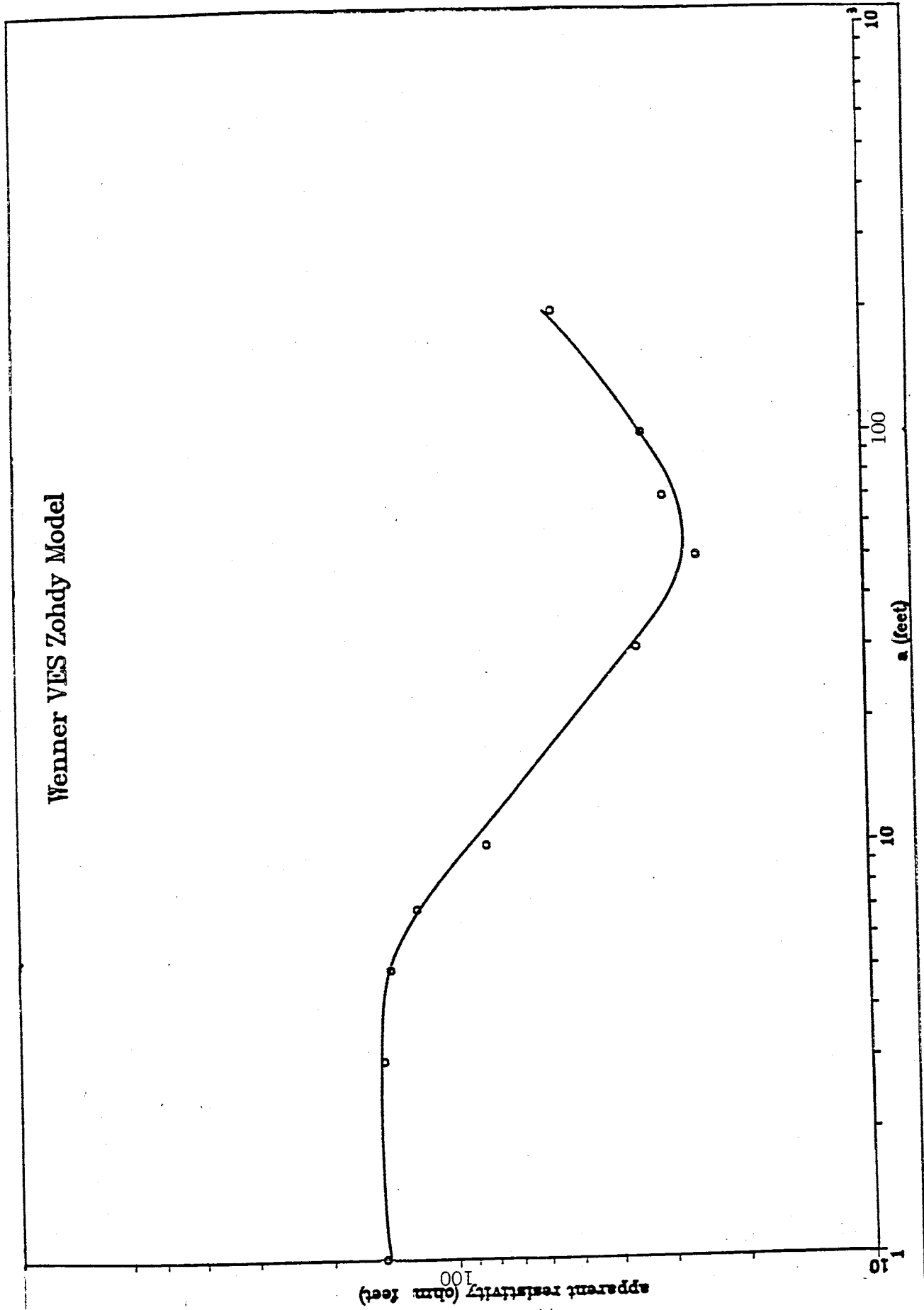


Figure 20. Log-log plot of La Union, lower landfill Wenner VES. Points = field measurements. Solid curve = model using Zohdy inversion program.

COMPARISON OF EFFECT OF SOIL TYPE
ON WENNER VES

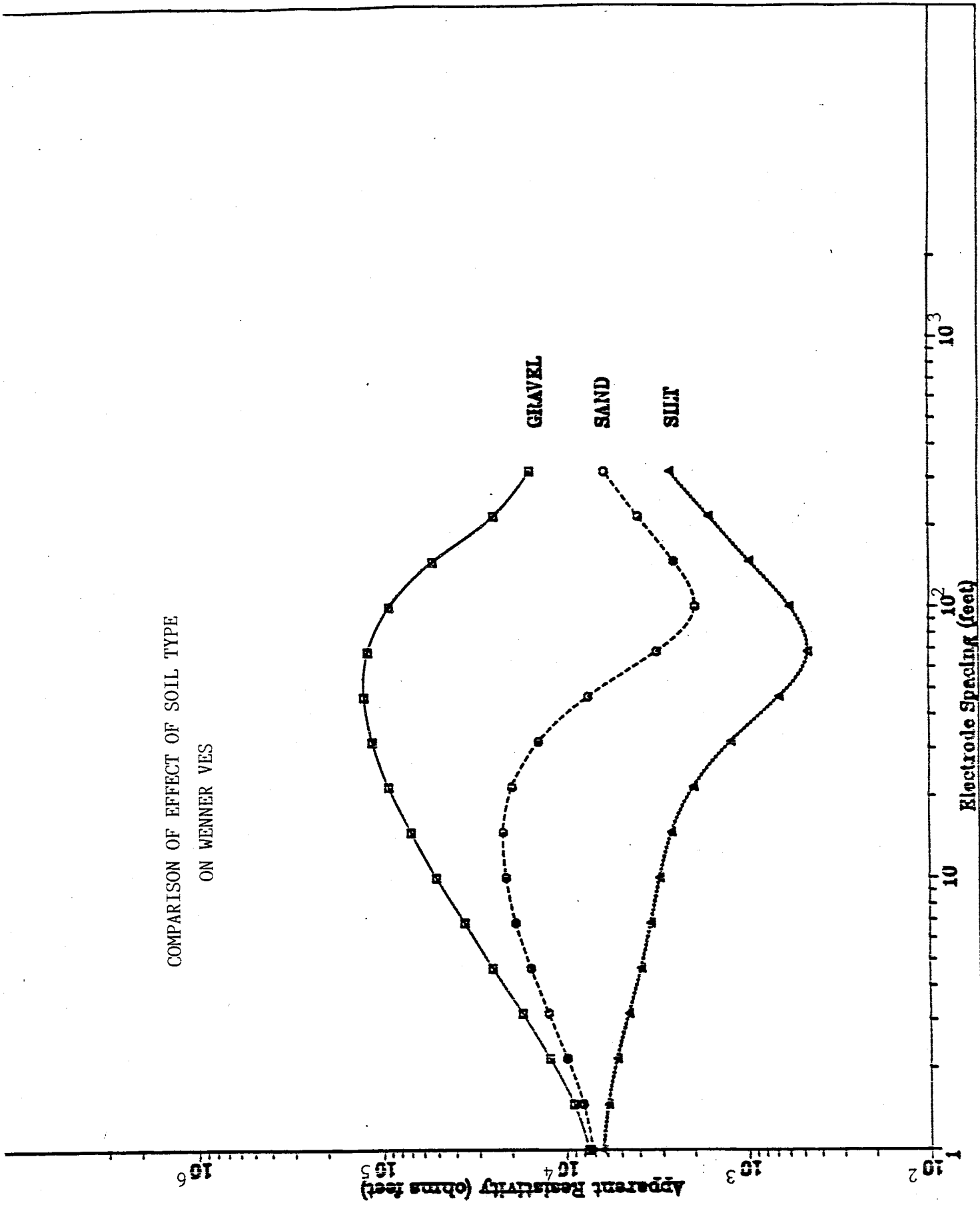


Figure 21. Comparison of effect of soil type on Wenner VES. 3 layer model, 2nd layer saturated, 3rd layer basement rock.